UNIVERSITY OF SOUTHAMPTON

Enzyme kinetics and electrochemical polymer transistor detection of enzyme reactions

By Yann Astier

DOCTOR OF PHILOSOPHY

Department of Chemistry

March 2001

UNIVERSITY OF SOUTHAMPTON

ABSTRACT

FACULTY OF SCIENCE

CHEMISTRY

Doctor of philosophy

Enzyme kinetics and electrochemical polymer transistor detection of enzyme reactions

By Yann Astier

The aim of the research reported in this thesis is to adapt the polymer microelectrochemical transistor technology to *in-vitro* immunological detection. *In-vitro* immunological detection or immunoassay is a routine diagnostic tool in medicine.

A wide variety of mono-specific antibodies can be obtained commercially with alkaline phosphatase attached as a label, consequently we describe a sensor offering a rapid detection (less than 60 s) of very low alkaline phosphatase concentrations (0 to 4 nM). We show how a poly(aniline) transistor may be switched from conductive to insulating by a redox enzyme. We show that this is still true when the polymer transistor is physically separated from the enzyme reaction in a chemical battery set-up. This set-up enabled us to use different pH conditions in both compartments of the battery like electrochemical device. Our sensor retains the polymer transistor electrochemical properties in acid while alkaline conditions are used in cell B. Electron transfer reaction from *p*-aminophenol at pH 9 in cell B to poly(aniline)-poly(vinylsulfonate) in 2 M sulfuric acid (cell A) is obtained, resulting in a change of polymer potential and hence a change of polymer conductivity. Also we describe the fabrication of 70 similar polymer transistors designed for one off detection experiments. We present a detailed account of *p*-aminophenol electrochemical properties above pH 7. We also show spectroscopic evidence of *p*-aminophenol forming

aggregates in solution above pH 7. An electrochemical study of *p*-aminophenyl phosphate showed its ability to poison platinum working electrodes. We present a kinetic study of quinone imine reduction by glucose oxidase and *p*-aminophenyl phosphate catalysed hydrolysis by alkaline phosphatase using rotating disc potential step electrochemical methods. Finally we describe the ability of our polymer transistor to detect *p*-aminophenol concentrations ranging from 100 to 400 nM as well as alkaline phosphatase concentrations ranging from 0 to 4 nM. In this chapter every polymer transistor is only used once.

Acknowledgements

I would like to thank Prof. Phil Bartlett for his supervision.

I thank MediSense Ltd. for financial support, and for providing chemicals needed in this work.

I thank the staff of the Chemistry Department of Southampton University for infallible support.

TABLE OF CONTENTS

Chapter 1: General introduction

Chapter 2: Experimental

Chapter 3: Poly(aniline)-poly(vinylsulfonate) transistors

Chapter 4: Disposable transistors

Chapter 5: The mediator

Chapter 6: *p*-aminophenyl phosphate

Chapter 7: Enzyme kinetics

Chapter 8: The sensor

Microelectrochemical Enzyme Transistors

1 Introduction

This chapter is an adaptation of: *Microelectrochemical transistors.* Phillip N. Bartlett and Yann Astier *Chem. Commun.*, 2000.

Electrochemical biosensors have been extremely successful as disposable devices for the measurement of blood glucose for use by diabetics world-wide. This success is based on ease of manufacture at low cost but with high control of quality and reproducibility combined with ease of use. The clinical range for glucose in blood lies between 1 and 20 mM. In this concentration range direct amperometric measurement at millimetre sized electrodes yields readily measured currents in the microamp range. Future applications will require much smaller devices so that more assays can be carried out in a single drop of blood and assays for analytes such as hormones, drugs or enzymes present at much lower concentrations (typically nano and micromolar). Taken individually and together these requirements will be difficult to meet with present types of amperometric biosensor because as the size of the electrode and/or the concentration of the analyte decreases the current measured also decreases. It is therefore appropriate to look for other types of electrochemical biosensor which, while retaining the simplicity of use and low cost of the amperometric devices, also provide the potential for greater sensitivity and small size.

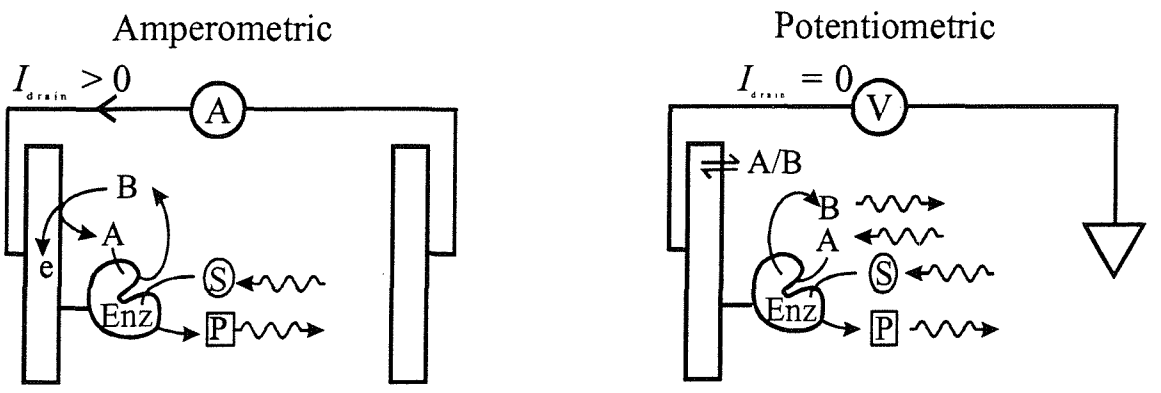

Figure 1: Schematic representations of an amperometric enzyme electrode and a potentiometric enzyme electrode. In the amperometric enzyme electrode the conversion of substrate, S, to product, P, by the enzyme is linked to the electrode through the mediator couple A/B. The current for the conversion of B to A is then related to the rate of the enzyme catalysed reaction and thus to the substrate concentration. In the potentiometric enzyme electrode the electrode senses the concentrations of A and B at the electrode surface. These concentrations depend on the rate of the enzyme catalysed reactions and the rates of mass transport of the A/B couple and the substrate in solution.

The majority of electrochemical biosensors are based on either potentiometric or amperometric detection, Figure 1. In the case of a potentiometric enzyme electrode the electrode senses the steady state concentration of some species, usually a product of the enzyme catalysed reaction (such as H^+, NH_4^+, etc.), at the electrode surface. This steady state concentration is determined by the kinetics of the enzyme catalysed reaction and by the mass transport of reactants to, and products away from, the electrode. Under suitable circumstances this steady state concentration is directly related to the concentration of the analyte in the solution. The operation of potentiometric enzyme electrodes suffers from a number of problems which limit their sensitivity for many applications.[1] In addition an accurate and stable reference electrode is essential and this is not easy to fabricate as a disposable structure. Consequently amperometric approaches have generally been favoured, although this is not always possible (for example in measurement of urea or penicillin). In an amperometric enzyme electrode the current is a direct measure of the rate of the enzyme catalysed reaction and therefore, under suitable circumstances, is directly related to the concentration of analyte. The great majority of redox enzymes or coenzymes such as NADH and NADPH do not undergo rapid, direct electrochemical reaction at electrode surfaces and consequently in is necessary to provide some means to couple the enzyme catalysed reaction to oxidation or reduction at the electrode surface. In

the first amperometric enzyme electrodes, such as the Clark glucose electrode,[2] this was done by oxidising or reducing one of the co-reactants or products of the enzyme catalysed reaction at a metal electrode. The enzyme glucose oxidase (E.C. 1.1.3.4) catalyses the reaction of β-D-glucose with oxygen to give D-glucono-δ-lactone and hydrogen peroxide. This reaction occurs in two stages. In the first step the oxidised flavin prosthetic group, FAD, bound in the enzyme active site is reduced by reaction with glucose to give the bound reduced flavin, $FADH_2$, and the product gluconolactone which undergoes hydrolysis to give gluconic acid. In a subsequent step the reduced flavin is reoxidised by reaction with molecular oxygen.

$$GOx(FAD) + \beta\text{-D-glucose} \rightarrow GOx(FADH_2) + \text{D-glucono-}\delta\text{-lactone}$$

$$\text{D-glucono-}\delta\text{-lactone} + H_2O \rightarrow \text{D-gluconate} + H_3O^+$$

$$GOx(FADH_2) + O_2 \rightarrow GOx(FAD) + H_2O_2$$

These reactions can be followed electrochemically by either measuring the rate of consumption of molecular oxygen or by measuring the rate of production of hydrogen peroxide. Although both approaches have been adopted they suffer from a number of problems. At high glucose concentrations, or in situations where the supply of oxygen is restricted, the response can be limited by the oxygen supply rather than by the concentration of glucose. In addition both oxygen and hydrogen peroxide are difficult species to measure electrochemically because of their poor electrode kinetics. Consequently measurements in whole blood, serum or other biological media are often difficult because of interference from other, readily oxidised compounds such as uric acid or ascorbate present in the sample. For these reasons it is preferable to avoid the use of oxygen and replace the second reaction by one in which a redox mediator is used to reoxidise the enzyme

$$GOx(FADH_2) + 2M^+ + 2H_2O \rightarrow GOx(FAD) + 2M + 2H_3O^+$$

Using this approach the mediator can be chosen so that it has both a fast reaction with the reduced enzyme, good stability and fast electrode kinetics at a potential where the interferences from other species present in the sample are minimal. The most successful example of this approach has been the use of ferrocene derivatives to mediate oxidation of glucose oxidase first suggested by Cass *et al.*[3] and subsequently the basis of a very successful commercial disposable glucose sensor.

For glucose oxidase, direct electrochemical oxidation of the enzyme is slow because the active site is buried deep within the enzyme core.[4] Homogeneous solution mediators, such as the ferrocene derivatives, are presumably able to diffuse into and out of the enzyme's active site and thus to act as a shuttle carrying electrons from the active site to the electrode. Although the use of homogeneous, freely diffusing mediators has proved a very successful and flexible approach to the problem it is not ideal for all applications because the mediator can diffuse away from the electrode surface and be lost. For this reason other approaches have been investigated including the co-immobilisation of the enzyme and mediator in carbon paste electrodes and sol-gel electrode structures, the covalent modification of the enzyme by attachment of the redox mediator to amino acid residues of the protein,[5,6] and the immobilisation of the enzyme in redox polymer films containing the covalently attached mediator. This last approach, pioneered by Heller,[7] has been very successful in linking the re-oxidation of several flavoproteins, including glucose oxidase, to electrodes for use in amperometric biosensors.

Despite these successes in designing amperometric enzyme electrodes there are important limitations to their performance if we wish to go towards either smaller sensors or analytes at lower concentrations. In an amperometric enzyme electrode the current is directly related to the rate of turnover of the enzyme. For example for glucose oxidase the maximum rate of turnover of the enzyme is 800 s^{-1}. For a monolayer coverage of the enzyme (1.6×10^{-12} moles cm^{-2})[8,9] on a 1 cm^2 electrode this corresponds to a maximum current of 240 μA. As the size of the electrode is decreased the current will also decrease because the number of enzyme molecules decreases. For a 70 micron diameter electrode (the diameter of a human hair - area 3.85×10^{-5} cm^2) the maximum current for a monolayer coverage of glucose oxidase will be 9.2 nA; for a 1 micron diameter electrode (area 7.85×10^{-9} cm^2 - a realistic size using present fabrication techniques) the current will be reduced to 1.9 pA. Clearly, in principle, this current can be increased if the enzyme

coverage is increased from a monolayer to multilayer. However the increase in current will be less that linear with increasing enzyme coverage because of the restriction on diffusion of the substrate through the enzyme layer at the electrode surface. Thus, realistically we can probably only expect an increase of one or two orders of magnitude in the current if we use multilayer enzyme coverage on the electrode.

These currents are for high concentrations of the analyte (> 20 mM) and for an enzyme with fast kinetics. At lower concentrations, or for many other enzymes, the currents would be less. This also becomes a problem when we try to develop amperometric biosensors for analytes such as hormones or drugs which are biologically active at much lower concentrations.

To address these problems it is appropriate that we investigate other electrochemical sensing strategies which maintain the advantages of electrochemical biosensors in terms of low cost, ease of use and manufacture but which offer other mechanisms to allow enhanced sensitivity at low analyte concentrations for devices of small size. One such approach is provided by the microelectrochemical transistor or switch devices first described by Wrighton and colleagues.[10] These devices make use of the ability to switch the conductivity of thin conducting polymer films by five or more orders of magnitude on oxidation or reduction. This large change in conductivity of the polymer leads to amplification of the signal and can be used as the basis of a chemical sensor or biosensor which acts as a electrochemical transistor analogous to a junction field effect transistor in its operation and characteristics. In addition these devices can be made very small so that they may be suitable for use in small sample volumes.

2 Conducting polymers

The microelectrochemical transistors and diodes described by Wrighton make use of the very large changes in the conductivity of electronically conducting polymers which accompany oxidation or reduction of the polymer backbone. Conducting polymers, such as poly(pyrrole) or poly(3-methylthiophene) are formed by oxidative coupling of the respective monomers. This coupling can be carried out chemically or electrochemically. The latter approach has the advantage that the polymerisation process is localised at the electrode surface and that the amount of polymer deposited can be controlled through the

total amount of charge passed. On cycling the potential of the conducting polymer film in a solution of background electrolyte the polymer can be repeatedly oxidised and reduced, Figure 2. The amount of charge passed in this process depends on the amount of polymer present. For polymers such as poly(pyrrole) and poly(3-methylthiophene) the oxidised form is conducting and the reduced form is insulating. Conduction in the oxidised form of the polymer is through the mobile bipolarons[11] Figure 2.

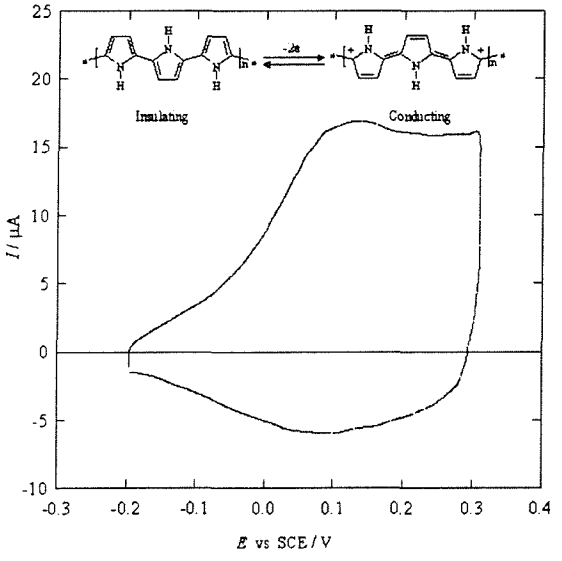

Figure 2: A cyclic voltammogram of a poly(pyrrole) film recorded at 200 mV s^{-1} in 2 mol dm^{-3} H_2SO_4. The film was grown on a 0.5 mm diameter platinum electrode at 0.65 V vs. SCE from a solution of 0.5 mol dm^{-3} pyrrole in 1 mol dm^{-3} KCl. The inset shows the schematic structures for the insulating and conducting forms of the polymer. Note that in the fully oxidised polymer there is typically one charge for every 4 monomer units.

The oxidation and reduction of the conducting polymer is also accompanied by the ingress and egress of anions, cations and solvent and by polymer chain relaxation process. Thus the dynamics of the redox transformation of these films is a complex process and one which we are only now beginning to full comprehend through the use of a variety of *in situ* techniques.[12,13] This movement of ions is essential to maintain electroneutrality of the polymer film. This requirement for the motion of ions to accompany the oxidation and

reduction of the polymer constrains the maximum rate at which these films can switch between conducting and insulating states.

3 Microelectrochemical transistors and diodes

The first microelectrochemical transistor, described by Wrighton and colleagues in 1984,[10,14] comprised a poly(pyrrole) film deposited across the gaps between three independent gold microband electrodes 1.4 μm apart on a oxidised silicon substrate, Figure 3. By analogy with a junction field effect transistor the three gold electrodes are referred to as the source, gate and drain. By using the central gate electrode Wrighton and colleagues were able to alter the redox state of the poly(pyrrole) film. With the gate at potentials, V_{gate}, negative of -0.2 V vs. SCE the polymer is insulating and no current flows through the polymer film between the outer source and drain electrodes when a voltage, V_{drain}, is applied between them - the device is in the "off" state. When the gate potential, V_{gate}, is changed to more positive values the poly(pyrrole) film becomes oxidised and changes to its conducting state. Now when a voltage is applied between source and drain a significant drain current, i_{drain}, flows between the source and drain electrodes through the poly(pyrrole) film - the device is in the "on" state. Figure 3 shows the current voltage characteristics of the device at different gate voltages. In this device a small signal applied to the gate electrode leads to a large change in the drain current flowing through the polymer; thus the device amplifies the signal in the same way that a solid state transistor can be use to amplify a signal.

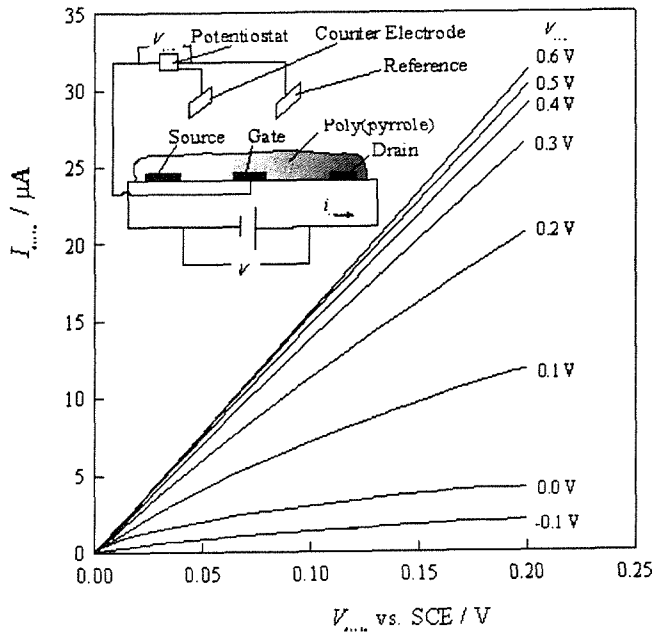

Figure 3: Plots of the drain current, i_{drain}, as a function of the drain voltage, V_{drain}, for a poly(pyrrole) based microelectrochemical transistor operated in acetonitrile containing 0.1 mol dm^{-3} [n-Bu_4N]ClO_4. Each curve corresponds to a different value of the gate voltage, V_{gate}. As the gate voltage increases from –0.1 V vs. SCE to 0.6 V the resistance of the poly(pyrrole) film decreases. The inset shows the arrangement used to make the measurements. (Adapted from White *et al.*[10])

power amplification up to frequencies of 10 kHz.[17] Nevertheless this is still considerably slower than for solid-state devices.

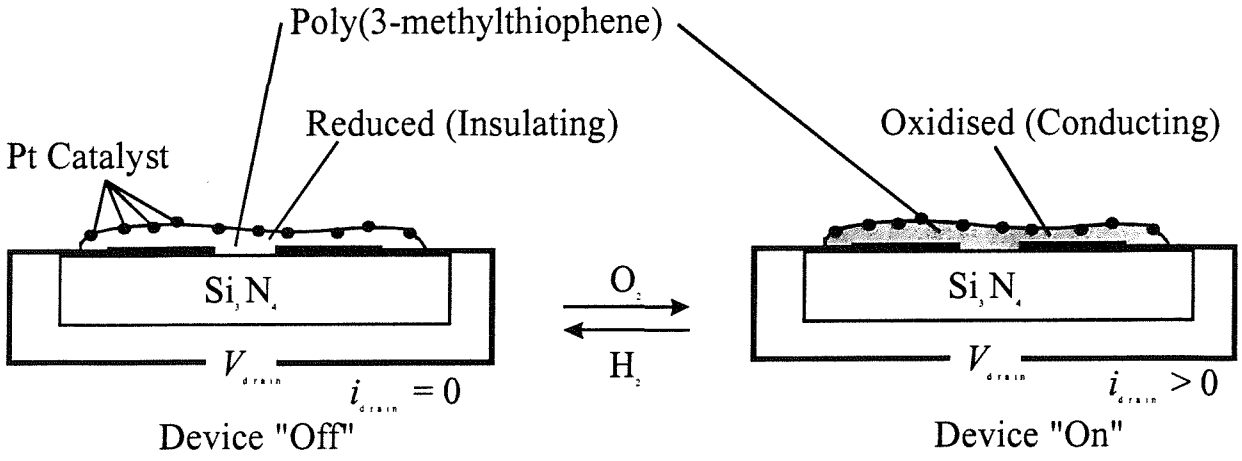

Figure 4: A two terminal poly(3-methylthiophene) based microelectrochemical enzyme transistor. The device can be turned "off" by reduction with hydrogen or "on" by oxidation with oxygen. The platinum particles are necessary to catalyse the reactions of the gases at the surface of the polymer. (Adapted from Thackeray *et al.*[19])

However although switching in microelectrochemical transistors is slow they have other properties which solid state devices do not possess, notably that the devices can be switched by chemical reactions and therefore can, in principle, be used as chemical sensors. Thus, instead of using a potentiostat and external circuit the redox state of the polymer film can be changed by oxidation or reduction by a species in solution and this change can again be sensed by a change in the drain current flowing through the device - the chemical reaction switches the device between "on" and "off" states. The first examples of this used simple outer sphere redox couples such as $[Fe(CN)_6]^{3-/4-}$ or $[Ru(NH_3)_6]^{3+/2+}$ to turn devices based on poly(aniline) films "on" and "off" respectively.[16] The amount of redox reagent which can be detected with this type of device is very small. For example for a poly(3-methylthiophene) based transistor Wrighton *et al.* were able to detect the injection of 1 x 10^{-9} mol of $[IrCl_6]^{2-}$ corresponding to the reaction of 8 x 10^{-16} mol of the reagent at the polymer surface.[18] Subsequently responses to molecular hydrogen and oxygen were demonstrated for microelectrochemical transistors based on poly(3-methylthiophene) films modified with platinum particles to catalyse the reactions of hydrogen and oxygen,[19] . Despite the use of the platinum particles to catalyse the reduction of oxygen the response of the devices was still rather slow, taking around 2 min to respond to 1 atm of dissolved molecular oxygen. In these devices the

microelectrochemical transistor acts as a sensor for the redox potential of the solution without any particular chemical selectivity for the species present.

Whilst these initial studies by Wrighton and colleagues demonstrated the concept of using a microelectrochemical transistor as a chemical sensor they did not go on to demonstrate selective devices or to look at the possible use of other types of catalyst to provide selectivity in the device response.

4 Microelectrochemical enzyme transistors

An obvious way to impart chemical selectivity to a microelectrochemical transistor is to use an immobilised enzyme as the catalyst.[20] However this has proved to be difficult because of the problems of coupling the enzyme electrochemistry to the conducting polymer film and finding the right conducting polymer with the correct properties for the application. The obvious starting point is to use poly(pyrrole) or one of its derivatives since these polymers can be deposited from neutral aqueous solutions and can be use to entrap enzymes such as glucose oxidase during deposition of the polymer.[21-23] This was the approach adopted by Matsue to make the first microelectrochemical enzyme transistor, a NADH responsive device based on diaphorase.[24] They used an interdigitated platinum electrode structure fabricated on glass with 10 μm wide bands separated by 10 μm wide gaps. These were coated with a thin electropolymerised film of co-polymerised pyrrole and N-methylpyrrole containing diaphorase (E.C. 1.6.99.- purified from *Bacillus stearothrmophilus*). In order to couple the enzyme catalysed reaction to the reduction of the polymer 1 mM anthraquinone-2-sulphonate was added to the solution as a mediator. On addition of NADH the oxidation of NADH, catalysed by the diaphorase, led to reduction of the pyrrole/N-methylpyrrole copolymer film causing the device to switch from "on" to "off". This change in the conductivity of the polymer was observed by recording the change in the drain current, i_{drain}, flowing through the device as a function of time after exposure to NADH, Figure 5. After exposure to NADH the device is in its "off" state and must be reset by reoxidising the polymer before it can be used to make another measurement of NADH. This was achieved by electrochemical oxidation of the polymer film.

Despite proving to be a useful way of immobilising enzymes at electrode surfaces for amperometric enzyme electrodes[21-23] poly(pyrrole) and its derivatives are not the most suitable polymers for the fabrication of microelectrochemical enzyme transistors because the stability of the polymer in solution at neutral pH is not good, it is hard to reproducibly deposit the films from neutral aqueous solutions and because the electrical conductivity of the polymer is irreversibly destroyed by reaction with hydrogen peroxide.[25,26] This is a particularly serious problem if one wants to use flavoproteins, such as glucose oxidase, which inevitable generate some peroxide even when a redox mediator are incorporated into the film with the enzyme.[27]

These problems can be overcome by using poly(aniline) which is stable, does not react with hydrogen peroxide and which can be deposited very reproducibly by electrochemical methods. The electrochemistry of poly(aniline) is more complex that that of poly(pyrrole) because there are three accessible oxidation states: the leucoemeraldine, emeraldine, and pernigraniline forms,[28,29] Figure 6. Of these three forms only the protonated emeraldine form is electronically conducting. The emeraldine base, Figure 6, is an insulator. Thus poly(aniline) generally only exists in its conducting form in acidic solution and the polymer is normally electrochemically deposited from acidic solutions (such as 1 M H_2SO_4). Poly(aniline) films can be cycled between the three redox states electrochemically in acidic solutions, Figure 6, but at low pH the pernigraniline form is unstable and undergoes hydrolysis leading to degradation of the film.

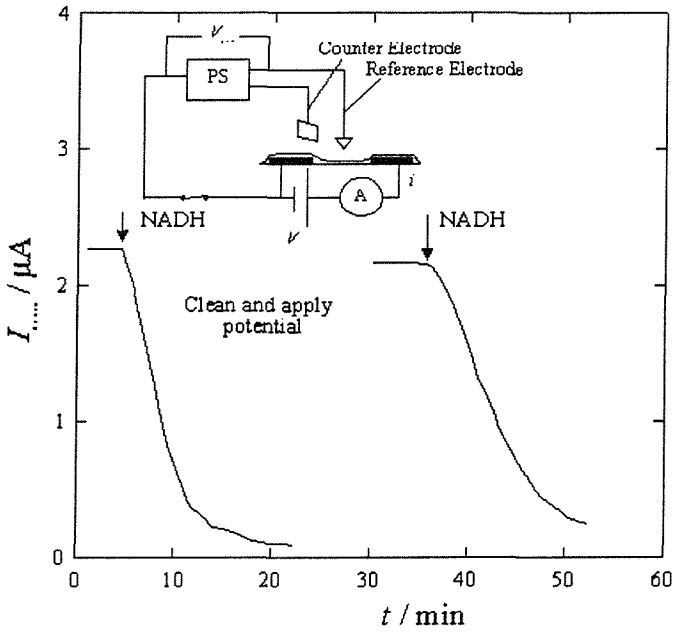

Figure 5: Response of the drain current, i_{drain}, to the addition of 1 mmol dm^{-3} NADH for a microelectrochemical enzyme transistor based on a copolymer of pyrrole and N-methylpyrrole and incorporating diaphorase and anthraquinone-2-sulfonate. The device was operated at a drain voltage of 20 mV in 0.1 mol dm^{-3} KNO_3 in 20 mmol dm^{-3} phosphate buffer at pH 6.8. The inset shows the experimental arrangement for the measurement (adapted from Matsue *et al.*[24]).

In order to use poly(aniline) films with flavoproteins it is essential to work in neutral, or at best weakly acidic, solutions to avoid the destruction of the enzyme. The workable pH range for poly(aniline) films grown from sulfuric acid solution is determined by the pK_a of the emeraldine form of the polymer. This is around 5.5, so that these films can be operated in buffered solutions at pH 5.

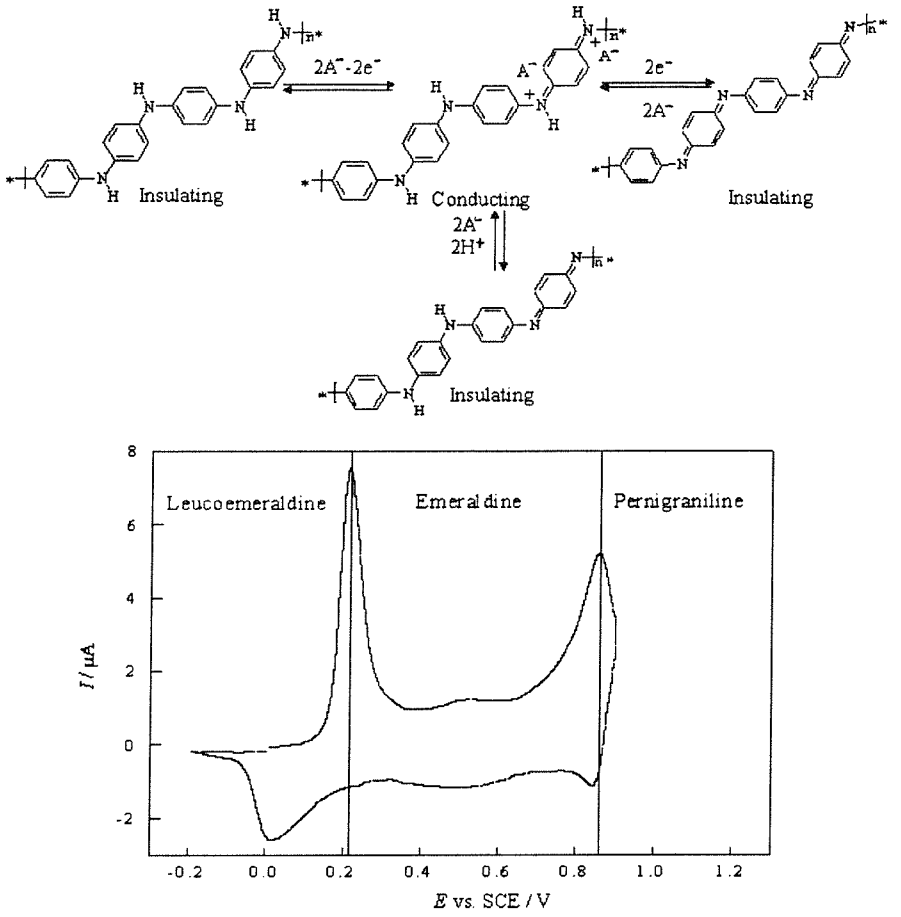

Figure 6: Cyclic voltammogram for a poly(aniline) film recorded at 20 mV s^{-1} in 2 mol dm^{-3} H_2SO_4. The film was grown on a 0.5 mm diameter platinum electrode at 0.9 V vs. SCE from a solution of 0.4 mol dm^{-3} aniline in 2 mol dm^{-3} H_2SO_4. The three different forms of the material are indicated. Of the three only the protonated emeraldine form is electronically conducting. The diagram also shows schematic representations of the structures of the different forms.

selectivity against interference from solution species. The fact that the film is deposited electrochemically also means that it coats the surface of the device evenly. The construction of the device is shown in Figure 7. To couple the enzyme catalysed oxidation of glucose to the reduction of the poly(aniline) film tetrathiafulvalene (TTF) was used as a mediator. The overall reaction scheme is then

$$GOx(FAD) + \beta\text{-D-glucose} \rightarrow GOx(FADH_2) + \text{D-glucono-}\delta\text{-lactone}$$

$$\text{D-glucono-}\delta\text{-lactone} + H_2O \rightarrow \text{D-gluconate} + H_3O^+$$

$$GOx(FADH_2) + 2TTF^+ + 2H_2O \rightarrow GOx(FAD^+) + 2TTF + 2H_3O^+$$

$$TTF + PANI(ox) \rightarrow TTF^+ + PANI(red)$$

where PANI(ox) represents the fully oxidised, insulating, pernigraniline form of poly(aniline) and PANI(red) the partially oxidised, conducting, emeraldine form. Thus the enzyme catalysed reaction turns the device from "off" to "on", Figure 7. Following exposure to glucose the device can be reset by electrochemical oxidation of the poly(aniline) to the pernigraniline form at 0.5 V vs. SCE.

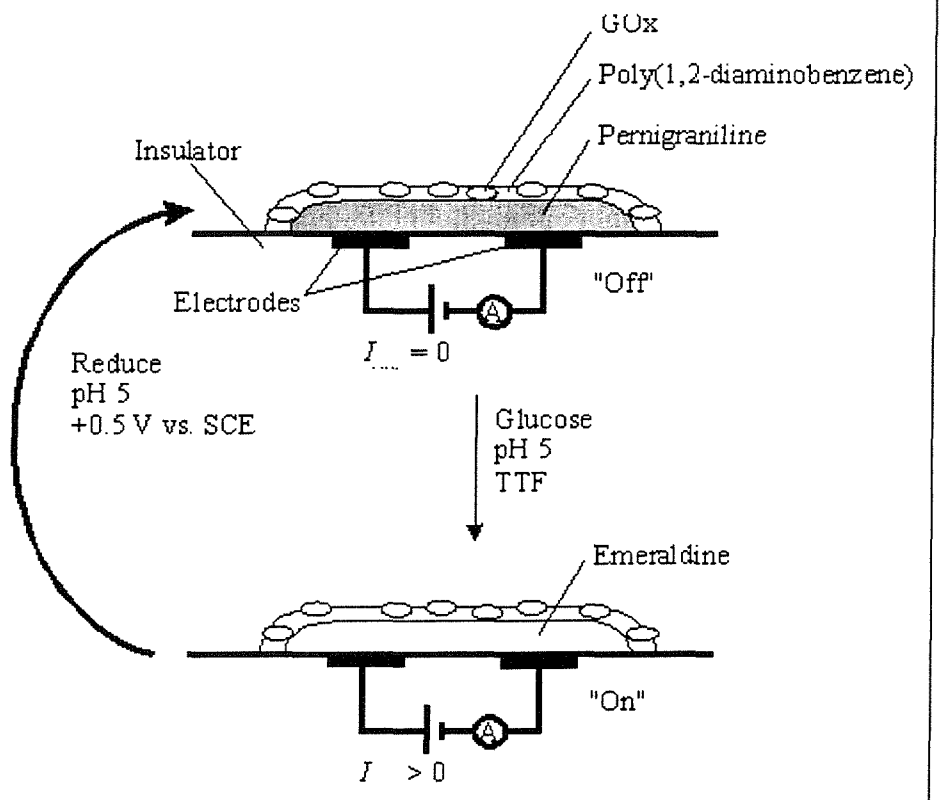

Figure 7: The construction and operation of a microelectrochemical enzyme transistor responsive to glucose. The device is based on a poly(aniline) film deposited across the gap between two electrodes. On top of the film the enzyme glucose oxidase (GOx) is immobilised in a electropolymerised film of poly(1,2-diaminobenzene). The device is switched from "off" to "on" on exposure to glucose. The device can be reset by electrochemical oxidation of the poly(aniline) film at +0.5 V vs. SCE at pH 5.0 to the insulating pernigraniline state.

For a device of this type the rate at which the drain current increases upon exposure to the analyte and the time taken for it to switch between states depend on the concentration of analyte.

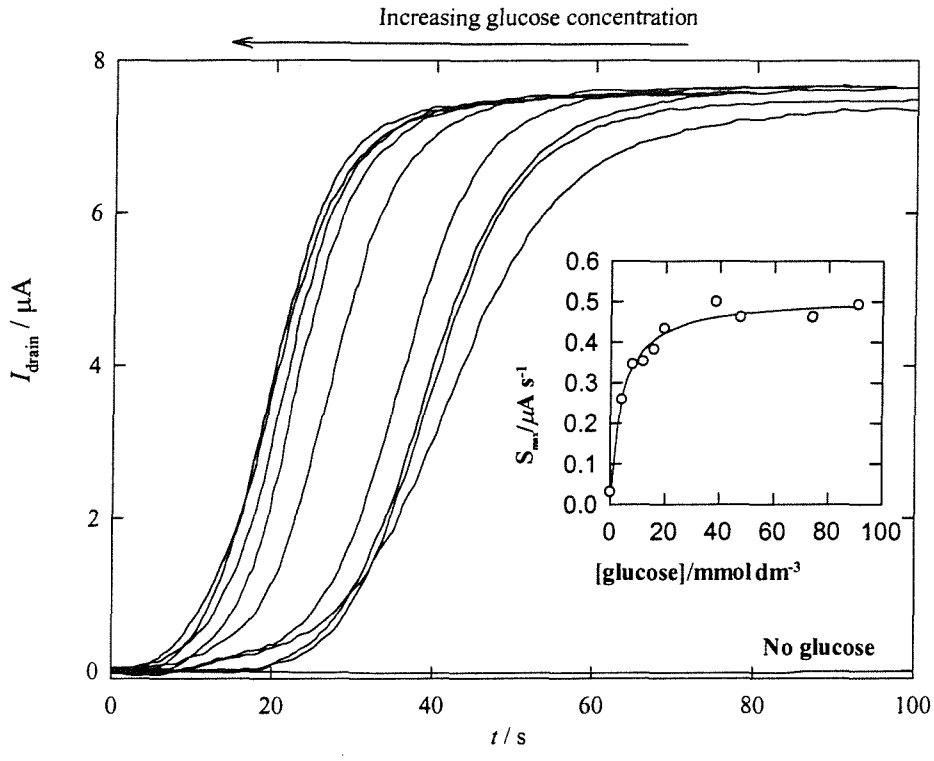

Figure 8: A set of response curves for a glucose oxidase based microelectrochemical enzyme transistor. The structure of the transistor is shown in figure 7. Between each measurement the device was reset electrochemically to its insulating state at 0.5 V vs. SCE. Measurements were made with a drain voltage, V_{drain}, of 20 mV in pH 5 phosphate/citrate buffer containing 0.5 mol dm^{-2} Na_2SO_4 and 0.5 vol % Triton X100 saturated with tetrathiafulvalene. In each case aliquots of sample solution were added at time zero. In the absence of glucose the drain current, i_{drain}, flowing through the device does not change. When an aliquot of glucose is added the drain current increases with time following the addition until it eventually reaches a plateau when the device is in the "on" state. The time taken for the device to switch on and the maximum switching rate, S_{max}, (defined as the maximum slope of the plot of drain current against time) depends on the concentration of glucose. The inset shows the calibration curve for this device. (Reprinted from Bartlett and Birkin.[30])

Figure 8 shows a set of response curves for a single device exposed to different concentrations of glucose. First it is clear that the device can be reused at least nine times with no apparent loss in function, in fact many more than nine consecutive operations are possible for this device under these conditions. It is also clear that the response of the device depends on the concentration of glucose added to the solution. Without added glucose there is no change in the drain current over the course of the experiment. When glucose is added there is initially no change in the drain current flowing through the poly(aniline) film but then, as the enzyme catalysed reaction begins to reduce the polymer

it is converted to its conducting, emeraldine state and the drain current increases eventually reaching a plateau when the polymer is highly conducting and the drain current is limited by the base resistance of the carbon microband structure (in this case about 3 kΩ). Note that on switching from "off" to "on" the resistance of this device changes by around 3 orders of magnitude. It can shown that the device does indeed operate through changes in the oxidation state of the poly(aniline) film by following the potential of the film during switching, Figure 9a. Before addition of glucose the potential of the polymer is around +0.28 V vs. SCE where the poly(aniline) film is insulating. On addition of glucose the potential immediately begins to shift cathodic as the poly(aniline) is reduced and then the drain current increases as the polymer becomes more conducting. Figure 9b shows the variation of the polymer resistance with potential.

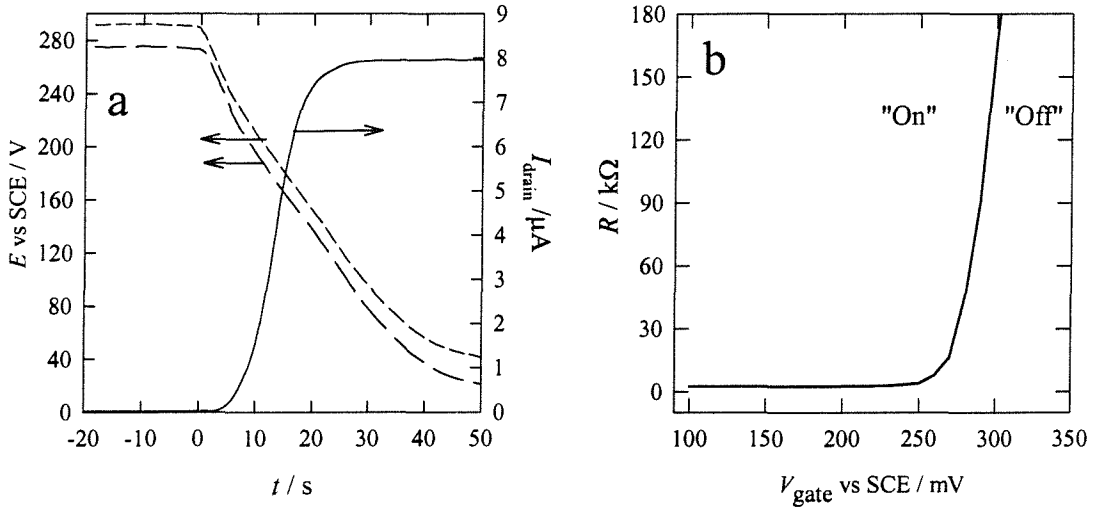

Figure 9: a) Simultaneous measurement of the drain current, i_{drain}, and the potentials of the two microband electrodes as a function of time after addition of glucose. b) resistance of a poly(aniline) film as a function of the redox potential at pH 5 (Reprinted from Bartlett and Birkin.[31])

Studies of the effect of varying the amount of polymer deposited onto the device and the enzyme loading allow the speed of response of these devices to glucose to be optimised and support the model for the operation of these devices.[31] By optimising the amount of poly(aniline) deposited across the 20 μm gap a switching time of less than 10 s can be achieved. This is significantly faster than the best switching times reported by Matsue *et al.* for their NADH responsive device.[24] The selectivity of this type of device for glucose over other sugars is largely determined by the selectivity of the enzyme itself with D-(+)-

glucose giving much faster switching rates than D-(+)-mannose or D-(+)-galactose, Table 1.

Substrate	relative homogeneous rate[53]	Amperometric response / μA	switching rate / s^{-1}
D-(+)-glucose	100	63	0.209
2-deoxy-D-glucose	25	42.5	0.218
D-(+)-mannose	0.98	8.8	0.081
D-(+)-galactose	0.14	3.3	0.034

Table 1: Comparison of the relative homogeneous rates, amperometric response, and switching rate recorded for a single device in the presence of 0.15 mol dm^{-3} substrate and 1.4 mmol dm^{-3} TTF^{+}. (From reference 31)

5 Advantages of microelectrochemical enzyme transistors

Microelectrochemical enzyme transistors have a number of potential advantages as biosensor devices which could be beneficial in some applications. First the devices do not require a potentiostat or a reference electrode to operate. Measurement of the drain current can be achieved with very simple instrumentation and, at least for devices operating in the "off" to "on" direction (see below), the instrumentation required to re-set the device after each measurement can be very simple. Second the devices can be made very small without loss of sensitivity. As the gap between the electrodes is decreased and the polymer film is made thinner the speed of response will increase and the magnitude of the drain current will increase. Third these devices can be thought of as counting the number of molecules which have reacted with the enzyme. Thus it will take a certain number of glucose molecules to switch the device from its "off" state to its "on" state. This number of molecules depends on the amount of poly(aniline) in the device - for a device 50 μm by 50 μm Bartlett *et al.* estimate that 60 fmol of glucose is required to reach the halfway point where i_{drain} is one half its maximum value. As the size of the device decreases the number of moles of glucose will also decrease. Fourth, the device integrates the analytical signal. Thus if the device is removed from the solution containing glucose the drain current does not fall back to zero but stays at the value reached. If the device is returned to the glucose solution the drain current increases once more. This is because the

enzyme catalysed reaction causes the reduction of the polymer so that each molecule of glucose which reacts injects one charge carrier into the polymer and these charge carriers accumulate there leading to the increase in conductivity. This is in direct contrast of the operation of superficially similar devices also based on conducting polymer films and enzymes which operate by sensing a local change in pH caused by the enzyme catalysed reaction.[33-35] In these devices the response returns to the baseline value when the analyte is removed and in their operation they resemble potentiometric enzyme electrodes and suffer from the same problems as these devices in terms of sensitivity and effect of solution buffer concentration.[1]

Bartlett *et al.* have made use of this ability of the microelectrochemical enzyme transistor to integrate the analyte signal in the measurement of low glucose concentrations using a device of the type described above.[36] In this work the authors were able to show that by the choice of suitable deposition and fabrication conditions they can make microelectrochemical enzyme transistors responsive to glucose with good reproducibility and that they can be used with good repeatability to make measurement of glucose concentration down to 2 μM in air saturated buffer at pH 5. This was 40 times better than the performance of the corresponding amperometric device.

Despite the success in fabricating working devices responsive to glucose some problems and disadvantages remain. First it is important to realise that devices of this type will suffer from similar problems of interference, enzyme kinetics and selectivity as amperometric enzyme electrodes. Indeed if a device works as a microelectrochemical enzyme transistor then it will generally also function as an amperometric sensor simply by holding it at the appropriate potential and measuring the current. The advantages of the microelectrochemical enzyme transistor over the amperometric enzyme electrode lie in its sensitivity and simplicity of measurement. Second, for the devices described above freely diffusing mediator species have been necessary to couple the enzyme reaction to the reduction or oxidation of the polymer. Third, the use of poly(aniline) with bisulfate counterion is restricted to pH 5 and below and this is not compatible with all enzymes or enzyme assays. In the next section we address some of these challenges.

6 Further developments

Not all enzymes require the use of redox mediators to achieve oxidation or reduction at electrode surfaces. For glucose oxidase the flavin redox active site is buried deep within the core of the protein making direct oxidation at an electrode very difficult but this is not the case for all enzymes. For horseradish peroxidase (E.C. 1.11.1.7) the haem redox site is located at the periphery of the enzyme and is solvent accessible. In this case direct reduction of the haem at electrode surfaces is possible.[37-39] Horseradish peroxidase can also be directly reduced at poly(aniline) coated electrodes[40] and so it is possible to make microelectrochemical enzyme transistors responsive to hydrogen peroxide using horseradish peroxidase as the catalyst.[41] In this case the reactions are

$$H_2O_2 + HRP(red) \rightarrow HRP(compound\ I) + H_2O$$

$$HRP\ (compound\ I) + PANi(red) \rightarrow HRP(red) + PANi(ox)$$

In this case the poly(aniline) is converted from its reduced, conducting, emeraldine form to its oxidised, insulating, pernigraniline form so that the device operates in the "on" to "off" direction, see Figure 9a, rather that the other way around as was the case for the glucose responsive device. This has an important consequence. Because the device starts in the conducting state the time taken to switch the device in any given concentration of analyte is much more sensitive to the choice of setting potential for the poly(aniline) film (the initial value of V_{gate}). This is because the more cathodic the initial gate potential the greater the amount of charge that must be removed from the polymer before its conductivity will change significantly switching the device "off". In contrast, for the glucose responsive device the poly(aniline) starts in the insulating state where the capacitance of the polymer is orders of magnitude lower. As a result small differences in the initial gate voltage make no difference in the switching time for the device and for the same reason the switching times are significantly faster.[41] The clear conclusion from this comparison is that, if possible, it is better to configure devices so that they operate in the "off" to "on" direction than *vice versa*.

The work described above for both glucose and hydrogen peroxide responsive devices was all carried out using poly(aniline) at pH 5. It is obviously desirable to remove this constraint and to be able to work at neutral pH. For poly(aniline) the problem is that the

emeraldine form of the polymer deprotonates above about pH 5 (see Figure 6 above) and that the deprotonated form is not an electronic conductor. For a poly(aniline) film the deprotonation of the emeraldine form is associated by the egress from the film of both the protons and the associated counter anions, Figure 10a. This is only possible if the counter anions are small and mobile, for example chloride or bisulfate anions. If these mobile counter anions are replaced by long chain polymeric counter anions these become trapped within the poly(aniline) film and the overall process changes, Figure 10b. Now if the protons leave the film they must be replaced by cations from the solution in order to maintain electroneutrality. As a consequence of this change the conductivity of the poly(aniline) can be maintained to much higher pH[42] (in effect there is a Donnan type potential established across the poly(aniline) solution interface which alters the electrochemical potential of the protons within the film). We have made use of this effect to deposit films of poly(aniline) with polymer counterions such as poly(vinylsulfonate) or poly(styrenesulfonate) which remain electrochemically active and conducting at neutral pH. These composite films can be used to make microelectrochemical enzyme transistors responsive to glucose[43] and to make devices responsive to NADH operating at pH 7.[44] In the latter case no enzyme is required because poly(aniline) is an excellent catalytic surface for the oxidation of NADH to NAD^+.[45]

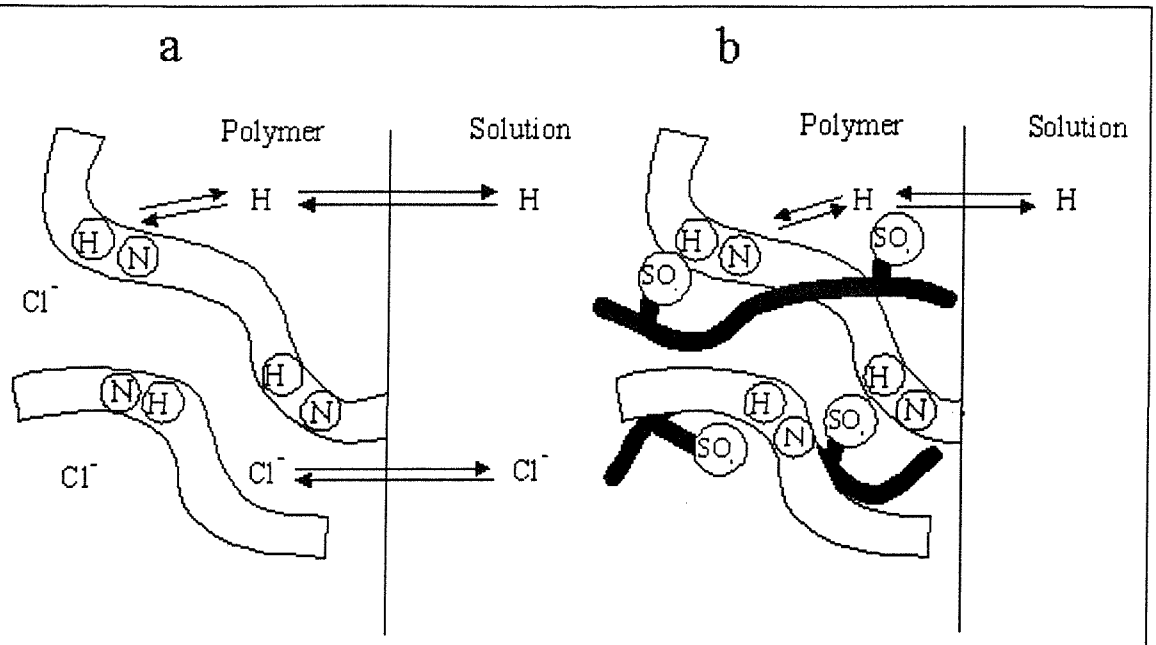

Figure 10: Protonation equilibria for poly(aniline) films. For poly(aniline) grown with a mobile anion (a), such as chloride, the emeraldine state of the polymer can deprotonate on contact with neutral solutions by simultaneous expulsion of protons and chloride ions to leave the insulating emeraldine base. In contrast, for poly(aniline) films grown with long chain polymeric anions (b), such as poly(styrenesulfonate), the polymer can only deprotonate if it exchanges protons for cations from the solution. As a result the emeraldine form of the polymer remains protonated even when placed in contact with neural solution.

Thus for glucose Bartlett *et al.* have shown that we can make microelectrochemical enzyme transistors which respond rapidly and reproducibly,[25,30,31] that such devices show sensitivity to low glucose concentrations,[36] and that we can make them operate at pH 7.[43] However in all cases it has been necessary to use a freely diffusing redox mediator to couple the oxidation of the reduced flavin to the reduction of the poly(aniline). There are two potential strategies to overcome this problem. The first, following the work of Heller on redox hydrogels,[7] is to use a redox polymer deposited on top of the poly(aniline) to establish electrochemical communication between the enzyme and the conducting polymer. Another alternative is to covalently attach the redox mediator to the enzyme.[5,6,46] Both approaches have been demonstrated in amperometric measurements and should work with microelectrochemical enzyme transistors if the redox potentials and rate constants for mediation are suitable.

7 Conclusions

Microelectrochemical enzyme transistors are good examples of integrated chemical systems as described by Wrighton[47] and Bard.[48] They are constructed by combining together, in a spatially organised manner, a number of distinct chemical components. These components (conducting polymer, insulating polymer, redox enzyme, redox mediator etc.) are each individually selected to perform a particular role in the final device and each possess different specific properties. By combining these discrete components in the proper way one is able to make functioning molecular devices. An important aspect of this approach is in the methods used to construct the final devices. These methods need to allow spatial control over the localisation of the different components. In constructing their microelectrochemical enzyme transistors Bartlett and coworkers have used electrochemical polymerisation and adsorption to localise and immobilise the different components onto structures made using screen printing or photolithographic methods.

The prospects from the exploitation of microelectrochemical enzyme transistors and related devices are good. Their construction and operation is compatible with the current developments of disposable microsensor structures, sensor arrays[49-51] and conducting polymer based electronic circuits.[52] Microelectrochemical enzyme transistors offer significant advantages for the detection of analytes at low concentrations as a result of the inherent integration of the analyte signal and amplification that they provide. These features could be of significant benefit in developing small, disposable devices for immunoassay and DNA assay applications. However, the development of such disposable devices will rise a number of problems in terms of interference from contaminants in solution, protein adhesion to the polymer film, and pH conflicts due to enzyme pH activity range. As a result, a complete re-design of the sensor would be necessary for every new enzyme to be tested.

8 Our project

The aim of the research reported in this thesis is to adapt the microelectrochemical transistor technology summarised in this general introduction to *in-vitro* immunological

detection. *In-vitro* immunological detection or immunoassay is a routine diagnostic tool in medicine. However, to date only a pregnancy and an albumin urine immunological test have been successfully put on the market for home use. This is due to the fact that even though the use of monospecific antibodies in immunoassays guaranty the specificity of the test, revealing the yield of the reaction proves to be extremely delicate in terms of experimental procedures. The commercial application of home use pregnancy test is made possible because the concentration of human chorionic gonadotropin to be detected is large enough to trigger a precipitation of the antibody-antigen complex, resulting in a change of colour of the supporting material. Even then, a laboratory based immunoassay is carried out to confirm the pregnancy. In this case, the full detection experiment involves up to six experimental steps over an average of 24h. The result of the immunoreaction is not directly observed, at the moment the most common revealing method in medical biochemistry is the use of enzymes attached to antibodies. These enzymes are used to reveal their presence in the media by adding substrates that are transformed into colorimetric enzyme products. Monitoring the concentration of substrate by spectrophotometry, involves measuring the activity of the enzyme and hence the concentration of the enzyme. This method requires bound antibodies to be isolated from unbound antibodies resulting in numerous experimental steps. By using electrochemistry instead of spectrophotometry, we are able to resort to using microelectrochemical transistors.

In this work we will prove that microelectrochemical transistors are a reliable revealing method for immunoassays, besides we will show that this method is more sensitive than laboratory based spectrophotometric protocols. The major interest of our method is its portable format, which increases the possibility of seeing home based basic blood analysis.

9 Our approach

In order to simplify the development of multipurpose polymer transistor sensors, we chose to separate the polymer transistor from the enzyme reaction. This implies that there is no direct contact between the redox enzyme and the polymer. This approach provides the possibility of using a different pH for the polymer electrochemistry and the biochemical

reaction simultaneously. In this way, the same polymer transistor can be used to create sensors involving enzymes operating at different pH, for each different enzyme the pH conditions can be adjusted without affecting the electrochemical properties of the polymer. This aim is achieved by dividing the sensor into two separate electrochemical cells as shown in Figure 11. The polymer potential is relayed to the collecting electrode in cell B, enabling an electron transfer between the mediator in cell B and the polymer film in cell A. Cells A and B are in contact via a salt bridge.

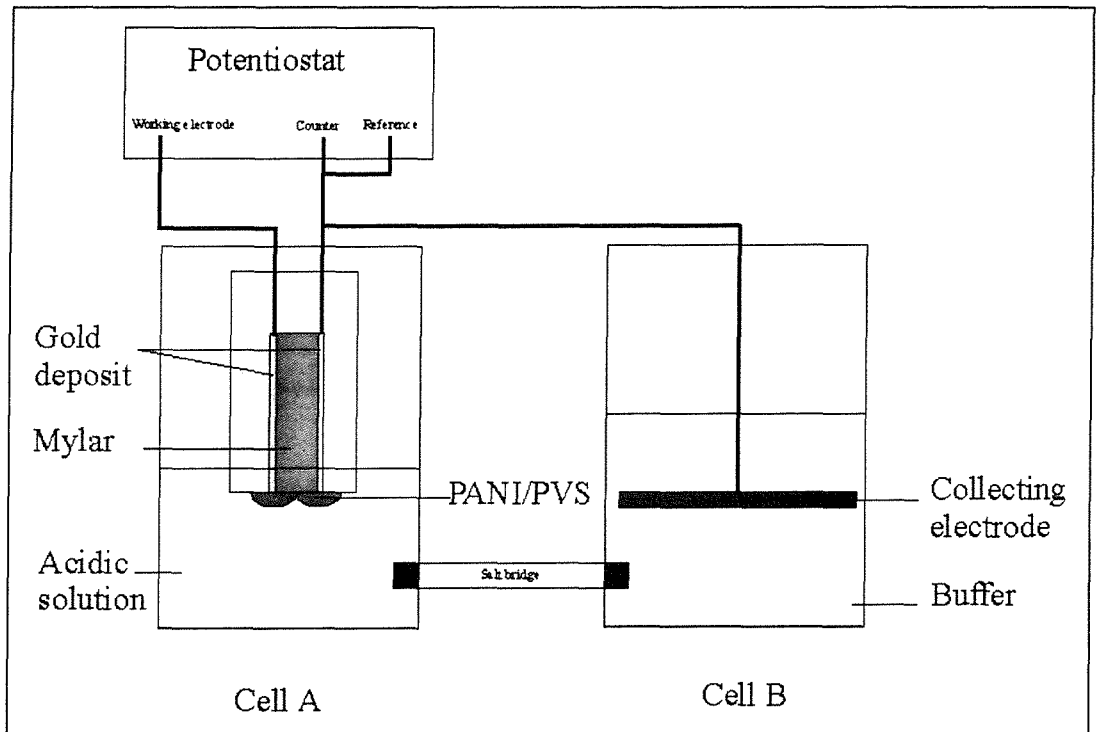

Figure 11: Cell A contains acid. Cell B contains the buffer that best suits the bioelectrochemical reaction. The polymer is connected to the collecting electrode and the charge transfer is enabled between the two cells by a salt bridge. The potentiostat is used to apply a potential difference between the two electrodes of the polymer transistor and record the resulting drain current.

10 General overview of thesis

This section contains a brief summary of the work that will be presented in the subsequent chapters. This work is directed towards the development of disposable sensors to detect immunoassay reactions. A wide variety of mono-specific antibodies can be obtained commercially with alkaline phosphatase attached as a label, consequently we describe a

sensor offering a rapid detection (less than 60 s) of very low alkaline phosphatase concentrations (0 to 4 nM). In chapter 2 the experimental procedures used to obtain the data presented in the subsequent chapters are outlined. Chapter 3 provides evidence that the sensor described in Figure 11 retains the polymer transistor electrochemical properties in acid while alkaline conditions are used in cell B. This chapter shows that electron transfer reaction from *p*-aminophenol at pH 9 in cell B to poly(aniline)-poly(vinylsulfonate) in 2 M sulfuric acid (cell A) is obtained, resulting in a change of polymer potential and hence a change of polymer conductivity. In chapter 4 we describe the fabrication of 70 similar polymer transistors designed for one off detection experiments. Chapter 5 is a detailed account of *p*-aminophenol electrochemical properties above pH 7. It will also show spectroscopic evidence of *p*-aminophenol forming aggregates in solution above pH 7. Chapter 6 is an electrochemical study of *p*-aminophenyl phosphate including evidence about its ability to poison platinum working electrodes. Chapter 7 presents a kinetic study of quinone imine reduction by glucose oxidase and *p*-aminophenyl phosphate catalysed hydrolysis by alkaline phosphatase using rotating disc potential step electrochemical methods. Finally chapter 8 describes the ability of our polymer transistor to detect *p*-aminophenol concentrations ranging from 100 to 400 nM as well as alkaline phosphatase concentrations ranging from 0 to 4 nM. In this chapter every polymer transistor is only used once.

11 References

1. M. J. Eddowes, D. G. Pedley, and B. Webb, *Sens. Actuators*, 1985, **7**, 233.
2. L. C. Clark, *Biosensors and Bioelectronics*, 1993, **8**, iv.
3. A. E. G. Cass, G. Davis, G. D. Francis, H. A. O. Hill, W. J. Aston, I. J. Higgins, E. V. Plotkin, L. D. L. Scott, and A. P. F. Turner, *Anal. Chem.*, 1984, **56**, 667.
4. H. J. Hecht, H. M. Kalisz, J. Hendle, R. D. Schmid, and D. Schomburg, *J. Mol. Biol.*, 1993, **229**.
5. P. N. Bartlett, R. G. Whitaker, M. J. Green, and J. Frew, *J. Chem. Soc., Chem. Commun.*, 1987, 1603.
6. Y. Degani and A. Heller, *J. Phys. Chem.*, 1987, **91**, 1285.
7. A. Heller, *J. Phys. Chem.*, 1992, **96**, 3579.
8. C. Sun, P.-H. Ho-Si, and D. J. Harrison, *Langmuir*, 1991, **7**, 727.

9. A. Szucs, G. D. Hitchens, and J. O. M. Bockris, *J. Electrochem. Soc.*, 1989, **136**, 3748.

10. H. S. White, G. P. Kittlesen, and M. S. Wrighton, *J. Am. Chem. Soc.*, 1984, **106**, 5375.

11. J. Heinze, in "Topics in Current Chemistry", vol. 152, Springer Verlag, Berlin, 1990, 3.

12. E. J. Calvo, R. Etchenique, P. N. Bartlett, K. Singhal, and C. Santamaria, *J. Chem. Soc., Faraday Discuss.*, 1997, **107**, 141.

13. A. R. Hillman, D. C. Loveday, M. J. Swann, S. Bruckenstein, and C. P. Wilde, *J. Chem. Soc., Faraday Trans.*, 1991, **87**, 2047.

14. G. P. Kittlesen, H. S. White, and M. S. Wrighton, *J. Am. Chem. Soc.*, 1984, **106**, 7389.

15. E. P. Lofton, J. W. Thackeray, and M. S. Wrighton, *J. Phys. Chem.*, 1986, **90**, 6080.

16. E. W. Paul, A. J. Ricco, and M. S. Wrighton, *J. Phys. Chem.*, 1985, **89**, 1441.

17. T. E. Turner Jones, O. M. Chyan, and M. S. Wrighton, *J. Am. Chem. Soc.*, 1987, **109**, 5526.

18. J. W. Thackeray, H. S. White, and M. S. Wrighton, *J. Phys. Chem.*, 1985, **89**, 5133.

19. J. W. Thackeray and M. S. Wrighton, *J. Phys. Chem.*, 1986, **90**, 6674.

20. M. S. Wrighton, J. W. Thackeray, M. J. Natan, D. K. Smith, G. A. Lane, and D. Belanger, *Phil. Trans. R. Soc. Lond. B*, 1987, **316**, 13.

21. M. Umãna and J. Waller, *Anal. Chem.*,, 1986, **58**, 2979.

22. N. C. Foulds and C. R. Lowe, *J. Chem. Soc., Faraday Trans., I*, 1986, **82**, 1259.

23. P. N. Bartlett and J. Cooper, *J. Electroanal. Chem.*, 1993, **362**, 1.

24. T. Matsue, M. Nishizawa, T. Sawaguchi, and I. Uchida, *J. Chem. Soc., Chem. Commun.*, 1991, 1029.

25. P. N. Bartlett and P. R. Birkin, *Synthetic Metals*, 1993, **61**, 15.

26. D. Belanger, J. Nadreau, and G. J. Fortier, *J. Electroanal. Chem.*, 1989, **274**, 143.

27. P. N. Bartlett, Z. Ali, and V. Eastwick-Field, *J. C. S., Faraday Trans.*, 1992, **88**, 2677.

28. G. Inzelt and G. Horanyi, *Electrochim. Acta*, 1990, **35**, 27.

29. W. S. Huang, B. D. Humphrey, and A. G. MacDiarmid, *J. Chem. Soc., Faraday Trans. I*, 1986, **82**, 2385.

30. P. N. Bartlett and P. R. Birkin, *Anal. Chem.*, 1993, **65**, 1118.

31. P. N. Bartlett and P. R. Birkin, *Anal. Chem.*, 1994, **66**, 1552.

32. C. Malitesta, F. Palmisano, L. Torsi, and P. G. Zambonin, *Anal. Chem.*, 1990, **62**, 2735.

33. M. Nishizawa, T. Matsue, and I. Uchida, *Anal. Chem.*, 1992, **64**, 2641.

34. M. Nishizawa, T. Matsue, and I. Uchida, *Sensors and Actuators B*, 1993, **13-14**, 53.

35. D. T. Hoa, T. N. Suresh Kumar, N. S. Punekar, R. S. Srinivasa, and R. Lal, *Anal. Chem.*, 1992, **64**, 2645.

36. P. N. Bartlett, J. H. Wang, and W. James, *Analyst*, 1998, **123**, 387.

37. L. Gorton, G. Jonsson-Peterson, E. Csoregi, K. Johansson, E. Dominguez, and G. Marko-Varga, *Analyst*, 1992, **117**, 1235.

38. U. Wollenberger, J. Wang, M. Ozsos, E. Gonzalez-Romero, and F. Scheller, *Bioelectrochem. Bioenerg.*, 1991, **26**, 287.

39. G. Jonsson and L. Gorton, *Electroanalysis*, 1989, **1**, 465.

40. P. N. Bartlett, P. R. Birkin, F. Palmisano, and G. De Benedetto, *J. Chem. Soc., Faraday Trans.*, 1996, **92**, 3123.

41. P. N. Bartlett, P. R. Birkin, J. H. Wang, F. Palmisano, and G. De Benedetto, *Anal. Chem.*, 1998, **70**, 3685.

42. G. E. Asturias, G. W. Jang, A. G. MacDiarmid, Z. Doblhofer, and C. Zhong, *Bunsen-Ges. Phys. Chem.*, 1991, **95**, 1381.

43. P. N. Bartlett and J. H. Wang, *J. Chem. Soc., Faraday Trans.*, 1996, **92**, 4137.

44. P. N. Bartlett, J. H. Wang, and E. N. K. Wallace, *J. Chem. Soc., Chem. Commun.*, 1996, 359.

45. P. N. Bartlett, P. R. Birkin, and E. N. K. Wallace, *J. Chem. Soc., Faraday Trans.*, 1997, **91**, 1951.

46. P. N. Bartlett, S. Booth, D. J. Caruana, J. D. Kilburn, and C. Santamaria, *Anal. Chem.*, 1997, **69**, 734.

47. M. S. Wrighton, *Comments Inorg. Chem.*, 1985, **4**, 269.

48. A. J. Bard, 'Integrated Chemical systems. A Chemical Approach to Nanotechnology', Wiley, New York, 1994.

49. M. B. Madaras, I. C. Popescu, S. Ufer, and R. P. Buck, *Anal. Chim. Acta*, 1996, **319**, 335.

50. M. B. Madaras and R. P. Buck, *Anal. Chem.*, 1996, **68**, 3832.

51. G. Nagy, X. X. Clarke, and R. P. Buck, *Anal. Chem.*, 1998, **70**, 2156.

52. C. J. Drury, C. M. J. Mutsaers, C. M. Hart, M. Matters, and D. M. de Leeuw, *App. Phys. Lett.*, 1998, **73**, 108.

53. M. Dixon and E. C. Webb, 'Enzymes', Longman, London, 1979.

Chapter 2: Experimental

1 Chemicals.

All aqueous solutions were freshly prepared using water purified by a Whatman RO 50 and a Whatman 'still plus' system. Aniline (99.5 %, Aldrich) was distilled under vacuum prior to use and stored under argon, poly(vinylsulfonic acid) supplied as a sodium salt solution in water (25 % estimated molecular weight 980-1100 g; m_n 800-995 g, no polydispersity data, Aldrich), sulfuric acid (Aldrich 97-99%), HCl (BDH, AnalaR) were used as received. Phosphate buffers were prepared from stock solutions of (A) citric acid (0.1 M, Aldrich, Ultrapure grade) and (B) di-sodium hydrogen orthophosphate 12 hydrate (0.2 M BDH, AnalaR). For pH 5 48.5 ml A and 51.5 ml B were made up to 100 ml and adjusted to pH 5 using a pH meter (Corning 145). Glucose oxidase (E.C. 1.2.4.4., type VII from Aspergillus niger, MW 186000, 100 units mg^{-1} (pH 5), 271.2 mg ml^{-1}) stock solution was a gift from MediSense U.K. glucose (BDH AnalaR), glucose solutions were always prepared 24 h before use and stored at 4 °C. pH 8 and 9 Tris-HCl buffers were made with TRISMA Base (SIGMA 99.9%). *p*-aminophenol came from Aldrich 98% pure and was recrystalised and stored under argon before use. *p*-aminophenol phosphate was kindly supplied by MediSense. Alkaline phosphatase EC 3.1.3.1 from bovine intestinal mucosa 2047 U / mg, Mr = 140000 was purchased from Fluka. KCl (BDH, Analar) was used as background electrolyte. Epoxy resin was Araldite CY1300 GB with hardener HY 1300 GB both supplied by Ciba Giegy Plastics used in ratio of 100 parts of resin to 39 +/- 1 parts of hardener by volume.

2 Equipments.

Electrochemical experiments were carried out using either a Ministat potentiostat (Thompson Electrochem) or an Oxford Electrodes portable potentiostat (Oxford Electronics, model PP2) used in conjunction with an home made voltage follower, and recorded with an XY/t chart recorder (Gould, series 60000), a Pharmacia LKB REC 102 Y/t recorder, and Keithley 175A digital voltmeter. Rotating disc studies were performed using an EG&G potentiostat with an Oxford Electrodes rotator and glassy carbon or

platinum rotating disc electrodes (area 0.38 cm^2). The electrodes were hand polished directly prior to use with a slurry of 1.0 and then 0.3 μm alumina (Buehler) to produce a mirror finish on the electrode surface. A large area platinum gauze was used as the counter electrode. All potentials are reported with respect to saturated calomel (SCE) reference electrode, this was used with a double frit separation to prevent KCl contamination in the case of gold cyclic voltammetry experiments on photolithographically fabricated electrodes. Poly(aniline) composite films deposited from poly(vinylsulfonate) solution were grown at 25 °C by water jacketing the stock solution. All other experiments were carried out in a thermostated cell at 25 +/- 0.1 °C. UV/Vis studies were performed using a Hewlett-Packard (8452A) UV/Vis spectrophotometer, a quartz cell was used in all experimentation. SEM images were obtained using a Joel 300 scanning electron microscope. NMR studies were carried out with a Brucker DPX 400 and Brucker AC300. Infra-red spectrometry was carried out on a Biorad Golden Gate FTS 135. Mass spectrometry studies were done with a VG platform quadrupole electrospray ionisation mass spectrometer. All pH measurements were carried out using a 145 pH ion selective electrode probe, supplied by Corning Science Products. The photolithographically fabricated electrodes MB4000 were purchased from Smart Microsystems.

3 Electrochemical cells and set-up

Pyrex water jacketed cells were used for all experiments described in this thesis with the exception of the deposition of poly(aniline) / poly(vinylsulfonate) films on photolithographically fabricated electrodes, which was carried out in a 10 μl drop from the water jacketed stock solution (Figure 1), and the detection experiments carried out from a 100 μl drop from the water jacketed stock solution directly on the 1 cm^2 basal plane HOPG (Goodfellows) collecting electrode (Figure 2).

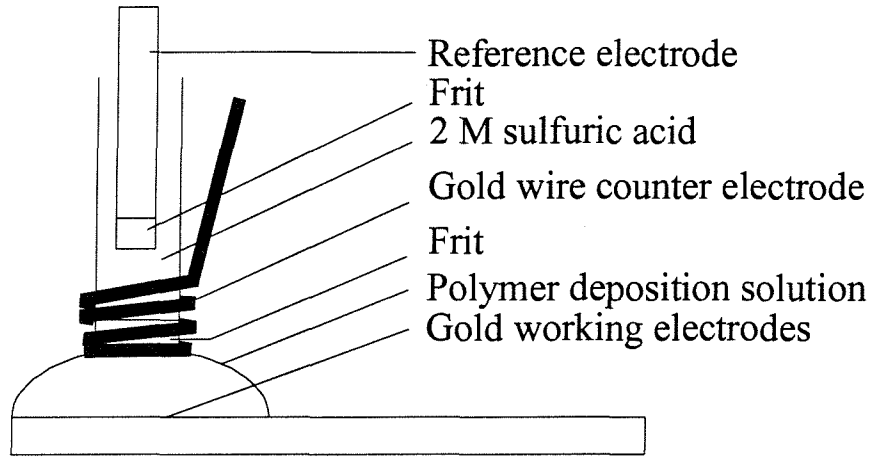

Figure 1: Polymer electrodeposition setup on photolythographically fabricated electrodes.

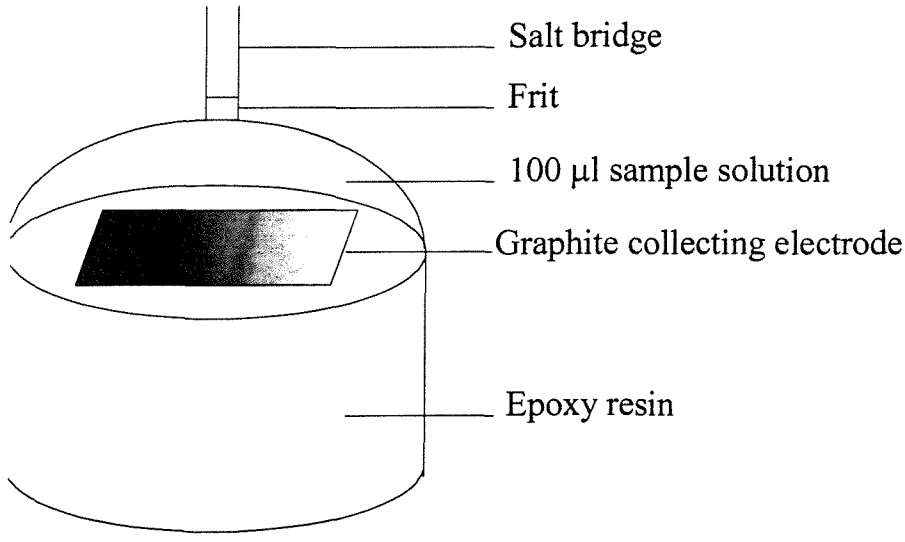

Figure 2: Bioelectrochemical detection experiment, sample set up.

3.1 Electrodes

The double gold foil electrode

The double gold foil electrodes are designed to provide two identical conducting areas separated by a very small insulating gap. Here the gold electrodes are 300 nm wide and 3 mm long, the gap can either be 6 or 10 µm wide between them. This precision is achieved by coating both sides of an insulating mylar sheet (Goodfellows) with a thin gold film

using vacuum metal vaporisation. The thickness of the mylar determines the size of the insulating gap between the electrodes.

The Mylar sheet is placed in the clutch, the vacuum is applied and an electric discharge creates gold vapor. The gold deposits uniformly in the clutch, the thickness of the gold deposition can be controlled down to 300 nm, beyond this the homogeneity of the coated layer is uncertain. This protocol is repeated on both sides of the Mylar.

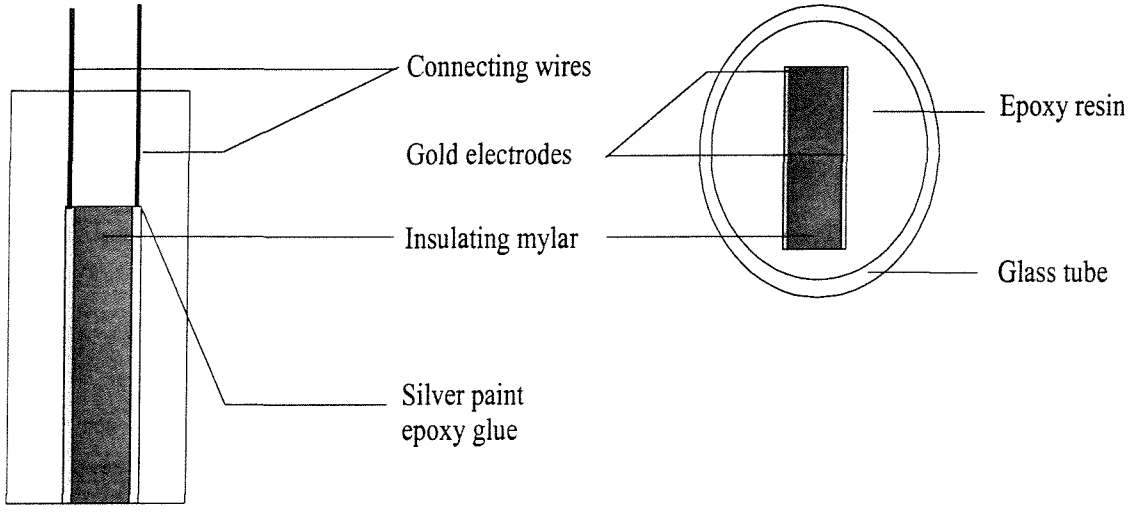

Figure 3: Displays a side view of the mylar and the gold layers inside the glass tube. It explains how the thickness of both mylar and gold enable to control the parameters of our electrode. The connecting wires are attached to their gold layer with silver paint and epoxy glue. The cut view of the electrode shows which part is used for electrochemistry. The length of the electrodes depends on the cut of the Mylar sheet after the gold deposition and usually is about 4 mm long.

The gold coated Mylar sheet is cut to the desired dimension and electric wires are connected with both gold layers. To do so, silver paint (Aldrich) is used to maximise the conductivity between the wire and the gold. Once the paint is dry some epoxy glue is laid over the connections to secure them.

Finally the setup is introduced into a glass tube which is filled with epoxy resin. After 24 h in the 40 °C oven, the electrodes are dry and need to be polished until the cut of the coated Mylar appears at the surface of the resin.

A lot of devices happen to be shorted during the fabrication, it is essential to check every device after polishing. This is done by measuring the resistance between the two gold electrodes with a digital voltmeter.

4 Computer softwares

In this thesis all data was analysed by using the SigmaPlot 2000 software, the data simulation was done using DigiSim. The statistic analysis according to the student test was done using the statistical analysis option in SigmaPlot.

5 Experimental procedures

5.1 polymer deposition

The double gold foil electrode was polished with 1 μm and 0.3 μm alumina. It was rinsed with deionised water and checked for short circuit. The polymerisation is undertaken in a 0.4 M Aniline solution in 2 M H_2SO_4 and 22 % by weight of poly(vinylsulfonate). The counter electrode is a platinum mesh, and 0.9 V are applied against an SCE reference, the working electrode is the two gold foils wired together. The potential is maintained until the polymerisation charge reaches 0.7 mC. We notice that below this polymerisation charge value, contact was not always made by the polymer between the two gold electrodes.

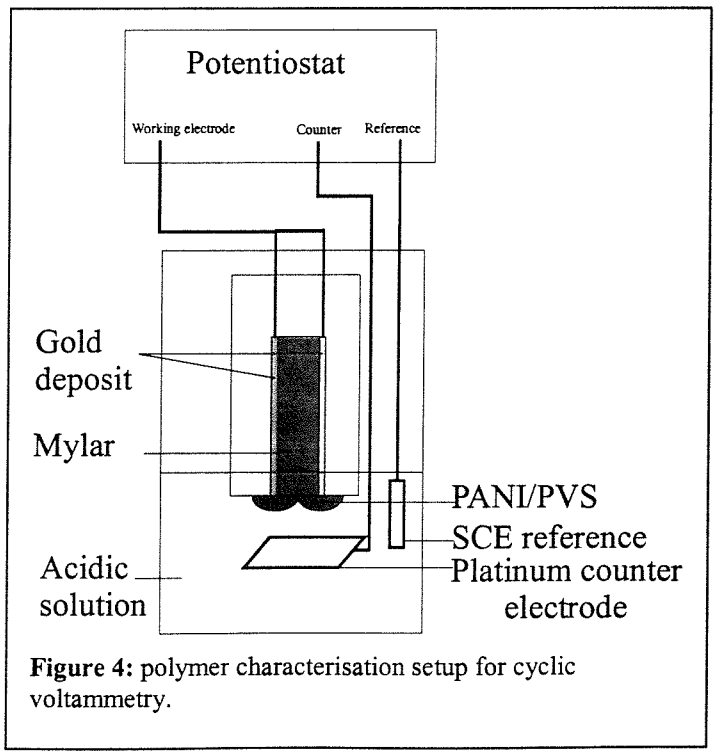

Figure 4: polymer characterisation setup for cyclic voltammetry.

5.2 polymer characterisation

The two gold electrodes bearing the polymer film (Figure 4) are connected together as the working electrode. Cyclic voltammetry is carried out in 2M sulfuric acid. The potential starts at 0 V and rises to 0.5 V and decreases to –0.2 V at 50 mV / s. In this way the electrochemistry of each polymer film can be compared.

5.3 Resistance measurements

For the resistance measurements of the polymer films laid across two gold electrodes, the use of two potentiostats was required. One potentiostat is used to apply a constant potential difference between the two gold electrodes, the other potentiostat is used to cycle the potential of the polymer film against SCE.

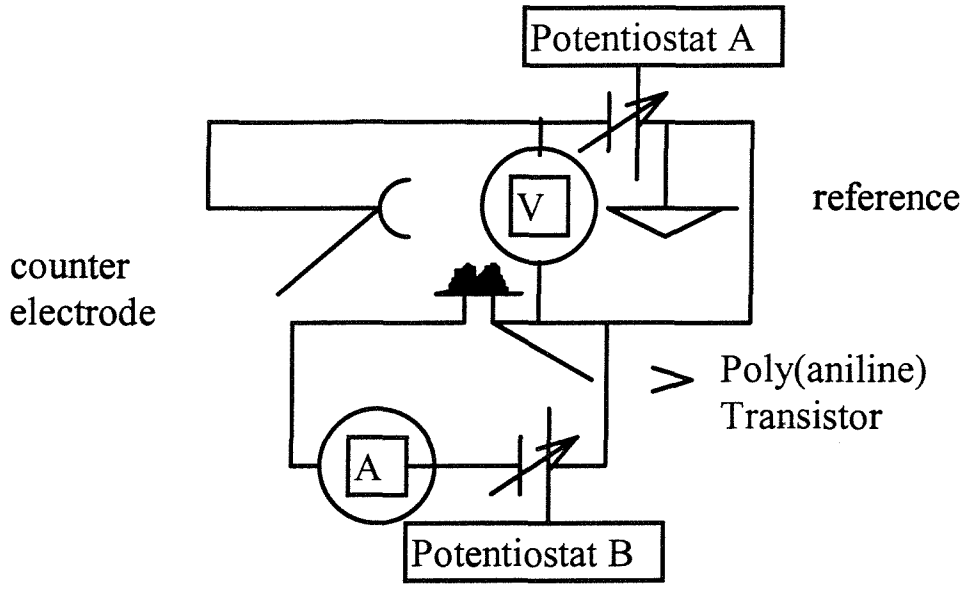

Figure 5 Circuit setup to measure the drain current while controlling the potential. One gold foil is connected to the working electrode outputs of potentiostat A and B. Potentiostat A is otherwise connected to a Pt mesh counter electrode and an in house build S.C.E. reference electrode. The second gold foil is connected to the counter and reference outputs of potentiostat B.

The setup is shown in Figure 5. One gold foil is connected to the working electrode outputs of potentiostat A and B. Potentiostat A is otherwise connected to a Pt mesh counter electrode and an in house built SCE reference electrode, it will control the potential vs SCE all the way through the experiment. The X-scale of the chart recorder is

linked to the potential output of potentiostat A. The second gold foil is connected to the counter and reference outputs of potentiostat B, which will maintain a 30 mV potential difference between the gold foils regardless of the potential of the film. The Y-scale of the chart recorder is connected to the current output of potentiostat B, in order to record the current induced by the potential difference between the two foils during the potential variation of the film. In this way a current / voltage curve is obtained from which the resistance of the polymer can be calculated as a function of potential.
The starting potential applied through potentiostat A is 0.5 V, it goes down to 0 V and back up to 0.5 at 5 mV / sec.

Meanwhile potentiostat B maintains a 30 mV potential difference between the two gold foils. The plot represents the potential of the film on the X scale and the corresponding drain current on the Y scale.

5.4 Drain current measurement

To measure the drain current through the polymer when a potential difference is applied between the two electrode supporting the polymer film, the following experimental conditions were used (Figure 5). One gold foil is connected to the working electrode outputs of potentiostat A and B. Potentiostat A is otherwise connected to a Pt mesh counter electrode and an in house built SCE reference electrode, it will maintain the potential at 0.31 Volts vs SCE all the way through the experiment. The X-scale of the chart recorder is linked to the potential output of potentiostat B. The second gold foil is connected to the counter and reference outputs of potentiostat B, which will apply 0 to 250 mV potential difference between the gold foils regardless of the potential of the film. The Y-scale of the chart recorder is connected to the current output of potentiostat B, in order to record the current induced by the gate potential between the two foils.
The potential applied by potentiostat A is measured through a Digital Voltmeter and is set at 0.31 Volts. The potential applied by potential B is varied at 50 mV / s from 0 to 250 mV. The chart recorder plots the potential difference on the X scale and the corresponding drain current on the Y scale.

5.5 Change of polymer potential by p-aminophenol oxidation at different pH.

The double gold foil electrode was polished with 1 μm and 0.3 μm alumina. It was rinsed with deionized water and checked for short circuit. The polymerisation is carried out in a 5 ml 2M sulfuric acid solution with 124 μl distilled aniline and 714 μl poly(vinylsulfonate). 0.9 volts are applied until the charge reached 0.7 mC.

The polymer was maintained in sulfuric acid and was used as working electrode, the counter electrode was a platinum mesh and the reference was an in house built SCE electrode. The potential was set at 0.5 Volts and applied to the polymer by the potentiostat. An in house built voltage follower was connected to the polymer and the reference. Once the potential has been applied during 5 minutes, the potentiostat was disconnected. The potential of the polymer can be checked using the voltage follower to ensure it did not change. At this stage, a second cell was used where the pH was buffered at 1, 7, and 9. A 1 cm^2 graphite electrode was placed in the buffer. A salt bridge filled with saturated KCl solution connecting both cells. As the potential was recorded, the graphite electrode was connected to the polymer. When the potential stabilizes, 1 μl of 800 μM *p*-aminophenol solution was added to the second cell yielding a total concentration of 8 μM *p*-aminophenol. The chemical reaction of *p*-aminophenol at the collecting electrode causes a change in potential of the polymer which was recorded.

5.6 Preparation of SEM samples

Poly(aniline)-poly(vinylsulfonate) films were deposited onto photolithographically fabricated electrodes and characterised in 2 M sulfuric acid using the methods outlined in 5.2. After polymer characterisation and the use of these electrodes in the bioelectrochemical experiment, these electrodes were carefully fractured to produce mountable sample sizes. The resulting samples were then set onto stubs using conducting carbon cement (Ciba-Geigy) and gold spluttered prior to transfer to the SEM.

5.7 Determination of diffusion coefficients

5.7.1 *p*-aminophenol

A bare glassy carbon rotating disc electrode (Oxford electrodes) (area 0.38 cm^2) was immersed into 130 cm^3 of deoxygenated 0.1 mol dm^3 pH 7.4 PBS Tween buffer (Sigma) 0.5 M KCl, thermostated at 25 °C. A cyclic voltammogram was recorded between the limits of -0.1 V and 0.3 V vs SCE at 5 mV/s, then freshly recrystalised *p*-aminophenol was added to the solution to obtain 1 mM *p*-aminophenol concentration. The counter electrode was separated from the rest of the solution by a glass frit. The potential sweep was repeated with the previous limits for the following rotation rates 2, 4, 9, 16, 25, 36, 49 Hz, the electrode was removed between scans and polished with 0.3 μm alumina (Buehler) to remove inaccuracies in plateau currents caused by electrode fouling due to *p*-aminophenol oxidation.

The procedure was repeated for 0.5 and 0.2 mM *p*-aminophenol concentrations. And repeated again for all three *p*-aminophenol concentrations using a platinum (area 0.38 cm^2) rotating disc working electrode.

5.7.2 *p*-aminophenyl phosphate

A bare glassy carbon rotating disc electrode (area 0.38 cm^2) was immersed into 130 cm^3 of deoxygenated 0.1 mol dm^3 pH 9.5 Tris-HCl buffer 0.5 M KCl, thermostated at 25 °C. A cyclic voltammogram was recorded between the limits of 0 V and 0.5 V vs SCE at 5 mV/s, then *p*-aminophenyl phosphate was added to the solution to obtain 1 mM *p*-aminophenyl phosphate concentration. The counter electrode was separated from the rest of the solution by a glass frit. The potential sweep was repeated with the previous limits for the following rotation rates 2, 4, 9, 16, 25, 36, 49 Hz, the electrode was removed between scans and polished with 0.3 μm alumina to remove inaccuracies in plateau currents caused by electrode fouling due to *p*-aminophenyl phosphate oxidation.

The procedure was repeated for 0.5 and 0.2 mM *p*-aminophenyl phosphate concentrations. The experiment was reproduced with a platinum (area 0.38 cm^2) rotating disc working electrode. This experiment showed an enhanced contamination of the platinum working electrode by *p*-aminophenyl phosphate oxidation products.

5.8 Electrolysis experiments

All electrolysis experiments were carried out in 130 ml degassed solutions, in water jacketed pyrex electrochemical cells (25 °C). The counter electrode (platinum mesh) was separated from the main solution by a glass frit. The working electrode was a 5 cm × 10 cm platinum mesh, the oxidation charge was recorded by an EG&G potentiostat. Regularly during the experiment, cyclic voltammetry experiments were carried out using a platinum 7 mm diameter freshly polished working electrode.

5.9 pKa titration and UV/VIS study of p-aminophenol

A 25 ml solution of *p*-aminophenol.HCl 4 mM was degassed with argon, its pH was monitored by a pH meter while aliquots of NaOH 4.34 mM solution were added. After each addition a 200 µl sample was placed into a quartz crystal UV cell and diluted to 1 ml with distilled water. The UV spectrum was recored directly before carrying on with the base titration.

5.10 Enzyme kinetic measurements

5.10.1 Glucose oxidase

Glucose oxidase kinetic studies were carried out in a 30 ml water jacketed pyrex electrochemical cell. All solutions were water jacketed at 25 °C and degassed before and during each experiment. The measurements were carried out with a glassy carbon rotating disc electrode (area 0.38 cm^2).

5.10.2 Alkaline phosphatase

Alkaline phosphatase kinetic studies were carried out in a 30 ml water jacketed pyrex electrochemical cell. All solutions were water jacketed at 25 °C and degassed before and during each experiment. The measurements were carried out with a glassy carbon rotating disc electrode (area 0.38 cm^2). *p*-aminophenyl phosphate solutions were prepared in 10 ml distilled water immediately before the measurement, to do so 1 ml of this *p*-aminophenyl phosphate solution was added to the 29 ml pH 9.5 Tris-HCl buffer (0.1 M) in the pyrex cell. The reaction was started by adding 1 to 3 µl alkaline phosphatase stock solution.

Chapter 3: Poly(aniline)-poly(vinylsulfonate) transistor

1 Introduction

In this chapter, we will describe a new bio-electrochemical sensing device designed to simplify the analysis of *in-vitro* immunological reactions. The new sensor only requires a 30 mV power supply and a ammeter to be operated. This offers the possibility of creating a portable electronic unit, to reveal home use enzyme or immuno assays. Our sensor is made of a conductive polymer (poly(aniline)-poly(vinylsulfonate)) laid across two electrodes between which a constant potential is applied by a power supply. In this chapter we will show how this polymer is reduced by an organic compound (*p*-aminophenol) reacting on a graphite electrode. The polymer film operates in strong acidic conditions (2 M sulfuric acid) while the organic compound reacting on the graphite electrode may be dissolved in neutral or alkaline buffers. The sensing device is sketched in Figure 1.

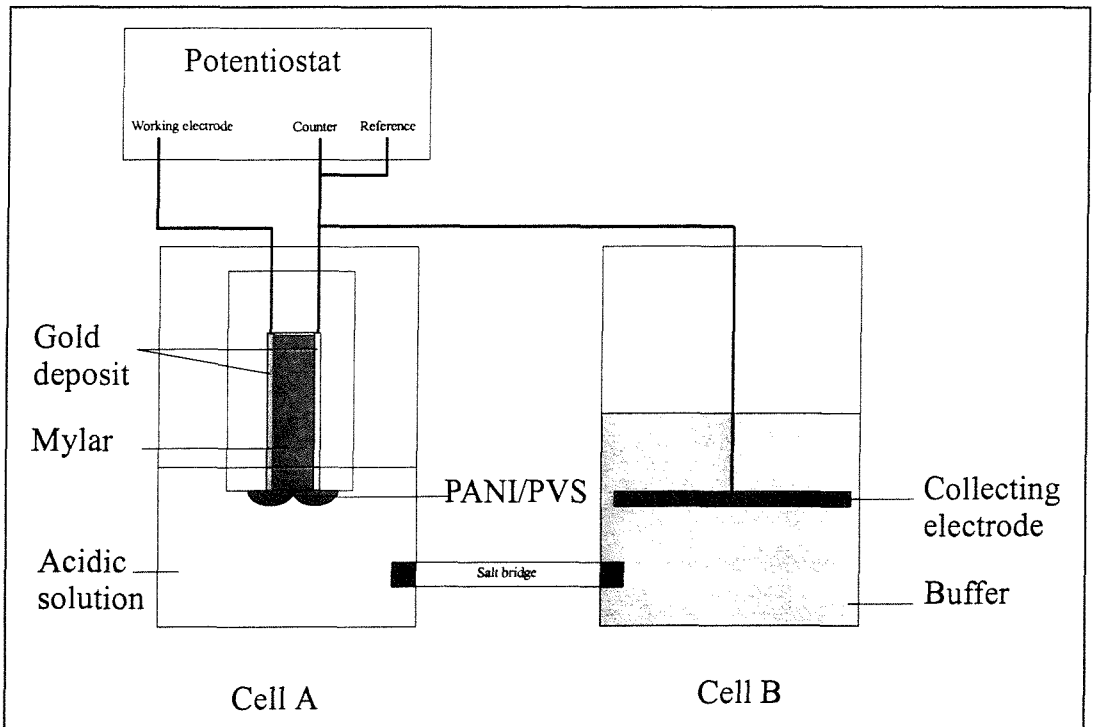

Figure 1: Cell A contains acid. Cell B contains the buffer that best suits the bioelectrochemical reaction. The polymer is connected to the collecting electrode and the charge transfer is enabled between the two cells by a salt bridge. The potentiostat is used to apply a potential difference between the two electrodes of the polymer transistor and record the resulting drain current.

Figure 1 shows how the polymer film laid across two gold electrodes kept apart by a mylar insulating sheet is electrically connected to a large collecting electrode bathing in a different solution. The different solutions are linked together by a salt bridge allowing charge transfer from one solution to the other. The polymer is electrically connected to the collecting electrode.

The sensor is based on the technology developed by Matsue *et al.* and Bartlett *et al.* in the area of "Enzyme transistors". The work from these authors derives from the use made by Wrighton *et al.* of conducting polymers laid between several electrodes. Wrighton[1] showed that conducting polymers could be used to electrically connect or disconnect two or more electrodes by changing the redox state of the given polymer. The change of redox state causes the polymer to change between a conductive state to an insulating state or *vice versa*. The transition from conducting to insulating and *vice versa* was monitored by applying a potential difference between the electrodes connected together by the polymer with a battery, and reading the resulting current with an ammeter. Several conductive polymers were shown to display changes in electrical resistance when their potential was varied: poly(aniline)[2], poly(pyrrole) and poly(N-methyl pyrrole)[3], and poly(3-methylthiophene)[4, 5]. The change of redox state was achieved by methods we describe next, resulting in a change of potential of the given polymer with respect to a reference electrode. One method was to vary the potential of the polymer using a potentiostat connected to a counter, a reference electrode and the polymer. This arrangement is shown in Figure 2, in this drawing the source and drain electrodes are the electrode between which a potential difference, V_{drain}, is applied, and the current, I_{drain}, is detected by the ammeter. A third electrode connected to the polymer (the gate electrode) is used to apply a potential, V_{gate}, via a potentiostat connected to a counter and a reference electrode. By varying the gate potential, one can change the redox state of the polymer film, and hence its resistivity to the drain current.

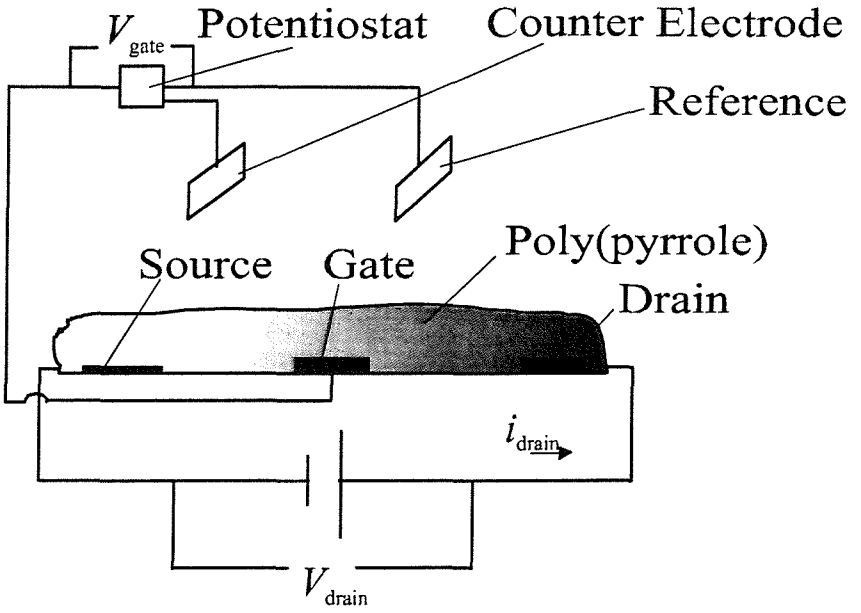

Figure 2: Poly(pyrrole transistor described by Wrighton *et al.* showing how the polymer film is connected to three electrodes. The drain current I_{drain} passing through the polymer from the drain to the source electrode, is induced by the drain potential V_{drain} applied between these two electrodes. If the gate potential V_{gate} is varied by the potentiostat, the redox state of the polymer changes. As a result the resistivity of the polymer is changed and I_{drain} is affected.

To obtain a change of redox state in the polymer film, another method is to reduce or oxidise the polymer chemically[4], as sketched in Figure 3. In this case, only two electrodes are connected to the polymer film and a drain voltage, V_{drain}, is applied between them. In this case the change of redox state in the polymer was obtained by Pt catalysed oxidation by oxygen or Pt catalysed reduction by hydrogen. The resulting effect of the change of redox state varies the resistivity of the polymer to the drain current, which varies accordingly. Thus the change of drain current may be used to monitor the presence of oxygen or hydrogen. However, as reported by the author the redox reactions of oxygen and hydrogen with the polymer film catalysed by platinum are unspecific, and are of little use in the fabrication of oxygen and hydrogen sensors *sensu-stricto*.

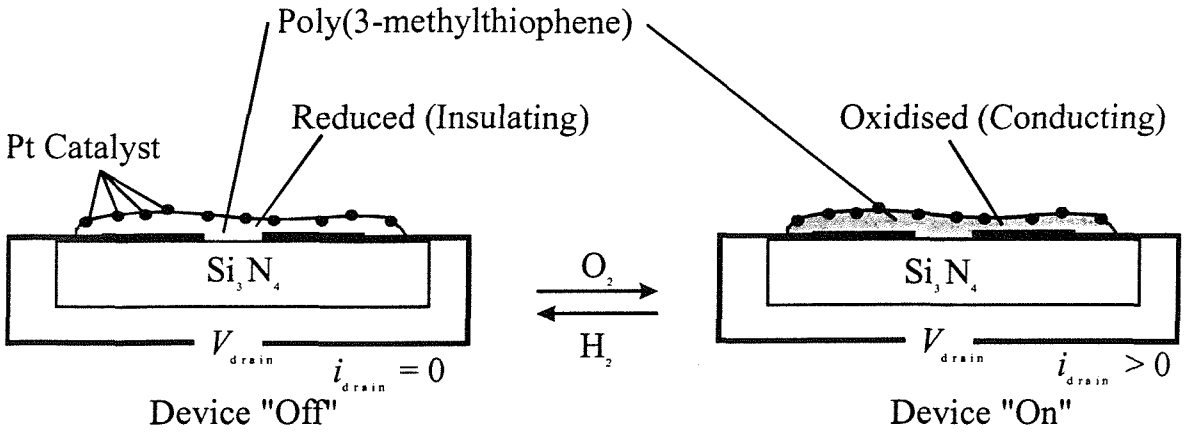

Figure 3: polymer transistor responding to oxygen oxidation or hydrogen reduction. The polymer film is laid across two electrodes between which a drain potential is applied. Pt micro-particules deposited at the surface of the film catalyse oxidation of the polymer by oxygen or reduction by hydrogen. When the polymer is reduced, no drain current is observed, when the polymer is oxidised, drain current is detected.

We are interested in using this type of structure (Figure 3) to monitor redox processes through changes in drain current as they do not require a potentiostat.

The idea of monitoring a chemical reaction by reading a current through a polymer was adapted to biosensors by using redox enzymes attached to the surface of the polymer. These enzymes specifically react with their substrate, therefore the changes of current through the polymer would only occur when the enzyme substrate is present. In this way conducting polymer sensors were used for the detection of glucose[6], and galactose[7, 8]. In each case an enzyme reacts with its substrate, and transfers its charge to a dissolved redox mediator, which in turn either oxidises or reduces the polymer as described in Figure 4.

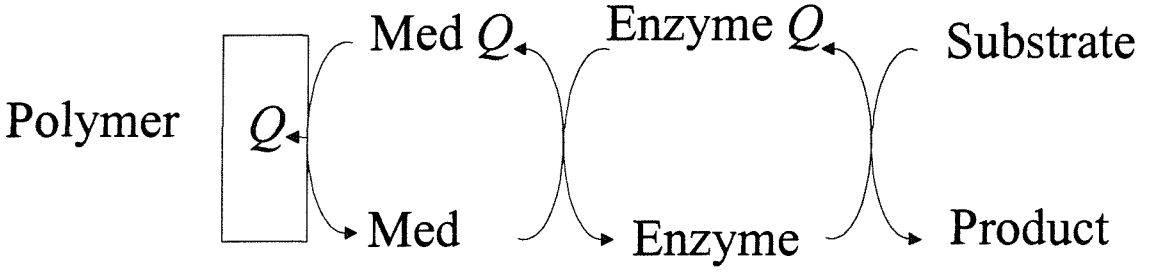

Figure 4: Reaction scheme of polymer electrochemical reaction induced by specific enzyme activity. The redox enzyme is charged by reacting with its substrate, and reacts with the dissolved mediator, which in turn transfers its charge to the polymer modifying the polymer redox state in the process.

In the case described in Figure 4, the change of polymer redox state is indirectly generated by the enzyme reaction.

Having the polymer, the mediator, the enzyme, and the enzyme substrate in the same solution imposes some restrictions due to the pH requirements of each one of the elements taking part in the bioelectrochemical reaction. In other words, the polymer film may prove to be more stable in acidic conditions, whereas the enzyme we wish to use, depending on its properties, may prove inactive or may denature in acidic conditions. In this study the goal is to provide an alternative method for carrying out immunoassays. Most immunoassay methods are based on the determination of the activity of an enzyme label. The most commonly used enzyme is alkaline phosphatase for which the optimal pH value is near pH 10[9, 10]. Considering this aspect of immunodetection highlights the difficulty of satisfying the acidic conditions needed for poly(aniline) electrochemistry, and the alkaline conditions required by the enzyme label[11].

We will show that our sensor solves this problem and allows the use of pH 0 for the polymer electrochemistry while pH up to 10.5 may still be used to operate the enzyme reaction.

First we will summarise the electrochemical processes which occur in poly(aniline) films under acidic conditions. We will then describe the conductive properties of in-house built poly(aniline)-poly(vinylsulfonate) transistors when poly(aniline) is in the conductive emeraldine redox state. We will show how this conductivity varies when the potential of the polymer film is varied and the redox state of poly(aniline) is changed. Finally we will prove the efficiency of our device demonstrating a change of polymer potential by carrying out a chemical reduction at various pH values, and show the subsequent change of conductivity through the polymer transistor.

2 Poly(aniline) electrochemistry

In this section we will explain how the change of redox state takes place in poly(aniline) by discussing poly(aniline) cyclic voltammetry in 2 M sulfuric acid.

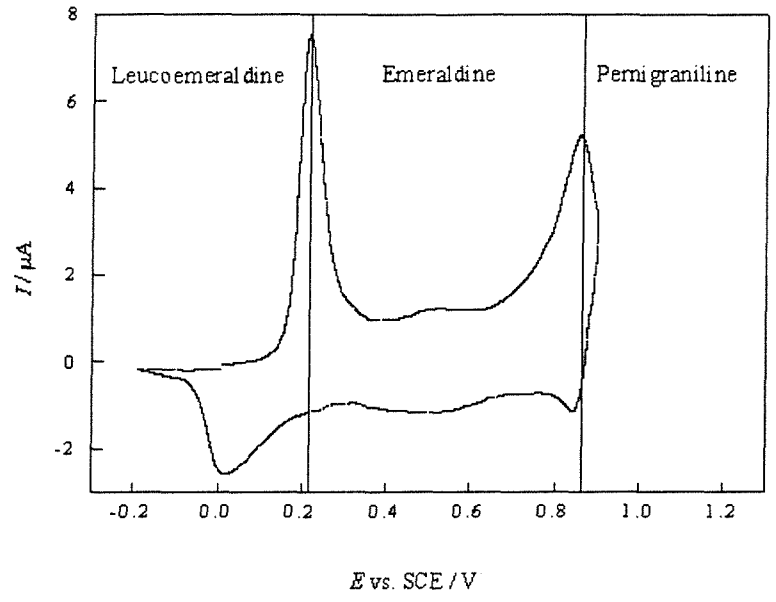

Figure 5: The cyclic voltammetry is carried out in 2 M sulphuric acid on a 500 μm platinum electrode. The potential starts at 0 V, rises to 0.9 V and decreases to –0.2 V at 20 mV / s. The polymerisation charge is 1.5 mC.

As a poly(aniline) film is cycled in acid, starting from 0 V up to 0.9 V, we observe a first oxidation peak assigned to the oxidation of leucoemeraldine into emeraldine. Near 0.9 V a second oxidation from emeraldine into pernigraniline is observed. On the reverse sweep the reduction of pernigraniline produces a sharp reduction peak, as the potential reaches 0V, a large reduction signal is observed.

The redox states of poly(aniline) in acid have different pK_a values. They are shown in Figure 6[12]. Three redox states are represented: leucoemeraldine, emeraldine, and pernigraniline. Two of these are known to form a salt in acidic conditions (the emeraldine and leucoemeraldine forms).

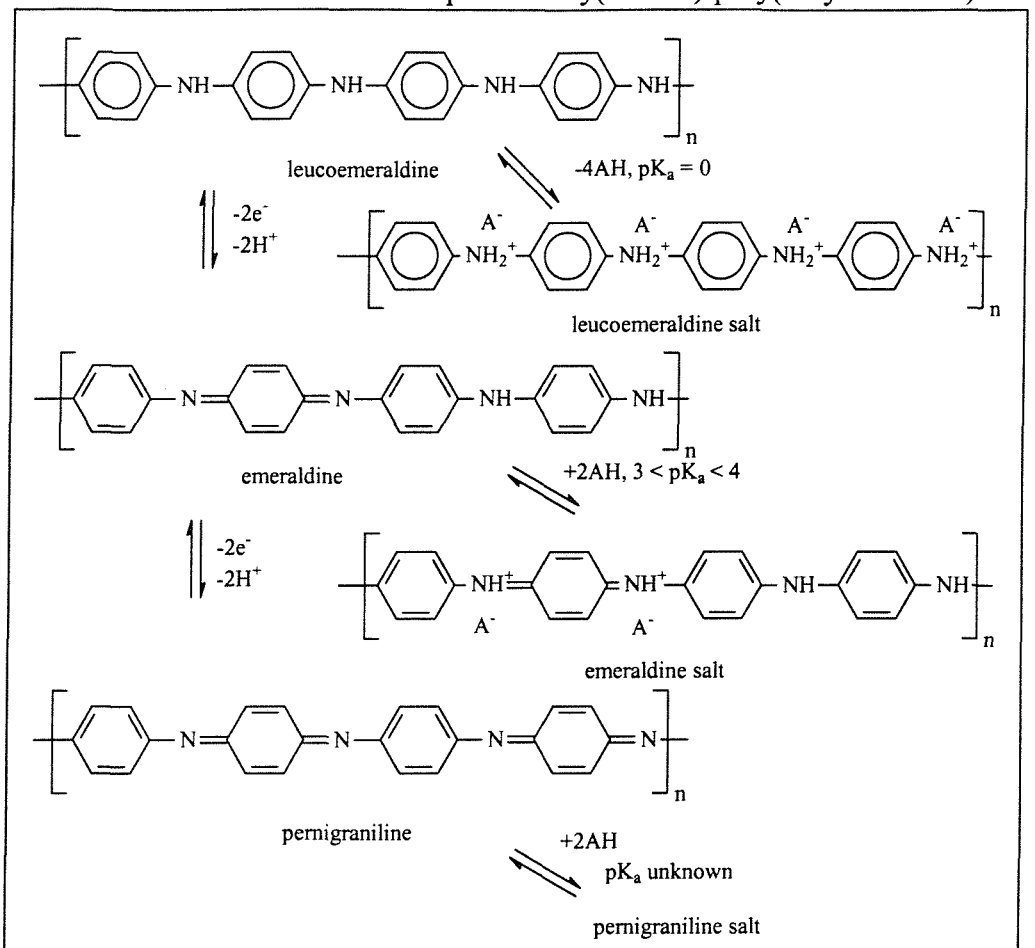

Figure 6: Poly(aniline) is known to exist in three different redox states: fully reduced polymer leucoemeraldine, oxidised (2e$^-$ each 4 polymer unit) emeraldine, and fully oxidised (1e$^-$ per polymer unit with respect to leucoemeraldine) pernigraniline. Both leucoemeraldine and emeraldine may be protonated to form a salt.

We will now discuss the conducting properties of a polymer film connecting two electrodes in 2 M sulfuric acid.

2.1 Poly(aniline)-poly(vinylsulfonate) deposition

In this study we will be using poly(aniline)-poly(vinylsulfonate) films deposited across gold electrodes. The electrodes are 2 mm long, 300 nm wide and separated by a 12.5 μm insulating mylar sheet (chapter 2).

Figure 7 shows the polymerisation current for a film grown by potential step at 0.9 V vs SCE in 2 M sulfuric acid.

In order to grow our polymer across two electrodes we apply the same potential to each of them. The polymerisation of aniline takes place on each electrode, as the size of the polymer increases the gap between the electrodes is progressively closed until the polymers films growing on each electrode make contact[13]. In the presence of poly(vinylsulfonate), the poly(aniline) traps poly(vinylsulfonate) anions within its structure as it grows[14-16].

To obtain electro-active poly(aniline) films deposited on electrodes we used potential step electro-polymerisation of aniline in sulfuric acid. The fact of having poly(vinylsulfonate) inserted in the poly(aniline) matrix does not affect the cyclic voltammetry of poly(aniline) because poly(vinylsulfonate) is not electrochemically active[17]. However this co-polymer was shown to facilitate ion transfers during the change of redox state of poly(aniline)[18]. Other methods such as galvanostatic or potential dynamic electro-polymerisation of aniline in other acids like HCl, HNO_3, $HClO_4$, and CF_3CO_2H have also been discussed in the literature [19].

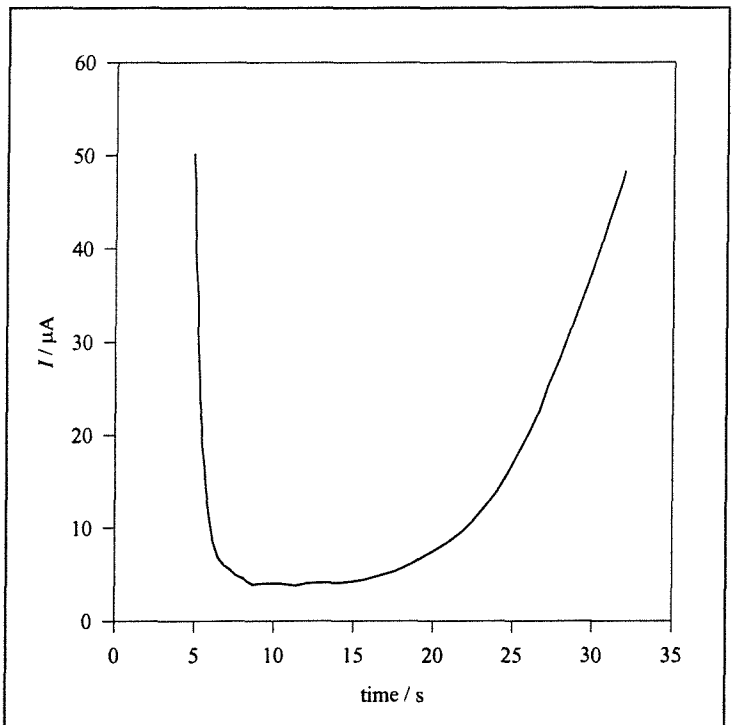

Figure 7: Current transient for aniline poly(vinylsulfonate) polymerisation. Polymerisation reactions are carried out at 0.9 V vs SCE on gold electrodes. The polymerisation solution is 5 ml 2 M H_2SO_4 containing 124 µl distilled aniline and 714 µl PVS. The potential is maintained until the polymerisation charge reaches 0.7 mC.

In Figure 7 we observe an instant rise of current when the electrode is switched from open circuit potential to 0.9 V vs SCE. This rise of current is related with the polarisation of the electrode (double layer charging) and decreases rapidly. After 15 s we observe an increase of current due to the polymerisation process. The experiment is stopped by switching the potentiostat back to open circuit. By integrating the current against the time in this experiment, we can estimate the polymerisation charge for the polymer film obtained. We found that the amperometry experiment of described above affords different transients from one electrode to another, but is very reproducible on a given electrode.

The poly(aniline)-poly(vinylsulfonate) film obtained is characterised by performing the cyclic voltammetry of the film in 2 M sulfuric acid from -0.2 V to 0.5 V at 50 mV / s. The cyclic voltammogram of the film is shown in Figure 8.

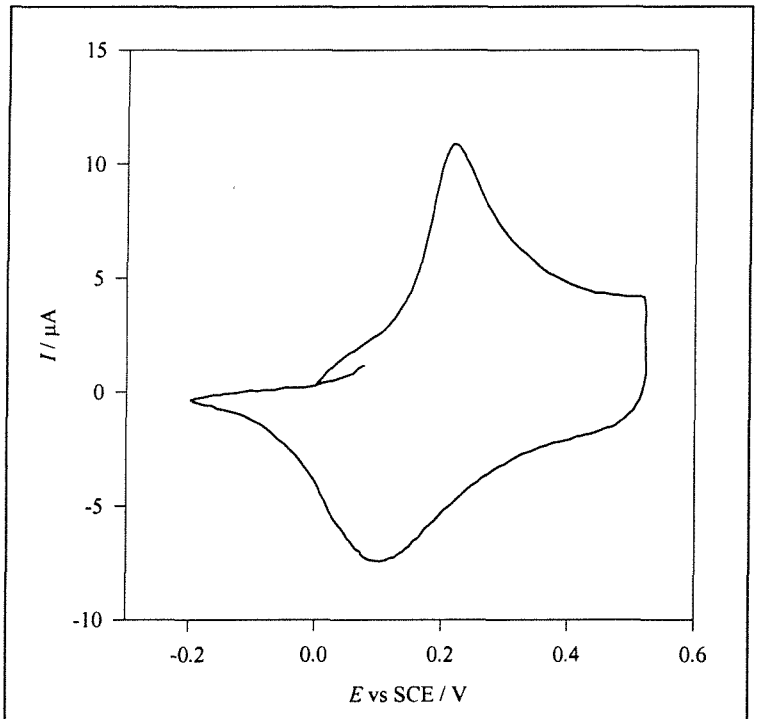

Figure 8: The cyclic voltammetry is carried out in 2 M sulphuric acid with a poly(aniline)-poly(vinylsulfonate) polymer film connected to two gold electrodes shorted together. The potential starts at 0 V vs SCE, rises to 0.9 V and decreases to -0.2 V at 50 mV / s. The polymerisation charge used for the electrodeposition of the polymer is 0.7 mC.

The cyclic voltammetry experiment shows the emeraldine / leucoemeraldine redox transition. The potential is not cycled beyond 0.5 V to avoid the formation of pernigraniline state, which is unstable in acid[20].

By calculating the polymerisation charge from the electropolymerisation experiment shown in Figure 7 and recording the cyclic voltammogram in acid between -0.2 and 0.5 V (Figure 8), we were able to ensure that all the polymer films we used during the study were similar in polymerisation charge and current intensities during the cyclic voltammetry (approximately 60 replicates on six different electrodes over two years).

2.2 Conductivity as a function of gate potential

In this section we will be using a poly(aniline)-poly(vinylsulfonate) film laid across two electrodes. We will describe the behaviour of the drain current when the gate potential is cycled from 0 to 0.5 V vs SCE. The drain potential does not vary during this study. The electrical circuit is sketched in Figure 9.

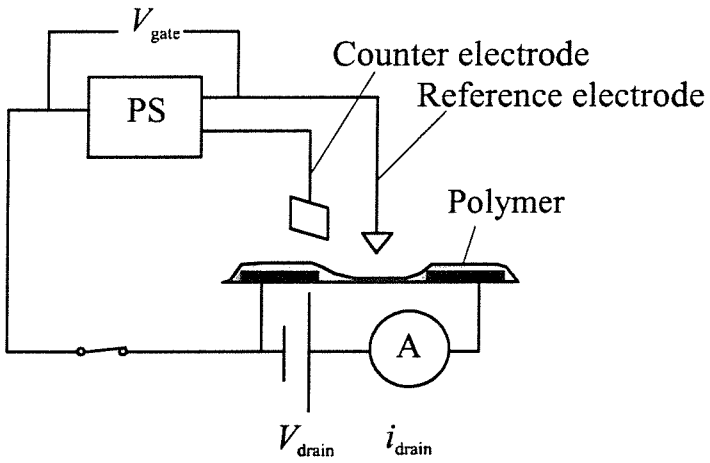

Figure 9: Electrical circuit used to study the resistance of the polymer. The potentiostat (PS) varies the gate potential of the polymer against an SCE reference. Meanwhile, a power suply applies a constant drain voltage between the two electrodes connected to the polymer. An ammeter detects the resulting drain current passing through the polymer.

As shown in Figure 9, the polymer (poly(aniline)-poly(vinylsulfonate)) is laid across two electrodes. Between these electrodes, a constant drain potential is applied. An ammeter detects the drain current between these electrodes. One of these electrodes is also used as

a gate electrode since it is connected to a potentiostat, which varies the potential of the polymer against an SCE reference.

By applying a constant 200 mV drain voltage and cycling the gate potential with the triangular wave generator of the potentiostat, we obtain the current displayed in Figure 10.

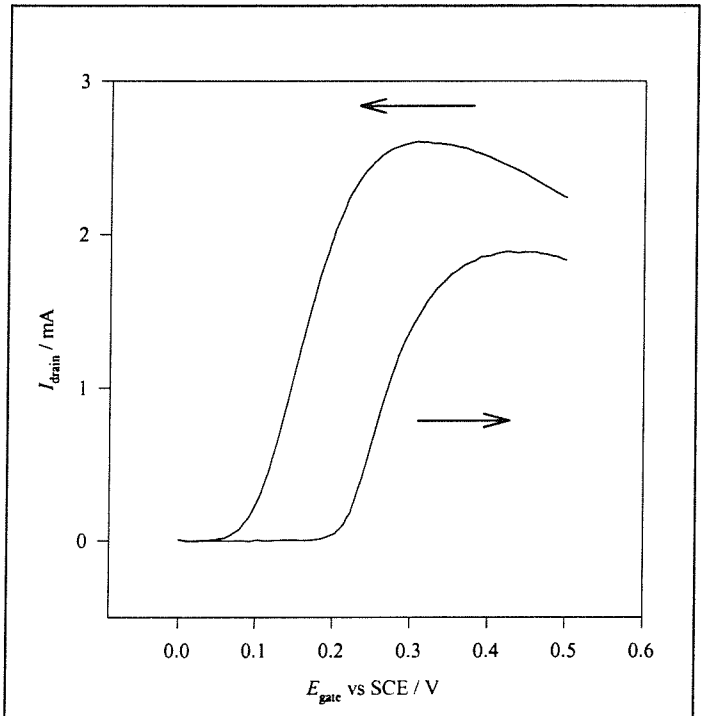

Figure 10: The gate potential is changed from 0.5 to 0 V vs SCE and back at 50 mV / s in 2M H_2SO_4. The drain voltage is maintained at 200 mV and the drain current is recorded.

In 2 M sufuric acid, the gate potential is held at 0.5 V vs SCE to form emeraldine salt, when the potential drops to 0.31 V, a maximum drain current is observed. A steep decrease of drain current is followed as the potential reaches 0 V. On the reverse scan, drain current is not seen to rise before 0.2 V, then the maximum drain current is observed at 0.45 V and is lower than the maximum drain current on the initial scan. If the potential is held at 0.5 V the drain current increases to reach its initial value and the experiment may be repeated.

It is important to point out that the amplitude of the decrease in drain current is more important as the gate potential decreases from 0.31 V to 0.1 V vs SCE than the amplitude of the increase of the drain current when the gate potential increases from 0.2 V to 0.4 V. When measuring the drain current to monitor the redox state of the polymer in our sensor,

Figure 10 shows that reducing emeraldine into leucoemeraldine will produce a larger drain current intensity response than oxidising leucoemeraldine into emeraldine.

Besides we note that the maximum drain current does not correspond to the same potential during the reduction and the oxidation of the film. This experiment was reproduced over 60 times, we noticed a very good reproducibility in terms of drain current intensity from different polymer films deposited on the same electrode, and the general behaviour of the drain current with respect to the gate potential was the same as described in Figure 10 every time at a given scan rate (here 50 mV / s).

2.3 Conductivity of emeraldine salt as a function of the drain voltage

We now study the drain current through the polymer when the gate potential is held at 0.31 V vs SCE. This optimal gate potential value was determined according to the drain current against gate potential plot from Figure 10. It is important to note that the optimal gate potential depends on the potential scan direction, in Figure 10 we see that the maximum drain current does not correspond to the same potential when the polymer is reduced and when it is oxidised. To obtain an optimal drain current at 0.31 V vs SCE, the gate potential needs to be brought down from 0.5 to 0.31 V vs SCE. To do so the same circuit as in the previous experiment is used (Figure 9). In this experiment, the gate potential is maintained at 0.31 V vs SCE (after being held at 0.5 V vs SCE for 1 min), then the drain potential is varied from 0 to 250 mV. The corresponding drain current against drain voltage plot is shown in Figure 11.

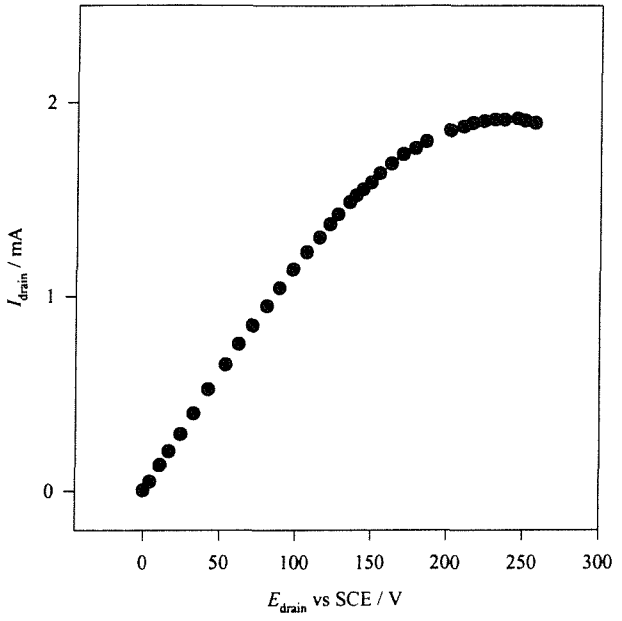

Figure 11: The gate potential is controlled through a Digital Voltmeter and is set at 0.31 Volts. The drain potential applied is varied manually from 0 to 250 mV. The chart recorder plots the potential difference on the X scale and the corresponding drain current on the Y scale.

Figure 11 displays a linear increase of drain current with drain voltage until 150 mV, beyond this value the drain current reaches a maximum at 240 mV and decreases slightly. The gate potential is held at 0.31V and the drain voltage maintains the potential difference between the source and the drain electrode. Because the source electrode is also the gate, while the gate remains at 0.31V, the drain electrode varies from 0.31 V to 0.56 V vs SCE. This explains the loss of conductivity beyond 250 mV drain potential, because the drain electrode is then beyond the potential of emeraldine.

This experiment shows that the use of poly(aniline)-poly(vinylsulfonate) films may afford currents that are large enough (mA) to be detected without any amplification. A portable electronic device designed to detect such large currents would be made simple by the absence of interference to the signal.

2.4 Conductivity against reduction charge

After showing the large drain current that our polymer film may afford, we will study the sensitivity of the polymer to reduction charge, and how it affects the resistance of the film. To do so, we consider the change in drain current with gate potential as the potential is decreased from 0.31 V to 0 V vs SCE (50 mV / s) as shown in Figure 10. Then we integrate the reduction current between these two potentials from the cyclic voltammetry experiment carried out at the same scan rate on the same polymer film (Figure 8). We then have both the reduction charge and the drain current related to potential, and knowing the drain voltage, we can plot the resistance of the film against reduction charge during the gate potential scan from 0.31 V to 0 V vs SCE. The results of this procedure are shown in Figure 12.

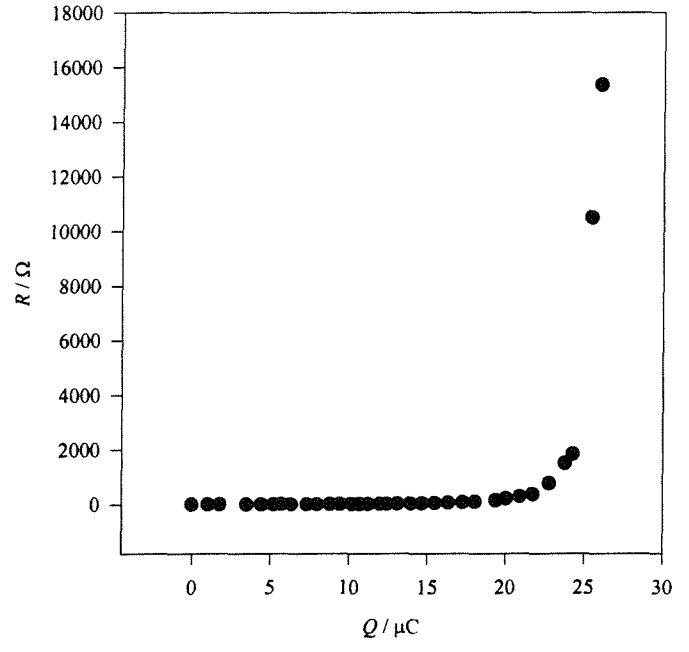

Figure 12: The resistance of the poly(aniline)-poly(vinylsulfonate) film is calculated from the drain current transient (Figure 10) and plotted against the reduction charge from the integration of the reduction current with time between the 0.31 V and 0.1 V vs SCE obtained from the cyclic voltammetry Figure 8. This result is obtained with a polymer film of 0.7 mC polymerisation charge.

Figure 12 shows that the change of resistance with charge is very fast beyond 20 μC. This implies that the polymer connecting our electrodes can be adjusted so that its potential is such that it retains a very low resistance while being at the threshold of the exponential rise in resistance. This makes our sensor extremely sensitive to a 5 μC reduction charge resulting in a 10^5 increase of resistance.

When varying the thickness of the polymer film deposited between our electrodes, we noticed that the reduction charge involved to obtain the resistance increase varied. If a thicker polymer film (larger polymerisation charge, same electrode) is used, a larger reduction charge is needed and *vice versa*. This fact is demonstrated by the reduction charge needed to obtain the exponential increase of resistance in Figure 13, which is plotted for a much thicker polymer film than Figure 12. Figure 13 shows that the reduction charge needed for the polymer film to become insulating is 10 times as much as in Figure 12, where the polymer deposition charge is 20 times less. This result shows that a smaller polymer requires less reduction charge to become insulating.

However we observe that the threshold in the reduction charge before the increase of resistance always corresponds to the same gate potential: 0.2 V vs SCE (data not shown), when the potential is decreased from 0.31 V to 0.2 V vs SCE at 50 mV / s, and is independent of film thickness.

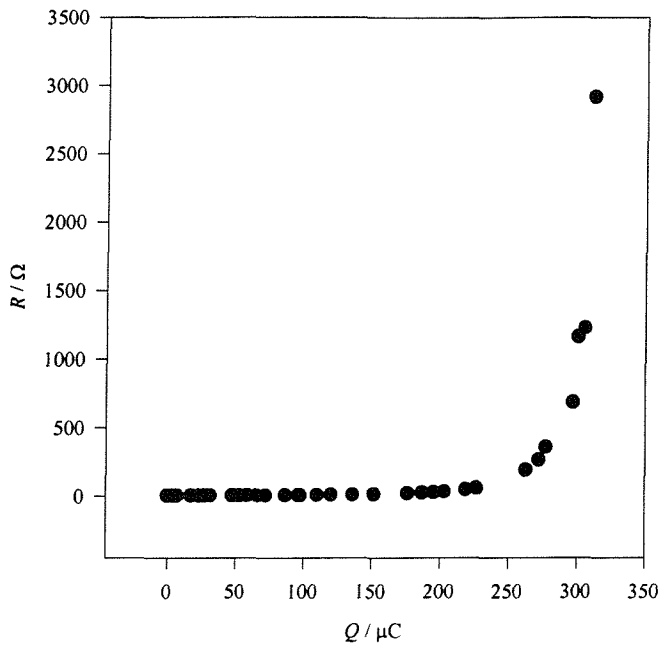

Figure 13: The resistance of the poly(aniline)-poly(vinylsulfonate) film is calculated from the drain current transient (Figure 10 same polymer film) and plotted against the reduction charge from the integration of the reduction current with time between the 0.31 V and 0.1 V vs SCE obtained from the cyclic voltammetry (Figure 8 same polymer film). This result is obtained with a polymer film of 4.24 mC polymerisation charge.

We conclude from this section that our poly(aniline)-poly(vinylsulfonate) film, when kept in sulfuric acid, displays a larger increase in resistance when it is reduced from emeraldine to leucoemeraldine than on the reverse process. But once the potential is maintained at 0.5 V vs SCE at the end of the scan, the drain current slowly rises back to its initial value at the start of the experiment. We showed that a film covering a 12.5 μm gap could afford drain currents up to 2 mA. And we showed that by taking the gate potential from 0.31 V to 0.2 V vs SCE, we could trigger a 10^5 increase of the film resistance for a 5 μC reduction charge.

3 Change of polymer potential by a redox reaction at a different pH

In this section we will prove that our sensor can be operated by reducing the polymer film in acid with an organic compound in a solution of a different pH via a collecting electrode.

The polymer and the organic compound reducing it are not in direct contact with each other and the reduction reaction takes place through a graphite electrode.

During this set of experiments, we will be using the set up described in Figure 1. We will show that the change of potential of the polymer, taking place during the experiment, is due to the addition of the chemical in cell B.

First we will describe how *p*-aminophenol affects the potential of the polymer. The experimental arrangement is shown in Figure 14. We should remember here that in this experiment the electrodes supporting the polymer are shorted together, because we monitor the potential of the polymer; we do not apply any drain voltage. In this experiment, the polymer is first oxidised to the emeraldine state in 2 M sulfuric acid using a potentiostat and a SCE reference. The potentiostat is disconnected and the polymer is connected to a voltage follower, which records the polymer potential against SCE. Then the collecting electrode from cell B is connected to the polymer film. The potential is recorded for a few seconds before adding *p*-aminophenol to the solution in cell B. The experiment is repeated with the same polymer, with various pH buffers in cell B, and the results are shown in Figure 15.

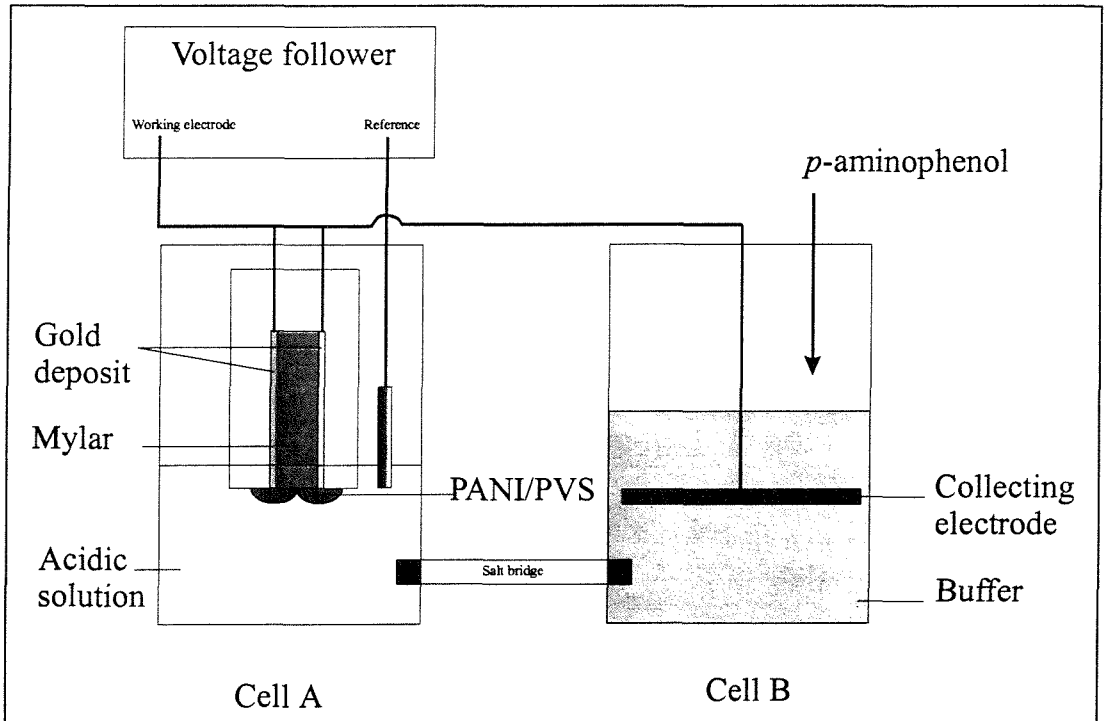

Figure 14: Cell A contains acid and provides the best conditions for the electrochemistry of the polymer. Cell B contains the buffer that best suits the bioelectrochemical reaction. The polymer is connected to the collecting electrode and the charge transfer is enabled between the two cells by a salt bridge. The voltage follower is used to monitor the potential of the polymer against SCE.

The polymer is initially oxidised potentiostatically between 0.3 and 0.4 V vs SCE. Figure 15 shows three potential curves corresponding to the addition of the same amount of *p*-aminophenol to cell B in three different pH buffers. Curve (a) corresponds to pH 2, curve (b) to pH 7 and curve (c) to pH 9.5. In each case we observe that the polymer potential remains stable until the addition of *p*-aminophenol (10 μM) to cell B. The addition is indicated by the arrows in Figure 15.

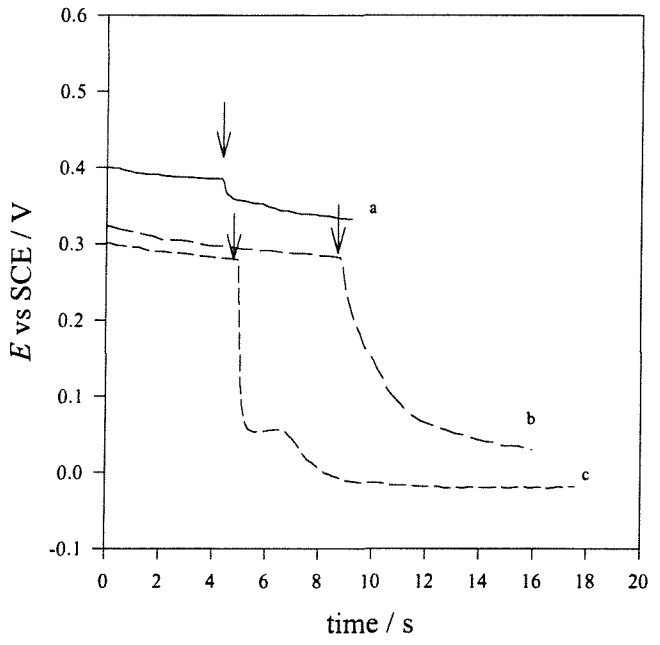

Figure 15: potential against time curve. Cell A (Figure 14) contains 2 M sulfuric acid, cell B (Figure 14) contains (a) pH 2 HCl / KCl buffer, (b) pH 7 citrate phosphate, and (c) pH 9.5 Tris-HCl buffer. all buffers are 0.1 M. The arrows indicate the addition of *p*-aminophenol to reach 10 μM.

The potential recorded after the addition of *p*-aminophenol varies with the pH in cell B. We suspect that the difference of potential to corresponds to the effect of pH on the *p*-aminophenol redox potential. This is confirmed by the cyclic voltammetry of *p*-aminophenol at the three pH values used in the potential shift experiment (Figure 16).

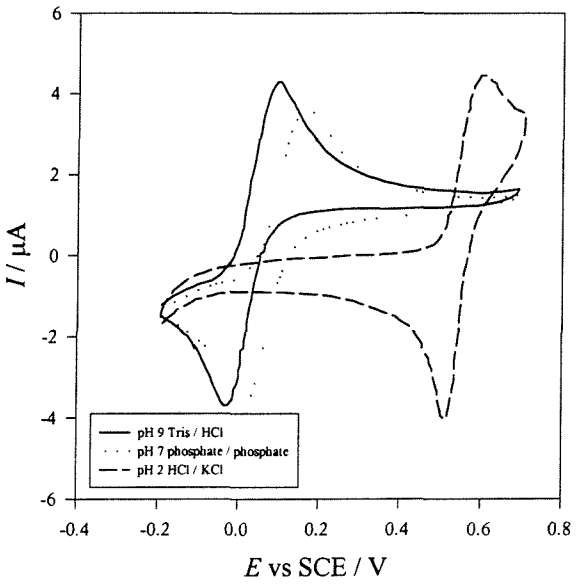

Figure 16: Cyclic voltammetry of *p*-aminophenol 10 µM in pH 2 HCl / KCl, pH 7 phosphate / phosphate and pH 9 Tris / HCl buffer at 50 mV / s on 3 mm diammeter glassy carbon electrode.

Figure 16 shows a clear relation between the final potential of the polymer when *p*-aminophenol is added to cell B (Figure 15), and the redox potential of *p*-aminophenol in the same pH during cyclic voltammetry experiments. This subject will be thoroughly described in chapter 5.

In Figure 15, we note a peculiarity in curve (c), which is a momentary rise of potential near 0 V vs SCE. This phenomenon has only been observed when using freshly deposited polymers, this phenomenon is systematically observed in these conditions. After three experiments with the same polymer film, this potential rise is no longer observed. Despite a lot of effort to identify the cause of this phenomenon, the experiments undertaken failed to provide enough evidence to reach a firm conclusion. However, we infer from this observation that a freshly deposited polymer is slightly different from a polymer that has been reduced and oxidised several times.

4 Change of drain current through the polymer with a redox reaction at pH 9.5

Having showed the direct relation between the *p*-aminophenol addition to cell B and the change of polymer potential, we now show the effect of the change of potential on the resistance of the polymer by applying a drain voltage to the polymer (emeraldine state) and recording the drain current through the polymer while adding *p*-aminophenol to cell B.

We use the setup described in Figure 1, the potentiostat is used as a power supply (counter and reference are shorted together) to apply a drain voltage between the two electrodes connected by the polymer. The polymer is previously set at 0.5 V vs SCE. A voltage follower records the change of potential while the potentiostat records the change in drain current. The potential and drain current start varying when *p*-aminophenol is added to cell B. Results are displayed in Figure 17.

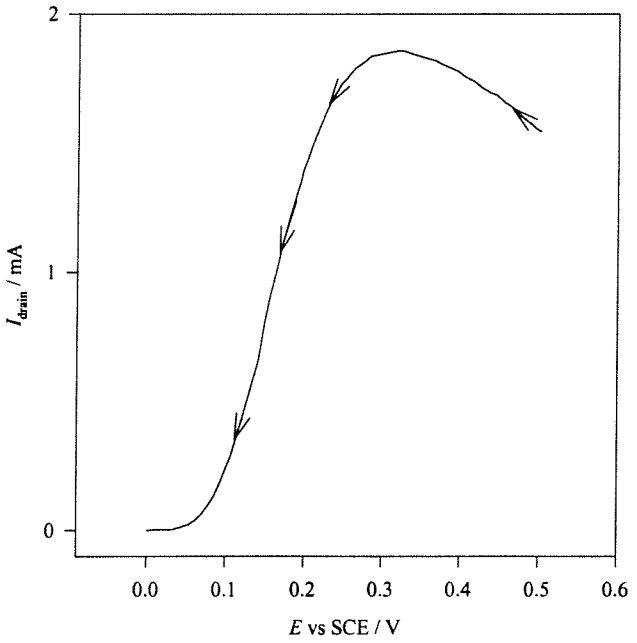

Figure 17: Drain current against polymer potential. The polymer potential is initially set at 0.5 V vs SCE. Cell A and B are connected according to Figure 1, The potentiostat reads the drain current and a voltmeter reads the polymer potential against SCE. When *p*-aminophenol is added to cell B the polymer potential and the drain current vary simultaneously.

This experiment proves the relation between the addition of reducing agent to cell B and the change of potential and resistance of the polymer in cell A.

5 Conclusion

In this chapter we demonstrated the viability of our new sensor. This new concept enables us to separate entirely the polymer electrochemistry from the analyte electrochemistry. As a result any redox enzyme regardless of its physiological origin can be used to transform its substrate and affect the redox state of the polymer.

We saw that the poly(aniline)-poly(vinylsulfonate) film requires its gate potential to be held at 0.5 V for 1 min before being set at 0.31 V vs SCE where the drain current intensity will be the highest.

We showed that the polymer resistance increases exponentially with reduction charge. When a thick polymer (high polymerisation charge: 4.24 mC) is used, the reduction charge needed to obtain the exponential rise of the polymer resistance is greater than with a thin polymer (small polymerisation charge: 0.7 mC). However the threshold of the resistance increase for any polymer film corresponds to bringing the gate potential from 0.31 V to 0.2 V vs SCE at 50 mV / s in both cases.

We proved that the pH buffer used in cell B could be changed at will according to any physiological requirements for the detection of the targeted analyte.

Another advantage of this device is the possibility to use as small a polymer film as is technically possible, thus requiring a very small charge to operate its redox transition, and use as big a collecting electrode as is practical for the type of detection required, while the charge of the polymer remains greater than the double layer charge of the collecting electrode. The result being an electrode size amplification. In our case, we estimate the polymer surface to be $2.5\ 10^{-8}\ m^2$, which would be the surface available for reaction with the redox agent if this one was dissolved in the same cell, and our graphite collecting electrode is $10^{-4}\ m^2$, which corresponds to a 4000 fold surface amplification.

6 References

1. Ofer, D., R.M. Crooks, and M.S. Wrighton, *Potential dependence of the conductivity of highly oxidized polythiophenes, polypyrroles, and polyaniline: Finite windows of high conductivity.* J. Am. Chem. Soc, 1990. **112**: p. 7869-7879.
2. Paul, E.W., A.J. Ricco, and M.S. Wrighton, *Resistance of polyaniline films as a function of electrochemical potential and the fabrication of polyaniline based microelectronic device.* J. Phys. Chem., 1985. **89**: p. 1441-1447.
3. Kittelsen, G.P., H.S. White, and M.S. Wrighton, *Chemical derivatization of microelectrode arrays by oxidation of pyrrole and N-methylpyrrole: Fabrication of molecule-based electronic devices.* J. Am. Chem. Soc., 1984. **106**: p. 7389-7396.
4. Thackeray, J.W. and M.S. Wrighton, *Chemically responsive microelectrochemical devices based on platinized poly(3-methylthiophene):Variation in hydrogen, oxygen, or pH in aqueous solution.* J. Phys. Chem., 1986. **90**: p. 6674-6679.
5. Chao, S. and M.S. Wrighton, *Solid-state microelectrochemistry: Electrical characteristics of a solid state microelectrochemical transistor based on poly(3-methylthiophene).* J. Am. Chem. Soc., 1987. **109**: p. 2197-2199.
6. Bartlett, P.N., J.H. Wang, and W. James, *Measurment of low glucose concentrations using a microelectrochemical enzyme transistor.* Analyst, 1998. **123**: p. 387-392.
7. Shaolin, M., X. Huaiguo, and Q. Bidong, *Bioelectrochemical responses of the polyaniline galactose oxidase electrode.* J. Electroanal. Chem., 1991. **304**: p. 7-16.
8. Shaolin, M., *Bioelectrochemical response of the polyaniline galactose oxidase electrode.* J. Electroanal. Chem., 1994. **370**: p. 135-139.
9. Christie, I.M., et al., *Simplified measurement of serum alkaline phosphatase utilizing electrochemical detection of 4-aminophenol.* Anal. Chim. Acta, 1992. **257**: p. 21-28.
10. Kokado, A., H. Arakawa, and M. Maaeda, *New electrochemical assay of alkaline phosphatase using ascorbic acid 2-phosphate and its application to enzyme immunoassay.* Anal. Chim. Acta, 2000. **407**: p. 119-125.
11. Rosen, I. and J. Rishpon, *Alkaline phosphatase as a label for heterogeneous immunoelectrochemical sensor.* J. Electroanal. Chem., 1989. **258**: p. 27-39.

12. Kalaji, M., L. Nylholm, and L.M. Peter, *A microelectrode study of the influence of pH and solutio composition on the electrochemical behaviour of polyaniline films.* J. Electroanal. Chem., 1991. **313**: p. 271-289.

13. Bartlett, P.N. and P.R. Birkin, *A microelectrochemical enzyme transistor responsive to glucose.* Anal. Chem., 1994. **66**: p. 1552.

14. Kang, E.T., et al., *Self doped polyaniline and polypyrrole. A comparative study by X-ray photoelectron spectroscopy.* Polymer Communications, 1991. **32**(13): p. 412-414.

15. Kuramoto, N., et al., *Modification of growth rate and structure of electropolymerised aniline by sodium polyvinyl sulphonate.* J. Chem. Soc. Chem. Commun., 1990: p. 1478-1480.

16. Bartlett, P.N., J.H. Wang, and E.N.K. Wallace, *A carbon dual microband electrode coated with a poly(aniline)-poly(vinylsulfonate) composite film exhibits an off-to-on switching response when exposed to NADH at pH 7; the device takes a few minutes to fully switch conductivity and has a linear response for NADH concentration up to ca> 4 mmol* dm^{-3}. Chem. Commun., 1996.

17. Wallace, E.N.C., *Poly(aniline) composites as bioelectrochemical sensors.* Thesis submitted for degree of Doctor of Philosophy, 1997.

18. Morita, M., et al., *Electrochemical behaviour of polyaniline-poly(styrene sulfonate) composite films in organic electrolyte solutions.* J. Electrochem. Soc., 1994. **141**(6): p. 1409-1413.

19. Desilvestro, J. and W. Scheifele, *Morphology of electrochemically prepared polyaniline.* J. Mater. Chem., 1993. **3**(3): p. 263-272.

20. Kobayashi, T., H. Yoneyama, and H. Tamura, *Oxidative Degradation Pathway of Polyaniline Film Electrodes.* J. Electroanal. Chem., 1984. **177**: p. 293.

Chapter 4: Disposable Transistors

1-Introduction

Our sensor is designed to detect a biochemical reaction through the chemical reduction of a polymer transistor. The change of potential in the polymer generates a drop in the current flowing through the transistor.

In chapter 3 we focused upon the understanding of the polymer. In this chapter we will report how the knowledge acquired earlier can prove to be useful for the design of a disposable transistor. The mechanisms we brought to light in chapter 3 helped us in the choice of the polymer film, the potential window it should remain within, and the initial and final potentials.

In chapter 3 we showed that a small polymer film (0.7 mC electropolymerisation charge) would require a smaller reduction charge (25 μC) to operate a transition from conductive emeraldine salt to insulating leucoemeraldine, whereas a larger polymer film (4.24 mC electropolymerisation charge) would require a larger reduction charge (300 μC) to operate the same transition. We also noticed changes of behaviour, during chemical reduction by *p*-aminophenol, between freshly deposited polymers and polymers, which had been reduced and oxidised several times implying that the polymer film should not be reused to guarrantee reliable results.

The reduction of the polymer is the result of *p*-aminophenol oxidation, therefore the concentration of *p*-aminophenol determines the number of charges available for the polymer reduction within the sample volume, and hence the flux of redox compounds to the electrode surface over the experiment time. This means that the smaller the polymer is ($Q < 1$ mC electropolymerisation charge), the more sensitive the sensor will be to small concentrations of *p*-aminophenol for a given measurement time.

Our aim is then to create a number of poly(aniline)-poly(vinylsulfonate) films connected to two electrodes, that will only be used once in the sensor. The difficulty of the procedure is to obtain identical polymer films.

We described the general operational conditions for our device and will now focus upon the fabrication of reproducible transistors.

A key factor for us to obtain good reproducibility from one transistor to another was to find reproducible supporting electrodes.

2-Photolithographically fabricated electrodes

In this section we will describe the type of gold electrodes we used to electrodeposit our polymer films in a reproducible manner.

We will be using commercially available interdigitated gold electrodes, in which each electrode is individually addressable. Each gold electrode is 10 μm wide and 2 mm long, the gap between each electrode is 10 μm wide. An SEM photograph of the electrodes is shown in Figure 1.

2.1-SEM

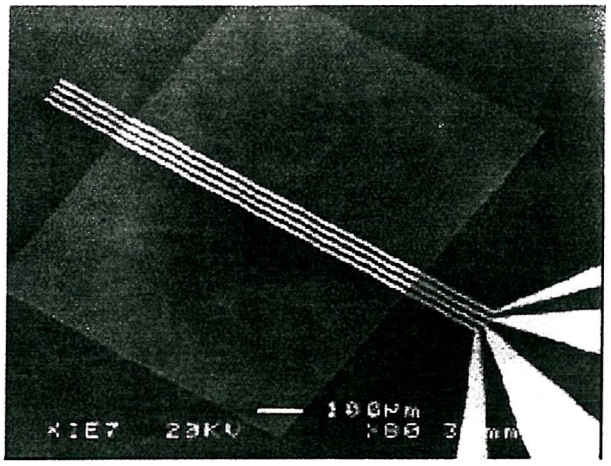

Figure 1: perspective view of the photolithography fabricated (MB4000 Smart Microsystems) 4 band electrodes used to build our transistor. Four gold bands can be seen. The dark shade around the gold bands is due to the presence of a photoresist insulating film. The clearer rectangle in the middle is where no film was deposited to allow electrochemistry to take place.

Our supporting electrodes are supposed to have similar surface areas, which should help for a reproducible electrodeposition of the polymer film on them. The handling of these electrodes is made easier by the protecting, insulating photoresist film deposited over the connections. To determine the statistical distribution of the electrode areas, we carried out gold cyclic voltammetry of the electrodes in acid and compared the gold oxide reduction peak of all our devices.

2.2-Cleaning procedure

Given the structure of the interdigitated gold electrodes, these cannot be polished before carrying out the cyclic voltammetry experiment. Even if photolithographycally fabricated gold electrodes guarantee similar electrode areas from one device to the other, gold oxides and other contamination may challenge electrochemistry. This is why a set of new electrodes will rarely yield consistent cyclic voltammetry if they are not cleaned previously. Organic solvents tend to dissolve plastic constituents of the device such as the photoresist material covering the electrode connections. The only efficient way to clean our gold electrodes was found to be hot piranha*. The solution is deposited on the electrodesfor 10 seconds and then rinsed away with deionised water. After doing the cyclic votammetry, cleaning may be repeated.

2.3-Gold cyclic voltammetry and statistics

We will now describe the cyclic voltammetry of the interdigitated gold electrodes.

Given the small size of the interdigitated electrodes, the experimental arrangements are made so that cyclic voltammetry can be carried out in a 10 µl drop of acid. This is done by using a gold wire attached to the tip of the reference electrode in order to maintain them vertically on top of the sulfuric acid solution drop resting on the photolithographically fabricated electrodes. This set up can not be thermostatted or degassed. The temperature variations are limited by thermostatting the stock solution before the experiment.

The cyclic voltammetry is carried out in 10 µl of 2 M sulfuric acid. All four gold electrodes are shorted together and connected as the working electrode to the potentiostat. An SCE reference is used and the counter electrode is a gold wire. Given the small volume of solution we are using to undertake cyclic voltammetry, it is essential to prevent KCl contamination from the reference electrode by using a second glass frit between the reference and the solution. Temperature was set at 25 °C, and was checked to avoid more than 5 °C difference from one experiment to the other.

Gold cyclic voltammetry obtained from our electrodes is far from perfect and compromises have to be made (Figure 2). The oxidation sweep displays two wide

oxidation signals and the reduction shows the gold stripping peak. Our only indication about the available gold surface is the gold-oxide reduction peak. To decide if two electrodes are similar, we consider this reduction current.

All the electrodes where numbered and traced from the gold cyclic voltammetry to the detection experiment. Cleaning was repeated in order to obtain at least 125 nA reduction peaks. Some of the 74 cyclic voltammograms of the gold electrodes in 2 M sulfuric acid are displayed in Figure 2.

The statistics show that the gold-oxide reduction peak can be reproduced from one device to another. The mean value is 175 nA and 94.5% of the electrodes are between 150 and 200 nA.

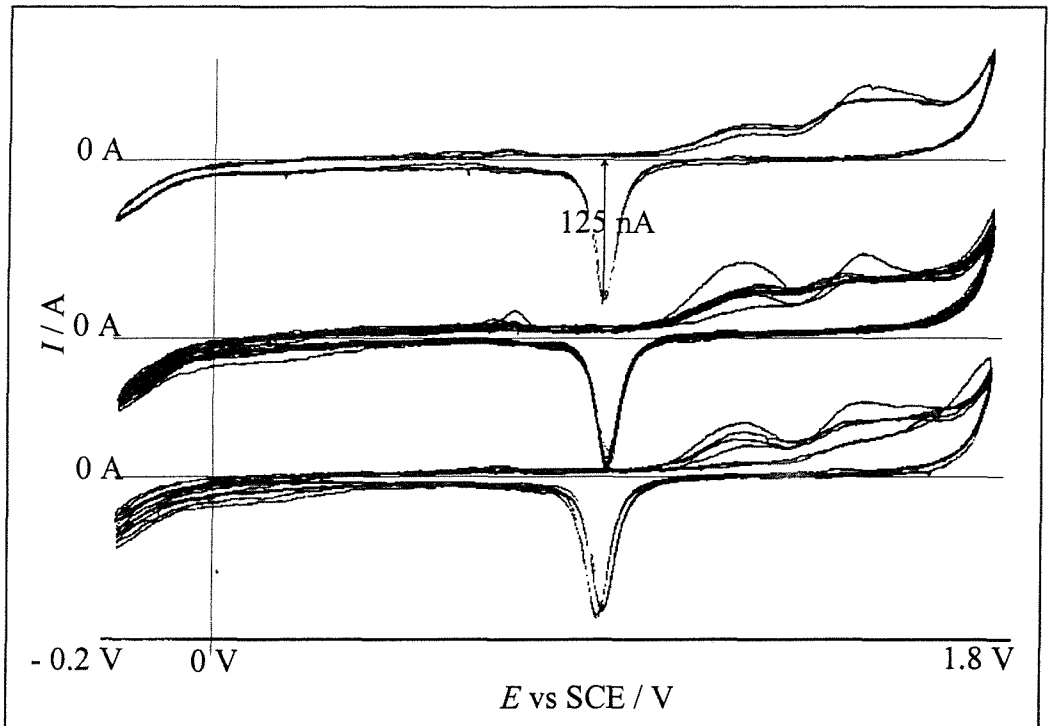

Figure 2: The cyclic voltammetry of all 4 gold electrodes of each device was carried at 100 mV / s, and the potential was cycled 10 times from –0.2 to 1.8 V vs SCE starting at 0 V. To prevent KCl diffusion, a double frit was used for the reference electrode. Cyclic voltammetry was carried out right after rinsing the piranha solution. The protocol was repeated until a minimum value of 125 nA was obtained for the gold stripping peak.

When comparing the cyclic voltammetry of our interdigitated electrodes with the cyclic voltammetry of a gold wire electrode (Figure 3), we notice several differences. In Figure 2, two oxidation peaks are observed at 1.2 V and 1.5 V vs SCE. In Figure 3 only one oxidation peak is observed at 1.2 V vs SCE. This implies that only one gold oxide is

* Piranha: 20% H_2O_2 / 80% sulfuric acid, extremely corrosive, should be handled with extreme care.

formed in the case of the gold wire electrode. This may be explained by the structure of the gold forming the electrode in each case. The photolithographically prepared electrodes are made of evaporated gold, which is not the same gold metal structure of the gold wire electrode.

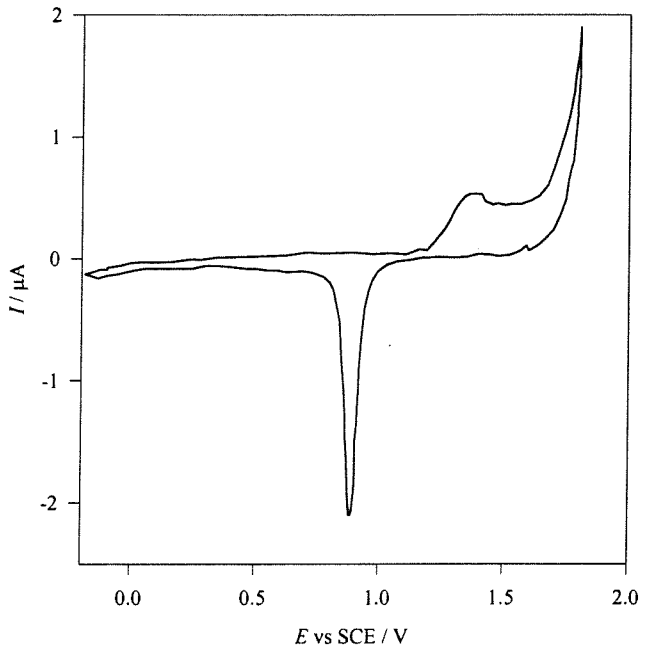

Figure 3: Cyclic voltammetry of a 0.2 mm diameter gold wire electrode in 2 M sulfuric acid at 100 mV / s from 0.2 V to 1.8 V vs SCE.

The reduction peak intensities for the gold electrodes on all 74 devices are reported in Figure 4.

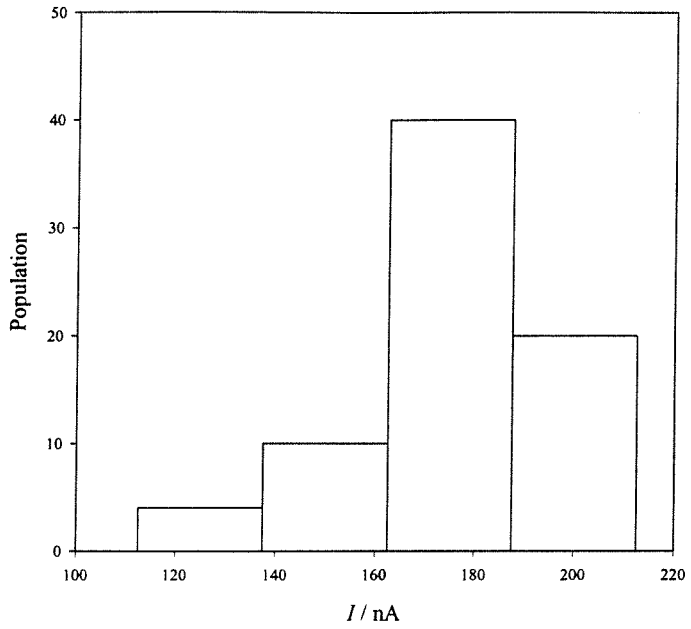

Figure 4: The columns represent the number of devices having the same stripping peak current. The X-scale is divided into four groups 125, 150, 175, and 200 nA.

The reduction peak intensity was measured for every experiment and studied according to the Student t test:

Population size 74 devices.

Mean value of the reduction peak intensity 175.6 nA.

Standard deviation 19.9 nA.

Standard error 3.2 nA.

95% confidence interval 6.6 nA.

99% confidence interval 8.9 nA.

The confidence interval at 99% represents a +/-5% variation of the reduction peak current throughout the transistor population of 74 devices.

3-Polymerisation reproducibility

Having studied the cyclic voltammetry of the gold electrodes from all interdigitated electrode devices, we will now describe the electropolymerisation of the poly(aniline)-

poly(vinylsulfonate) film on these electrodes. The polymerisation charge for each deposition will be analysed statistically according to the Student test.

The electrodeposition of the polymer was carried out as follows. Two neighboring gold electrodes are shorted together and connected to the potentiostat as the working electrode. A gold wire is used as the counter electrode and the reference electrode is separated from the solution by a double frit containing 2 M sulfuric acid to prevent KCl contamination of the gold electrodes. The polymerisation solution is 5 ml 2 M H_2SO_4 containing 124 µl distilled aniline and 714 µl poly(vinylsulfonate). As explained in section 2.3 the stock solution is kept at 25 °C with a waterbath in order to maintain identical conditions at the start of each experiment. For each polymerisation experiment 10 µl of aniline poly(vinylsulfonate) are deposited on the gold electrodes and the counter electrode together with the reference electrode (double frit) are approached to make contact with the solution with a micrometric screw clamp. The potential is switched from open circuit to 0.9 V vs SCE and the current is recorded against time. In this way the polymer film is connected to two neighbouring electrodes covering the 10 µm gap separating them. The SEM photographs of a poly(aniline)-poly(vinylsulfonate) film deposited on two gold electrodes according to this method are shown in Figure 5 and Figure 6.

3.1-SEM

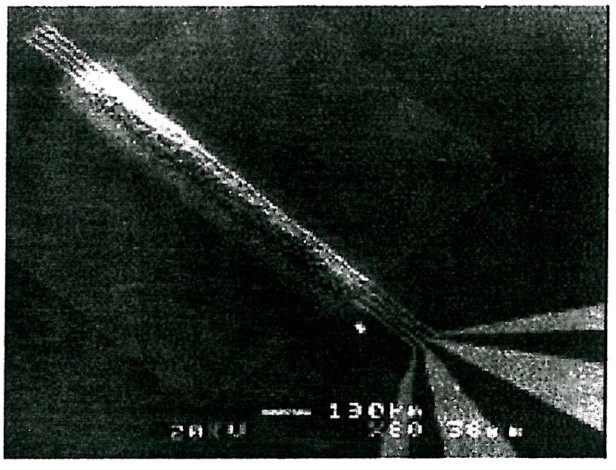

Figure 5: perspective view of the poly(aniline)-poly(vinylsulfonate) transistor deposited between two neighbouring gold electrodes.

As we can see on the SEM picture, the polymer deposition is very irregular it explains how difficult it is to make these transistors identical. As explained in the first chapter, given the conductivity processes, it is still possible to obtain similar conductive properties for transistors displaying different structures. Nonetheless there is no doubt that great improvements could be brought to the sensor by controlling the polymer structure.

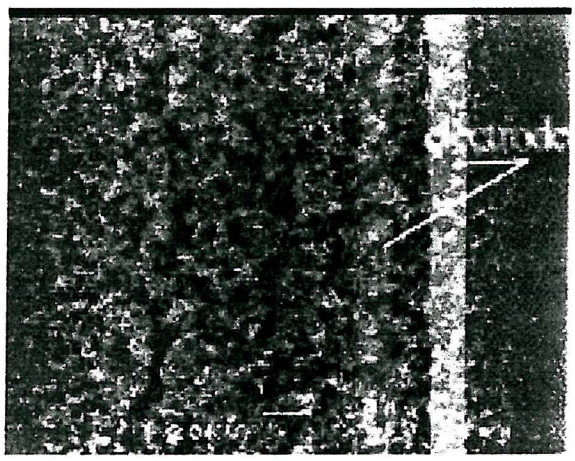

Figure 6: close up view of the polymer arrangement over the connecting electrodes. The two unused gold bands can be seen on the right, their width is 10 µm.

The perspective view of the transistor shows a good distribution of the polymer along the electrodes. It proves the reliability of the support electrodes and the efficiency of the insulating film.

3.2-Procedure

Having checked that the gold surface is similar (within 5% of mean value for reduction current) from one electrode to another, we shall now see if the polymerisation can be controlled to produce identical transistors. We only find out that a transistor is satisfactory on the final detection experiment. By controlling each step carefully we are able to eliminate devices that are too different from the rest of our samples.

Here we study the polymerisation transients carried out with the gold electrodes for which the statistics were displayed previously. The polymerisation has to be carried out within an

hour after the cleaning and the gold cyclic voltammetry is checked otherwise the electropolymerisation charge was found to be significantly smaller than the mean value of the charge from the rest of the statistical population.

In the polymerisation step, the indicator is the polymerisation charge. The statistics were calculated on three different sets of electrodes on different dates and different times of the day.

Polymerisation is the most delicate part of the preparation and must be temperature controlled as long as possible before the start of the experiment. In regular experimental conditions (see chapter 3) we observed a large influence of the temperature on the electropolymerisation of the polymer film (data not shown). Also as we work on a very small volume, KCl from the reference electrode is liable to interfere and a double frit was used to avoid KCl diffusion.

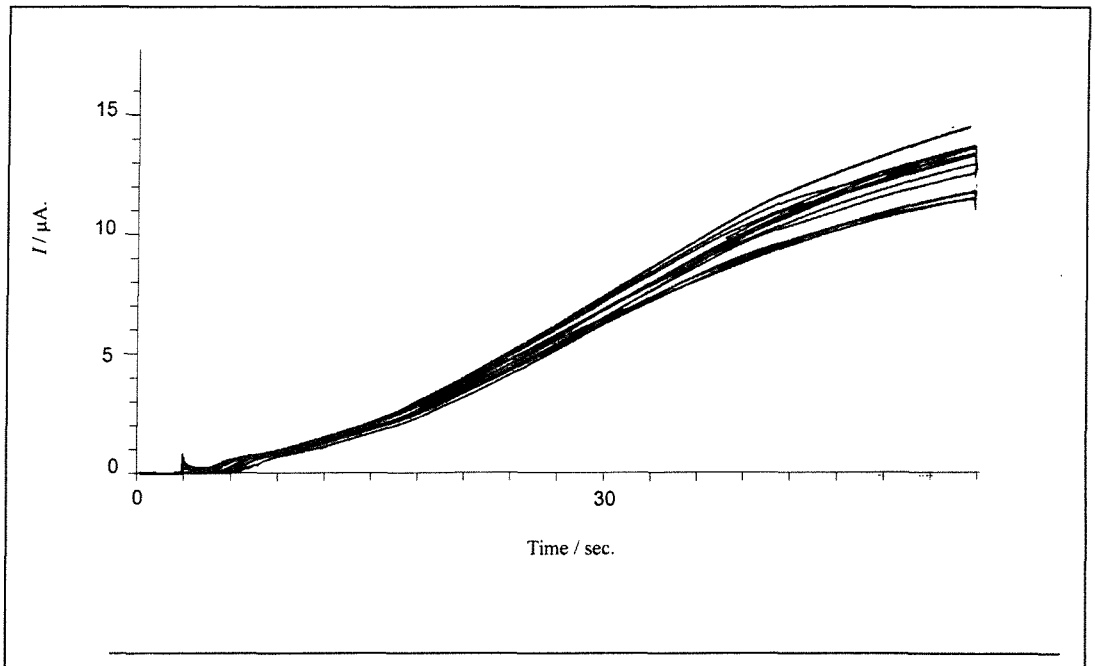

Figure 7: 10 current transients for polymerisation reactions carried out at 0.9 V on photolithographically defined electrodes. The polymerisation solution is 5 ml 2 M H_2SO_4 containing 124 µl distilled aniline and 714 µl poly(vinylsulfonate). The working electrode corresponds to two neighbouring electrodes on the disposable photolithography devices.

3.3-Statistics

The polymerisation charge is integrated from the current transient (see Figure 7). Each value is reported and statistics are calculated.

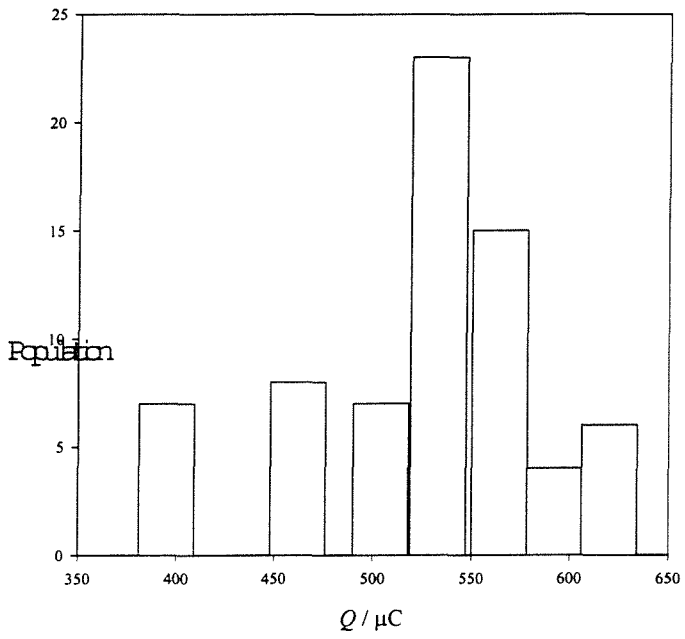

Figure 8: shows the distribution of the polymerisation charge for identical polymerisation time and potential. The charges were calculated from the polymerisation current transients. The statistics are calculated according to the student test. The data was collected from three different sets of experiments and polymerisations were carried out within an hour after cleaning the gold.

The electropolymerisation charge was calculated for every one of the 70 experiments (Figure 8) and studied according to the Student t test:

Population size 70 devices.

Mean value of the electropolymerisation charge 500 μC.

Standard deviation 71 μC.

Standard error 12 μC.

95% confidence interval 24 μC.

99% confidence interval 32 μC.

The mean value of the charge is 500 μC and 71% of the values are located between 450 and 550 μC (+/-20%).

4-Conductivity

4.1-procedure

Each transistor before each measurement is treated in 2 M sulfuric acid, first the potential is held at 0 V vs SCE for 1 min, this step is necessary to level the atmospheric oxidation[1] among our devices after the polymerisation.

The second step consists in the application of 0.35 V for 1 min. This step generates the conductive state of the polymer and is timed to allow the formation of emeraldine salt.

The last step is crucial to the signal amplification, the film is held at 0.2 Volts for 1 min. This potential was calculated from the average critical charge that can be observed in the charge against resistance plots from chapter 3.

After this potential treatment the measurements must be carried out within 1 minute.

4.2-statistics

The following statistics are obtained from the drain current values detected when a 30 mV drain voltage is applied between the two gold electrodes following the potential treatment described above. Here the gate potential is not maintained and is free to vary. The final stage of our experiment is the detection of *p*-aminophenol oxidation for which a different transistor will be used every time. Disposable transistors are only used as new and the initial conductivity is the only indication about the suitability of the device before the detection is carried out. Here we see that even if all the previous cleaning of the electrodes and electropolymerisation are kept under control, some important differences can be observed among our devices. The drain currents obtained after setting the gate potential of the polymer at 0.2 V vs. SCE with a 30 mV drain voltage, are shown in Figure 9. These

drain current intensities can be seen to vary from 300 to 650 μA. The average value is 455 μA and 40% of the transistors display an initial current value between 400 and 500 μA.

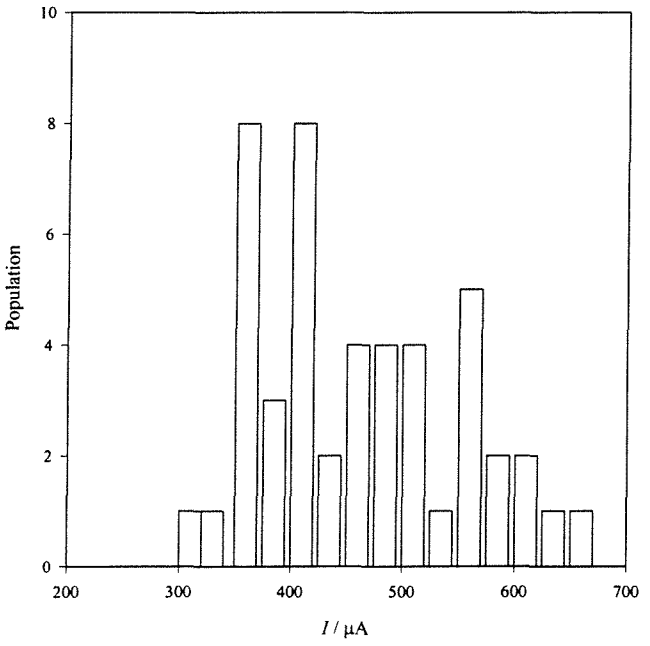

Figure 9: Displays the drain current through the transistors when 30 mV drain voltage is applied after the gate potential of the polymer transistor was set at 0.2 V vs SCE.

Population size 54 devices.

Mean value of the drain current intensity (30 mV drain voltage) 455 μA.

Standard deviation 88 μA.

Standard error 12 μA.

95% confidence interval 24 μA.

99% confidence interval 32 μA.

It is important to point out the population size is reduced to 54 transistors. These are the transistors that have been used for detection. 16 transistors have been discarded for several reasons such as having out of range drain currents or having their photoresist layer damaged, and their values were not included in the statistics.

The 7% variation needs to be taken into account for the calibration experiment.

5 Conclusion

These data describe the set of transistors that were used during our detection experiments. The difficulty to produce reproducible transistors in this work, could be greatly improved by studying the electrode configuration. In our case, we had to rely upon commercially available electrodes, and it was impossible to modify the devices in order to optimise the polymer deposition. Besides, the cost of these electrodes limited us in experimenting a large number of electro-polymerisation conditions. Also the cost of each electrode is related to the volume of units being fabricated, and it is interesting to note that were these electrodes produced in large quantities, there individual cost would drop drastically.

The transistors provide the signal amplification of our experiment. We shall now study the electrochemistry of *p*-aminophenol, which reduces the polymer.

1. Degani, Y. and A. Heller, *Direct electrical communication between chemically modified enzymes and metal electrodes.* Phys. Chem., 1987. **91**(6): p. 1285-1289.

Chapter 5 : The Mediator

Electrode processes consist of a chemical reaction involving a charge transfer across the interface between the electrode and the solution phase. Reaction will only take place with molecules within molecular distances of the electrode. Mass transport determines the rate supply of the reacting species to the electrode surface and the electron transfer reaction between the electrode and the molecules at the electrode surface determines how fast the reaction takes place once a reactive compound has reached the electrode surface.

The reactant diffuses to the electrode, undergoes charge transfer, and the product diffuses away from the electrode as new reactant comes to the electrode surface. Depending on the experimental conditions, other events may occur during this process. Chemical reactions may take place directly after the charge transfer occurs. The product may be unstable and decompose immediately after being generated, in some cases it may lead to adsorption of inert molecules on the electrode surface, resulting in electrode poisoning. All of these factors influence the overall rate of the electrode reaction.

Consider the ideal situation where both the reactant and the product are stable and highly soluble in the solvent used. In this case, if the product is recycled into reactant by a reverse reaction taking place in the solution, the current at the electrode may provide information about the kinetics of the recycling reaction. This requires that the charge transfer between the reactant and the electrode is well characterised.

These recycling reactions may be implemented by having redox enzymes reacting with the product of the electrode reaction, regenerating the initial reactant. In this situation, this reactant may be considered as a mediator to relay charges from the enzyme to the electrode. The current measured at the electrode becomes an indirect measure of the turn-over of the enzyme.

The enzyme will continue to transfer charge to the mediator only if the enzyme substrate is present in the solution. By transforming its substrate, the enzyme renews its charge and is able to transfer it to the mediator again.

The electrode reaction yielding oxidation or reduction current can be used to collect indirect information about the enzyme turn-over, and hence indirectly about the enzyme's substrate. The most successful example of this type of analysis is the electrochemical glucose sensor

published by Cass *et al.*[1]. The authors showed how the oxidation current for a ferrocene derivative can be related to the glucose concentration as glucose oxidase transfers electrons from glucose to ferricinium ion recycling it into ferrocene.

This experiment showed that this type of reaction could be used as the basis for sensors to detect enzyme substrates.

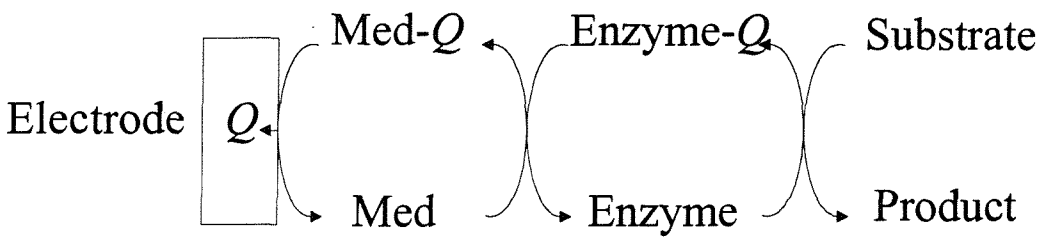

Figure 1: Illustration of the chain of reactions resulting in the charge transfer process. The redox enzyme is charged by transforming the substrate, the mediator is charged by the enzyme, the mediator transfers its charge to the electrode.

This concept was also adapted to immunoassays[2, 3]. In this case enzymes are covalently attached to antibodies. The aim of the experiment being to detect the concentration of antibodies in solution, the current from the mediator is related indirectly to the enzyme concentration, and hence to the antibody concentration. This in turn will be related to the concentration of antigen to which the antibody binds.

The implication of having enzymes and enzyme substrates in the solution where the electrode reaction takes place is difficult to evaluate where the mass transport and the electron transfer are concerned. A theoretical model was developed by Albery *et al.* [4] to relate the charge transfer at the electrode to the enzyme kinetics described in Figure 1. We use this model in chapter 7 to determine enzyme kinetic parameters by rotating disc voltammetry experiments.

But before any indirect information is interpreted from the reactant charge transfer at the electrode, the reactant reaction with the electrode must be thoroughly investigated.

1- *p*-aminophenol

Since it was first introduced as an electrochemical mediator by Thompson *et al.*[5] in 1991, *p*-aminophenol has been extensively used in the area of electrochemical immunoassays. Most antibodies are commercially available with alkaline phosphatase attached as a labeling agent. By using *p*-aminophenyl phosphate as a substrate for the enzyme, these protein conjugates can be used in electrochemical immunoassays without further modification. Several papers have been published reporting the degree of signal amplification that could be obtained by using *p*-aminophenol phosphate with alkaline phosphatase and recycling the electrode reaction product with another enzyme for this mediator at alkaline pH when used in electrochemical immunoassays [6-9]. Christie *et al.* showed that *p*-aminophenyl phosphate was very efficient for the detection of alkaline phosphatase in human serum by measuring the kinetic increase of *p*-aminophenol concentration in patient samples[6]. Ghindilis *et al.* described how alkaline phosphatase activity could be monitored with an oxygen electrode. In their work *p*-aminophenyl phosphate is hydrolysed to *p*-aminophenol by alkaline phosphatase. Then instead of detecting this product directly at the electrode, it is oxidised by laccase, which in turn reduces dissolved oxygen. The oxygen electrode detects the consumption of oxygen. In a subsequent step, quinone imine is recycled into *p*-aminophenol by glucose dehydrogenase. Again the authors show good calibration curves for their method but no detailed electro-analytical studies have been done[9]. Bier *et al.* published the same system as Ghindilis *et al.* applied to immunoassays [8]. Despite this interest in the use of *p*-aminophenol in assays, to the best of our knowledge no extensive work on the electrochemistry of *p*-aminophenol at neutral or alkaline conditions has ever been published. The articles related to *p*-aminophenol electrochemistry focus on the description of a variety of sensors without ever characterising *p*-aminophenol electrochemical properties: e.g. progesterone immunosensor in cows' milk[10] or an heterogeneous immunoelectrochemical sensor[11]. In each case the electrochemistry of *p*-aminophenol is only briefly sketched.

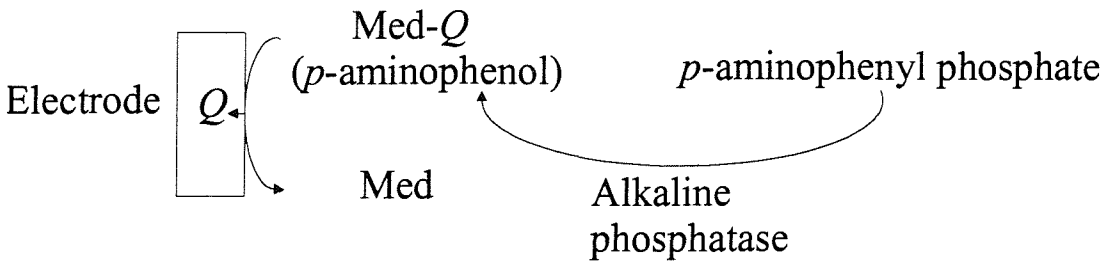

Figure 2: Illustration of alkaline phosphatase electrochemical detection. The mediator is the product of the enzyme reaction. In this case the mediator is generated by the enzyme.

A recycling reaction described in Figure 1 can be applied to the alkaline phosphatase reaction described in Figure 2. This combined system will generate a higher current, which can be used to detect lower concentrations of mediator[5, 9]. Thompson *et al.* reported zeptomolar detection [5].

The first issue we will address in this chapter is the stability of *p*-aminophenol.

1.1 Structure and mesomeric forms

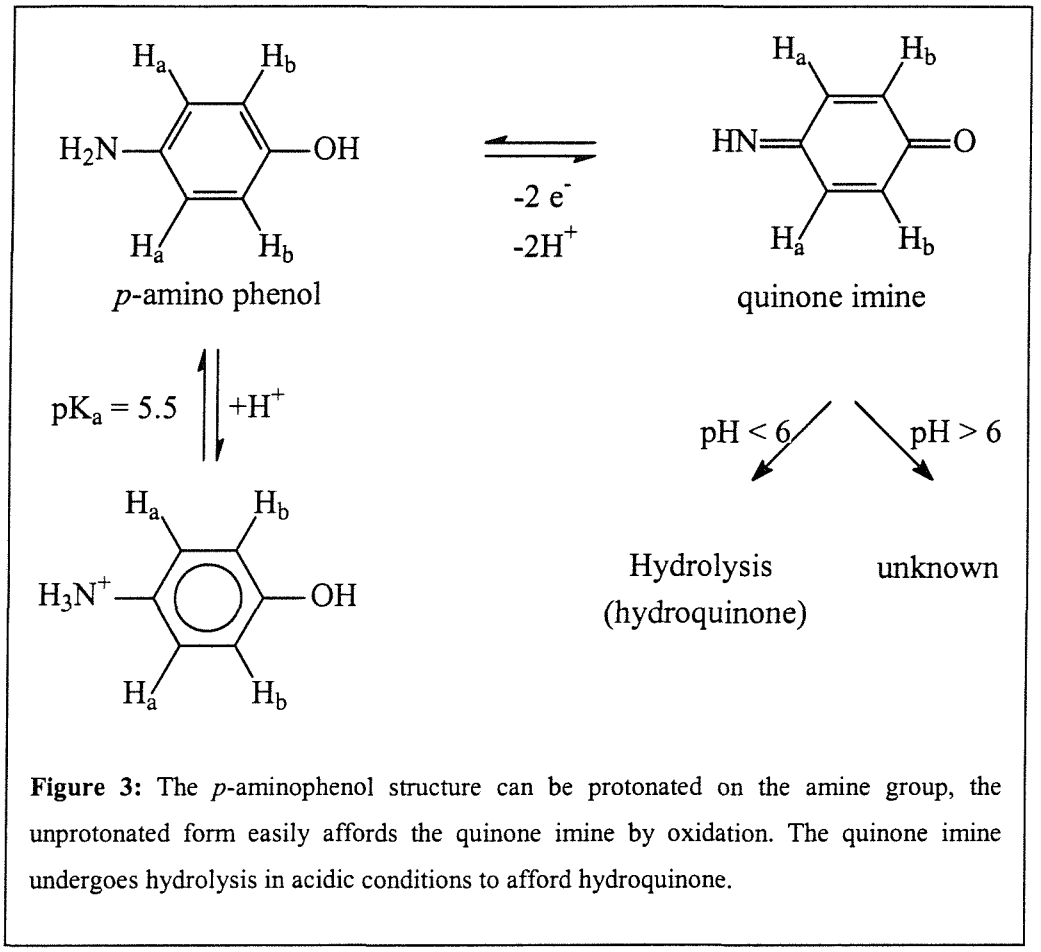

Figure 3: The *p*-aminophenol structure can be protonated on the amine group, the unprotonated form easily affords the quinone imine by oxidation. The quinone imine undergoes hydrolysis in acidic conditions to afford hydroquinone.

Both the hydroxyl and amine groups can act as electron donors and the molecule is conjugated. In acidic conditions, the protonation of the amine group prevents the delocalisation of one non bonding electron pair on to the aromatic ring. And the oxidation of the compound requires a higher potential.

In alkaline conditions one electron pair on the amine group and two electron pairs on the oxygen are free to delocalise on the aromatic ring as there is no protonation of the amine group.

The oxidation product, quinone imine, reacts according to different pathways depending on the pH. In acidic conditions (below pH 6), hydrolysis[12] was reported to take place affording hydroquinone. In alkaline conditions (above pH 6) the compound is reported to have a half

life of 15 min to 25 min depending on pH and buffering agent[5] but the reaction products have not been characterised although 1-4 addition of *p*-aminophenol on quinone is suspected[13].

1.2 Melting point and NMR

p-aminophenol was recrystalised under argon before use. The melting point reported in the literature is 188-190°C[14].
mp: 189°C under argon.

^{1}H-NMR (300 MHz, DMSO-d^{6}) δ 6.45 (q, 4H, $^{3}J_{Hb\text{-}Ha}$=13 Hz, $^{4}J_{Ha\text{-}Ha}$=9Hz). δ 4.4 (s, 2H, NH_2). δ 8.45 (s, 1H, OH).

^{13}C-NMR (300 MHz, DMSO-d^{6}) δ 115, C_{Ha}, C_{Hb}. δ 140. δ 145.

1.3 Hydrolysis process in acid

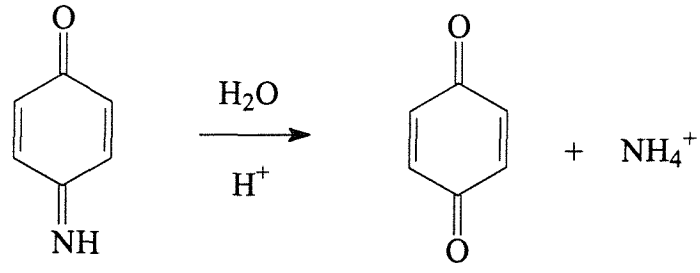

Figure 4: *p*-aminophenol hydrolysis is catalysed by protons. It is unclear whether the substitution with water is concerted. The reaction yields quinone and amonium ion[12].

The hydrolysis of quinone imine in acid was reported to be an irreversible pseudo-first-order reaction[15] for which the kinetic constants in acidic conditions were measured using several electrochemical techniques: cyclic chronopotentiometry, thin layer chronopotentiometry [12], spectroelectrochemical studies [16, 17], and chronopotentiometry with current reversal [18].

The possibility of water addition to quinone imine leading to *p*-hydroxyphenylhydroxylamine was put forward by Alberts and Shain [19] but ruled out by Hawley and Adams [13] who proved the formation of the quinone radical by EPR.

The hydrolysis constant ranges from 0.0194 s^{-1} in 0.5 M H_2SO_4 to 0.129 s^{-1} in pH 4 buffer. Above pH 5, no values are reported due to interference from side reactions that will be discussed next. The values were all measured at 25°C.

1.4 Reaction process in neutral and alkaline conditions.

In neutral and alkaline conditions, the amine group is deprotonated and oxidation by atmospheric oxygen takes place. It is assumed [13] that quinone is formed by hydrolysis and that *p*-aminophenol undergoes 1-4 additions with the quinone yielding 2,5-bis(4-hydroxyanilino)-*p*-benzoquinone and various other unidentified addition products. These seem to foul the working electrode during cyclic voltammetry experiments [5].

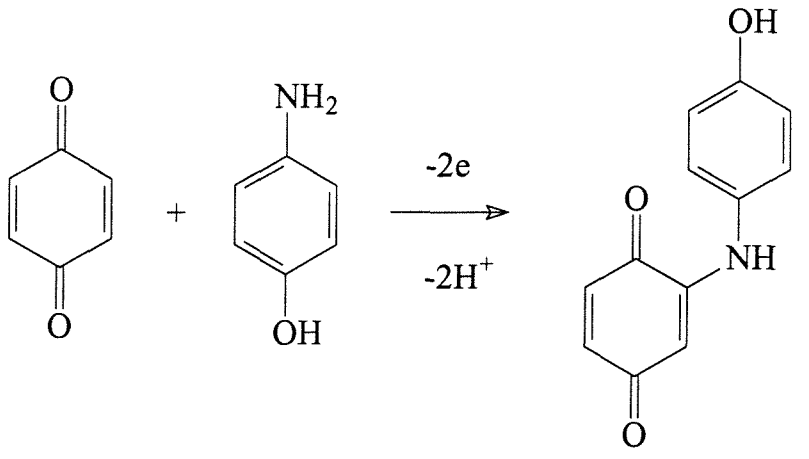

Figure 5: *Once quinones appear in the solution it is assumed that they react with the starting material. Nucleophilic 1-4 addition of the amine on the quinone is suspected[13]. Up to two p-aminophenol molecules can substitute on the quinone.*

1.5 p-aminophenol degradation in solution followed by UV spectroscopy.

The kinetics of this 1-4 addition would depend on the quinone concentration, which varies with the amount of oxygen in solution, the reaction does not take place when the solution is under argon bubbling. The effect of light was investigated, but does not seem to have any influence on the product in solution. The literature only provides half life estimates for *p*-aminophenol at alkaline pH from which oxidation constants are deduced. Thompson *et al.*[5] showed that the stability at pH 10 is influenced by the choice of buffer. Their research proved that ethanolamine and 2-(methylamino)ethanol prevent degradation for nearly 30 min, diethanolamine and 2-(ethylamino)ethanol for 20 min, tris-(hydroxymethyl)aminomethane (Tris) and triethanolamine hydrochloride for only 15 min. The study was carried out with 5 μM *p*-aminophenol solutions.

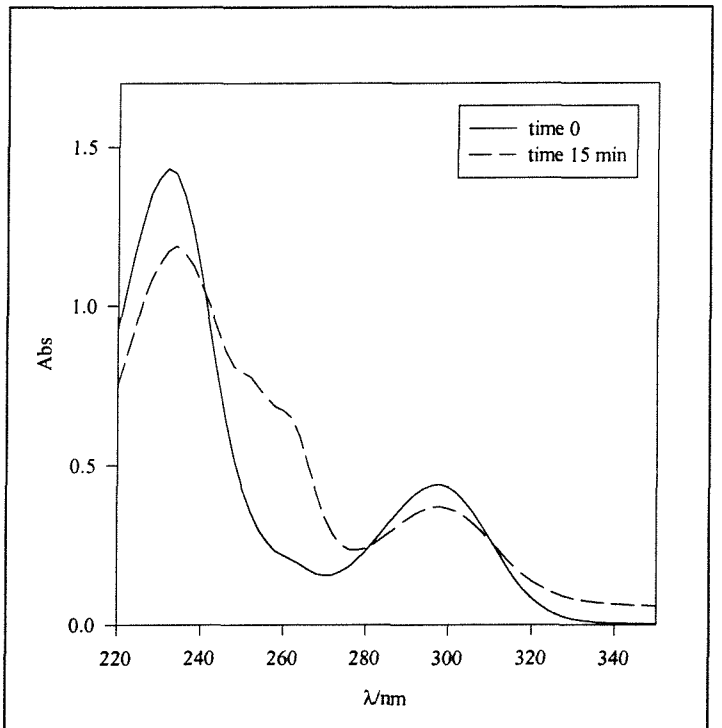

Figure 6: UV spectrum of 2 mM *p*-aminophenol at pH 9.6 unbuffered. Two main absorptions are observed at 240 and 300 nm, with time an absorption appears at 260 nm.

The UV absorption at 300 nm (Figure 6) is assigned to a para hydroxy substituted phenyl ring $\varepsilon = 200\ dm^{-3}\ mol^{-1}\ cm^{-1}$[20]. The 230 nm absorption is likely to account for both the para

amino and para hydroxy groups. The extinction coefficient is calculated from a diluted solution in order to obtain an absorbance value less than 1: ε = 1270 dm^{-3} mol^{-1} cm^{-1}. The absorption at 300 nm is very broad and does not allow us to observe the n to π^* transition from the quinone, but an absorption at 260 nm increases with time proving a structural modification of the compound in solution. This absorption appears, while the original clear solution becomes very dark showing a reaction process. The modification of the UV spectrum with pH was studied and will be discussed later. The spectral changes provide evidence for a reaction taking place in the presence of dissolved oxygen. A similar absorption signal evolution at 260 nm also was reported during the electrochemical reduction of *p*-benzoquinone[16].

In unbuffered distilled water, the evolution of *p*-aminophenol suggested by the changes in the spectrum takes place on a longer time scale. An attempt was made to purify the product of the reaction by leaving freshly recrystalised *p*-aminophenol in distilled water stirring over 48 h in air.

At the end of the reaction, a black precipitate was collected, filtered and dried under vacuum for three days. Thin layer chromatography on silica in ethyl acetate and 2% methanol showed two different compounds. The first being identified as starting material. The two species were separated on a silica column using ethyl acetate until all the starting material was eluted. 5% methanol were then added to the eluant, a brown solution was collected and dried on the vacuum line.

1.6 NMR of oxidation product:

The NMR spectrum was recorded in DMSO-d^6.

^{1}H NMR (400MHz): δ 10.1 (broad singlet, 1H), δ 9.1 (broad singlet, 3H), δ 7.18 (q, 4Har, J^3 = 14Hz, J^3 = 8.5Hz), δ 6.89 (q, 4Har, J^3 = 9Hz, $J^3_{Hb\text{-}Hb}$ = 7Hz), δ 6 (s, 1H), δ 5.58 (s, 1H).

2D ^{1}H NMR (400 MHz):

The coupling constants correspond to ortho couplings exclusively and no meta coupling is observed. This does not support the hypothesis of 1-4 Michael addition.

The two dimensional ^{1}H NMR displays only one proton-proton coupling between the two quartets at δ 7.18 and δ 6.89.

^{13}C NMR (400MHz): δ 155.224 (CR_4, Dept -ve), δ 154.852 (CR_4, Dept -ve), δ 151.601 (CR_4, Dept -ve), δ 131.978 (CR_4, Dept -ve), δ 130.663 (CR_4, Dept -ve), δ 125.487 (CH, Dept +ve), δ 124.984 (CH, Dept +ve), δ 116.173 (CH, Dept +ve), δ 116.142 (CH, Dept +ve), δ 115.983 (CH, Dept +ve), δ 115.726 (CH, Dept +ve), δ 94.837 (=CH, Dept +ve), δ 93.943 (=CH, Dept +ve).

1.7 The two dimension ^{1}H-^{13}C NMR shows:

-C δ 93.943 coupled with H δ 5.58 singlet.

-C δ 94.837 coupled with H δ 6 singlet.

-C δ 115.983 to116.173 coupled with 4H δ 6.89 quartet.

-C δ 124.984 and 125.487 coupled with 4H δ 7.18 quartet.

The carbon signals at δ 93 and δ 94 are non-aromatic and both are linked with one proton, their likely structure being alkyl CH functions.

The carbon signals at δ 116 are consistent with aromatic rings and the coupling indicates 4 CH. This situation is also observed with the carbons around δ 125. The ^{1}H NMR of the corresponding protons is consistent with aromatic protons but both quartets integrating 4 H each display 4 equal intensity signals where a para substituted ring would yield a 1, 3, 3, 1 quartet due to coupling between the two groups of equivalent protons.

1.8 Infrared spectrum:

A broad vibrational signal is observed at 3200 cm^{-1} assigned to secondary amide N-H stretch and amide NH_2. Several vibrations in the range 1500 to 1600 cm^{-1} are related to C-H and C=C vibrations of aromatic rings, they are as expected broad and unresolved and the spectrum is made even less clear by the signals of several benzene rings on the same

molecule. At 1700 cm^{-1} a very weak vibration signal is consistent with an αβ unsaturated ketone.

1.9 Mass spectrometry:

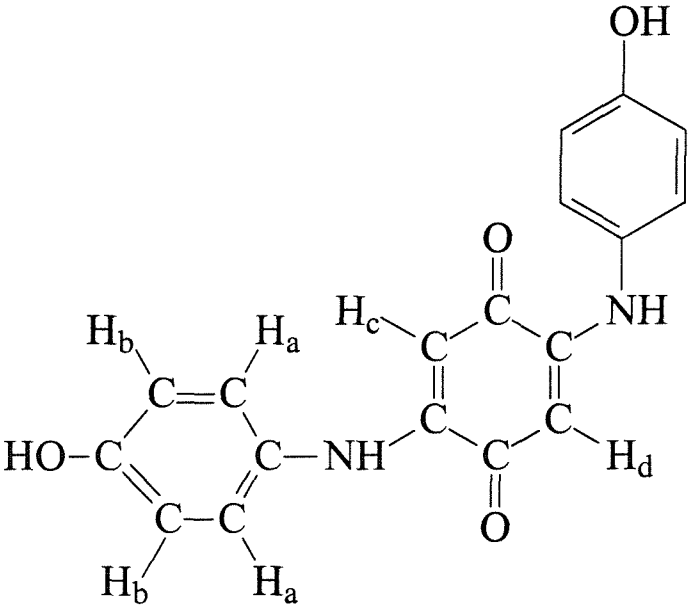

Figure 7: The 2,5-bis(4-hydroxyanilino)-*p*-benzoquinone structure suggested by Hawley *et al.*[13] is not consistent with our NMR data.

The electrospray MS analysis displayed different results in negative and positive ionisation. We observe signals at m/e = 800 and 391 in positive spray and no signal in negative spray. None of them correspond to the expected mass of M+1=323. Given the mass of the possible reagents: *p*-aminophenol M = 109, quinone imine M = 107, hydroquinone M = 110 or benzoquinone M = 108, the mass m/e = 391 can only be obtained by the breaking up of a benzene ring. This is unheard of.

1.10 Discussion:

The NMR and mass spectrometry are not consistent with the suspected product of 1-4 addition of *p*-aminophenol on quinone (Figure 7), it is unclear why the protons H_c and H_d have different signals since the molecule is assumed to be symmetrical. The three dimensional representation of the molecule does not display any difference between them. The quartets (δ 6.89 and δ 7.18 ^{1}H NMR) display equal intensity signals. The ortho coupling constants (J^3 = 8 Hz) and the lack of para coupling constants (J^4 = 3 Hz) rules out the possibility of a 1-4 Michael addition. The 4 symmetric protons on the same benzene ring should display a 1, 3, 3, 1 signal intensity quartet, and both ortho and para coupling constants. Another possibility is the condensation of oxidised benzoquinone observed during benzoquinone oxidation at pH 5[21].

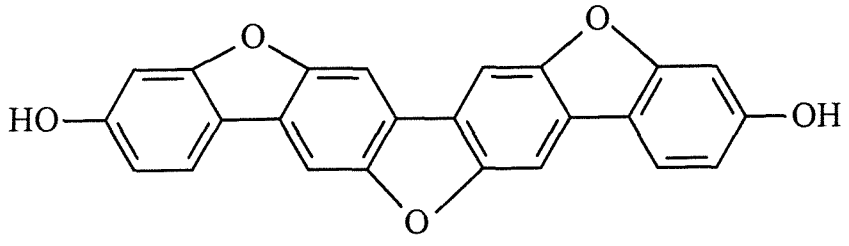

Figure 8: *Condensation product of oxidised benzoquinone suggested by Feng et al.*[21]

The formula shown in Figure 8 is closer to the mass spectrometry result (M/e = 364) and has non equivalent proton singlets. But this compound does not have any nitrogens and therefore does not correspond to the broad NMR signals we observe.

1.11 Conclusion

1-4 Michael addition is certainly not the right mechanism, but it is also clear that benzoquinone condensation is incorrect. Possibly a combination of both processes is taking place. Unfortunately, the analysis of the compound is inconclusive.

Having studied the evolution of *p*-aminophenol in solution, we will now try to characterise its electrochemistry in neutral and alkaline conditions where it is normally used for biochemical sensing.

2- Electrochemistry

Even though the EC mechanism of *p*-aminophenol electrochemistry in acid is a thoroughly documented subject[12, 13, 15, 18, 19], very little information is available about neutral and alkaline conditions.

2.1 Electrochemical processes

The mechanism of *p*-aminophenol electro-oxidation (Figure 9) described in the literature and presented above does not take into account the protonation of the amine group at acidic pH.

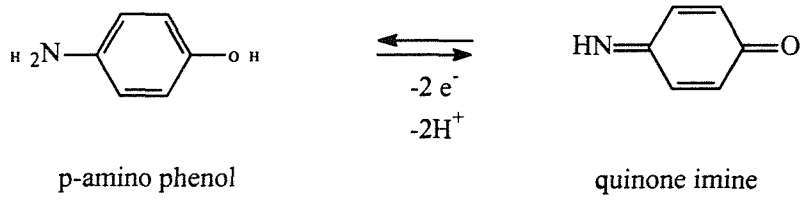

Figure 9: Oxidation reaction of *p*-aminophenol at the electrode at neutral and alkaline pH affording quinone imine, 2 protons and 2 electrons.

The cyclic voltammetry of *p*-aminophenol at pH 7.4 citrate buffer is shown in Figure 10.

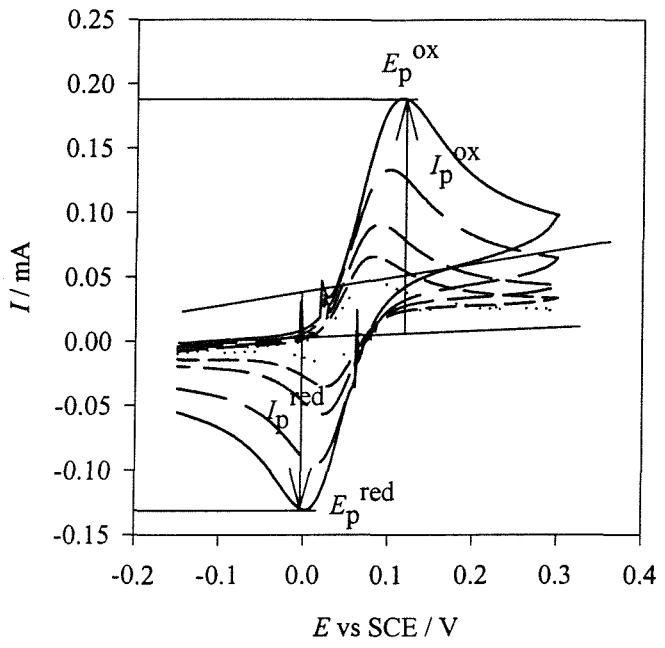

Figure 10: Cyclic voltammograms of *p*-aminophenol 1 mmol in pH 7.4 citrate buffer, 0.5 M KCl. 7 mm diameter platinum working electrode, the voltammograms were recorded at 5, 10, 20, 50, and 100 mV/s.

The voltammogram displays a low charging current (1 μA at 100 mV / s). The oxidation potential E_p^{ox} at 100 mV / s is 120 mV vs SCE and the reduction potential E_p^{red} is 0 V. With n being the number of electrons involved in the electrochemical process, the peak potential difference ΔE_p = 120 mV (100 mV / s) is higher than $59/n$ mV, therefore it is not a reversible system. In these conditions, the resistance of the solution is estimated to be 20 Ω (section 4.3), which means that the IR drop effect does not significantly affect these values ($\Delta E_{IR} \approx 7$ mV).

The maximum oxidation (Figure 10) current I_p^{ox} is 190 μA (100 mV / s) and the reduction maximum current I_p^{red} is 170 μA (100 mV / s), the ratio is close to unity (0.89).

The anodic and cathodic signals have similar shapes and the separation of peak potentials varies with the scan rate. These properties characterise our system as a quasi reversible system.

2.2 Electrochemistry at various pH

As proton exchange is part of the electrochemical process pH affects the electrochemistry of the compound. A shift of the redox potential can be observed when pH conditions are changed from acidic to alkaline.

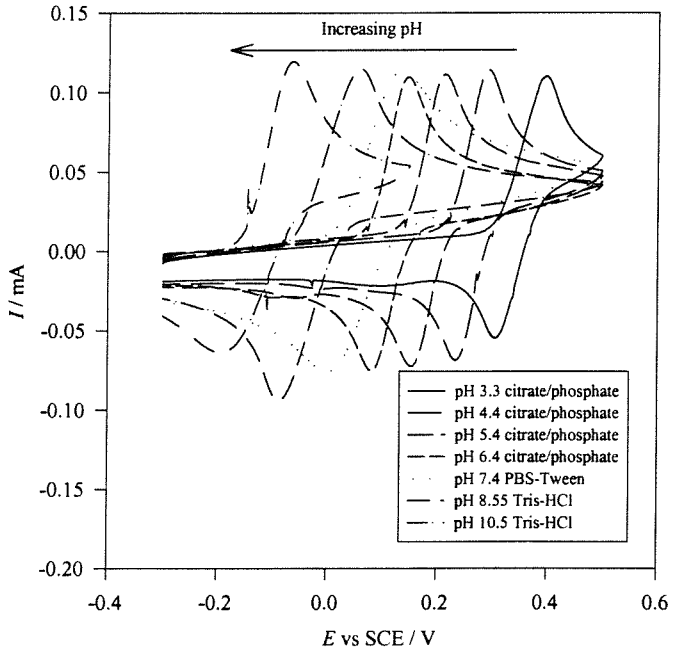

Figure 11: Cyclic voltammgrams at different pH. Currents where recorded in 1 mmol *p*-aminophenol solutions at 50 mV/s with a 7 mm diameter platinum working electrode. 0.1 M KCl.

The shift of the redox potential, $E_{1/2}$, with pH is linear from pH 1 to 6.5, and from 7.4 to 10.5 (Figure 12). The cyclic voltammetry retains a symmetric shape from acidic pH to pH 8.5. At pH 10.5 we observe a broad reduction peak and a sharp oxidation peak displaying a difference in kinetics between oxidation and reduction. The slower reduction process is understood by the kinetics of protonation at such an alkaline pH. At acidic pH we see similar

signals on both sweeps but the reduction signal displays a smaller intensity which seems to be compensated by an extra peak consistent with hydroquinone reduction (right hand side Figure 11). This second reduction reaction is no longer observed as pH becomes more alkaline and the reduction peak corresponding to quinone imine reduction has a larger intensity. The second reduction peak is consistent with hydroquinone reduction resulting from the hydrolysis of quinone imine[22].

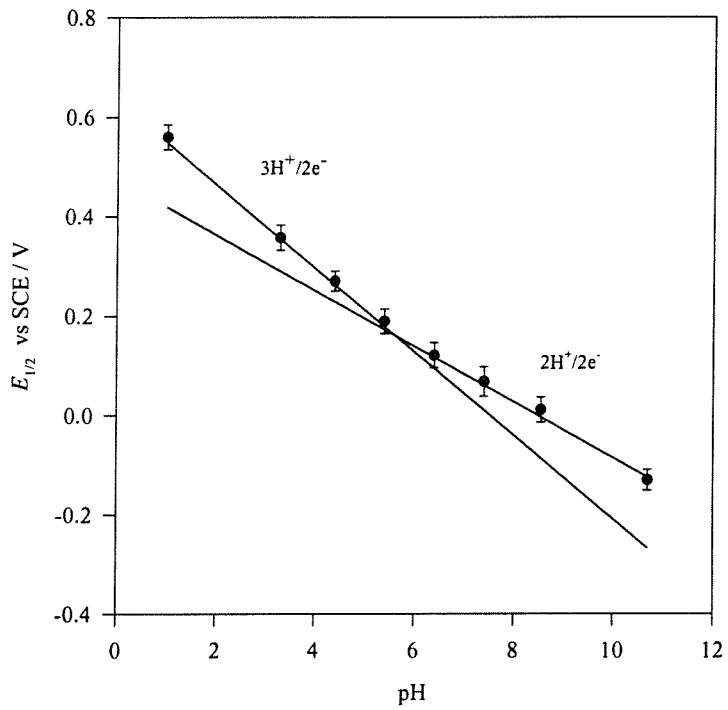

Figure 12: Variation of redox potential values against pH obtained from five sets of experiments. Regression lines are calculated for $E_{1/2}$ values for pH 1 to 5.4 and 7.4 to 10.5. The respective slopes are -84 mV and -58 mV / pH unit. Both correlation coefficients are better than to 0.99.

By plotting the redox potential $E_{1/2}$ from cyclic voltammetry against pH, we can investigate the effect of protonation on the redox potential Figure 12. According to the slope of $E_{1/2}$ vs pH, we are able to determine the pK_a of the compound. The slope of the shift in acidic conditions is -84 mV / pH unit and -58 mV from neutral to alkaline. The slopes were fitted with equation (2).

The Nernst equation shows that the slopes of the plots of $E_{1/2}$ vs pH depend on the number of protons exchanged during the electrochemical reaction.

$$\Delta E = \frac{RT}{nF} \log \Delta \left[H^+\right]^m \quad (1)$$

Where ΔE is the change of redox potential, $\Delta[H^+]$ is the change of proton concentration, the number of electrons exchanged is n and the number of protons is m. From equation (1) we obtain:

$$\Delta E = -\frac{0.056m}{n} \Delta pH \quad (2)$$

From equation (2) the slope for a $3H^+ / 2e^-$ reaction is -84 mV / pH unit and -56 mV for a $2H^+ / 2e^-$ process. The redox potentials displayed in Figure 12 were fitted with equation 3 using a $3H^+ / 2e^-$ exchange in the acidic part of the curve and $2H^+ / 2e^-$ exchange for the alkaline pH value.

The analysis of the redox potential according to pH suggests that the amine group of *p*-aminophenol is protonated below pH 5.4. Therefore this pK_a value should be verified by acid-base titration and the UV analysis of the compound.

2.3 pK_a titration

The titration of *p*-aminophenol.HCl in distilled water with NaOH is shown in Figure 13. We see a titration plot, as the volume of NaOH solution added is increased. At first the pH increases slowly from pH 4 to pH 6. As we approach the equivalence point the pH increases from 6 to 10 over a 1 ml addition of NaOH solution. In the third part of the plot the pH reaches 11 as NaOH volume is increased to 22 ml. No other equivalence point can be observed by further addition of basic solution (not shown).

The pKa is determined as corresponding to the pH value at the half volume of NaOH solution at the equivalence. The equivalence is determined by graphical methods pointing out the pH for which $C_{acid}\ V_{acid} = C_{base}.V_{base}$.

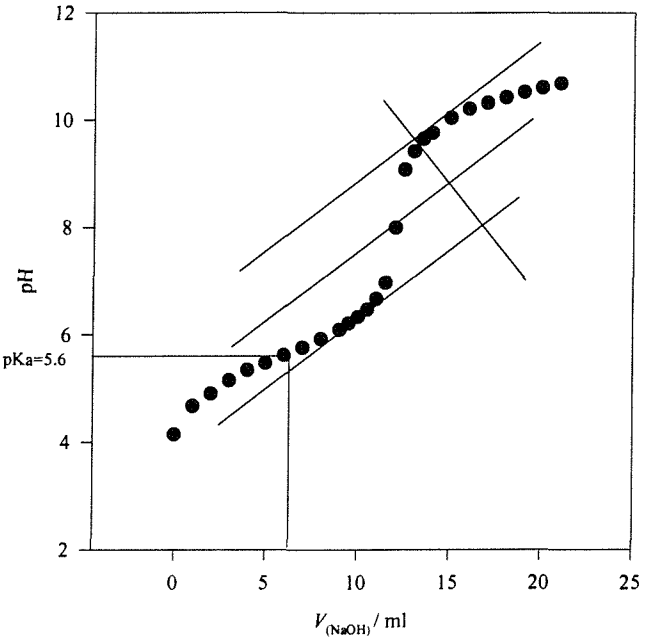

Figure 13: Titration of 25 ml *p*-aminophenol.HCl 4mM by NaOH 4.34 mM. The pH at the equivalence is determined by the parallel lines technique. Half the volume of NaOH at the equivalence determines the pKa = 5.6.

During the titration of *p*-aminophenol.HCl a deprotonation of the amine group is assumed to take place when pH is equal or above the pKa value. This structural modification of the compound implies changes in absorption that can be investigated through UV spectroscopy. The calculated pK_a is 5.6. The maximum pH value is 11, up to this value, we conclude that only one deprotonation is taking place.

A UV study was carried out through the titration experiment.

2.4 UV study

The UV spectra of *p*-aminophenol at different pH display two pairs of absorptions (Figure 14). One pair at 220 and 272 nm in acid is replaced by an other pair at 232 and 298 nm when the pH reaches the pKa value determined by titration (Figure 13). The shorter wavelength absorption at 200 nm remains unchanged.

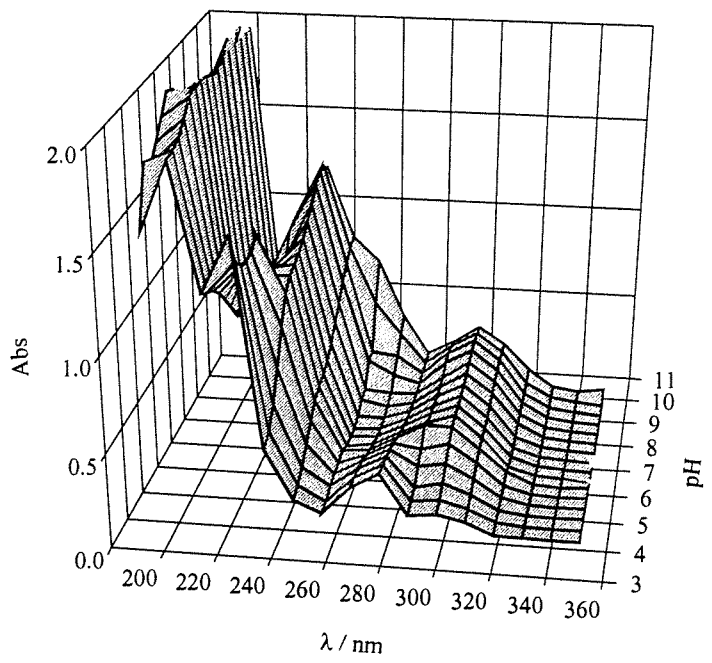

Figure 14: Three dimension graph showing the evolution of the UV spectrum with pH of *p*-aminophenol.

The pH independent signal near 200 nm is attributed to the aromatic ring. The absorption at 298 nm is assigned to a para hydroxy substituted phenyl ring. The 232 nm absorption accounts for both the para amino and para hydroxy electronic transition. The transition from the protonated to the unprotonated form results in two non bonding electrons now available for conjugation. It is generally accepted that conjugation has a bathochromic effect on the signal of the molecule [20]. Therefore we assume that both signals observed with the protonated form are shifted to longer wavelengths when deprotonation takes place at the pK_a.

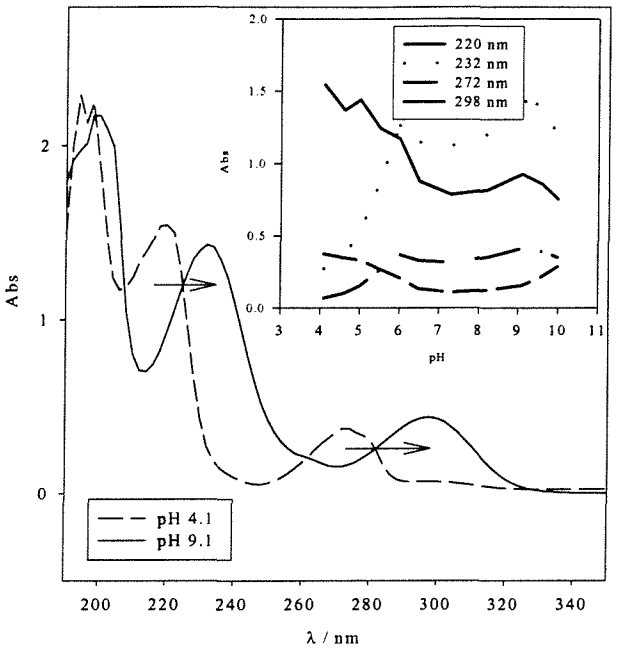

Figure 15: Two dimension representation of UV spectra during base titration. The inserted graph shows the cross over of the two pairs of peaks near the pKa value of *p*-aminophenol.

The two dimension projection of the UV spectra display isosbestic points at 225 nm and 285 nm the insert graph (Figure 15) clearly shows the shift of wavelength occurring over our estimated value of $pK_a = 5.5$.

A possible explanation for the modification of absorption above the pK_a value is supra-molecular aggregation in solution following deprotonation. In order to investigate if rearrangements such as dimerisation were involved, the same solution was succesively diluted in order to disrupt any molecular aggregates in solution.

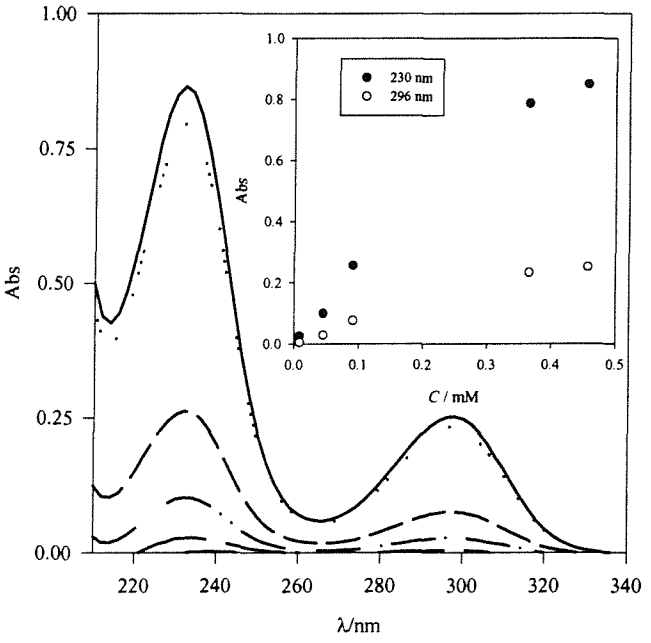

Figure 16: UV spectra of deprotonated *p*-aminophenol from 0.45 mM to 9 μM at pH 8. The insert graph shows absorption intensity against concentration.

The dilution of a solution of *p*-aminophenol in the unprotonated state yields a smaller absorption as expected. The insert graph (Figure 16) shows that the loss of absorption is not linear with dilution above 0.2 mM. But no modification of wavelength can be observed throughout the dilution experiment.

We divide the absorption by the concentration in each spectrum from Figure 16. The result is a plot of the extinction coefficient for each solution against the wavelength (Figure 17). The change of extinction coefficient from one concentration to another reveals supra-molecular aggregates in solution.

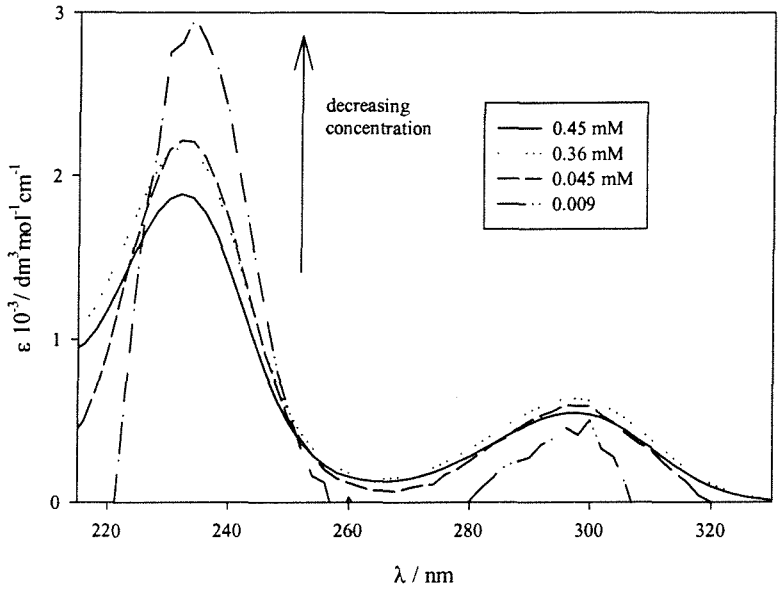

Figure 17 Extinction coefficients of deprotonated *p*-aminophenol from 0.45 mM to 0.9 μM at pH 8. The insert graph shows absorption intensity against concentration.

Figure 17 shows the extinction coefficient of *p*-aminophenol at pH 8 against the wavelength. This graph clearly shows an increase of the extinction coefficient value at 235 nm when the concentration decreases. At 300 nm, there is no clear evolution of ε with the change of concentration. This evidence suggests that *p*-aminophenol forms supra-molecular aggregates in solution. These tend to dissociate as the concentration decreases.

The absorption at 235 nm is assigned to the aromatic ring, whereas the absorption at 300 nm is assigned to the amine and para hydroxy groups. The change of extinction coefficient with concentration at 235 nm implies that the rearrangement affects the arromatic ring, but does not affect the amine and hydroxy groups as the extinction coefficient at 300 nm remains unchanged when concentration is varied.

During the electrode oxidation of *p*-aminophenol, the electron transfer triggers a molecular rearrangement. If the reagent is arranged in dimers or trimers, the electron transfer will induce a supra-molecular rearrangement in addition to the molecular rearrangement. A possible consequence of *p*-aminophenol undergoing both molecular and supra molecular rearrangements during the electron transfer reaction at the electrode surface, is slower electron transfer kinetics.

This implies that the electron transfer rate constants may vary with *p*-aminophenol concentration because the later is responsible for the formation of supra molecular structures in solution.

2.5 Conclusion

In this section, we characterised three states of *p*-aminophenol according to pH (from pH 0 to pH 12) and potential. These were confirmed by electrochemistry, UV spectroscopy and base titration.

3- Electrolysis experiments

To verify that the electrochemistry of *p*-aminophenol always involves a two electron process in any pH conditions, the electrolysis of the compound was carried out in acid, neutral and alkaline conditions.

3.1 Electrolysis at pH 4.5 citrate / phosphate buffer.

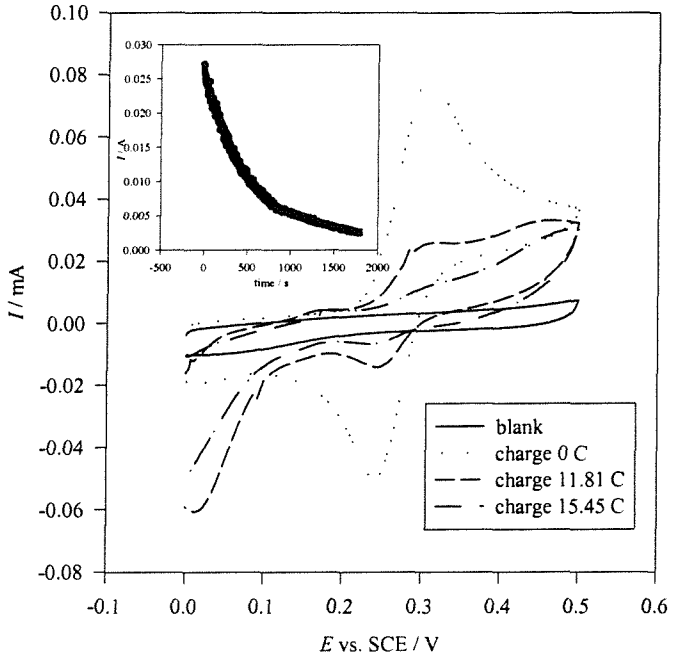

Figure 18: Cyclic voltammetry of *p*-aminophenol 0.5 mM (130 ml) in degassed 0.5 M KCl, pH 4.5 citrate/phosphate buffer 0.1 M. The working electrode is 7 mm platinum disc and counter is platinum mesh. The scan rate is 50 mV / s. Voltammograms are recorded without *p*-aminophenol in solution (blank), before any charge is passed, after 11.81 C oxidation charge is passed and finally when 15.45 C have been passed. The electrolysis is achieved by setting the potential at 0.35 V with a 5 cm x 5 cm platinum mesh electrode. The electrolysis current transient is shown in the insert.

Figure 18 shows cyclic voltammograms for *p*-aminophenol recorded before, during and after the electrolysis experiment. The electrolysis was stopped after 1800 s. The charge was obtained by integrating the current against the time from the insert figure.

The experiment is carried out using a divided cell where the counter electrode is separated by a glass frit.

The current intensity from the cyclic voltammetry experiment at charge 0 C is considered as 100 % of 0.5 mM *p*-aminophenol solution. The following experiments give different current intensities at the same potential, these intensities are converted to molar values by referring to the 100 % equivalent, which is 0.5 mM. Converting the corresponding charge to electron moles the ratio electron / molecule could be estimated at 2.2 e^- / molecule. The theoretical

value should be 2 e^- / molecule. The difference may be explained by experimental error or/and a contamination by the catholyte.

The oxidation hydrolysis of quinone imine into benzoquinone is taking place. We can observe an oxidation signal at 0.45 V and a reduction signal at 0.01 V showing the increasing concentration of the benzoquinone / hydroquinone system[23, 24] when the electrolysis charge reaches 11.81 and 15.45 C.

3.2 Electrolysis at pH 7.4

Following the same protocol, a ratio of $2e^-$ / molecule was calculated from the electrolysis in buffer PBS-Tween pH 7.4.

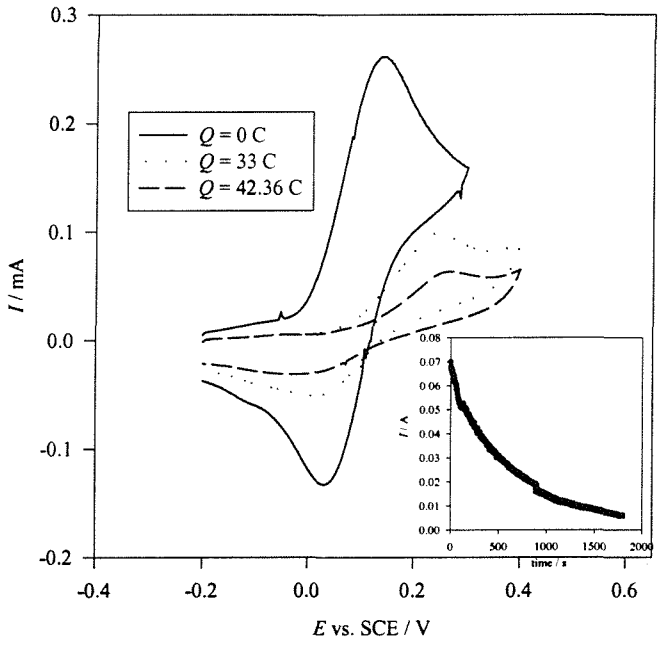

Figure 19: Cyclic voltammetry of *p*-aminophenol 2.11 mM (130 ml) in degassed 0.5 M KCl, pH 7.4 PBS-Tween buffer 0.1 M. The working electrode is 7 mm platinum disc and counter is platinum mesh, the scan rate is 50 mV / s. Voltammograms are recorded before any charge is passed, after 33 C oxidation charge is passed and finally when 42.36 C have been passed. The electrolysis is achieved by setting the potential at 0.2 V with a 5 cm x 5 cm platinum mesh electrode. The electrolysis current transient is shown in the insert.

The cyclic voltammetry during the electrolysis at pH 7.4 displays a potential shift of the oxidation potential. The electron per molecule ratio for each of the voltammograms remains $2e^-$ / molecule. As we saw in Figure 24, pH 7.4 represents a critical value for the electrochemistry of *p*-aminophenol.

The UV spectrum remains unchanged before and after the experiment (data not shown).

3.3 Electrolysis at pH 10.5

At alkaline pH the solution has to be carefully degassed before and during the experiment. This is achieved by maintaining a large argon flow through the cell while the electrolysis takes place. It seems that the absence of atmospheric oxygen prevents rapid degradation of *p*-aminophenol.

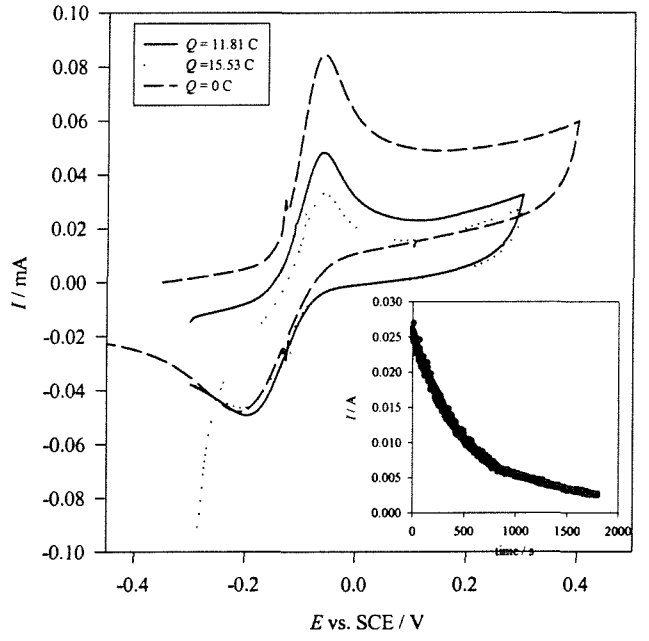

Figure 20: Cyclic voltammetries of *p*-aminophenol 0.5 mM (130 ml) in degassed 0.5 M KCl, pH 10.5 Tris-HCl buffer 0.1 M. The working electrode is 7 mm platinum disc and counter is platinum mesh, the scan rate is 50 mV / s. Voltammograms are recorded before any charge is passed, after 11.81 C oxidation charge is passed and finally when 15.53 C have been passed. The electrolysis is achieved by setting the potential at 0.15 V with a 5 cm x 5 cm platinum mesh electrode. The electrolysis current transient is shown in the insert.

The electrolysis at alkaline pH gives a ratio of $2e^-$ / molecule. When 15.53 C have been passed we see a reduction current at the beginning of the voltammetry. This is due to the product being now mainly in its oxidised form, the starting potential for the cyclic voltammetry reduces the compound. But the electron per molecule ratio is unchanged through out the experiment.

3.4 Conclusion

This section shows that *p*-aminophenol electrochemistry always involves a two electrons oxidation process. Whether *p*-aminophenol is protonated or not, does not affect the number of electrons involved.

4 Electron transfer kinetics at various pH

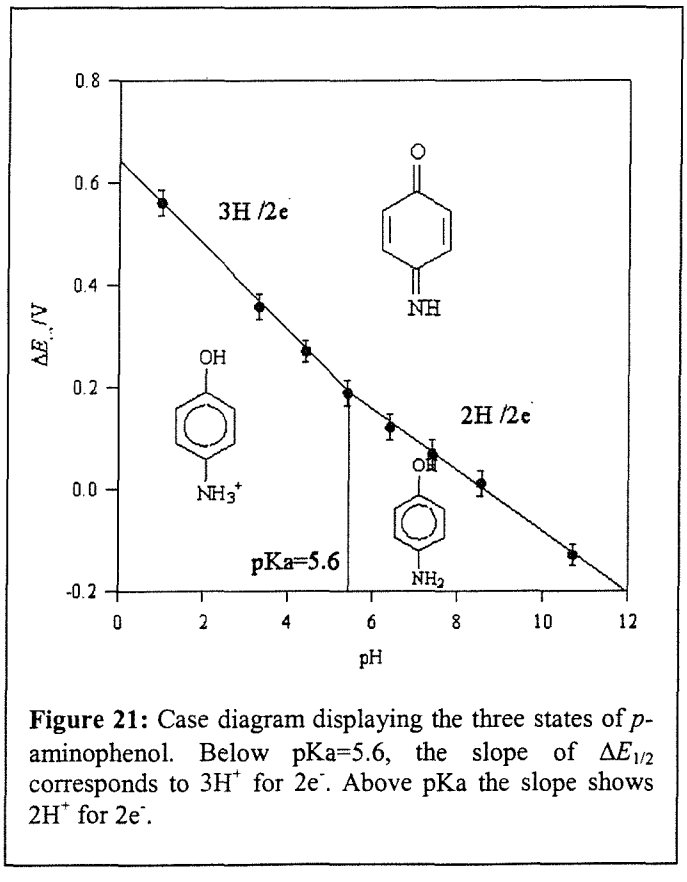

Figure 21: Case diagram displaying the three states of *p*-aminophenol. Below pKa=5.6, the slope of $\Delta E_{1/2}$ corresponds to $3H^+$ for $2e^-$. Above pKa the slope shows $2H^+$ for $2e^-$.

Figure 21 summurises the information obtained from cyclic voltammetry, base titration, electrolysis and UV study. It shows the three states of *p*-aminophenol according to pH and potential.

We shall now study the kinetics of the electrochemistry of *p*-aminophenol. To do so, we first characterise the diffusion coefficient at pH 7.4 using rotating disc voltammetry.

4.1 Diffusion coefficients

The diffusion coefficient of *p*-aminophenol was accurately determined at 25 °C by rotating disc voltammetry experiments. The maximum currents were plotted against the square root of the rotation speed and the diffusion coefficient was calculated from the slope according to the Levich equation.

$$I = 1.554nF\nu^{-1/6}CD^{2/3}W^{1/2}A \qquad (3)$$

Where I is in amps, n is the number of electrons transferred hence $n = 2$, F is the Faraday constant 96484 C mol^{-1}, C is the concentration of *p*-aminophenol in mol cm^{-3}, D is the diffusion coefficient in cm^2 s^{-1}, W is the rotation speed of the electrode in Hz, A is the electrode area in cm^2, and ν is the kinematic viscosity of the solution.

The kinematic viscosity of PBS-Tween was compared to that of water by the dropping ball method[25], and no significant difference was observed.

Two sets of experiments were carried out under identical conditions using both glassy carbon and platinum rotating disc electrodes.

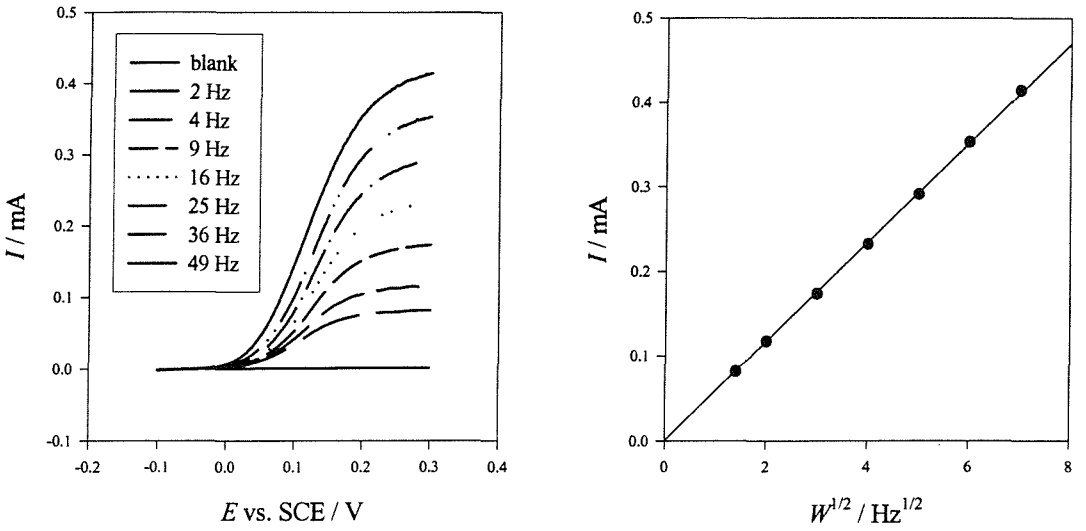

Figure 22: Shows the current against potential obtained for a 0.5 mM *p*-aminophenol solution, 0.5 M KCl, pH 7.4 PBS 0.1 M at various rotation speeds. SCE reference, platinum counter and 7 mm diameter glassy carbon electrode. The plot displays the maximum current values plotted against the square root of the rotation speed and their corresponding regression line passing through the origin. Slope 5.864 10^{-5} A $Hz^{-1/2}$.

From the Levich equation, the following diffusion coefficients were determined with a glassy carbon rotating disc electrode:

C / mM	**0.2**	**0.5**	**1**
D / cm^2 s^{-1}	**8.57×10^{-6}**	**1.02×10^{-5}**	**7.76×10^{-6}**

Table 1: Diffusion coefficient values calculated from the slope of the regression line for each concentration of *p*-aminophenol in 0.5 M KCl, pH 7.4 PBS 0.1 M, using a glassy carbon rotating disc electrode at 25°C.

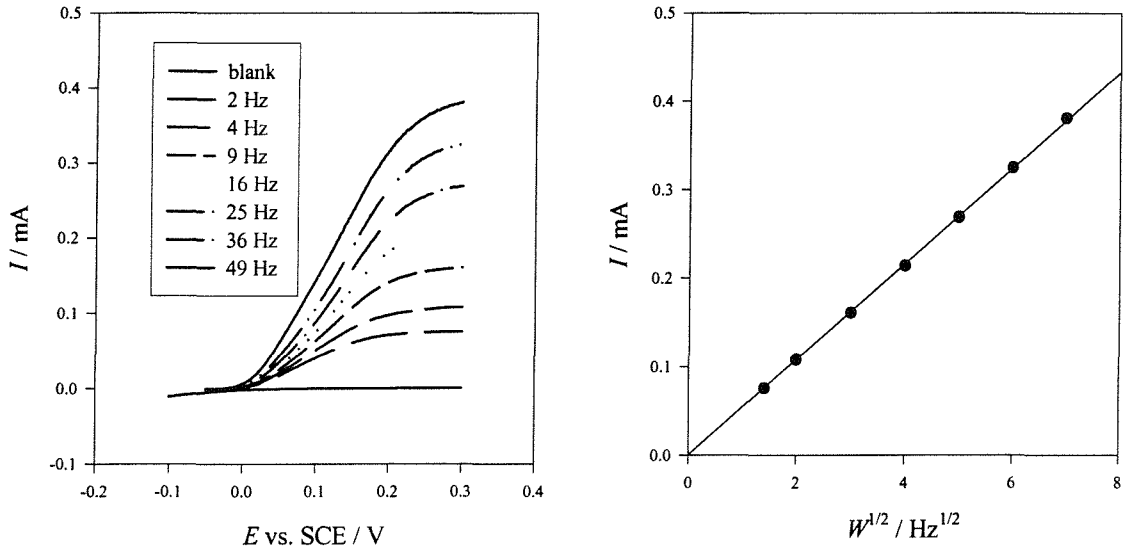

Figure 23: Shows the current against potential obtained for a 0.5 mM *p*-aminophenol solution, 0.5 M KCl, pH 7.4 PBS 0.1 M at various rotation speeds. SCE reference, platinum counter and 7.01 mm diameter rotating disc platinum electrode. The plot displays the maximum current values plotted against the square root of the rotation speed and their corresponding regression line passing through the origin. The slope is $5.405\ 10^{-5}$ A $Hz^{-1/2}$.

The currents recorded during the experiments start increasing at 0 V and reach a maximum value near 0.2 V. The current increases linearly over 200 mV from 0 V to 0.2 V. A fast electrochemical system like ferrocyanide in KCl solution will have a current rise over 56.4 mV at 290 K reaching a plateau[26]. By comparison, *p*-aminophenol is a slow electrochemical system.

The same experiment was repeated for different concentrations of *p*-aminophenol and the following diffusion coefficient values were calculated using a platinum rotating disc electrode:

C / mM	0.2	0.5	1
D / cm^2 s^{-1}	8.34×10^{-6}	9.06×10^{-6}	8.06×10^{-6}

Table 2: Diffusion coefficient values calculated from the slope of the regression line for each concentration of *p*-aminophenol , 0.5 M KCl, pH 7.4 PBS 0.1 M with a platinum rotating disc electrode at 25°C.

These values are consistently higher than the diffusion coefficient measured by Robinson *et al.* at pH 7.4[27], which was 6.6 x 10^{-6} cm^2 s^{-1}. The difference between our values and the published results may be explained by the use of different experimental methods. Robinson *et al.* used the chemical as received from the supplier in a flow injection device producing a measurement over 10 h. From the results in this work, we showed that *p*-aminophenol has to be freshly sublimed and solutions above pK_a have to be replaced after 15 min. Otherwise secondary reactions occuring in the solution bring the concentration of *p*-aminophenol below its initial value. Their value is lower, because of dividing the current by a concentration, which is higher than the real value.

4.2 Different types of buffer

The peak separation in *p*-aminophenol cyclic voltammograms is highly influenced by the pH (Figure 24). We observe a 70 mV separation between the oxidation and the reduction peaks from pH 3.3 up to pH 7.5. pH 7.5 shows an important variation for all types of buffers whether glassy carbon or platinum electrodes are used. Beyond this pH value the peak separation is close to 120 mV up to pH 10.5.

Some variations are observed when comparing different buffer species at the same pH. Phosphate buffer displays consistently smaller ΔE_p values than the corresponding pH citrate buffer. Also PBS-Tween at pH 7.4 has the same ΔE_p as Tris-HCl for higher pH values. In the case of PBS-Tween, dodecanoic acid ($C_{12}H_{24}O_2$) causes the peak separation to be higher than in the corresponding phosphate buffer. From simulation experiments described in the last section of this chapter, we found that Tween may induce a large solution resistivity, which would account for the 120 mV peak separation. Another possibility is that Tween may partially passivate the electrode inducing slower electrode kinetics.

Nonetheless it is essential for us to determine the conditions in PBS-Tween because it is a common buffer for immunoreactions.

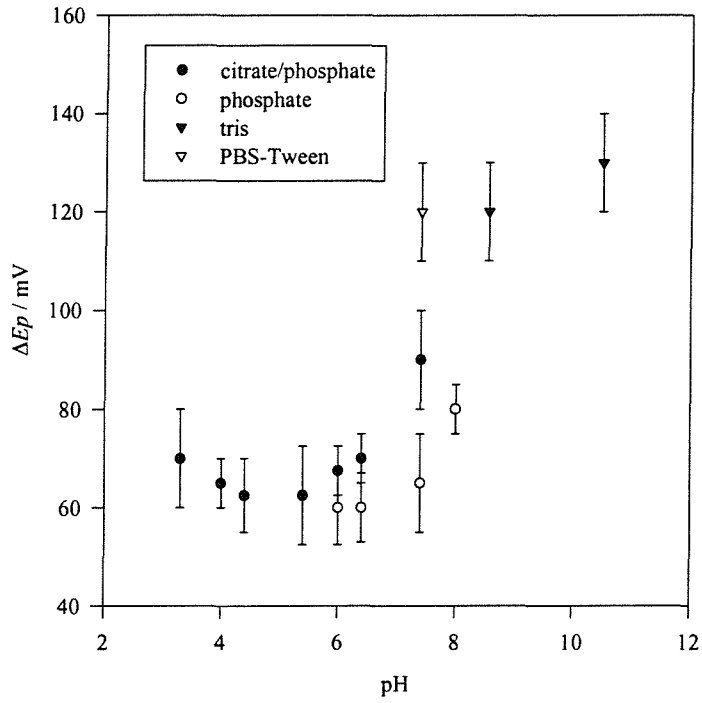

Figure 24: plot representing ΔE_p values obtained from cyclic voltammetry at 50 mV/s of 1 mM solutions of *p*-aminophenol 0.1 M KCl at various pH values and various buffering agents all at 0.1 M. The potential difference between the oxidation peak and the reduction peak are plotted against pH. Standard errors are calculated from 5 sets of data obtained with both glassy carbon and Pt working electrodes.

We notice that the pK_a does not influence the peak separation, this confirms that protonation of the amine has no effect on the electrode kinetics. The change of peak separation at pH 7.4 does not correspond to the pK_a value of *p*-aminophenol, therefore does not seem to be related to the protonation of the amine group. The peak separation in PBS-Tween is 120 mV, by simulation (section 4) we could reproduce this peak separation by assuming a solution resistivity over 100 Ω, which is probably due to the Tween surfactant. Nonetheless we can not assert that this effect is due to resistivity of the solution as it could also be the result of electrode coating by the surfactant (Tween). This value may not reflect a change in electron

transfer rate constant. In both citrate and phosphate buffers, we observe an increase of the peak separation near pH 7.4.

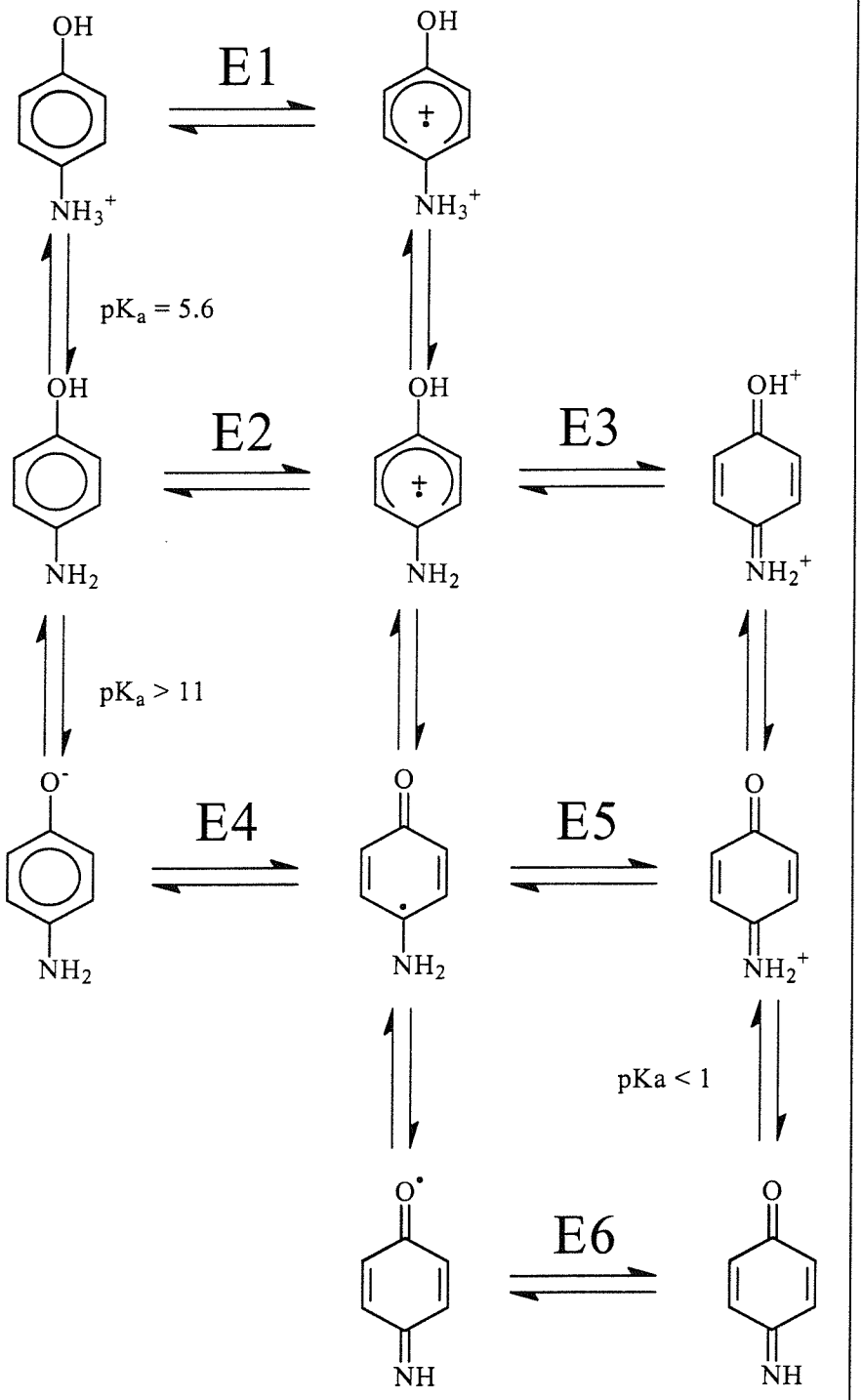

Figure 25: Square scheme diagram for *p*-aminophenol electrochemistry. Electrochemical steps are represented horizontally and chemical steps are represented vertically.

To explain this change, the scheme of squares for the reaction (Figure 25) is studied. Chemical steps are represented vertically and electrochemical steps are represented horizontally.

Figure 25 displays the different mechanistic pathways that may be involved in *p*-aminophenol oxidation. Protonated *p*-aminophenol (top left) is present in solution when the pH is kept below the pK_a = 5.6. Above pK_a *p*-aminophenol is mainly in its deprotonated form (middle left). These are the only two forms we could observe as deprotonation of the hydroxy group did not occur below pH 12 (Figure 13) during the titration experiment.

From pH 7 to pH 10, on the basis of the UV-spectrum (Figure 14), we assume that deprotonated *p*-aminophenol is the main reagent in solution. When the oxidation potential is reached by the working electrode the product of the electrode reaction is quinone imine (bottom right). To form quinone imine by electrochemical oxidation of deprotonated *p*-aminophenol a one electron oxidation step (E2) should take place to form *p*-aminophenol radical cation. At this stage another one electron oxidation step may take place (E3), or a deprotonation. If E3 occurs directly after E2, this should be followed by two chemical steps consisting in two deprotonation steps leading to quinone imine. This being an E2E3CC mechanism.

If deprotonation occurs directly after E2, the next step may either be E5 followed by a deprotonation, or a second deprotonation followed by a second one electron oxidation step. This leads respectively to either E2CE5C and E2CCE6.

The change in peak separation between pH 7 and pH 8 may be due to a change of mechanism as the reaction would change from EECC where both electrons are transfered one after the other leading to a fast electrode oxidation, to ECEC, in which the kinetics of the chemical reaction slows the second electrochemical step.

The hypothesis for the oxidation of *p*-aminophenol is E2E3CC between pH 5.6 (pKa) and pH 7.4, then E2CE5C above this pH value. The chemical step slows the electron transfer kinetics, this is reflected by a larger peak current separation.

To explain the change of electron transfer kinetics between pH 7 and pH 8, another hypothesis may be formulated on the grounds of UV-spectroscopy evidence. The spectra of diluted solutions of *p*-aminophenol at pH 8 (Figure 16) showed an evolution of the extinction

coefficient for the absorption signal assigned to the benzene ring with concentration (Figure 17). This result suggests the formation of supra-molecular aggregates of *p*-aminophenol in pH 8 solution. A possible effect of such aggregates is the diminution of electron transfer kinetics during the electrode reaction of the compound, as explained earlier. The new hypothesis is that such aggregates are only formed above pH 7.4. To verify this hypothesis, a new set of spectra of *p*-aminophenol diluted solutions was recorded in pH 6 phosphate buffer. pH 6 is chosen because it is close to the pK_a = 5.6 and we saw (Figure 14) that at this pH, the absorption of both the protonated and unprotonated species are observed.

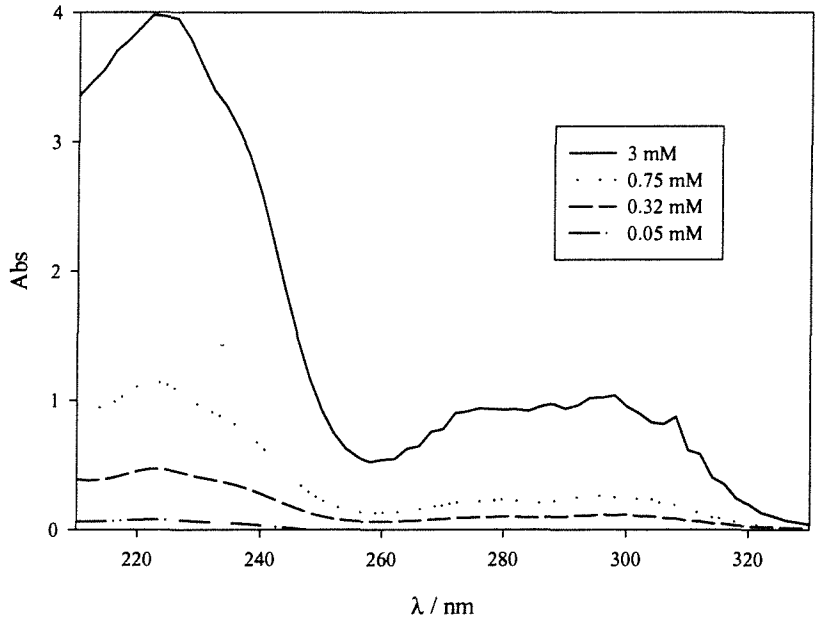

Figure 26: UV spectra of deprotonated and protonated *p*-aminophenol from 3 mM to 50 μM in pH 6 phosphate buffer.

Figure 26 shows the UV-spectra of different dilutions of *p*-aminophenol in pH 6 phosphate buffer. As commented for Figure 15 we see an absorption signal at 220 nm assigned to the benzene ring of protonated *p*-aminophenol, and we see an absorption at 235 nm assigned to the benzene ring of deprotonated *p*-aminophenol. Two other absorptions are observed at 280 and 300 nm these are assigned to the amine and hydroxy groups of respectively protonated

and deprotonated *p*-aminophenol. By dividing the absorption values by the corresponding concentrations, we obtain the plot of extinction coefficient against wavelength (Figure 27).

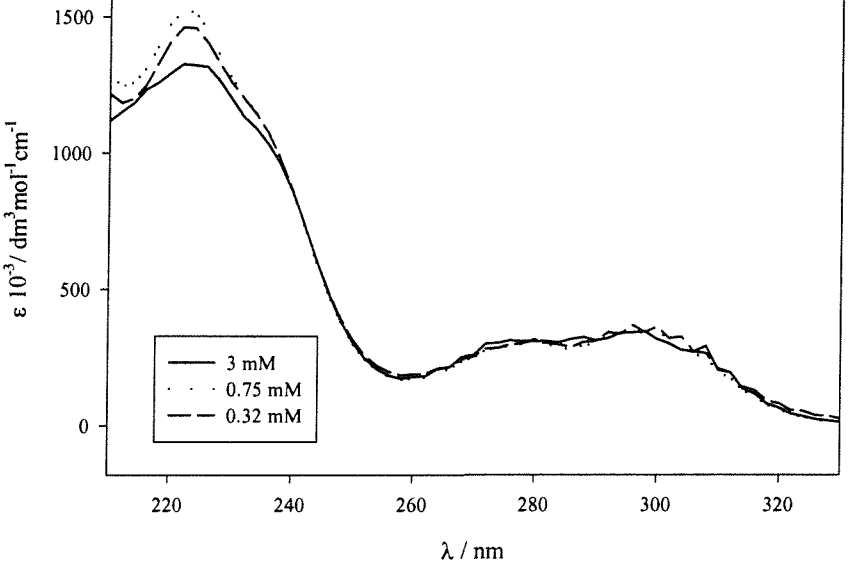

Figure 27: Extinction coefficients of deprotonated and protonated *p*-aminophenol from 3 mM to 50 μM in pH 6 phosphate buffer.

In Figure 27 the extinction coefficient is plotted against the wavelength, we do not see a systematic increase or decrease of the extinction coefficient with the change of concentration at 220 and 230 nm. Besides, we see an overlap of the plots for all three concentration at 280 and 300 nm.

This result suggests that supra-molecular aggregates is not taking place at pH 6, whereas it does occur at pH 8. This phenomenon may also be involved in the increase of redox peaks separation from pH 7 to pH 8 (Figure 24). However, a spectroscopic study would be needed for this hypothesis to be verified, and the eventual supra-molecular structures to be characterised.

4.3 Electrochemical rate constants

In order to study electron transfer kinetics, solutions of several pH using several buffers were used. In each solution cyclic voltammetry was carried out from 5 to 100 mV/s. By studying the shape of the current voltage curves, the influence of the pH as well as the choice of buffer can be evaluated. The reason for using cyclic voltammetry instead of rotating disc voltammetry to determine these constants is the unstability of *p*-aminophenol over the time scale of the rotating disc experiment at the various pH values. The accuracy of the results depends on precise concentration values that may not be maintained over 15 min in alkaline conditions.

Figure 28 shows two experiments at pH 7.4 with (left) a phosphate/citrate buffer and (right) a phosphate buffer. The current voltammograms show similar oxidation and reduction peaks in both cases. The voltammogram in citrate buffer is broader than in phosphate but the redox potential of the analyte is the same in both solutions. This may reflect different electron transfer kinetics that are studied through the ΔE_p values at each scan rate.

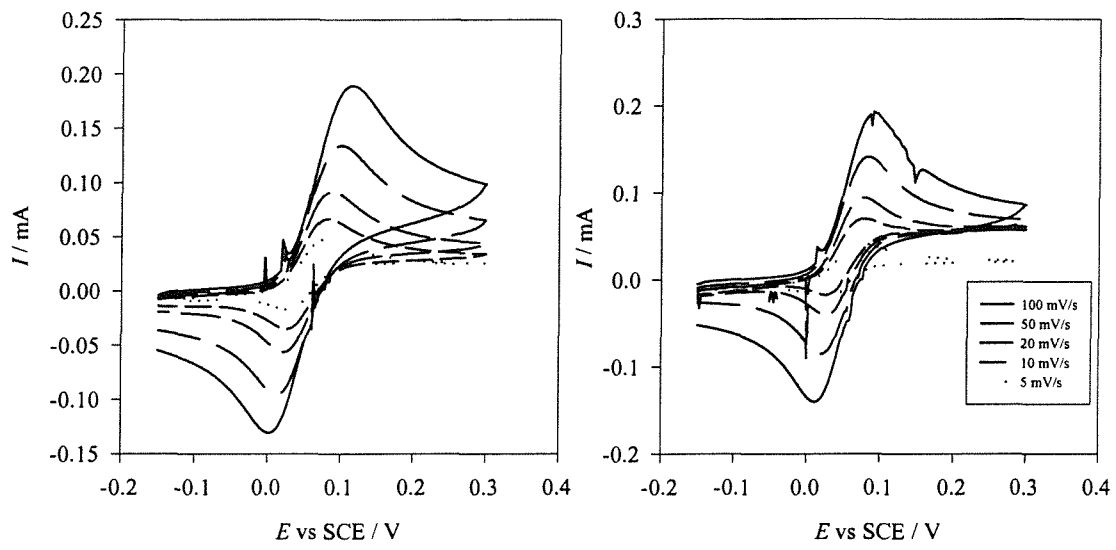

Figure 28: Cyclic voltammetry of *p*-aminophenol 1mM at pH 7.4: left citrate/phosphate buffer, right phosphate/phosphate buffer, both buffers at 0.1 M. These were carried out using a 7 mm diameter platinum working electrode, and a platinum mesh counter electrode. The working electrode is polished between each measurement while the solution is degassed.

The electrochemical rate constant is directly related to ΔE_p in semi reversible electrochemical systems[28]. The relation is given by equation

(4)[29].

$$\varphi = \gamma^{\alpha} k_s \Big/ \sqrt{\pi a D_o} \qquad \textbf{(4)}$$

Where:

$$\gamma = \sqrt{D_o / D_r}$$

$$a = {}^{nFv}/_{RT}$$

$$\alpha = 0.5$$

φ is given according to the peak current separation. These values are reported in the original paper by Nicholson *et al.*[29]. D_o is the diffusion coefficient of the oxidized form and D_r of the reduced form. The value for α is estimated at 0.5 as the intensity of the reduction and the oxidation currents are very similar. In all calculations n=2.

The values for φ were calculated from the experimental values for ΔE_p, using the data given in the original paper, k_s values were then calculated according to equation 4 and are displayed in Table 3:

$k_s/10^{-3}$.cm.s^{-1}						
	pH 4	pH 6		pH 7.4		pH 8
	citrate	citrate	phosphate	citrate	phosphate	phosphate
100 mV/s	3.04	2.28	3.1	1.52	3.04	2.28
50 mV/s	2.69	2.15	3.23	1.61	2.69	2.15
20 mV/s	3.75	2.4	3.75	1.36	2.72	2.04

Table 3: shows that k_s is maximum between pH 4 and pH 6 but in citrate buffer. It can be divided by 2 from pH 4 to pH 7.4. k_s is very small above pH 8.

Values below 20 mV/s were omitted because natural convection taking place in the cell distorts the results. This factor is not controlled and takes place to different extents from one experiment to the next. The scan rate being slow, this phenomenon influences the result. As a result the values of k_s obtained from cyclic voltammetry at 5 mV/s display a larger standard error than faster scan rates.

Rotating disc voltammetry would prove more accurate to determine electron transfer constants. However in this case it is not used because *p*-aminophenol is not stable over the time scale of the rotating disc experiment at the various pH values.

The values presented in Table 3 are influenced by the resistivity of the solution, which may vary between two buffering agents at the same pH. The simulation experiments in section 4 of this chapter suggest that in these conditions, uncompensated solution resistance is in the range of 20 Ω.

4.4 Conclusion

We saw that a possible change of electrochemical mechanism takes place when pH is increased above 7.4. We also showed that in alkaline conditions, *p*-aminophenol may form supramolecular aggregates that may slow electron transfer kinetics. The diffusion coefficient was accurately determined at pH 7.4. Electron transfer constants were calculated using cyclic voltammetry as rotating disc voltammetry could not be used at all pH values.

5 Simulation of voltammetry

In this section we describe the use of voltammetry simulation software (DigiSim) to check the accuracy of the constants calculated in the previous sections and test our understanding of the electrochemical processes in *p*-aminophenol electrochemistry.

5.1 rotating disc voltammetry simulation parameters

Simulation of current response may be obtained by including the constants we calculated in the DigiSim simulation software.

To simulate the rotating disc voltammetry experiment carried out in PBS-Tween from which the diffusion coefficient was obtained, the following parameters and constants presented below were used.

Mechanism: EECC

In DigiSim 2.1 some rules must be followed to enter the reaction mechanism.
The character "e" is used to denote the electron in an electron transfer reaction.
Only one electron transfers are allowed and should be entered in as oxidation steps.
Species names should be kept as simple as possible to minimise errors in entering mechanisms, A, B, C etc...
To enter an EECC mechanism the following syntax was used:

A + e = B, first oxidation step
B + e = C, second oxidation step
D + H = C, first deprotonation
E + H = D, second deprotonation

Parameters:

The first set of values define the cyclic voltammetry simulation parameters as used in the practical experiment. In this set of parameters, only the solution resistance and the electrode capacitance are defined empirically:

Starting potential: Estart(V)=-0.1
Reverse potential: Erev(V)= 0.3
Scan rate (V/s): 0.001
Solution resistance (Ohms): 120
Electrode capacitance (F): 10 10^{-6}
Temperature (K): 298
Number of cycles: 1
Electrode radius (cm): 0.35
Rotation speed (rad/s): 307.87 (49Hz) to 12.56 (2Hz)
Kinematic viscosity of solution (cm^2/s): 0.01

The second set of values defines the electron transfer reaction. The first oxidation potential is defined by cyclic voltammetry in section 2.2, and the first electron transfer rate constant was determined in section 4.3.

Potential of first oxidation step(V): 0.09
First electron transfer rate constant (cm/s): 0.003
Potential of second oxidation step (V): 0.09
Second electron transfer rate constant (cm/s): 0.03

The second oxidation potential may be changed to a lower potential value (0.8 V) without any consequence on the current potential. However, if the same potential is entered for both oxidation steps, the second electron transfer has to be at least 10 times faster than the first, whether it is 10 or 100 times faster does not make any difference.

Deprotonation parameters:

This parameter affects the chemical reactions taking place after the two electron transfers.

Proton concentration: $10^{-7.4}$

The proton concentration is given by the pH value we are using (pH 7.4), the corresponding rate constant k_f was found to have no influence on the simulation from 0 to 1000.

Diffusion and concentration values:

Here all parameters are known within experimental error, *p*-aminophenol concentration is set experimentally and the diffusion coefficient is obtained from section 4.1.
A initial concentration M: 0.0005
A diffusion coefficient (cm^2/s): $9\ 10^{-6}$
B initial concentration M: 0
B diffusion coefficient (cm^2/s): $9\ 10^{-6}$

Assumptions:

The electrode capacitance was set at 10 μF.

The resistance of the solution was approached by trial and error with several simulation experiments. This value influences the slope of the current transient. This parameter was the only varying value when trying to reproduce experimental data, as the other parameters were determined experimentally in the previous sections.

Assuming the first electron transfer is slower than the second one is motivated by the fact that increasing scan rates in cyclic voltammetry never display a separation of the oxidation wave into two distinct current peaks. Varying the second electron transfer constant did not affect the simulated current as long as it remained at least ten times bigger than the first.

The resulting simulation experiments are shown in Figure 29. The resistivity of PBS-Tween buffer may explain the large peak separation when cyclic voltammetry is performed (section 2.2), but we cannot differentiate the resistance from an electrode passivation as the later can not be simulated. The good correlation between the simulation and the experimental data confirms the estimated value for the diffusion coefficient.

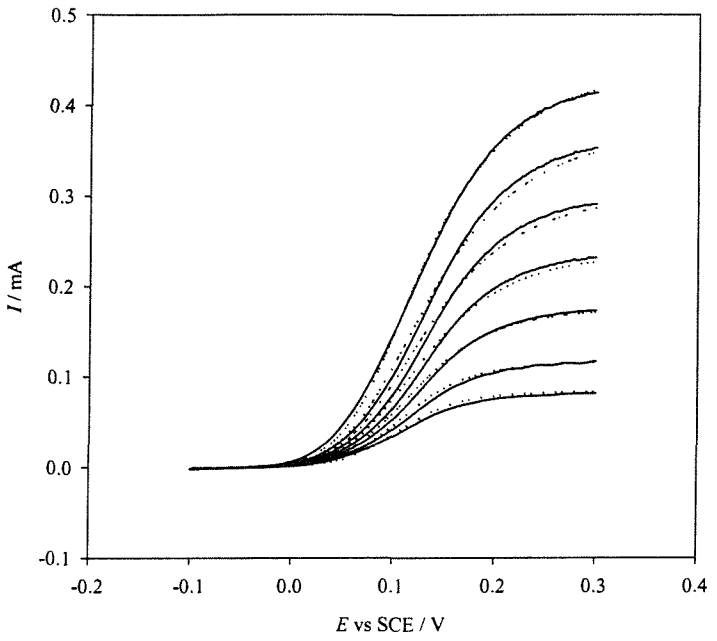

Figure 29: rotating disc voltammetry of *p*-aminophenol 0.5 mM in PBS-Tween pH 7.4 buffer on glassy carbon is represented in solid lines. Simulated data are plotted (dotted lines).

The simulation results (Figure 29) do not display any systematic error between the simulations and the experimental current waves.

5.2 Simulation results

Figure 29 displays a comparison of simulated and experimental data.

The main issue of this simulation is to assert the type of electrochemical mechanism. Both ECEC and EECC mechanisms were computed with result that ECEC gave results that were remote from the experimental data. On the contrary, the EECC mechanism provides a good fit to the experimental data estimate.

The electron transfer kinetic constant was determined according to the experimental measurements reported in section 4.3.

The diffusion coefficient was determined by rotating disc voltammetry (section 4.1).
The oxidation potential was determined by cyclic voltammetry.
The kinematic viscosity of water was chosen after comparing results of dropping ball experiments between aqueous phosphate buffer and PBS-Tween[25].
The experiment was maintained at 25°C during the experiment.

5.3 Cyclic voltammetry simulation

DigiSim was used to simulate cyclic voltammetry of *p*-aminophenol at pH 7.4.
The simulation parameters are given below.

Mechanism: EECC

A + e = B, first oxidation step
B + e = C, second oxidation step
D + H = C, first deprotonation
E + H = D, second deprotonation

Parameters:

As described in section 5.2, all parameters are set experimentally except for the electrode capacitance and the solution resistance, this time the experiment we are simulating does not contain Tween surfactant. This is taken into account by entering a lower solution resistance (20 Ω).

Starting potential: Estart(V)=-0.1
Reverse potential: Erev(V)= 0.3
Final potential: Estop(V)= -0.1

Scan rate (V/s): varied from 0.05 and 0.1
Solution resistance (Ohms): 20
Electrode capacitance (F): 10 10^{-6}
Temperature (K): 298
Number of cycles: 1
Electrode area (cm^2): 0.384
Kinematic viscosity of solution (cm^2/s): 0.01

For the following set of parameters, the same principles apply as in the rotating disk voltammetry simulation. The first oxidation potential and electron transfer rate constant are obtained from sections 4.1 and 4.3 respectively. The second oxidation potential may be changed for a lower potential value (0.5 V) without influencing the simulation, but if the same potential is entered for both electron transfers, the second electron transfer rate constant needs to be 10 times higher than the first one.

Potential of first oxidation step(V): 0.06
First electron transfer rate constant (cm/s): 0.003
Potential of second oxidation step (V): 0.06
Second electron transfer rate constant (cm/s): 0.03

Deprotonation parameters:

Proton concentration: $10^{-7.4}$

The proton concentration is given by the pH we are using, as in section 5.2, the deprotonation rate constant does not seem to affect the current wave when varied from 0 to 1000.

Diffusion and concentration values:

These parameters are set experimentally within experimental error, the diffusion coefficient was calculated in section 4.1.

A initial concentration M: 0.001

A diffusion coefficient (cm^2/s): 9 10^{-6}

B initial concentration M: 0

B diffusion coefficient (cm^2/s): 9 10^{-6}

The simulation experiment result at 50 mV / s is shown in Figure 30, where it is compared with the cyclic voltammogram recorded experimentally.

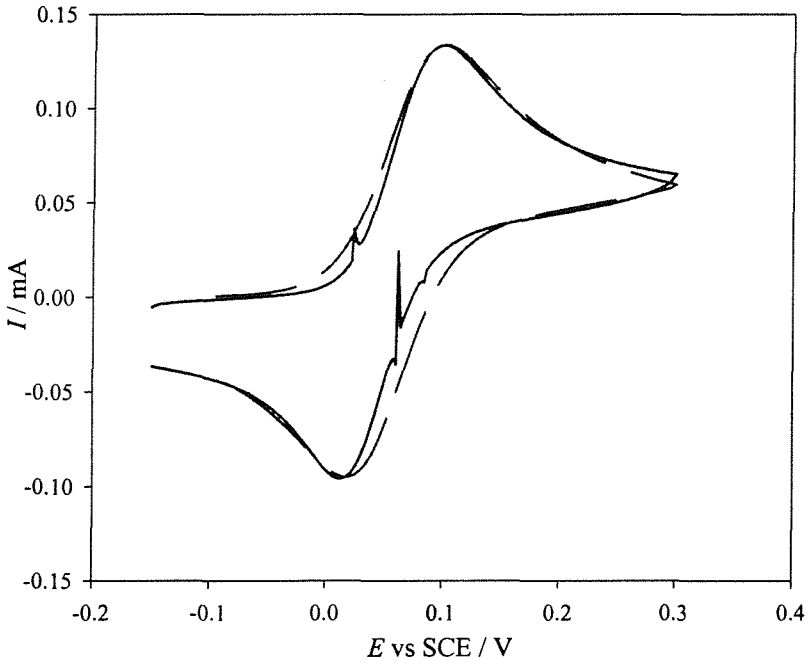

Figure 30: Overlay of cyclic voltammetry experiment at 50 mV/s in phosphate pH 7.4 buffer (solid line) and DigiSim simulation (dashed line).

We notice that the simulated data displays broader current peaks than the experimental data.

A similar simulation experiment was carried out using 100 mV / s scan rate, the result is compared to the experimental data in Figure 31.

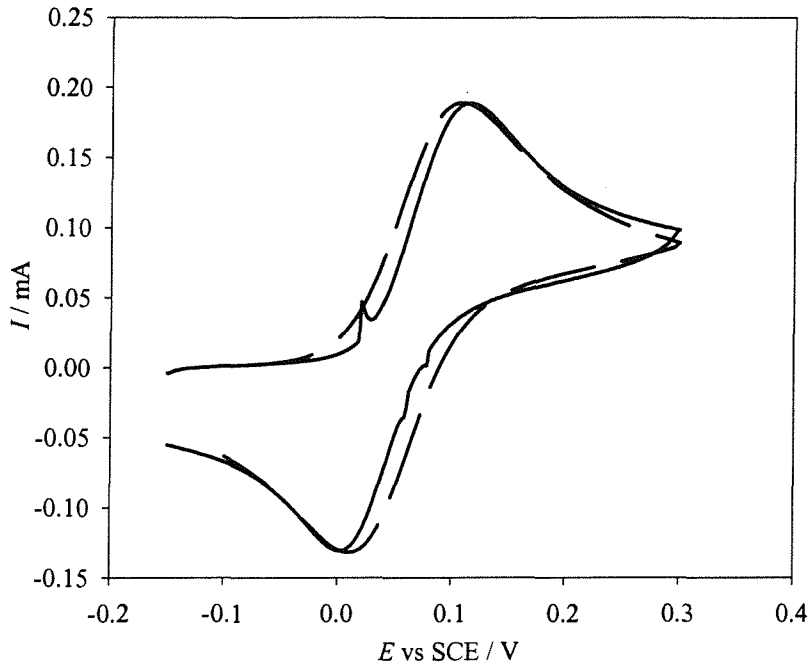

Figure 31: Overlay of cyclic voltammetry experiment at 100 mV/s in phosphate pH 7.4 buffer (solid line) and DigiSim simulation (dashed line).

Similarly to Figure 30, the simulated peak currents are broader than the experimental data.

5.4 Discussion

As in the rotating disc voltammetry simulation, few parameters were determined empirically. The simulation of cyclic voltammetry experiments was performed using values for electron transfer rate constants determined using cyclic voltammetry experiments section 4.3.
The resistance of the solution was approached by trial and error using the simulation software. The electrode capacitance was set arbitrarily at 10 μF. The similarity in current intensity, peak separation and peak potential with the experimental value shows that the EECC mechanism is possibly right. Also the diffusion coefficient seems to have been determined accurately.

Attempts to simulate cyclic voltammetry in alkaline conditions by supposing an ECEC electrochemical mechanism were successful in reproducing the peak separation and peak

potential observed experimentally. Unfortunately, they did not reproduce the experimental current intensities. This might be caused by the complexity of the system, which is not assimilated by the software.

6 Conclusion

This chapter showed that the degradation reaction of *p*-aminophenol in neutral and alkaline conditions is not 1-4 Michael addition of *p*-aminophenol on benzoquinone. It does not seem to be benzoquinone condensation. However the product can be purified and has a clear NMR spectrum, which suggests symmetry in the molecule.

The pK_a of *p*-aminophenol has been determined using cyclic voltammetry and has been confirmed by both UV spectroscopy and base titration. Three redox states of *p*-aminophenol were characterised with respect to pH and potential conditions. The electrochemical mechanism remained a two electron process in acidic, neutral and alkaline conditions. The transitions between the three redox states were studied. The electrochemical mechanism was shown to be EECC between pH 0 and pH 7.4, and we suspect an ECEC mechanism above pH 7.4. We calculated the electron transfer kinetic constants using cyclic voltammetry experiments, and the diffusion coefficient of *p*-aminophenol in aqueous solution at pH 7.4, $D = 9\ 10^{-6} cm^2/s$.

We were able to evaluate the accuracy of our results by entering them in a simulation program, and comparing the simulated data with the experimental data.

In the next chapter we study the electrochemical properties of *p*-aminophenyl phosphate. The aim of this chapter is to check that there is no interference between *p*-aminophenol and *p*-aminophenol phosphate electrochemistry.

7 References

1. Cass, A.E.G., et al., *Ferrocene-mediated enzyme electrode for amperometric determination of glucose.* Anal. Chem., 1984. **56**: p. 667-671.

2. Carlo, M.D. and M. Manscini, *Enzyme immunoassay with amperometric flow-injection analysis using horseradish peroxidase as a label.* Anal. Chim. Acta, 1996. **336**: p. 167-174.
3. Piras, L., et al., *Immunoenzymatic application of a redox potential biosensor.* Anal. Chim. Acta, 1996. **335**: p. 127-135.
4. Albery, W.J., et al., *Electrochemical sensors: theory and experiment.* J. Chem. Soc., Faraday Trans 1, 1986. **82**: p. 1033-1050.
5. Thompson, R.Q., et al., *Zeptomole detection limit for alkaline phosphatase using 4-aminophenylphosphate, amperometric detection, and an optimal buffer system.* Anal. Chim. Acta, 1993. **271**: p. 223-229.
6. Christie, I.M., et al., *Simplified measurement of serum alkaline phosphatase utilizing electrochemical detection of 4-aminophenol.* Anal. Chim. Acta, 1992. **257**: p. 21-28.
7. Tang, H.T., et al., *p-aminophenyl phosphate: an improved substrate for electrochemical enzyme immunoassay.* Anal. Chim. Acta, 1988. **214**: p. 187-195.
8. Bier, F.F., et al., *An enzymatic amplification cycle for high sensitive immunoassay.* Anal Chim. Acta., 1996. **328**: p. 27-32.
9. Ghindilis, A.L., et al., *Determination of p-amino phenol and catecholamines at picomolar concentrations based on recycling enzyme amplification.* Anal. Chim. Acta, 1995. **304**: p. 25-31.
10. Pemberton, R.M., et al., *A comparison of 1-naphtyl phosphate and 4 aminophenyl phosphate as enzyme substrates for use with a screen printed amperometric immunosensor for progesterone in cows milk.* Biosensors & Bioelectronics, 1999. **14**: p. 495-503.
11. Rosen, I. and J. Rishpon, *Alkaline phosphatase as a label for heterogeneous immunoelectrochemical sensor.* J. Electroanal. Chem., 1989. **258**: p. 27-39.
12. Christensen, C.R. and F.C. Anson, *Application of thin layer chronopotentiometry to kinetic studies.* Anal. Chem., 1964. **36**: p. 495-497.
13. Hawley, D. and R.N. Adams, *Homogeneous chemical reactions in electrode processes. Measurement of rates of follow-up chemical reactions.* J. Electroanal. Chem., 1965. **10**: p. 376-386.
14. Beil. **13**: p. 427.

15. Herman, H.B. and A.J. Bard, *Electron transfer with following chemical reaction.* Anal. Chem., 1964. **36**(3): p. 510-514.

16. Shim, Y.-B. and S.-M. Park, *Spectroelectrochemical studies of p-benzoquinone reduction in aqueous media.* J. Electroanal. Chem., 1997. **425**: p. 201-207.

17. Wang, Z., et al., *Spectroelectrochemistry for a coupled chemical reaction in the channel cell.*

Part II. Kinetics of hydrolysis and the absorption spectrum of p-bezoquinone imine. J. Electroanal. Chem., 1999. **464**: p. 181-186.

18. Testa, A.C. and W.H. Reinmuth, *Chronopotentiometry with current reversal. Application to p-benzoquinone imine hydrolysis.* Anal. Chem., 1960. **32**(11): p. 1512-1514.

19. Alberts, G.S. and I. Shain, *Electrochemical study of kinetics of a chemical reaction coupled between two charge transfer reactions.* Anal. Chem., 1963. **35**(12): p. 1859-1866.

20. Lambert, J.B., et al., *Introduction to organic spectroscopy*, ed. Macmillan. 1987: Macmillan.

21. Feng, J., et al., *Electrocatalysis of anodic oxygen-transfer reactions: The electrochemical incineration of benzoquinone.* J. Electrochem. Soc., 1995. **142**(11): p. 3626-3632.

22. Park, H., J.-S. Park, and Y.-B. Shim, *Redox reaction of benzoquinone on a lipid coated glassy carbon electrode.* J. Electroanal. Chem., 1997. **438**: p. 113-119.

23. Malinauskas, A. and R. Holze, *Electrocatalysis of the quinone/hydroquinone system by electrodes coated with substituted polyaniline.* Ber. Busenges. Phys. Chem., 1996. **100**(10): p. 1740-1745.

24. Babaei, A. and A.J. McQuillan, *In-situ spectroelectrochemical studies of decomposition of hydroquinones on platinum electrodes in dichloromethane solutions.* J. Phys. Chem. B, 1997. **101**: p. 7443-7447.

25. Gilmont, R., Inst. & Control Systems, 1963. **36**(121).

26. Pletcher, D., *A first course in electrode processes*, ed. T.e. consultancy. 1991: Alresford Press Ltd. 141.

27. Robinson, D., J.E. Anderson, and J. Lin, *Measurement of diffusion coefficients of some indoles and ascorbic acid by flow injection analysis.* J. Phys. Chem., 1990. **94**: p. 1003-1005.

28. Nicholson, R.S., *Theory and application of cyclic voltammetry for measurement of electrode reaction kinetics.* Anal. Chem., 1965. **37**(11): p. 1351-1355.

29. Nicholson, R.S. and I. Shain, *Single scan and cyclic methods applied to reversible, irreversible, and kinetic systems.* Anal. Chem., 1964. **36**(4): p. 706-723.

Chapter 6: *p*-aminophenyl phosphate

1 Introduction

p-aminophenyl phosphate is a substrate for alkaline phosphatase[1]. Similarly to *p*-aminophenol, the literature lacks a detailed account of its electrochemistry. As described in chapter 5, *p*-aminophenol phosphate is hydrolysed by alkaline phosphatase, the product of the enzyme catalysed reaction is *p*-aminophenol.

In chapter 5 we studied the electrochemistry of *p*-aminophenol, and determined its electron transfer kinetics under various conditions. This study enables us to relate the oxidation current intensity for *p*-aminophenol to its concentration under controlled conditions. However, we intend to design a sensor in which the concentration of *p*-aminophenol is not constant, but will increase as a result of alkaline phosphatase activity in the presence of *p*-aminophenyl phosphate. It is essential to be able to relate the change of oxidation current of *p*-aminophenol to its change of concentration with time. This will allow us to use the kinetics for the change of current to calculate enzyme activity. This is why we need to verify that *p*-aminophenol phosphate does not interfere with *p*-aminophenol electrochemistry.

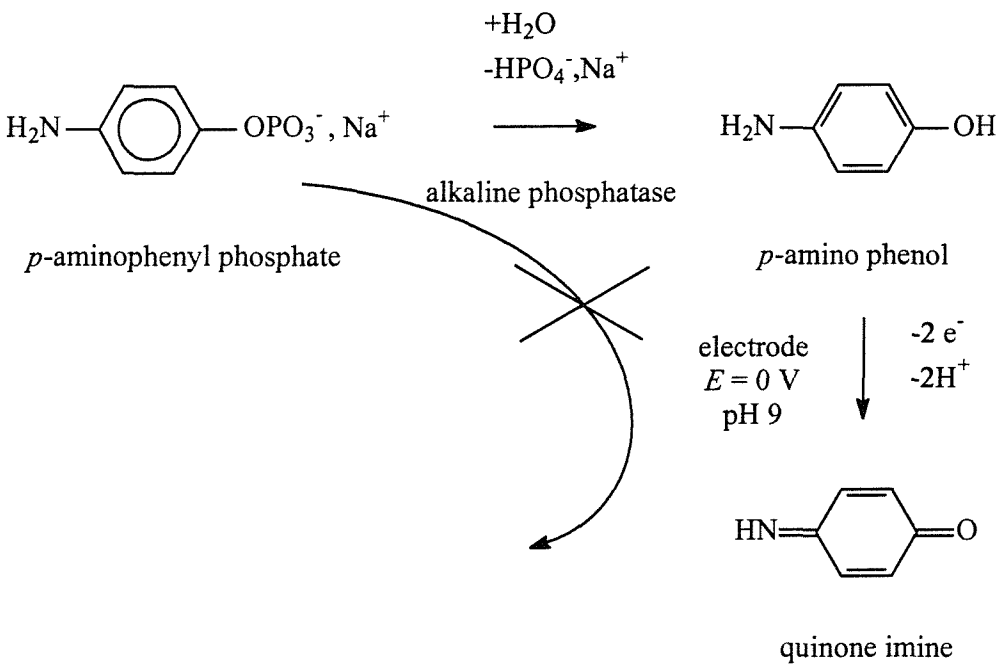

Figure 1: Scheme for reaction of *p*-aminophenyl phosphate with alkaline phosphatase yielding *p*-aminophenol. The reaction is followed by the oxidation of the product at the electrode $E = 0$ V at pH 9 affording quinone imine. Under these conditions, *p*-aminophenyl phosphate should not react at the electrode.

Figure 1 shows how the oxidation current from *p*-aminophenol is related to the hydrolysis of the phosphate bond by alkaline phosphatase. The aim of this chapter is to check the electrochemistry of *p*-aminophenyl phosphate and investigate the possible interference with *p*-aminophenol oxidation. Most publications reporting bioelectrochemical sensing devices involving *p*-aminophenyl phosphate show that it does not interfere with electrochemical oxidation of *p*-aminophenol[1-4].

In neutral and acidic conditions the phosphate is quickly hydrolysed without any enzyme. To maintain the solution stable over the time scale of the experiment, the pH has to remain above 8 [1].

We shall now report our results for the study of the electrochemistry of *p*-aminophenyl phosphate.

2 Cyclic voltammetry

The electrochemistry of *p*-aminophenyl phosphate is studied through cyclic voltammetry at pH 9.

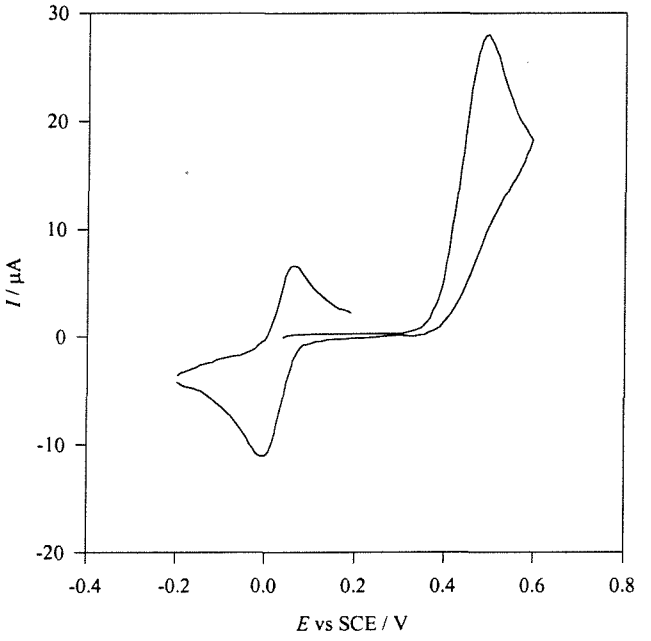

Figure 2: Cyclic voltammogram of *p*-aminophenyl phosphate 1mM in pH 9 Tris-HCl buffer 0.1 M. 3 mm diameter glassy carbon electrode, platinum mesh counter electrode. Sweep rate 20 mV / s, starting at 0 V up to 0.6 V and down to -0.2 V.

Figure 2 shows no current at 0 V on the initial sweep. At 0.5 V an irreversible peak is observed, as the potential is reversed to -0.2 V, a reduction peak is observed. This reduction signal is reversible as an oxidation peak may be observed when the potential is brought back to 0.2 V. If the potential is scanned initially from 0 to 0.3 V, the redox system near 0 V is not present. This redox system is consistent with that of *p*-aminophenol at pH 9. From this voltammetry, we conclude that *p*-aminophenyl phosphate is oxidised at 0.5 V, the oxidation product is quinone imine that is reduced into *p*-aminophenol on the reverse sweep.

By varying the scan rate, we checked that no reverse peak current is observed for the oxidation of *p*-aminophenol phosphate.

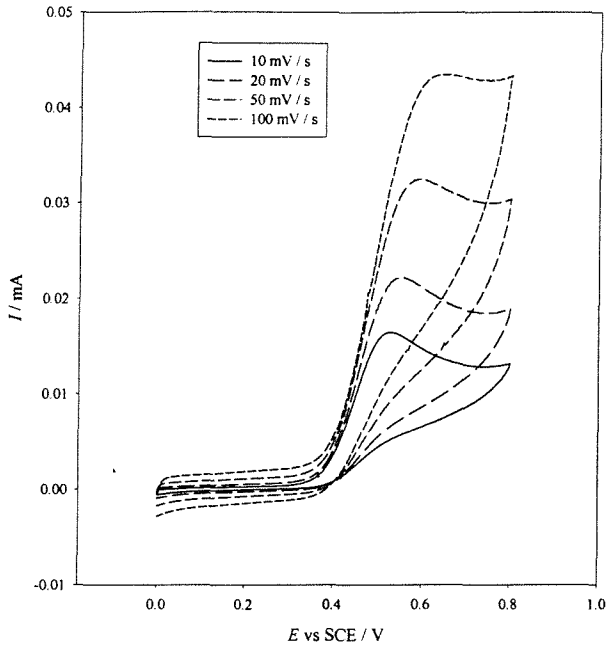

Figure 3: Cyclic voltammetry of *p*-aminophenyl phosphate 1mM in pH 9 Tris-HCl buffer 0.1 M, 0.1 M KCl. 7 mm diameter glassy carbon electrode, platinum mesh counter electrode. Sweep rate varies from 10 to 100 mV / s, starting at 0 V up to 0.8 V.

Figure 3 shows that varying the scan rate from 10 to 100 mV / s does not reveal any reduction current after the oxidation of *p*-aminophenol phosphate. We conclude that this oxidation is irreversible.

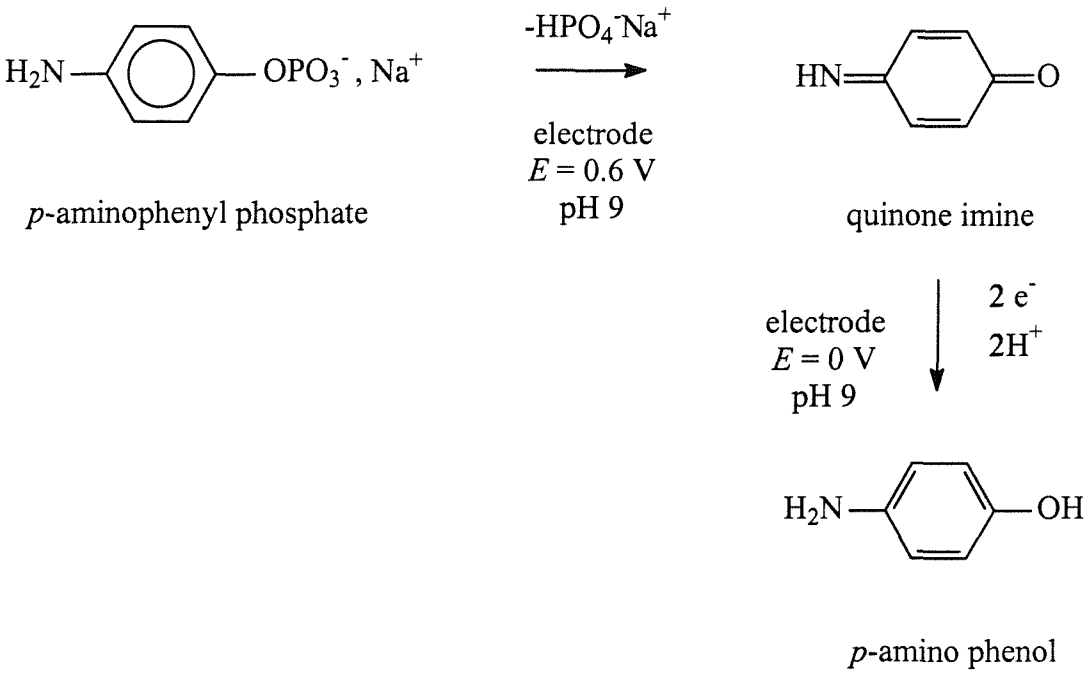

Figure 4: reaction scheme of *p*-aminophenyl phosphate oxidation affording quinone imine. The product is reduced at the electrode affording *p*-aminophenol. The mechanism for the oxidation process is unknown.

Figure 4 illustrates the suspected reaction scheme when *p*-aminophenyl phosphate is oxidised at the electrode. The result is the cleavage of the phosphate bond affording quinone imine.

The mechanism involved in the cleavage reaction of the phosphate group following *p*-aminophenyl phosphate oxidation is not known, but this study showed that irreversible oxidation of *p*-aminophenyl phosphate takes place at a higher potential (0.6 V at pH 9) than *p*-aminophenol / quinone imine electrochemistry (0 V at pH 9). As a result we do not expect any interference from *p*-aminophenyl phosphate in the electrochemical oxidation of *p*-aminophenol.

3 Rotating disc voltammetry

An attempt was made to determine the diffusion coefficient of *p*-aminophenyl phosphate at 25°C by rotating disc voltammetry experiments. The maximum currents were plotted against the square root of the rotation speed and the diffusion coefficient was calculated from the slope according to the Levich equation.

$$I = 1.554nFv^{-1/6}CD^{2/3}W^{1/2}A \qquad (1)$$

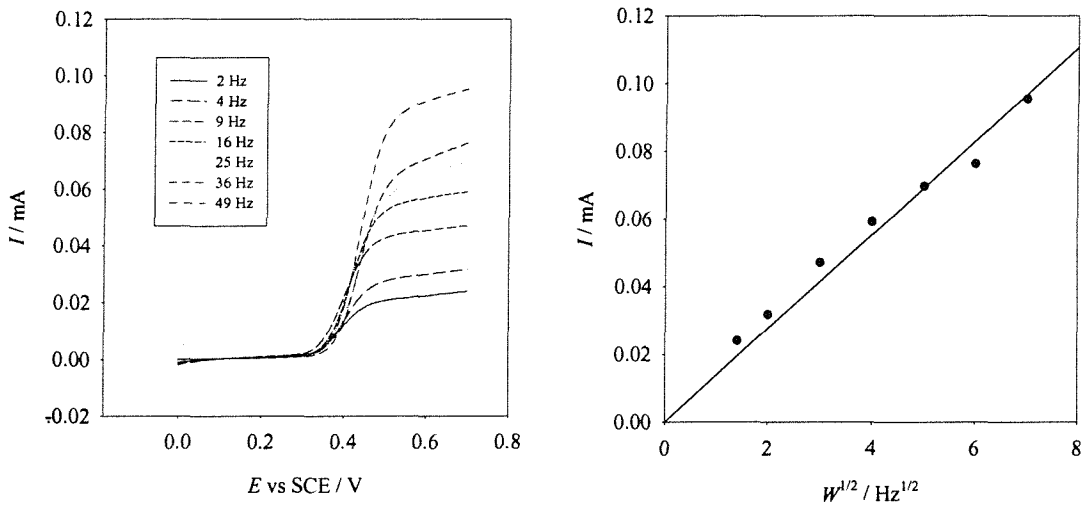

Figure 5: Rotating disc voltammetry of *p*-aminophenol phosphate 0.2 mM in pH 9.8 Tris-HCl 0.1 M, 0.5 M KCl. With a 7 mm diameter glassy carbon electrode, platinum mesh counter electrode at 5 mV/s. The working electrode was polished between each voltammetry.

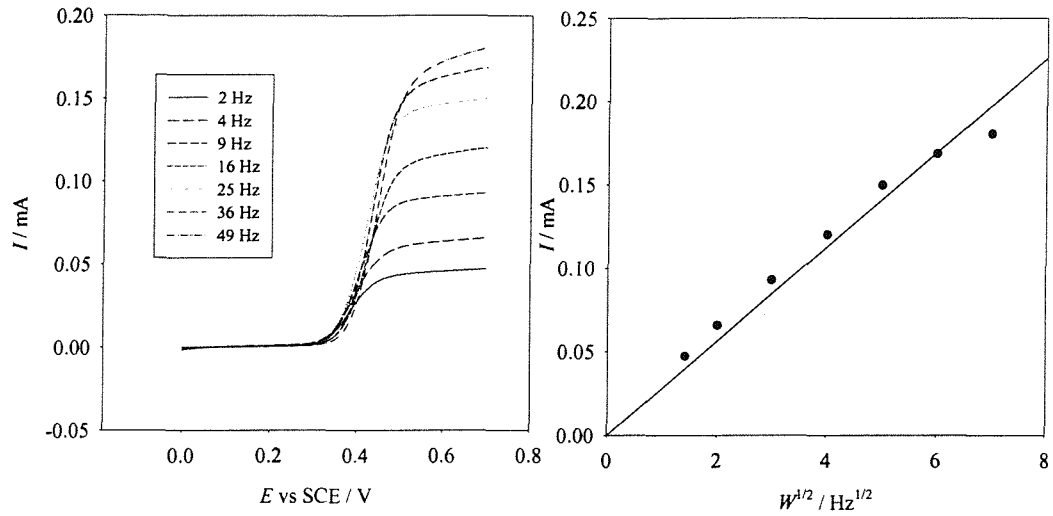

Figure 6: Rotating disc voltammetry of *p*-aminophenol phosphate 0.5 mM in pH 9.8 Tris-HCl 0.1 M, 0.5 M KCl. With a 7 mm diameter glassy carbon electrode, platinum mesh counter electrode at 5 mV/s. The working electrode was polished between each voltammetry.

I is in amps. n is the number of electrons transferred hence $n = 2$. F is the Faraday constant 96484 C mol^{-1}. C is the concentration of *p*-aminophenyl phosphate in mol cm^{-3}. D is the diffusion coefficient in $cm^2\ s^{-1}$. W is the rotation speed of the electrode in Hz. A is the electrode area in cm^2. ν is the kinematic viscosity of the solution.

From the slope of the regressions for each concentration, the diffusion coefficient may be estimated according to the Levich equation

Concentration M	0.2×10^{-3}	0.5×10^{-3}	10^{-3}
D_0 cm^2s^{-1}	4.6×10^{-6}	3.3×10^{-6}	2.6×10^{-6}

Table 1: displays the diffusion coefficient values calculated from each set of plots in Figure 5 andFigure 6, according to equation (1).

The diffusion coefficient values displayed in Table 1 show a decrease of the diffusion coefficient with *p*-aminophenyl phosphate concentration. Besides the maximum currents obtained from the rotating disc voltammetry currents displayed in Figure 5 andFigure 6 when plotted against the square root of the rotation speed, display a poor correlation with the corresponding linear regression. This happens despite the fact that the working

electrode was polished between each measurement. When the working electrode is not polished before each measurement, we obtain the rotating disc voltammetry current displayed in Figure 7.

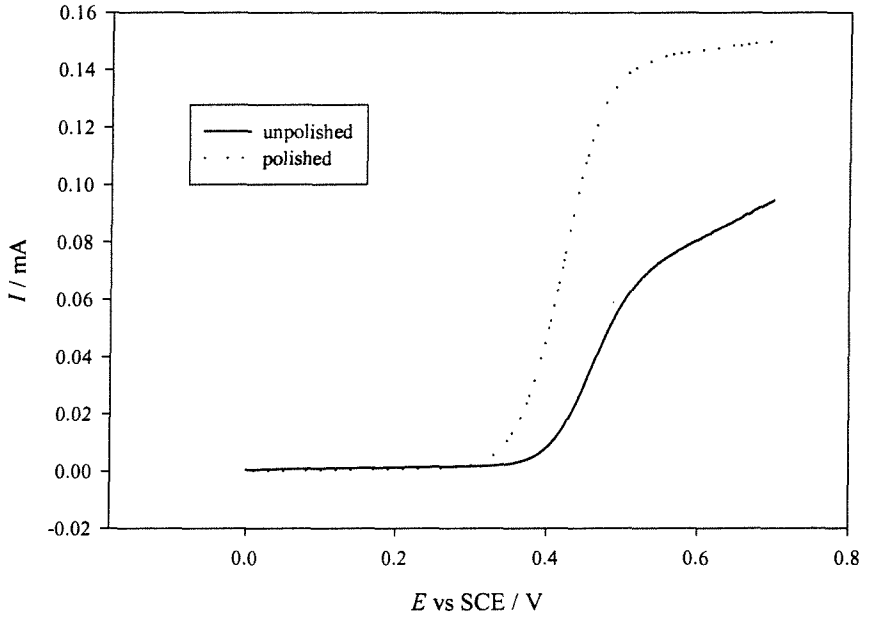

Figure 7: Rotating disc voltammetry (25 Hz) of *p*-aminophenol phosphate 0.5 mM in pH 9.8 Tris-HCl 0.1 M, 0.5 M KCl. With a 7 mm diameter glassy carbon electrode, platinum mesh counter electrode at 5 mV/s. The working electrode was polished before the first cyclic voltammetry but not before the second one.

Figure 7 shows the difference between the current wave during a rotating disc voltammetry experiment when the glassy carbon working electrode is freshly polished and when it is not. When the electrode is freshly polished, a current plateau is obtained, the current intensity is 0.15 mA. When the working electrode is not polished, no current plateau may be observed and the maximum current is 0.1 mA. We observe a potential shift between the two current transients, with a polished working electrode, the current increases at 0.35 V, whereas it increases beyond 0.4 V with the unpolished electrode.

From this experiment we conclude that *p*-aminophenyl phosphate oxidation causes electrode poisoning. As a result, we assume that the rotating disc voltammetry currents on glassy carbon electrodes are affected by the electrode poisoning. This would explain why in Table 1 diffusion coefficient values decrease with the increase in *p*-aminophenol concentration. Therefore, we conclude that the diffusion coefficient obtained from the 0.2 mM *p*-aminophenol is the closest to the exact figure, but since it is not possible to quantify

the effect of electrode poisoning with *p*-aminophenol concentration, this result is only an indicative estimation of *p*-aminophenyl phosphate diffusion coefficient.

We can compare the influence of the working electrode material on the electrode poisoning effect by doing a rotating disc voltammetry experiment with a platinum working electrode (Figure 8).

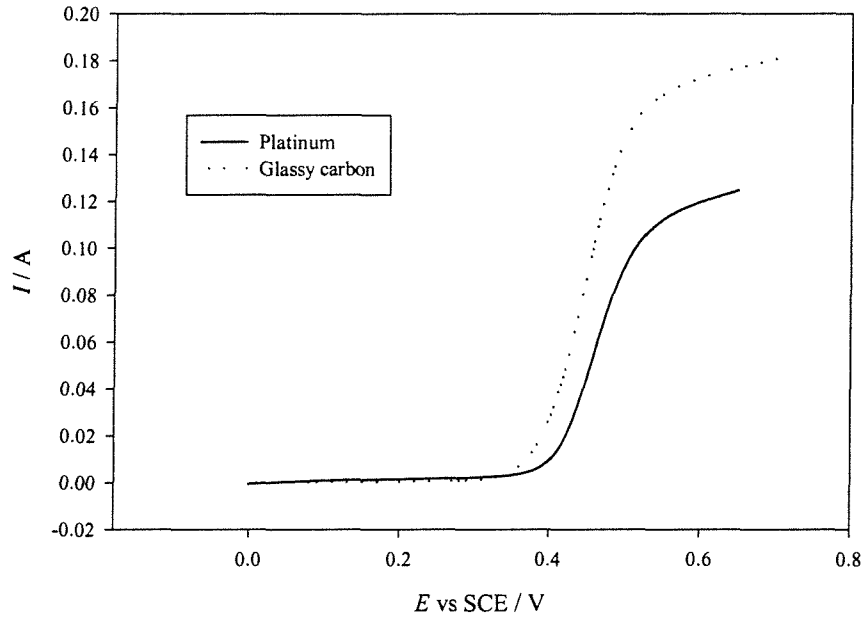

Figure 8: Rotating disc voltammetry (49 Hz) of *p*-aminophenol phosphate 0.5 mM in pH 9.8 Tris-HCl 0.1 M, 0.5 M KCl. With a 7 mm diameter glassy carbon and platinum electrode, platinum mesh counter electrode at 5 mV/s. The working electrode was polished before each experiment.

Figure 8 shows the rotating disc voltammetry of *p*-aminophenyl phosphate with polished platinum and glassy carbon electrodes. With the polished glassy carbon working electrode we see a maximum current at 0.18 mA. The current starts to increase near 0.35 V. With the polished platinum working electrode we see a maximum current reaching 0.12 mA, and the current increases above 0.4 V. In both cases, the working electrodes are polished immediately before the cyclic voltammetry is carried out. We see that platinum more readily fouled by *p*-aminophenyl phosphate in solution than glassy carbon.

This set of experiments gives us an estimate of *p*-aminophenyl phosphate diffusion coefficient. These values may not be considered as accurate due to the electrode poisoning, that seems to occur on glassy carbon as soon as the oxidation reaction takes place. The use of platinum as a working electrode was proved to yield a larger electrode than glassy carbon.

The use of platinum as well as carbon microelectrodes to carry out potential step experiments could have provided us with another means of checking *p*-aminophenyl phosphate diffusion coefficient[5]. Unfortunately, no sensible analysis could be made of the results as it seemed that platinum and carbon microelectrodes alike were subject to electrode poisoning.

4 *p*-aminophenyl phosphate interference with glucose oxidase

As explained in the introduction to chapter 5, we are trying to relate the change of oxidation current of *p*-aminophenol with time to alkaline phosphatase activity for the hydrolysis of *p*-aminophenyl phosphate into *p*-aminophenol. To amplify the oxidation current of *p*-aminophenol, we use a redox enzyme (glucose oxidase) and its substrate (β-D glucose) to reduce the quinone imine generated by the oxidation of *p*-aminophenol, so that the same molecule may undergo several electrode oxidation reactions by being reduced by the redox enzyme each time (Figure 9). In the previous sections, we showed that the electrode potential required to detect *p*-aminophenol was not high enough to cause *p*-aminophenyl phosphate oxidation. The aim of the experiment described here is to check that the presence of glucose oxidase and glucose in a *p*-aminophenyl phosphate solution does not cause *p*-aminophenyl phosphate to hydrolyse into *p*-aminophenol.

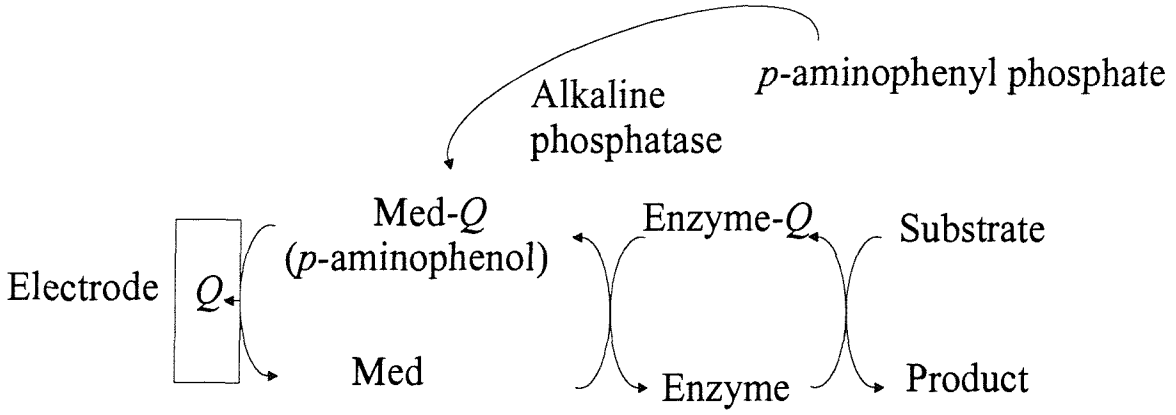

Figure 9: Reaction scheme of oxidation of *p*-aminophenol. *p*-aminophenol is generated during the hydrolysis of *p*-aminophenol phosphate catalysed by alkaline phosphatase. At the working electrode *p*-aminophenol is oxidised into quinone imine, quinone imine is rediced by a redox enzyme (glucose oxidase). Glucose oxidase is reduced after its reaction with quinone imine by oxidising its substrate (glucose).

The main concern at the level of the sensor is that *p*-aminophenyl phosphate should not be able to react with glucose oxidase. This guarantees that the current collected at the electrode is exclusively due to *p*-aminophenol and hence the result of alkaline phosphatase activity (Figure 9).

To verify this, a fresh pH 9 solution of *p*-aminophenyl phosphate at 23 μM was prepared. Glucose was added to the solution up to 100 mM and glucose oxidase up to 32 μM. The glucose was added from a concentrated solution that was prepared 24 h before. In Figure 10 we see that when 0 V are applied to the working electrode, the oxidation current remains close to 0 A. On the contrary, if alkaline phosphatase was added to the same solution up to 50 nM, an oxidation current could be observed when the potential of the working electrode was held at 0 V. The current rose to 7 μA after 70 s.

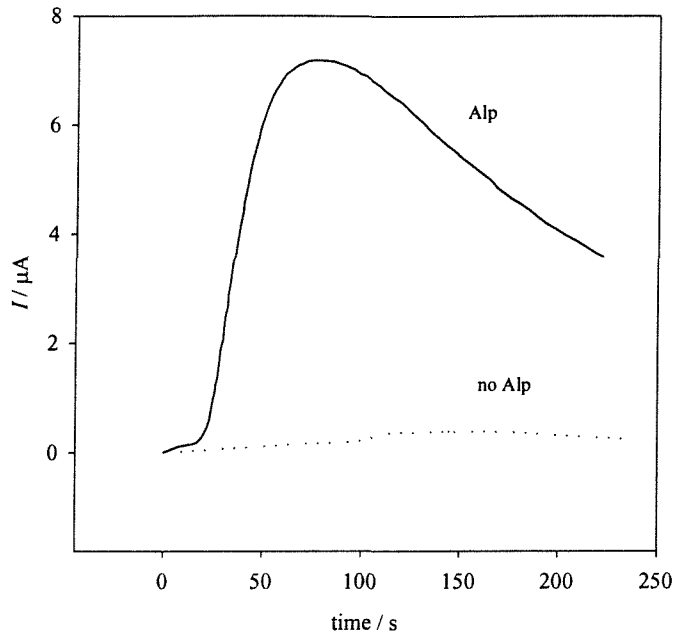

Figure 10: current transients obtained on a 1 cm^2 graphite working electrode, gold wire counter electrode. 'Alp' current transient is obtained from a pH 9.5 Tris-HCl solution with 23 µM *p*-aminophenyl phosphate, 100 mM glucose, 38 µM glucose oxidase and 50 nM alkaline phosphatase. 'No Alp' current transient is obtained from a solution made of 23 µM *p*-aminophenyl phosphate, 100 mM glucose, 38 µM glucose oxidase.

Figure 10 shows that oxidation of *p*-aminophenol at 0 V at pH 9 only occurs when alkaline phosphatase is present in solution, otherwise the detected current remains close to 0.

In the light of evidence collected in chapter 7, a hypothesis will be proposed in this chapter to explain the behaviour of the amplified current plotted in Figure 10.

5 Conclusion

This chapter shows that at pH 9 *p*-aminophenol phosphate will not generate *p*-aminophenol spontaneously if the working electrode potential is kept at 0 V. The irreversible oxidation of *p*-aminophenyl phosphate takes place at 0.6 V and the oxidation product is likely to be quinone imine. The rotating disc voltammetry with a glassy carbon working electrode enabled us to evaluate the diffusion coefficient of *p*-aminophenyl phosphate but also showed that platinum working electrodes could not be used to study this compound. We also checked that glucose oxidase and glucose in the *p*-aminophenyl phosphate solution did not cause the later to hydrolyse into *p*-aminophenol.

In chapters 5 and 6, we have shown that the oxidation current of *p*-aminophenol at 0 V at pH 9 is the only source of current in the solution. We have characterised the electrochemistry of both *p*-aminophenyl phosphate and *p*-aminophenol. We now have collected the necessary information to relate oxidation current intensities to *p*-aminophenol concentration, whether *p*-aminophenyl phosphate, glucose oxidase or glucose are present.

6 References

1. Thompson, R.Q., et al., *Zeptomole detection limit for alkaline phosphatase using 4-aminophenylphosphate, amperometric detection, and an optimal buffer system.* Anal. Chim. Acta, 1993. **271**: p. 223-229.
2. Tang, H.T., et al., *p-aminophenyl phosphate: an improved substrate for electrochemical enzyme immunoassay.* Anal. Chim. Acta, 1988. **214**: p. 187-195.
3. Ghindilis, A.L., et al., *Determination of p-amino phenol and catecholamines at picomolar concentrations based on recycling enzyme amplification.* Anal. Chim. Acta, 1995. **304**: p. 25-31.
4. Bier, F.F., et al., *An enzymatic amplification cycle for high sensitive immunoassay.* Anal Chim. Acta., 1996. **328**: p. 27-32.
5. Denuault, G., M.V. Mirkin, and A.J. Bard, *Direct determination of diffusion coefficients by chronoamperometry at microdisk electrodes.* J. Electroanal. Chem., 1991. **308**: p. 27-38.

Chapter 7: Alkaline phosphatase and glucose oxidase kinetics

Introduction

In the last two chapters, this study has focussed upon the electrode oxidation of the mediator. We now introduce enzyme reactions to the system. Glucose oxidase will oxidise glucose and reduce quinone imine, the result is a recycling process of *p*-aminophenol after its electrode oxidation. Due to this enzyme reaction, the same molecule of *p*-aminophenol will transfer electrons from the enzyme to the electrode several times, acting as a mediator. To characterise this recycling process, we need to determine the reoxidation kinetic constant of the enzyme, which reflects the affinity of the enzyme for the mediator.
In the second part of the chapter, we will study alkaline phosphatase kinetics. However we need to verify how the new experimental conditions (high glucose oxidase and glucose concentrations) affect *p*-aminophenol electrochemistry. The following experiments were carried out in Tris-HCl buffer pH 9.5.

The understanding of the enzymatic process in the sensor requires a full electrochemical characterisation of electron transfer from substrate to enzyme, enzyme to mediator, and mediator to electrode. Fulfilling this task requires the study of the system under carefully controlled homogenous conditions. The ideal tool in this case is the rotating disc because it provides controlled mass transport to the electrode. For the rotating disc the thickness of the diffusion layer, Z_D is given by:

$$Z_D = 0.642\nu^{1/6} D_A^{1/3} / W^{1/2} \quad (1)$$

Where ν is the kinematic viscosity of the solution, D_A is the diffusion coefficient of the redox compound, and W is the rotation speed of the electrode in Hz.

1- Mediating conditions, pH 9.5

1.1 Interference from the biochemical reagents

1.1.1 Interference at high concentrations of glucose oxidase

To be able to observe any effect of high glucose oxidase concentration on *p*-aminophenol electrochemistry, we prepared *p*-aminophenol solutions and recorded the oxidation current through cyclic voltammetry while increasing glucose oxidase concentration. The rotation speed of the electrode was set before starting the electrochemistry experiment. A potential of 0.0 V was applied to the glassy carbon working electrode, and the oxidation current was recorded. A concentrated solution of glucose oxidase was added to the cell in aliquots of 40 and 80 µl. After each addition, the current was seen to decrease. The total solution volume was 30 ml and the total volume of glucose oxidase added to this cell was 740 µl. The resulting dilution factor being 2.4 % for the *p*-aminophenol. This experiment was repeated for only three different rotation speeds as the amount of glucose oxidase consumed by this experiment is very large. The option of recording the current for each rotation speed at each increase of enzyme concentration could not be adopted because *p*-aminophenol is not sufficiently stable at pH 9.5 over the time scale of the experiment.

The current intensities recorded during this experiment proved not to be linear when plotted against the square root of the rotation speed. This implying that the Levich behaviour for *p*-aminophenol rotating disc voltammetry observed in chapter 5 no longer applies (different pH conditions).

The influence of a large protein concentration on the electrochemistry may be due to several factors. The viscosity of the solution may be affected, this will have consequences for the diffusion of all the constituents of the solution. In addition protein adsorption on the electrode surface will affect the electron transfer process.

By not adding any glucose to the solution, the catalytic reaction is prevented and we can see how, in the presence of glucose oxidase, the electrochemistry of *p*-aminophenol is changed.

By plotting the current values as $1/I=f(1/W^{1/2})$ (Figure 1), we can analyse the data according to the Koutecky-Levich equation:

$$\frac{1}{I} = \frac{1}{I_k} + \frac{1}{I_{l,c}} + \frac{1}{I_e} \tag{2}$$

In which I_e, I_k and $I_{l,c}$ are defined by:

$$I_k = nFAk_f(E)C_0^* \tag{3}$$

$$I_{l,c} = 1.554nFAC_0^* D_0^{2/3} \nu^{-1/6} W^{1/2} \tag{4}$$

$$I_e = nFAC_0^* \tag{5}$$

Where n is the number of electron involved, F is the Faraday constant (C mol^{-1}), A is the electrode area i.e. 0.384 cm^2, $k_f(E)$ is the electron transfer rate constant and depends on the potential, C_0^* is the bulk concentration of the solution in mol dm^{-3}, D_0 is the diffusion coefficient cm^2 s^{-1}, ν is the kinematic viscosity of the solution 0.01 cm^2 s^{-1}, and W is the rotation speed of the electrode Hz.

$I_{l,c}$ being a function of the rotation speed W, when the rotation speed is infinite: $1/I = 1/I_k$. This allows isolation of the kinetics of the electron transfer process. The slope of the regression lines in Figure 1 are given by $1/I_{l,c}$, and can be used to calculate the diffusion coefficient. I_e is the potential independent current.

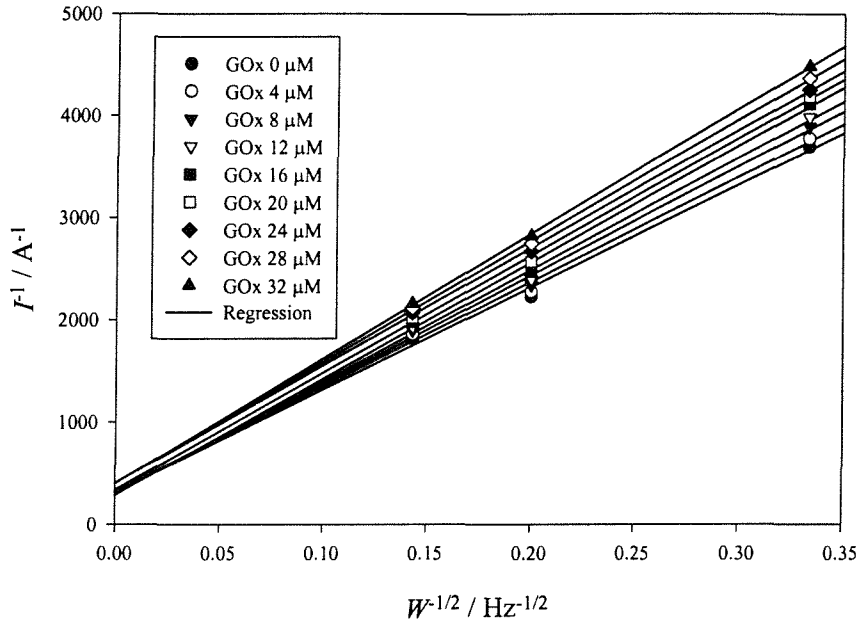

Figure 1: Koutecky-Levich plot of rotating disc voltammetry of *p*-aminophenol 1 mM solution in pH 9.5 Tris-HCl buffer 0.1 M, 0.1 M KCl in presence of various glucose oxidase concentrations. The glucose oxidase concentrations range from 0 to 32 μM at 49, 25, and 9 Hz, the working electrode is 7 mm diameter glassy carbon set at 0 V.

From Figure 1 we observe a change of the regression with increasing glucose oxidase concentration. An evaluation of the varying parameters such as electron transfer kinetics, viscosity and diffusion can be made. The change in slope may be related to a change in viscosity equation (4) and the change in intercept value may be related to a change in electron transfer kinetics (3). First we check if the change of intercept is significant by analysing the correlation between the intercept values and the the enzyme concentration (Figure 2). The intercept values from Figure 1 are reported in Table 1:

Enzyme 10^{-6}M	0	4	8	12	16	20	24	28	32
Intercept A^{-1}	317.7	326.5	304.5	300.6	286.8	334.8	401.5	400.5	399

Table 1: Intercept values from Figure 1 for each enzyme concentration.

This analysis shows that within experimental error there is no correlation between the variation in intercept value and enzyme concentration.

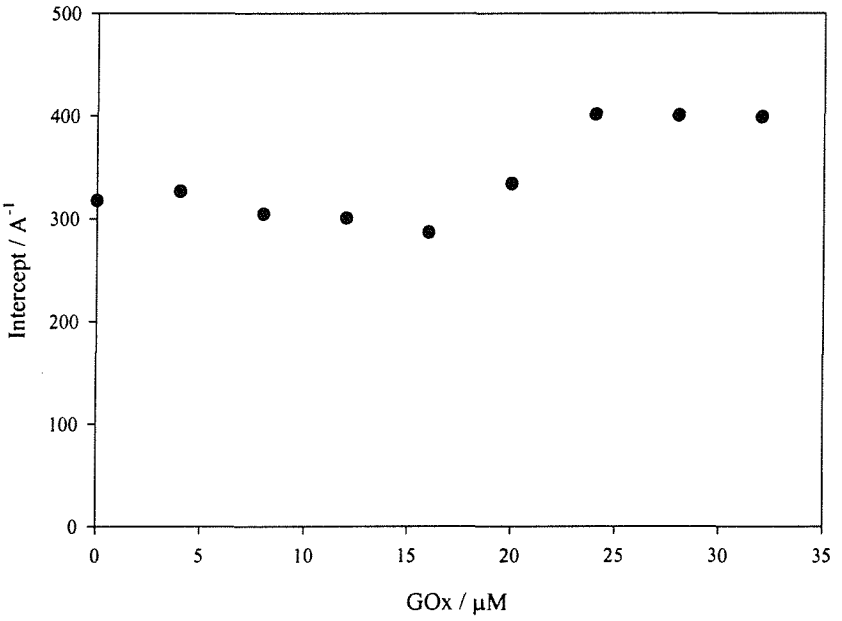

Figure 2: Intercept values from Figure 1 plotted against the corresponding glucose oxidase concentration.

Analysis of the intercept values with the studentttest provides the following information:

The mean value is 341 A^{-1}.

The standard deviation is 49.5 A^{-1}

The standard error is 17.5 A^{-1}

Confidence interval at 95 % is 41.4 A^{-1}

Confidence interval at 99% is 61.3 A^{-1}

The number of values is 8.

All values are within the confidence interval at 99% meaning that none of these values is significantly different from the mean value of the entire statistical population.

We conclude that no significant change in electron transfer kinetics is caused by the increasing glucose oxidase concentration.

On the other hand we observe a significant increase in the values of the slope from Figure 1 with enzyme concentration, these slopes are plotted against glucose oxidase concentration in Figure 3.

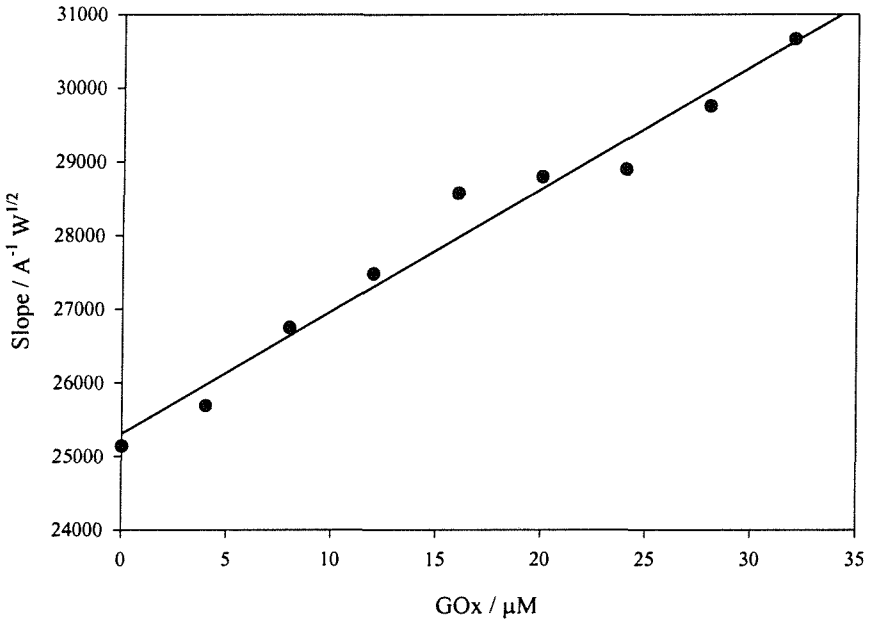

Figure 3: regression slopes from Figure 1 are plotted against glucose oxidase concentration the slope of this regression is 166 A^{-1} $W^{1/2}$ μM^{-1}.

Figure 3 shows how the slope of the regression from Figure 1 increases with enzyme concentration. The slope of the regression in this plot is 166 A^{-1} $W^{1/2}$ μM^{-1}.

To explain the behaviour of the current with increasing glucose oxidase concentration, we will try to identify the parameters of the electron transfer reaction that may be affected. We will now see what the implications of these results may imply for the diffusion of *p*-aminophenol under these conditions.

1.1.2 Influence on the viscosity

One hypothesis is that the increasing protein concentration affects the viscosity of the solution. In the Koutecky-Levich plot, the change in slope can be due to a change in viscosity as the concentration of *p*-aminophenol remains unchanged. In the Koutecky-Levich equation (2), $I_{l,c}$ (3) depends on $D^{2/3}\nu^{-1/6}$. According to the Stokes-Einstein equation.

$$D = \frac{kT}{6\pi\eta a} \tag{6}$$

Where k is the Boltzmann constant 1.38 10^{-23} kg m^2 s^{-2} K^{-1}, T is the temperature in K, a is the radius of the species (including its hydration shell) also known as hydrodynamic radius in m, η is the viscosity in kg m^{-1} s^{-1}, and D is the diffusion coefficient in m^2 s^{-1}.

Attempts were made to measure the diffusion coefficient of *p*-aminophenol accurately at pH 9.5 by rotating disc voltammetry, but the unstability of *p*-aminophenol at this pH prevented us from obtaining sensible results.

However, from equation (6), equation (7) is obtained (Levich).

$$D = \frac{Const_1}{\nu} \tag{7}$$

D is the diffusion coefficient and ν is the kinematic viscosity in cm^2 s^{-1}.

Equation (3) can be rearranged using equation (7) to give:

$$I_{l,c} = 1.554nFAC_0Const_1^{2/3}\nu^{-5/6}W^{1/2} \tag{8}$$

Using the D value calculated for *p*-aminophenol from the current slope value from Figure 1 when no glucose oxidase is present, where the kinematic viscosity is assumed to be similar to water, 0.01 cm^2 s^{-1}, $Const_1$ may be estimated as 2.06 10^{-8} cm^4 s^{-2}. The corresponding diffusion coefficient of *p*-aminophenol at pH 9.5 is 2.06 10^{-6} cm^2 s^{-1}. The kinematic viscosity may be calculated and related to the different enzyme concentrations used in this experiment from the Koutecky-Levich plot (Figure 1) according to equation (8).

By expressing the diffusion coefficient according to equation (7) in (8) we can relate the change in slope to the corresponding change in viscosity. Results are displayed in Table 2:

Enzyme 10^{-6}M	0	4	8	12	16	20	24	28	32
Slope $A^{-1}Hz^{-1/2}$	25141	25689	26749	27480	28573	28796	28894	29753	30663
ν $10^{-2}cm^2s^{-1}$	1	1.02	1.08	1.11	1.16	1.17	1.18	1.22	1.27

Table 2: kinematic viscosity values corresponding to the increase in protein concentration.

From Table 2 we observe a significant change of viscosity with glucose oxidase concentration. However, when the glucose oxidase concentration is 0, the value for the diffusion coefficient is not the same as the diffusion coefficient we calculated at pH 7.4 for *p*-aminophenol in chapter 5 as shown in Table 3

From equation (7) and the viscosity values showed in Table 2 the diffusion coefficients may be calculated as shown in Table 3

Enzyme concentration 10^{-6}M	0	4	8	12	16	20	24	28	32
D 10^{-6} cm^2s^{-1}	2.06	2.02	1.9	1.85	1.77	1.74	1.74	1.69	1.62

Table 3: Diffusion coefficient of *p*-aminophenol at pH 9.5 with increasing concentration of glucose oxidase.

We observe a linear decrease of diffusion coefficient with enzyme concentration. But the first value when no glucose oxidase is present, is different from the value we obtained from rotating disc voltammetry at pH 7.4 for *p*-aminophenol, D = 8.5 10^{-6} cm^2 s^{-1}. A likely explanation for this difference comes from the UV study of the compound at pH 9.5 (chapter 5), which leads us to think that at pH 9.5 *p*-aminophenol may form aggregates in solution. If this is the case, the Stokes radius of the diffusing structure is increased resulting in a smaller diffusion coefficient according to the Stokes-Einstein equation (6). According to this equation, the corresponding stokes radius of *p*-aminophenol for D = 8.5 10^{-6} cm^2 s^{-1} (chapter

5, pH 7.4) is $a = 2.56\ 10^{-10}$ m. At pH 9.5 we calculated $D = 2.06\ 10^{-6}$ cm^2 s^{-1} according to the Stokes-Einstein equation $a = 10^{-9}$ m, which implies the formation of tetramers of *p*-aminophenol in solution at pH 9.5. This is consistent with the UV data obtained from *p*-aminophenol solutions at alkaline pH.

The reason why glucose oxidase increases the viscosity of the solution may be due to the glycosilation of the protein surface. In the literature related to redox enzyme sensors, no mention of viscosity changes due to protein concentration has been mentioned.

1.2 influence of glucose

Having seen the influence of glucose oxidase concentration on the solution viscosity, we now study the influence of glucose at 100 mM without glucose oxidase in the solution. To do so a fresh solution of *p*-aminophenol was prepared containing 100 mM glucose. A potential of 0 V was applied to the glassy carbon working electrode, and the current was recorded at several rotation speeds. For comparison, the same experiment was carried out under the same conditions without glucose. The Koutecky-Levich plots of the currents recorded during this experiment are showed in Figure 4.

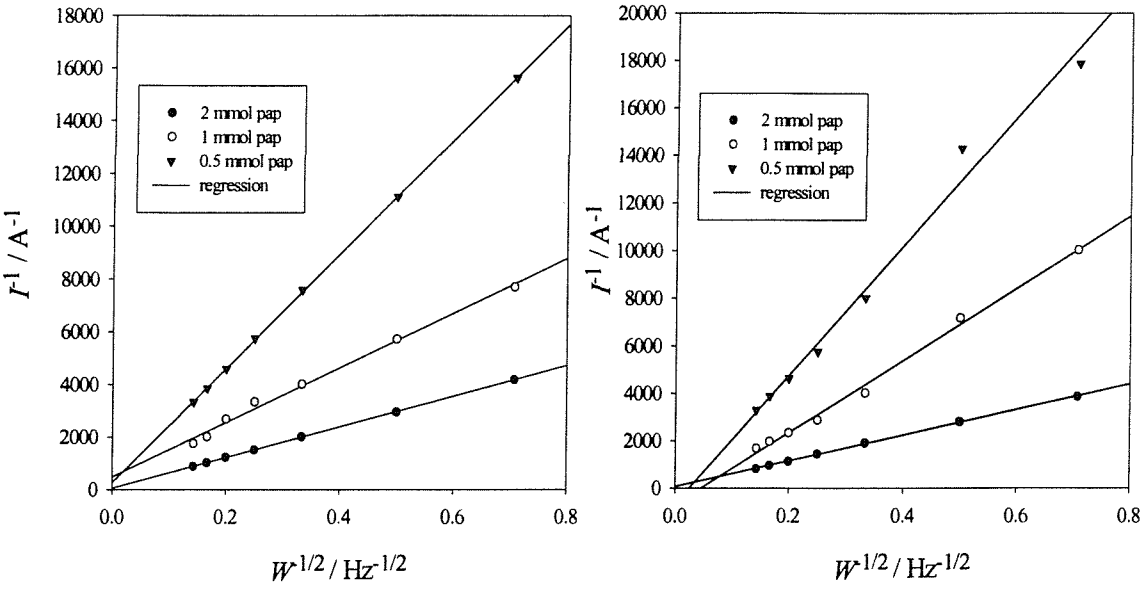

Figure 4 Koutecky-Levich plots of rotating disc electrode experiment at 0 V with *p*-aminophenol (pap) at 0.2, 0.5, 1 mM in Tris-HCl buffer pH 9.5. The background electrolyte is KCl 0.5 M. Left 7 mm glassy carbon working electrode, no glucose in solution, right 7 mm glassy carbon working electrode with 100 mM glucose present in solution.

Figure 4 shows all regressions on both plots to pass through the origin (within experimental error). However the slopes of the regression lines for each *p*-aminophenol concentration seem to be different when glucose is present or not.

Concentration / mM	Without glucose Slope / $A^{-1}Hz^{-1/2}$	100 mM glucose Slope / $A^{-1}Hz^{-1/2}$
2	22000	27000
1	10500	15000
0.5	5800	5800

Table 4: shows the slope values for the Koutecky-Levich plots from Figure 4. The slope of the linear regression is given for each concentration of *p*-aminophenol with and without glucose.

According to Table 4 there is a difference in the slope of the linear regression from the Koutecky-Levich plots in Figure 4 between the experiment carried out in presence of glucose (100 mM) and without glucose. The difference in slope on the Koutecky-Levich plot between the experiment with and without glucose for the same *p*-aminophenol concentration implies a difference of kinematic viscosity and diffusion coefficient between the two solutions. From the slope values it is possible to evaluate how the glucose in solution affects the viscosity. To do so, the diffusion coefficient in equation (4) is replaced by its expression in equation (7) leading to equation (8). By dividing the slope of the regression for a given concentration of *p*-aminophenol from Figure 4 with glucose by the slope of the linear regression from the same concentration of *p*-aminophenol without glucose, the following expression is obtained:

$$\left(\frac{S_1}{S_2}\right)^{6/5} = \frac{\nu_1}{\nu_2} \qquad (9)$$

Where S_1 is the slope of the regression from the Koutecky-Levich plot (Figure 4) in $A^{-1}\ Hz^{-1/2}$ from the experiment with glucose present, S_2 is the slope of the regression from the Koutecky-Levich plot in $A^{-1}\ Hz^{-1/2}$ from the experiment with no glucose present, and respectively ν_1 and ν_2 are the kinematic viscosities in $cm^2\ s^{-1}$ of the solution with and without glucose.

From equation (9) the difference of slope values showed in Table 4 show an average increase of kinematic viscosity of a factor 1.26 from the solution without glucose to the solution with glucose.

The same experiment was reproduced with a platinum working electrode. The corresponding Koutecky-Levich plots are displayed in Figure 5.

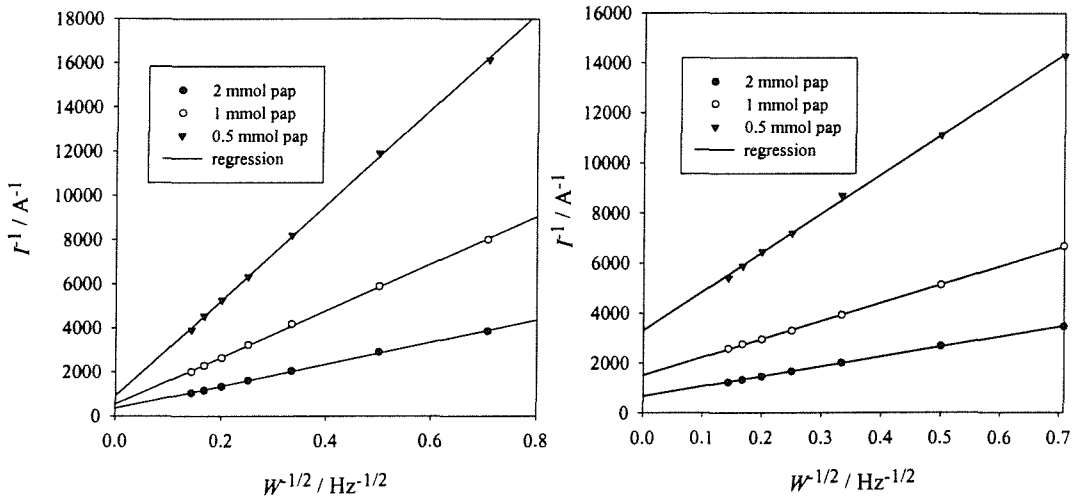

Figure 5: Koutecky-Levich plots of rotating disc electrode experiment at 0 V with *p*-aminophenol at 0.2, 0.5, 1 mM in Tris-HCl buffer pH 9.5. The background electrolyte is KCl 0.5 M. Left 7 mm platinum working electrode, no glucose in solution, right 7 mm glassy carbon working electrode with 100 mM glucose.

Figure 5 shows Koutecky-Levich plots of rotating disc experiments with a platinum working electrode. When glucose is present (Figure 5 right) the intercept of the linear regressions do not pass through the origin. When no glucose is present (Figure 5 left) the results are the same as the experiments carried out with the glassy carbon electrode (Figure 4 left). When the rotation speed tends to infinity, the mass transport limited current tends to infinity. In the case of mass transport limited current the intercept of the regression line is the origin within experimental error. If the current is kinetically limited, the intercept moves away from the origin. These results imply that interference to the electron transfer occurs when a platinum electrode is used in the presence of glucose. The glassy carbon working electrode does not seem to be affected. The interactions between glucose and noble metals is an important area of investigation, a significant amount of information has already been published on the subject [1-3]. Therefore it is not surprising that the electron transfer kinetics should be affected when electrochemistry is carried out with a platinum working electrode in presence of glucose.

This section showed that in alkaline conditions, the addition of a large concentration of glucose oxidase generates important changes of viscosity in the solution, that cannot be ignored. A large concentration of glucose (100 mM) increases the kinematic viscosity by a factor 1.26 with respect to the glucose free solution at pH 9.5. When a platinum working electrode is used, glucose will interfere with the electron transfer kinetics for *p*-aminophenol oxidation. As a result, only glassy carbon electrodes were used in the following kinetic analysis.

2- Glucose oxidase kinetic analysis at pH 9.5

This section is aimed at understanding glucose oxidase re-oxidation kinetics. As explained earlier, *p*-aminophenol is to undergo a cycle of oxidation at the electrode and reduction by reduced glucose oxidase. In chapter 5, we described the electrode oxidation reaction and we will now be studying the reduction of quinone imine by the reduced enzyme. The reason for this is to quantify the amplification of the current for *p*-aminophenol oxidation produced by the recycling of quinone imine by glucose oxidase in the presence of glucose. We know how to relate the oxidation current to the concentration of *p*-aminophenol when no glucose oxidase is present. When the amplification takes place, we need to understand the enzyme reaction kinetics in order to relate the oxidation current to the concentration of mediator. To determine the re-oxidation kinetic constant of the enzyme, we have used rotating disc voltammetry. Under these conditions we have been able to base our study on a mathematical model available from the literature.

Glucose oxidase kinetics were studied according to the mathematical model initially published by Albery *et al.* [4] in which homogenous conditions where the mediator is present in the bulk solution are discussed. Bartlett and Pratt[5] published a detailed kinetic analysis for glucose oxidase in homogenous catalytic conditions with ferrocene carboxylic acid working as mediator. Here we will use the same model to recalculate the kinetic constants at pH 9.5.

The theoretical model is extensively described in the above-cited literature and we will only recall the main outlines in this chapter. For further detail, the reader should refer to the published work.

2.1- Theory for homogenous enzyme catalysis

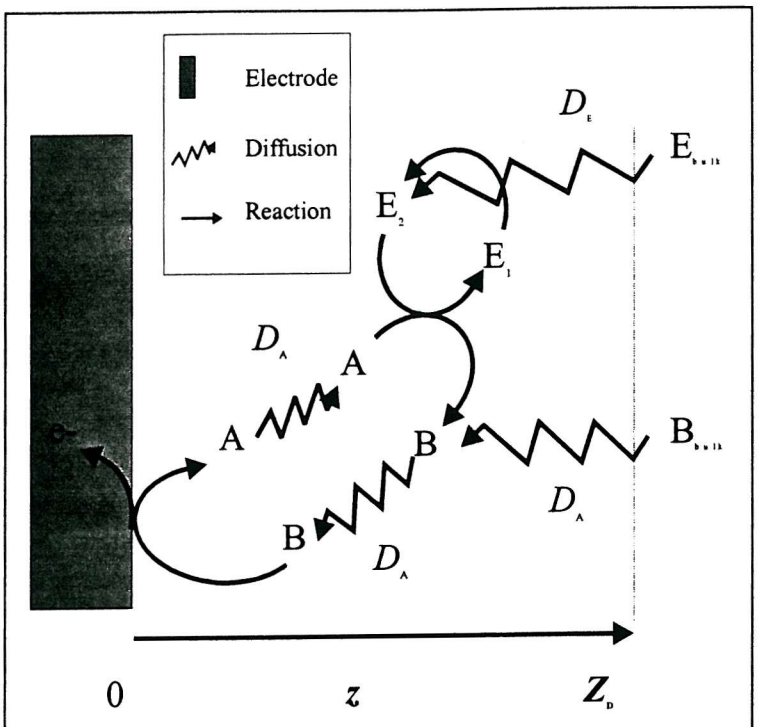

Figure 6: A schematic diagram of the homogeneous system as considered by Albery *et al.*[6] A and B are the oxidised and reduced forms of the mediator respectively. E_1 and E_2 are oxidised and reduced enzyme respectively. The substrate is not explicitly considered in this treatment, its effect on the rate of reduction of E_1 to E_2 is taken in consideration in the calculation of k_s. D_E is the diffusion coefficient of enzyme E_1 and E_2, D_A is the diffusion coefficient of mediator A and B. Z_D is the Levich diffusion length defined in equation (1). Inside the diffusion layer ($z<Z_D$) mass transport is by diffusion alone, whereas outside Z_D the bulk concentrations of B and E_2 are maintained at E_{bulk} and B_{bulk} respectively by convection. Oxidised mediator A is only produced at the electrode surface by re-oxidation of B.

In deriving the model (Figure 6) it is assumed that the substrate concentration is sufficiently high that substrate depletion at the electrode is insignificant.

The reactions occurring in solution are:

$$E_2 + A \xrightarrow{k_M} B + E_1 \qquad (10)$$

$$E_1 \xrightarrow{k_E} E_2 \tag{11}$$

Where

$$k_E = k_{cat}\ s_\infty / (K_M + s_\infty) \tag{12}$$

and s_∞ is the substrate concentration in the bulk solution. The reaction scheme is summurised in Figure 6.

Diffusion-reaction equations can then be written for the four species A, B, E_1 and E_2. Following Albery *et al.*

$$\frac{\partial a}{\partial t} = D_A \frac{\partial^2 a}{\partial z^2} - k_M e_2 a \tag{13}$$

$$\frac{\partial b}{\partial t} = D_A \frac{\partial^2 b}{\partial z^2} + k_M e_2 a \tag{14}$$

$$\frac{\partial e_2}{\partial t} = D_E \frac{\partial^2 e_2}{\partial z^2} - k_M e_2 a + k_E e_1 \tag{15}$$

$$\frac{\partial e_1}{\partial t} = D_E \frac{\partial^2 e_1}{\partial z^2} + k_M e_2 a - k_E e_1 \tag{16}$$

We are interested in the steady state response, therefore equations (13)-(16) are all set equal to zero.

The total concentration e_Σ is assumed to be uniform throughout the solution. This corresponds to taking the diffusion coefficients for the oxidised and the reduced forms of the enzyme as being equal. Then at any point in the solution:

$$e_1 + e_2 = e_\Sigma \tag{17}$$

Similarly, assuming equal diffusion coefficients for the oxidised and the reduced forms of the mediator and assuming that the mediator is entirely in its reduced form in bulk solution, we have:

$$a + b = m_\Sigma = b_\infty = a_0 \tag{18}$$

Where m_Σ is the total mediator concentration at any point, b_∞ is the bulk concentration of reduced mediator B and a_0 is the concentration of A at the electrode surface when we are in the limiting current region.

The following dimensionless variables are used in the model:

$$u = a / m_\Sigma \tag{19}$$

$$u' = b / m_\Sigma \tag{20}$$

$$v = e_2 / e_\Sigma \tag{21}$$

$$\chi = z / Z_D \tag{22}$$

$$\kappa_M = k_M Z_D^2 e_\Sigma / D_A \tag{23}$$

$$\kappa_E = k_E Z_D^2 / D_E \tag{24}$$

$$\gamma = k_M a_0 / k_E \tag{25}$$

Here Z_D is the Levich diffusion layer thickness given by:

$$Z_D = 0.642\, \nu^{1/6}\, D_A^{1/3} / W^{1/2} \tag{26}$$

Where ν is the kinematic viscosity in $cm^2\ s^{-1}$ and W / Hz is the rotation speed.

In dimensionless form equations (13) and (15) become:

$$\frac{d^2u}{d\chi^2} = \kappa_M uv \tag{27}$$

$$\frac{d^2v}{d\chi^2} = \gamma\kappa_M uv - \kappa_E(1-v) \tag{28}$$

The current I is calculated from the flux of mediator reacting at the electrode:

$$I = -nFAD_A \frac{da}{dz}\Big|_{z=0} \tag{29}$$

In dimensionless terms this becomes:

$$I = -\frac{nFAD_A m_\Sigma}{Z_D} \frac{du}{d\chi}\Big|_{\chi=0} \tag{30}$$

We are interested in the situation where the reduced mediator is present in the bulk solution. Therefore when $z = Z_D$ and $\chi = 1$:

$$a = 0 \qquad b = m_\Sigma \qquad u = 0 \tag{31}$$

At the electrode surface, where $z = 0$ and $\chi = 0$, in this situation unlike the related work published by Albery *et al.* and Bartlett *et al.* the electrode oxidation of the mediator is

kinetically limited. Therefore the assumption that the mediator is converted entirely into its oxidised form is not valid. Instead the boundary conditions are:

$$a < m_\Sigma \qquad b = m_\Sigma - a \qquad u = \frac{m_\Sigma - b}{m_\Sigma} \tag{32}$$

The electrode reaction being described by:

$$B \xrightarrow{k_b} A + e^- \tag{33}$$

Where B is p-aminophenol, A_1 is quinone imine, and k_b is the electron transfer reaction rate constant at the electrode.

We find that Cases I and VIII (according to Albery *et al.*) are defined by equation (34).

$$\frac{D\partial^2 a}{\partial x^2} = -k_m[E_\Sigma]a \tag{34}$$

at $x=\chi_D$; $a=0$

at $x=0$; $a=a_0$

If we consider the steady state conditions:

$$\left.\frac{D\partial a}{\partial x}\right|_{x=0} = -\left.\frac{D\partial b}{\partial x}\right|_{x=0} \tag{35}$$

Each term from equation (35) is defined by:

$$-k_b b_0 = -k_b(m_\Sigma - a_0) \tag{36}$$

Where $m_\Sigma = (a + b)$.

Determination of amperometric response I requires the solution of equations (35) and (36) with the boundary conditions from (31) and (32).

$$\chi_K = \sqrt{\frac{D}{k_m[E_\Sigma]}} \tag{37}$$

$$a = A_1 \sinh(x/\chi_K) + B_1 \cosh(x/\chi_K) \tag{38}$$

$$\frac{\partial a}{\partial x} = \frac{A_1}{\chi_K}\cosh(x/\chi_K) + \frac{B_1}{\chi_K}\sinh(x/\chi_K) \tag{39}$$

To solve this equation, we use the following boundary conditions:

$$0 = A_1 \sinh(\chi_D/\chi_K) + B_1 \cosh(\chi_D/\chi_K) \tag{40}$$

where:

$$\frac{A_1}{\chi_K} = \frac{-k_b(m_\Sigma - a_0)}{D} \tag{41}$$

and:

$$a_0 = B_1 \tag{42}$$

By inserting the expression of B in equation (40) we obtain:

$$A_1 = \frac{k_b \chi_K m_\Sigma}{\tanh(\chi_D/\chi_K)k_b\chi_K + D} \tag{43}$$

The new expression of A_1 is substituted in equation (29) give the following expression for the current:

$$I = \frac{nFAm_{\Sigma}k_b}{1+\frac{k_b\chi_K}{D}\tanh(\chi_D/\chi_K)} \quad (44)$$

2.2 Limiting cases

In order to define the right conditions that will enable us to relate the current to the re-oxidation rate of the enzyme $\gamma < 1$ (25), experiments were performed respecting the boundary conditions of case I and VIII. These are the boundary conditions required for a kinetically limited enzymatically amplified electrode oxidation (case I). In order to determine the experimental conditions necessary to meet this requirement, it is helpful to have estimates of the various rate constants and diffusion parameters for our system taken from the literature. These were used as a starting point for the design of our experiment. Approximate values for the relevant parameters are as follows:

$D_M \approx 10^{-6}$-10^{-5} cm^2 s^{-1}, $D_E \approx 10^{-7}$-10^{-6} cm^2 s^{-1}, $\nu \approx 10^{-2}$ cm^2 s^{-1}, $k_M \approx 10^5$ mol dm^3 s^{-1}, $k_{cat} \approx$ 500-1000 s^{-1}.

The maximum value of k_E is k_{cat} when $s_\infty >> K_M$. Therefore to achieve $\gamma<1$ it is best to make the substrate concentration as high as practical. This has the added benefit that it minimizes the chances of substrate depletion being significant since, if $s_\infty >> K_M$, a small decrease in substrate concentration will not affect k_E. Taking the worst case estimate for the rate parameters, the requirement for $\gamma<1$ is equivalent to $m_\Sigma < 2.5$ mmol dm^{-3} and therefore a mediator concentration of 1 mmol dm^{-3} was used.

The experiment was temperature controlled at 25°C, and each set of measurements were obtained from a fresh 30 ml *p*-aminophenol solution. The solutions were prepared immediately before each set of measurements was carried out and the buffer solution (pH 9.5 Tris-HCl 0.1 M) containing glucose (0.1 M) and background electrolyte (0.1 M KCl) was kept under argon bubbling in the 25°C water bath throughout. Once the solution was

prepared, the rotation speed of the working electrode was set at 49 Hz and a potential of 0 V was applied. The current was recorded varying the rotation speed from 49 to 0.5 Hz. These currents enabled us to ensure identical dilution of *p*-aminophenol from one experiment to the next. The rotation speed was reset at 49 Hz and glucose oxidase concentrate solution was added to the cell. The lowest enzyme concentration (0.312 μM) resulted in the addition of 6.42 μl of glucose oxidadase solution and the highest (32.6 μM) was 658 μl for a maximum dilution effect of 2% on the rest of the solution. 0 V were applied and the rotation speed was varied to 0.5 Hz while the current was recorded. For each change in rotation speed the current was recorded for 30 s to allow a steady convection through the solution. This experiment was reproduced 10 times in all. Results are displayed in Figure 8

These conditions are defined by equation (44), which is defined by three limiting conditions:

Condition 1: kinetically controlled current

$k_b\chi_K << 1 \qquad I \approx nFAk_b m_\Sigma$

(45)

Condition 2: catalytically controlled current

$k_b\chi_K >> 1;\ \chi_D >> \chi_K \qquad I \approx \frac{nFADm_\Sigma}{\chi_K}$

(46)

Condition3: potential independent current

$k_b\chi_K >> 1;\ \chi_D << \chi_K \qquad I \approx \frac{nFADm_\Sigma}{\chi_D}$

(47)

The above limiting cases can be illustrated as follows:

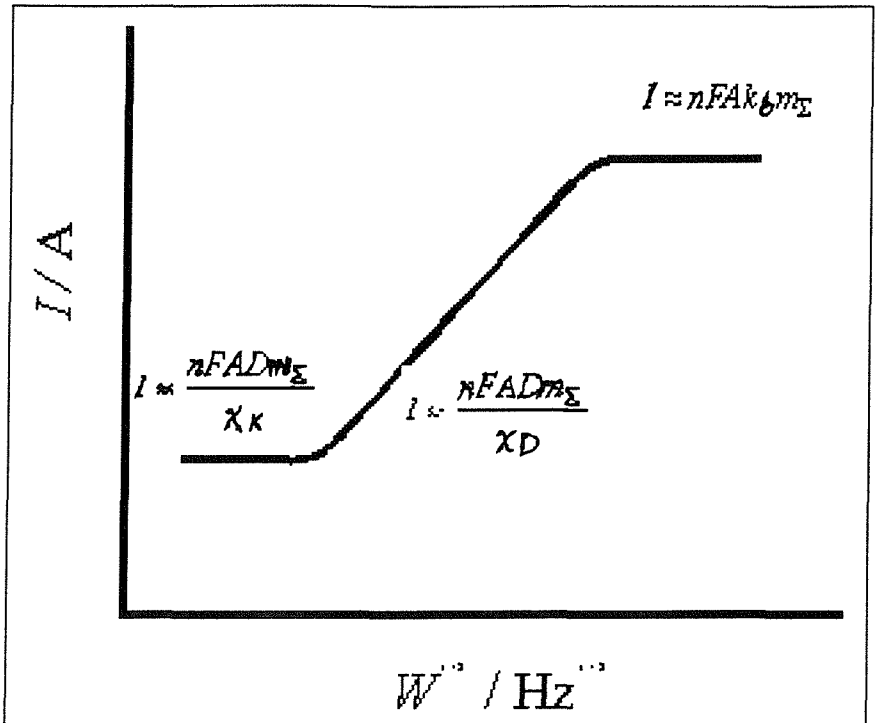

Figure 7: sketch of the current behaviour against rotation speed (equation (44)) according to the limiting case.

The experimental data displayed in Figure 8 are fitted with equation (44), each set of data is fitted individually. Three parameters are fitted in each case:

$$I = \frac{A}{1 + B[E_\Sigma]^{-1/2} \tanh\left(\frac{C[E_\Sigma]^{-1/2}}{W^{1/2}}\right)}$$

$$A = nFAm_{\Sigma}k_b \tag{48}$$

$$B = \frac{k_b}{\sqrt{D[E_{\Sigma}]}k_{\mathrm{M}}} \tag{49}$$

$$C = 0.643D^{-1/6}\nu^{1/6}\sqrt{k_M[E_{\Sigma}]} \tag{50}$$

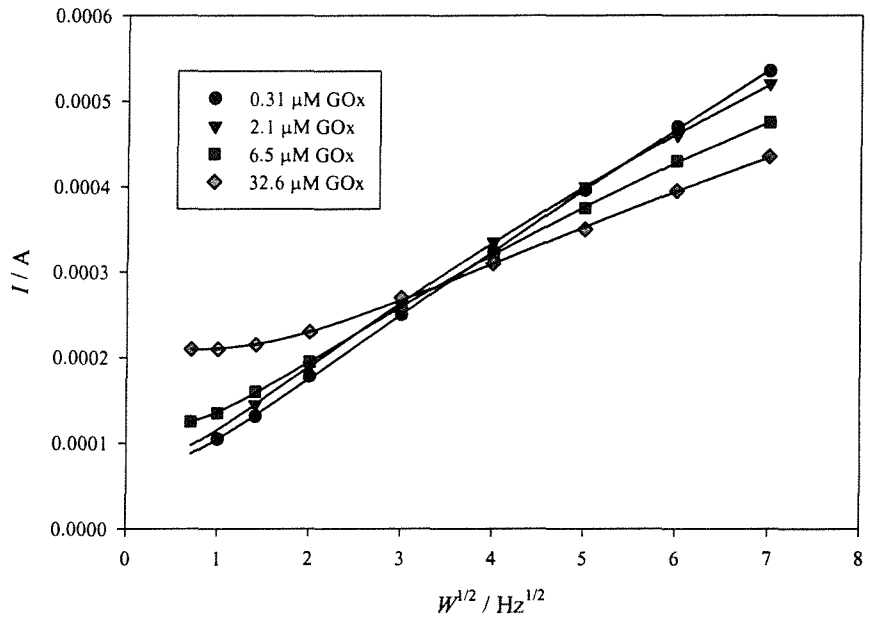

Figure 8: the conditions used are pH 9.5 Tris-HCl 0.1 M, KCl 0.1 M, glucose 0.1 M, with rotation speeds of 0.5, 1, 2, 4, 9, 16, 25, 36, 49 Hz for the following enzyme concentrations: 0.312 μM; 2.12 μM; 6.46 μM and 32.6 μM. The potential is 0 V using a 7 mm diameter glassy carbon working electrode.

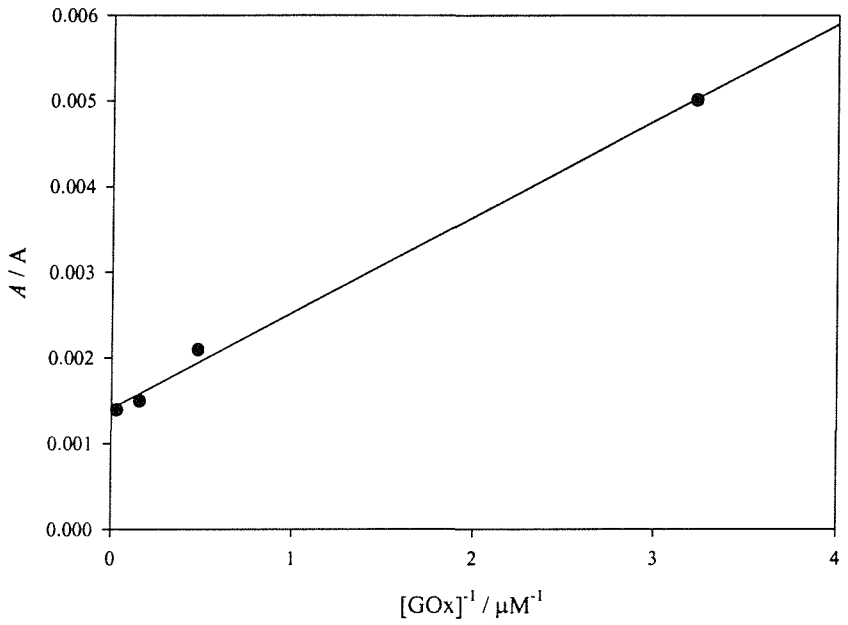

Figure 9: parameter *A* defined by (48) is plotted against the invert of glucose oxidase concentration.

2.3 Data analysis

Parameters *A*, *B*, and *C* defined by the equations (48), (49), and (50) are plotted against glucose oxidase concentrations in Figure 9, Figure 10, Figure 11.

Parameter *A* shows a dependence on the inverse of the glucose oxidase concentration, which is unexplained. However this dependence may be the result of a working electrode area diminution due to the reversible adsorption of glucose oxidase on the glassy carbon working electrode.

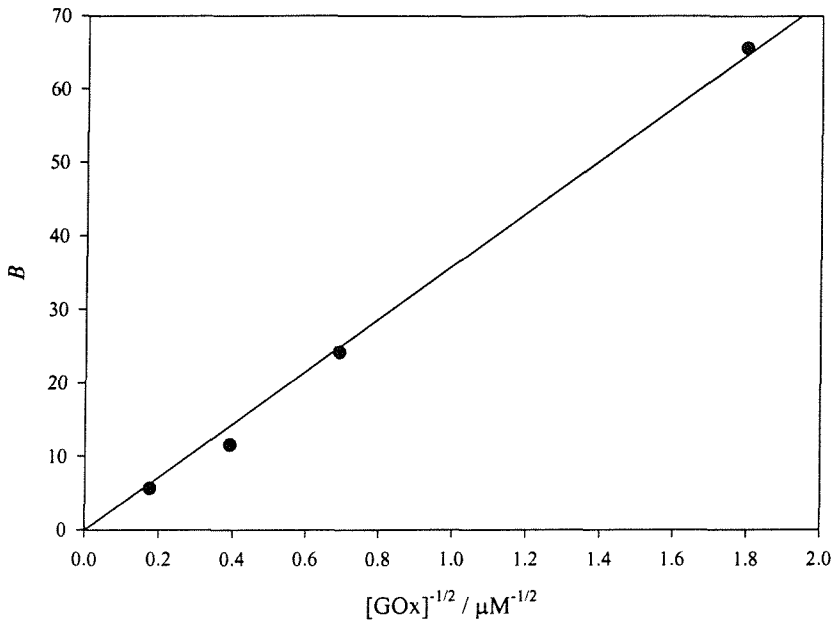

Figure 10: parameter B defined by **(49)** is plotted against $[GOx]^{-1/2}$ to obtain the slope of the regression.

Variation of B against the invert of the square root of glucose oxidase concentration is in perfect agreement with the theory and the slope value of the regression line is given by $\frac{k_b}{\sqrt{Dk_M}}$. The effect of the variation of D does not appear significant in this case

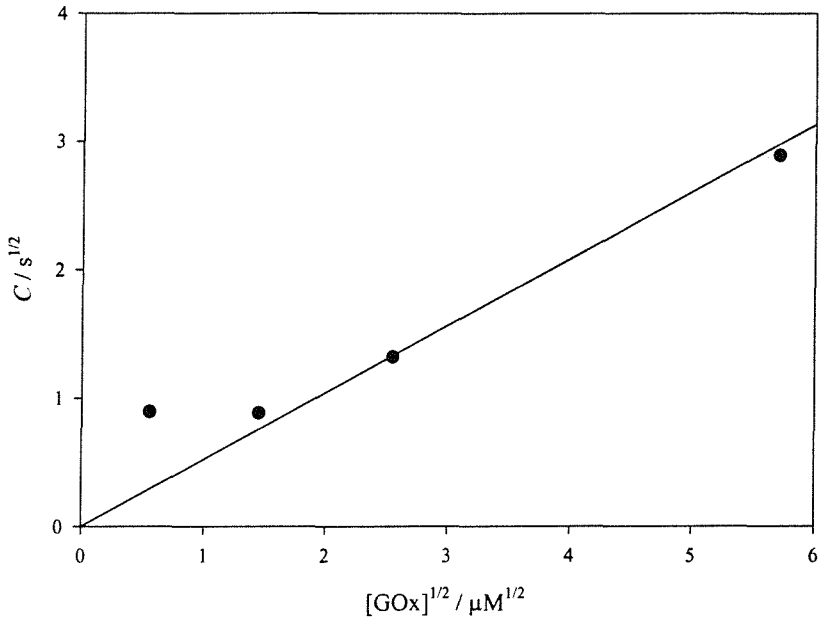

Figure 11: parameter C defined by (50) is plotted against the square root of glucose oxidase concentration.

Parameter C shows deviation from the theory at low glucose oxidase concentration, otherwise the fit to the theory is good. The slope of the regression line is given by $0.643D^{-1/6}\nu^{1/6}\sqrt{k_M}$.

2.4 Calculation of k_b, and k_M

In order to determine k_M from the fitting of parameter B, we need to determine k_b. This is done by plotting our experimental currents as $1/I$ against $W^{1/2}$. The intercept current value W tends to infinity is defined as follows:

$$1/I = \frac{1}{nFAm_{\Sigma}k_b} \tag{51}$$

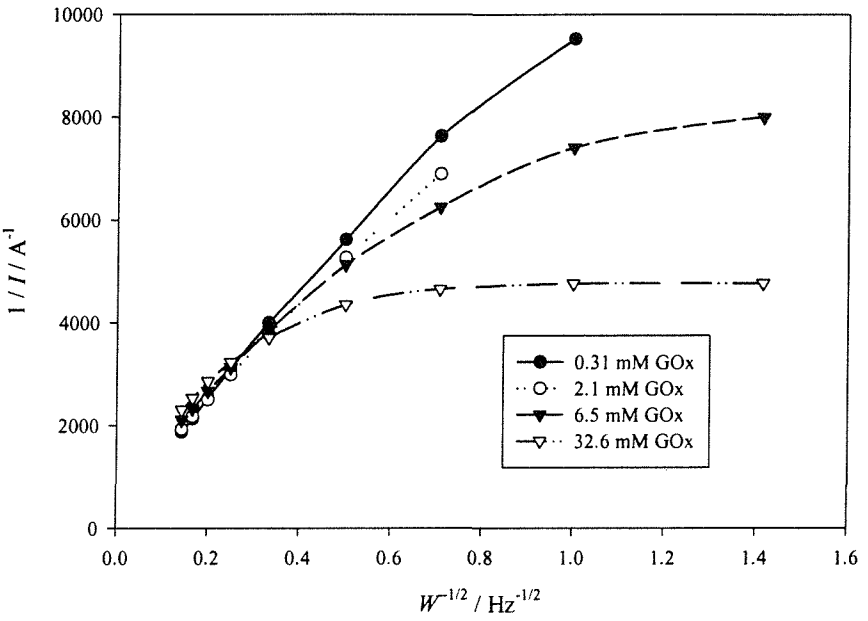

Figure 12: the data from Figure 8 is replotted to isolate the intercept value at $W^{-1/2} = 0$. The value is 342 A^{-1}.

From equation (52) and the intercept value obtained from Figure 12 we calculate k_b = 0.0394 cm s^{-1}.

The k_M was calculated to be between 0.57 10^5 (Figure 10) and 0.03 10^5 $mol^{-1}dm^3s^{-1}$ (Figure 11). It represents the rate constant for the re-oxidation of the enzyme. This value is approximately four times less the k_M value calculated by Bartlett *et al.*[5] in pH 7, when Ferrocene carboxylic acid is used as mediator.

3- Alkaline phosphatase

Now that the re-oxidation constant of glucose oxidase has been calculated (k_M = 0.57 10^5 mol^{-1} dm^3 s^{-1}), we are able to estimate the rate of amplification that will be provided by the redox enzyme. We now need to determine the kinetics of the alkaline phosphatase catalysed *p*-aminophenyl phosphate hydrolysis. This study will provide us with values for K_M and k_{cat} in these conditions.

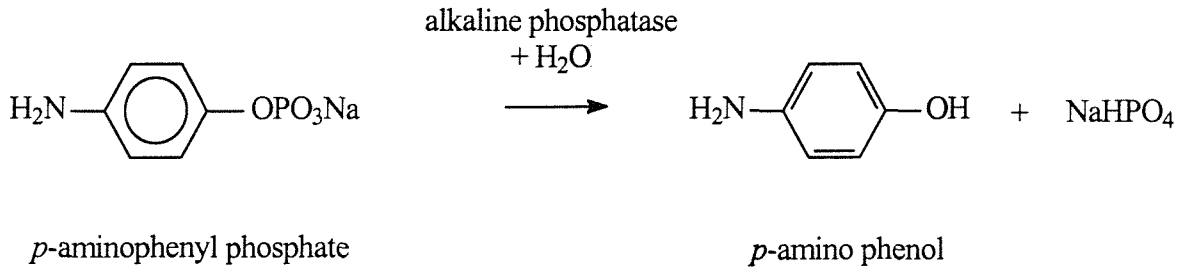

Figure 13: reaction scheme for *p*-aminophenyl phosphate hydrolysis catalysed by alkaline phosphatase. The products are *p*-aminophenol and phosphate.

The alkaline phosphatase catalysed *p*-aminophenyl phosphate hydrolysis is sketched in Figure 13.

3.1 *p*-aminophenyl phosphate electrochemistry

This subject was studied in the previous chapter, in that study we verified that at pH 9 *p*-aminophenol phosphate will not generate *p*-aminophenol spontaneously if the working electrode potential is kept at 0 V. The irreversible oxidation of *p*-aminophenyl phosphate takes place at 0.6 V and the oxidation product is likely to be quinone imine. The rotating disc voltammetry at the glassy carbon working electrode enabled us to evaluate the diffusion coefficient of *p*-aminophenyl phosphate but also showed that platinum working electrodes could not be used to study this compound. We also showed that glucose oxidase and glucose in the *p*-aminophenyl phosphate solution did not cause the later to hydrolyse into *p*-aminophenol.

3.2 Kinetic parameters

The system we are studying now does not involve any recycling process from glucose oxidase. Here we are interested in the rate of hydrolysis of *p*-aminophenyl phosphate. The hydrolysis product (*p*-aminophenol) is detected at the working electrode at 0 V. The reaction scheme is shown in Figure 14. In this case again, we have used rotating disc voltammetry in order to control mass transport to the electrode.

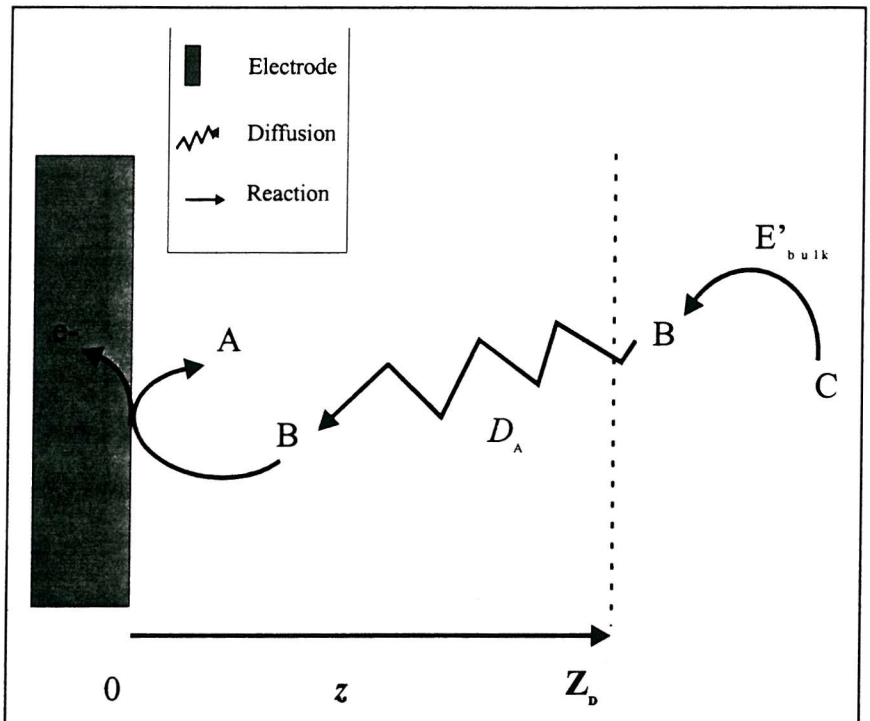

Figure 14: A and B are the oxidised and reduced forms of the mediator respectively. D_A is the diffusion coefficient of mediator A and B. Z_D is the Levich diffusion length defined in (1).

3.3 Calibration of *p*-aminophenol

The purpose of this section is to establish how the oxidation current of *p*-aminophenol at the electrode may be related to *p*-aminophenol concentration. To determine the kinetics of

alkaline phosphatase, we are working at pH 9.5 Tris-HCl buffer 0.1 M (KCl 0.1 M) with a glassy carbon rotating disc electrode.

With a rotating disc electrode set at 0 V in pH 9.5 buffer, the current increase due to *p*-aminophenol oxidation is linear with *p*-aminophenol concentration (Figure 15). To be able to resort to classical enzyme kinetic equations, this linear relation was taken advantage of to convert recorded currents into concentrations.

For this calibration experiment, 30 ml of buffer and background electrolyte solution were water jacketed at 25°C and degassed with argon . The rotation speed of the working electrode was set at 49 Hz and a 0 V potential was applied. A concentrated solution of *p*-aminophenol (0.3 M) was prepared, 10 µl fractions of the concentrated solution were added to the cell. The current was recorded throughout the experiment and the values of the current after each addition are plotted in Figure 15.

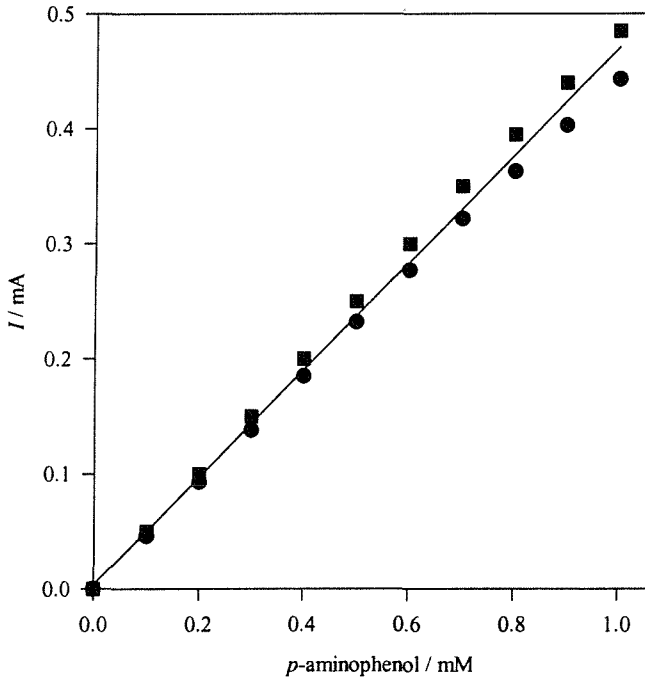

Figure 15: Calibration of *p*-aminophenol from 0 to 1 mM in pH 9.5 Tris-HCl buffer 0.1 M, KCl 0.1 M. The glassy carbon working electrode is 7 mm diameter and values are recorded at 49 Hz in a 30 ml solution previously degassed with argon. The counter electrode is platinum mesh, and reference is SCE. Square and circle symbols show extreme values from three sets of calibration results. The regression line was used to convert currents to concentrations.

This calibration experiment was carried out once a day (5 times) and proved to be reproducible. (Figure 15). The plots in Figure 15 show the current recorded from adding fractions of *p*-aminophenol from a freshly prepared *p*-aminophenol 0.3 M solution. We use the regression from this plot to convert our currents into concentration.

This section showed that at 49 Hz we can directly relate the current to *p*-aminophenol concentration. This will simplify the analysis of the data as all currents will be directly converted into mol dm^{-3}.

3.4 Alkaline phosphatase kinetics

In this section we will describe results for the study of the catalysed hydrolysis of *p*-aminophenyl phosphate. The reaction is catalysed by alkaline phosphatase. The product of the reaction is *p*-aminophenol and $NaHPO_4$. As shown earlier, by setting the potential of the working electrode at 0 V, we can detect *p*-aminophenol in the solution. By using a rotating disc electrode, the mass transport to the electrode is controlled and the stirring of the solution is maintained by a high rotation speed (49 Hz). At set potential, the current transient recorded against time is related to the hydrolysis reaction rate. The rates are given in A s^{-1}, which are later converted in M s^{-1}. To avoid a significant diminution of *p*-aminophenol in solution due to the amount of product reacting at the electrode, the total solution volume is 30 ml and the glassy carbon rotating disc electrode diameter is 7mm.

The enzyme catalysed reaction is expressed as:

$$E+S \underset{k_{-1}}{\overset{k_{+1}}{\rightleftharpoons}} ES \xrightarrow{k_{+2}} E+P \qquad (53)$$

where S is the substrate, E is the enzyme, ES is enzyme-substrate complex, and P is the product. The rate constants are $k_{+}1$ for the formation of the ES complex, $k_{-}1$ for the

dissociation of the ES complex into E and S, and $k_{+}2$ is the rate of dissociation of ES into E and P.

The E+P to ES rate constant is considered as insignificant, and hence conversion of ES into E + P irreversible.

The stationary state illustrates the case where most of the enzyme is in enzyme-substrate complex. At the early stage of the reaction no product is present, the reverse reaction of ES into E+S may be ignored for a very short time period. The initial reaction rate is assumed to be related to k_{+2}[E], which is the maximum rate for the reaction known as V_{max} when $[S] > k_M$. A new solution and a polished electrode were used for every experiment. The solution was degassed with argon and temperature controlled at 25°C. Alkaline phosphatase is an expensive consumable therefore before receiving it from the supplier, one has to schedule the experiments so that the enzyme does not deteriorate in storage, and also calculate the quantity required so that all experiments may be carried out. As a result, this kinetic study was done with the same alkaline phosphatase concentration throughout, and the substrate concentration was varied. Once the solution was prepared with the desired concentration of *p*-aminophenyl phosphate, the rotation speed of the rotating disc electrode was set at 49 Hz and 0 V were applied. At time zero, 13.5 ml of alkaline phosphatase solution were added to the cell yielding a final concentration of 25 nM. Every experiment was carried out in triplicate.

The slopes of the curves obtained from these experiments (in A s^{-1}) were analysed to determine the slope of the current near time zero (the initial rate), where the velocity of the reaction is closest to $k_{cat}[S]$. Each measurement was reproduced three times and the average values of these analyses are plotted in Figure 16. On the same figure, the error bars were calculated as the overage variance of all three values with respect to the average of the three values for a given substrate concentration.

Using the calibration curve displayed in Figure 15 initial velocity in A s^{-1} for various substrate concentrations are expressed in μM s^{-1}.

3.5 Michaelis-Menten

This representation was shown to follow the following equation:

$$v = \frac{V_{max}[S]}{K_m + [S]}$$

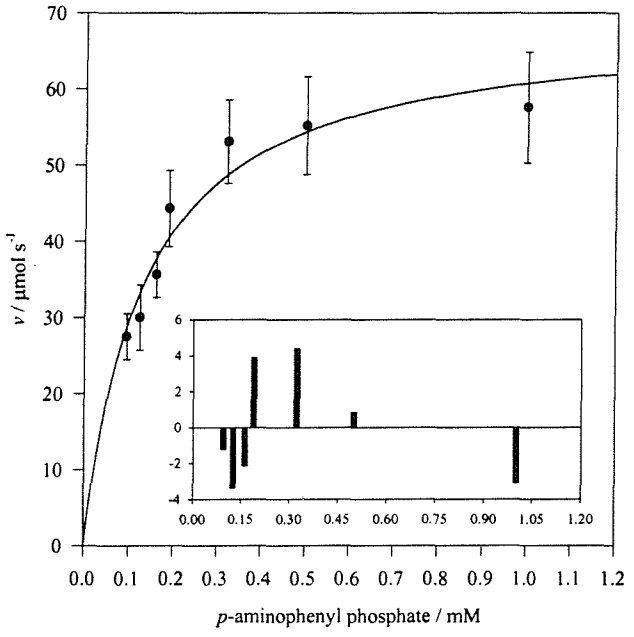

Figure 16: Michaelis-Menten representation of a substrate titration experiment. 25 nM alkaline phosphatase, 30 ml pH 9.5 Tris-HCl 0.1 M, KCl 0.1 M, *p*-aminophenyl phosphate is varied from 0 to 1 mM. The line shows the best fit of equation (54) to the data and the inset shows the residuals.

Figure 16 shows calibration data obtained for 25 nM alkaline phosphatase. The best fit of this data to equation (54) gives values of 1.32×10^{-4} mol dm^{-3} and 2.74×10^{3} s^{-1} for K_m and k_{cat} respectively under our conditions. The amperometric detection technique has an insignificant effect on the *p*-aminophenol concentration ($k \approx 8\times10^{-5}$ s^{-1}).

The literature provides varying values for these parameters Christie *et al.*[7] calculated K_m=1.25 mM at pH 10.2. But Thompson *et al.*[8] showed that both K_m and k_{cat} varied greatly with the pH, the buffering agent and the buffering agent concentration. For instance they showed that in 2-(methylaminoethanol) pH 10 buffer, K_m could vary from 0.2 mM for a 0.01 M buffer concentration to 7.6 mM for a 1 M buffer concentration. They also showed that alkaline phosphatase activity could be greatly improved by adding $MgCl_2$ to the solution whereas it was greatly reduced by the addition of $ZnCl_2$ to the solution.

From this section, we conclude that the calculated values of K_m and k_{cat} for alkaline phosphatase with *p*-aminophenyl phosphate substrate in our conditions are within the range of values indicated in the literature. However it seems that this activity could be optimised by studying the effect of different buffering agents and metal salts. One option would be to replace some KCl by $MgCl_2$ as a background electrolyte.

4- Combined glucose oxidase and alkaline phosphatase enzyme system

After studying both the glucose oxidase system (Figure 6) and the alkaline phosphatase system (Figure 14) separately, we are able to study the combined glucose oxidase alkaline phosphatase system, and evaluate the amplification of the current due alkaline phosphatase catalysed hydrolysis of *p*-aminophenyl phosphate by the glucose oxidase redox recycling.

The interest of combining alkaline phosphatase with glucose oxidase is to obtain a larger current from fewer *p*-aminophenol molecules as they are recycled. But we saw earlier that both the diffusion and the viscosity were affected by the addition of glucose and glucose oxidase having an effect on electrochemistry. Because of this complexity measuring the current from the alkaline phosphatase alone and comparing it with the combined alkaline phosphatase and glucose oxidase system is the only reliable way to evaluate the difference of oxidation current intensity. In this section we will analyse the amplification of the current while the concentration of *p*-aminophenol increases as a result of *p*-aminophenyl phosphate hydrolysis. We will study the amplification afforded by glucose oxidase and see what improvements can be made to optimise this amplification.

Also we will measure the amplification of the current under the same conditions when using a stationary working electrode.

First we describe the enzyme system that will be used (Figure 17), in this diagram E' stands for alkaline phosphatase and C for *p*-aminophenyl phosphate.

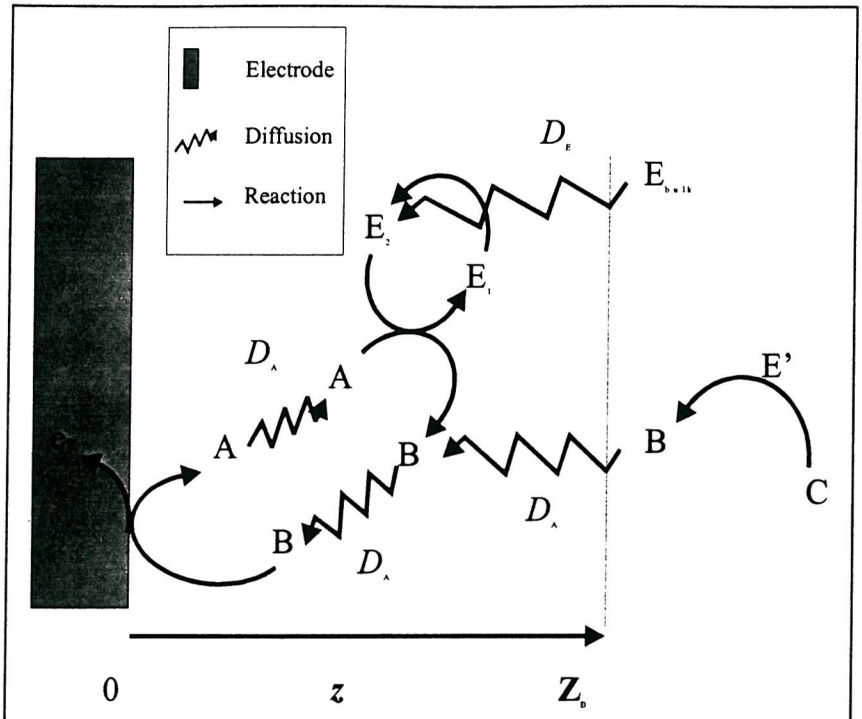

Figure 17: A schematic diagram of the homogeneous system as considered by Albery *et al.*[6] A and B are the oxidised and reduced forms of the mediator respectively. E_1 and E_2 are oxidised and reduced enzyme respectively. The substrate is not explicitly considered in this treatment, its effect on the rate of reduction of E_1 to E_2 is taken in consideration in the calculation of k_s. D_E is the diffusion coefficient of enzyme E_1 and E_2, D_A is the diffusion coefficient of mediator A and B. Z_D is the Levich diffusion length defined in (1. Unlike Figure 6, outside Z_D the bulk concentration of B varies according to the kinetics of the catalysed reaction C affords B. Oxidised mediator A is only produced at the electrode surface by re-oxidation of B.

The only difference between Figure 17 and Figure 6 is the variation of the concentration of B (*p*-aminophenol) in the bulk. This concentration depends on alkaline phosphatase activity and the original concentration of C (*p*-aminophenyl phosphate). Because the current is triggered by the addition of alkaline phosphatase, some convection is needed to homogenize the solution as 1 to 3 µl of alkaline phosphatase stock solution are added to 30 ml. For this reason the rotation speed of the working electrode was set at 4 Hz. This rotation speed affords a rapid homogenization of alkaline phosphatase concentration throughout the solution, yet it is slow enough to observe the current amplification by the glucose/glucose oxidase system.

The experiments were carried out in 30 ml pH 9.5 Tris-HCl 100 mM glucose and KCl background electrolyte. A new solution and a polished electrode were used for every experiment. The solution was degassed with argon and temperature controlled at 25 °C. Each measurement was made by setting the rotation speed at 4 Hz and applying 0 V potential. At time zero alkaline phosphatase was added to the solution and the current was recorded against time. Each experiment consisted in one measurement under the conditions described above and one measurement with the same solution containing 38 μM glucose oxidase.

4.1 Results

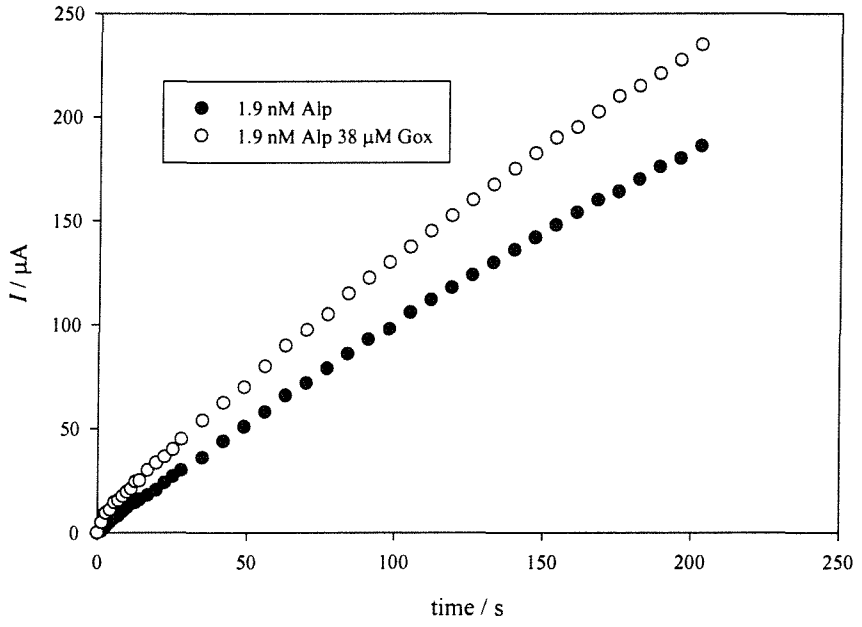

Figure 18: Current transients obtained with a 7 mm diameter glassy carbon working electron rotating at 4 Hz. The 30 ml solution is pH 9.5 Tris-HCl buffer 0.1 M, KCl 0.1 M, 100 mM glucose, 3 mM *p*-aminophenyl phosphate. It is water jacketed at 25°C. Time 0 is given by the addition of 1 μl of alkaline phosphatase stock solution to obtain a 1.9 nM final protein concentration. Black dots show current without glucose oxidase. White dots show current with 38 μM glucose oxidase.

The current increases as soon as the alkaline phosphatase is added. The experiment is stopped after 200 s. When glucose oxidase is present under the same conditions, a higher current is observed.

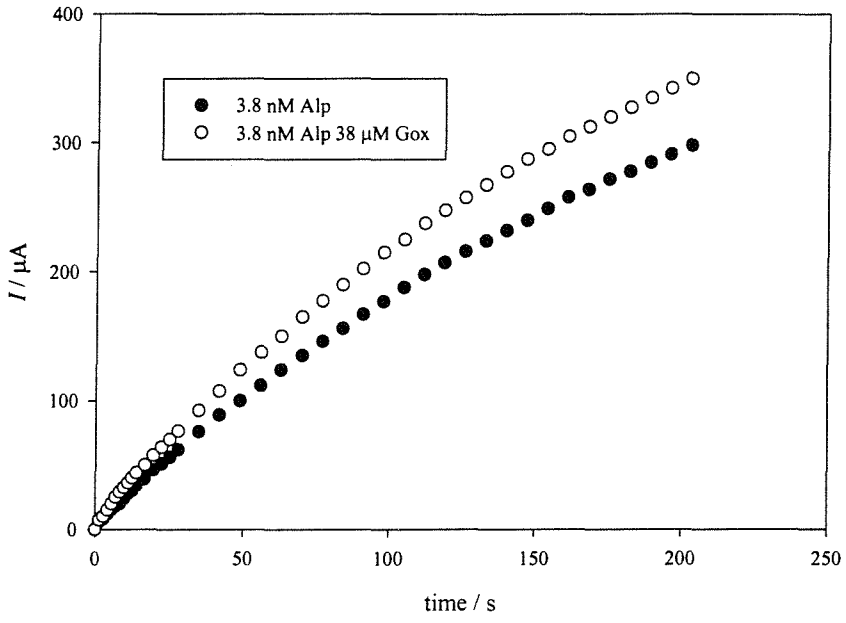

Figure 19: Current transients obtained with a 7 mm diameter glassy carbon working electron rotating at 4 Hz. The 30 ml solution is pH 9.5 Tris-HCl buffer 0.1 M, KCl 0.1 M, 100 mM glucose, 3 mM *p*-aminophenyl phosphate. It is water jacketed at 25°C. Time 0 is given by the addition of 2 µl of alkaline phosphatase stock solution to obtain a 3.8 nM final protein concentration. Black dots show current without glucose oxidase. White dots show current with 38 µM glucose oxidase.

The experiment was repeated with a higher concentration of alkaline phosphatase. By increasing the concentration of alkaline phosphatase, we increase the rate of *p*-aminophenyl phosphate hydrolysis and hence accelerate the increase in *p*-aminophenol concentration. When glucose oxidase is present, the same pattern of current amplification is observed in all three experiments.

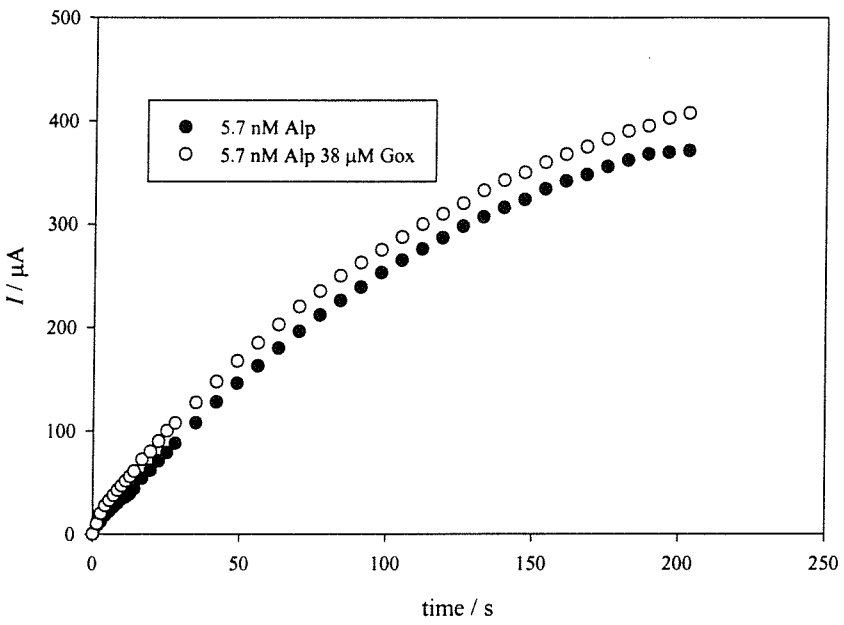

Figure 20: Current transients obtained with a 7 mm diameter glassy carbon working electron rotating at 4 Hz. The 30 ml solution is pH 9.5 Tris-HCl buffer 0.1 M, KCl 0.1 M, 100 mM glucose, 3 mM *p*-aminophenyl phosphate. It is water jacketed at 25°C. Time 0 is given by the addition of 3 µl of alkaline phosphatase stock solution to obtain a 5.7 nM final protein concentration. Black dots show current without glucose oxidase. White dots show current with 38 µM glucose oxidase.

The level of amplification generated by glucose oxidase is not large (1.2). The rotation speed of the electrode is the determining factor in the recycling process. Quinone imine is exclusively generated at the electrode surface. The intensity of recycling process within the diffusion layer varies according to the flux generated by the rotation of the working electrode. If the flux is important, the reduced compound is flushed away from the electrode before it has time to generate current. Therefore the level of amplification will be a maximum with stationary electrode.

4.2 Discussion

To reach a better understanding of the amplification process taking place in the system described in Figure 17, we divided the amplified current by the current obtained when no glucose oxidase is added to the solution, and hence no amplification of the current is taking place. Results of the analysis are given in Table 5:

Alkaline phosphatase concentration	1.9 nM	3.8 nM	5.7 nM
Mean value	1.58	1.23	1.20
Standard error	0.1	0.01	0.02
Confidence interval 99%	0.28	0.02	0.06

Table 5: statistical analysis of current intensity ratios (unit less) with the student t-test, from the glucose oxidase amplified current (circle symbols Figure 18, Figure 19, and Figure 20) divided by the current without glucose oxidase (black dots Figure 18, Figure 19, and Figure 20).

We observe that the mean amplification is larger for the lowest concentration of alkaline phosphatase. This indirectly implies that the amplification factor is higher for a lower *p*-aminophenol concentration. To verify this assumption, the current ratios for 1.9 nM and 5.7 nM alkaline phosphatase are plotted against time (Figure 21). This figure shows that amplification by glucose oxidase is uniform with time after 50 sec.

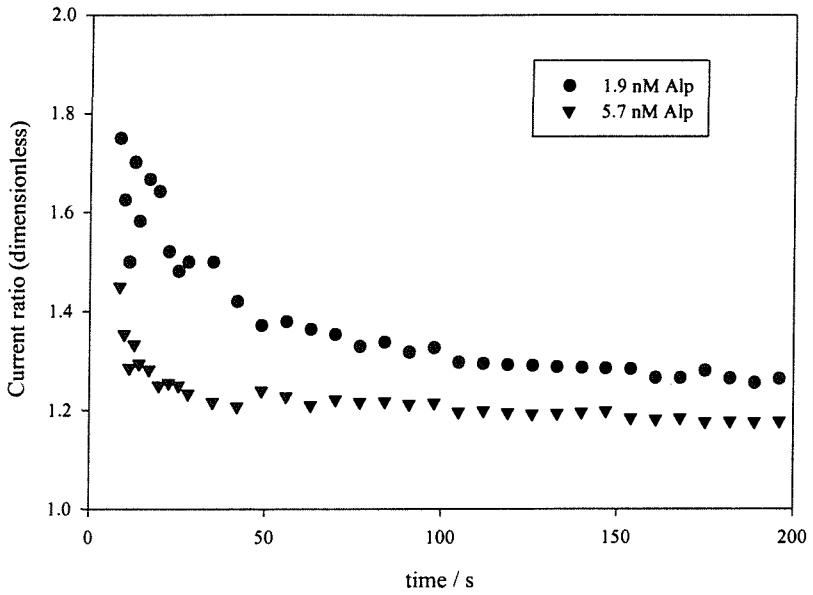

Figure 21: Current amplification ratio plotted against time. Ratios are obtained from dividing the glucose oxidase amplified current by the current obtained with alkaline phosphatase alone at 0V.

Figure 21 shows a rapid decay of the amplification coefficient from 0 to 50 s. However, at lower alkaline phosphatase concentration (1.9 nM) the amplification coefficient remains consistently higher than the amplification coefficient obtained from a higher alkaline phosphatase concentration (5.7 nM) from 50 to 200 s. We have shown in chapter 5 that in alkaline conditions *p*-aminophenol undergoes rapid evolution in solution forming aggregates. In this chapter, we estimated the diffusion coefficient of *p*-aminophenol at pH 9.5 ($2.06\ 10^{-6}$ $cm^2\ s^{-1}$), and showed that the corresponding Stokes radius is multiplied by 4 between pH 7 ($r = 2.5\ 10^{-10}$ m) and pH 9.5 ($r = 10^{-9}$ m). This result leads us to infer that *p*-aminophenol forms tetramer agglomerates in these conditions, these agglomerates being responsible for the decrease in affinity for glucose oxidase. As a result, the amplification coefficient is seen to decrease rapidly as these agglomerates form in solution.

4.3 Static working electrode

The next experiment was carried out to evaluate the amplification on a stationary electrode.

These experiments were carried out in a 100 µl drop laid on a 1 cm^2 graphite working electrode, the counter electrode was a gold wire and the reference was a home made SCE reference electrode. The solution was pH 9.5 Tris-HCl 100 mM glucose and KCl background electrolyte with *p*-aminophenyl phosphate. 0 V potential were applied and current was recorded when alkaline phosphatase was added to the solution. The same experiment was repeated with glucose oxidase present in the solution.

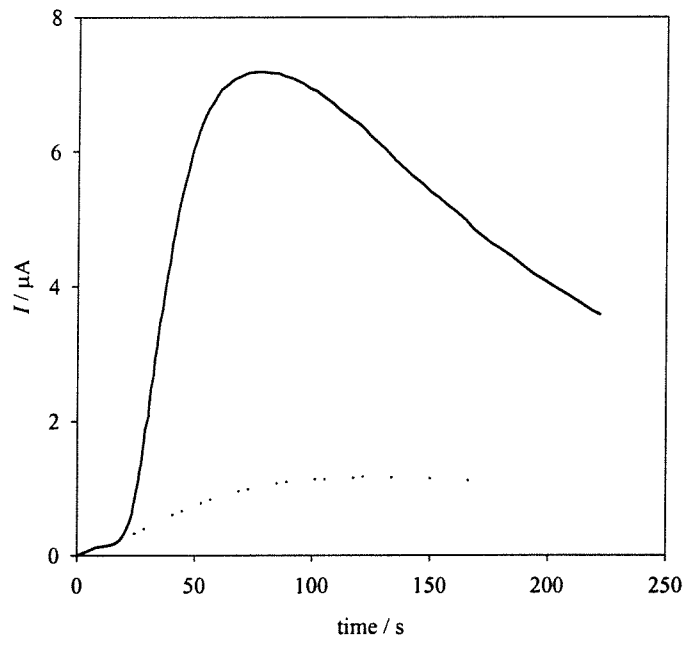

Figure 22: Current transients obtained on a 1 cm^2 graphite working electrode, gold wire counter electrode. Upper signal is obtained from a pH 9.5 Tris-HCl 100 µl solution with 23 µM *p*-aminophenyl phosphate, 100 mM glucose, 38 µM glucose oxidase and 50 nM alkaline phosphatase. The lower signal is 50 nM alkaline phosphatase and 23 µM *p*-aminophenyl phosphate, 100 mM glucose.

The current resulting from combined alkaline phosphatase and glucose oxidase represents a 7 fold increase over the current obtained with alkaline phosphatase alone in the same conditions. The drop of current after 100 s may be due to a rapid degradation of *p*-aminophenol as the small volume of solution is exposed to atmospheric oxygen.

In this situation, amplification is not constant and the working electrode is not rotating during the time of the experiment. However, there is an obvious hypothesis to explain the decrease of the glucose oxidase amplified current after 50 s in Figure 22. We saw in chapter 5 that the UV study of *p*-aminophenol at alkaline pH suggested the formation of *p*-aminophenol agglomerates in solution. The calculation of the diffusion coefficient of *p*-aminophenol at pH 9.5 from this chapter suggests that the Stokes radius of the molecule is multiplied by four. Figure 21 shows the amplification of the current by glucose oxidase to decrease between 0 and 40 s from the start of alkaline phosphatase catalysed hydrolysis of *p*-aminophenyl phosphate. In the light of this indirect evidence, we infer that as soon as *p*-aminophenol tetramers are formed, glucose oxidase ceases to recycle quinone imine into *p*-aminophenol.

5- Conclusion

In this chapter, we determined the kinetic parameters of our enzyme system. First we showed that in the presence of glucose and glucose oxidase at pH 9.5, the oxidation of *p*-aminophenol was kinetically limited. We also showed that increasing concentration of glucose oxidase affected the viscosity of the solution, which in turn diminished the diffusion coefficient of *p*-aminophenol. We estimated the diffusion coefficient of *p*-aminophenol at pH 9.5, from the corresponding change in Stokes radius between pH 7 and pH 9, we confirmed the formation of *p*-aminophenol agglomerates in alkaline conditions.

Having a kinetically limited electrochemical process led us to redefine the mathematical model from Albery *et al.* for these new conditions. From the new mathematical model, we determined the re-oxidation constant for glucose oxidase with *p*-aminophenol in excess glucose concentration to be 0.03×10^5 dm^3 mol^{-1} s^{-1} < k_M < 0.57×10^5 dm^3 mol^{-1} s^{-1}. This confusing result is probably due to the formation of *p*-aminophenol aggregates for which glucose oxidase has little or no affinity. The formation of these aggregates takes place during the rotating disc experiments undertaken to determine the re-oxidation kinetic constant of glucose oxidase, corrupting our values.

We also determined the K_M and k_{cat} values of alkaline phosphatase for *p*-aminophenyl phosphate under our conditions, and found values of 1.32×10^{-4} mol dm^{-3} and 2.74×10^{3} s^{-1} for K_m and k_{cat}.

Under the conditions for the sensor we will be using in chapter 8, we saw that the total amplification by glucose oxidase was only 7 fold. However, by changing the mediator, this value could be greatly improved.

6 References

1. Wilde, C. and M. Zhang, *Oxidation of glucose at electrodeposited platinum electrodes in alkaline solution.* J. Chem. Soc, 1993. **89**(2): p. 385-389.
2. Wilde, C. and Z. Meijie, *Oxidation of glucose at electrodeposited platinum electrodes.* J. Electroanal. Chem., 1992. **340**(1-2): p. 241-255.
3. Kokoh, K., et al., *"On line" chromatographic analysis of the products resulting from the electrocatalytic oxidation of D-glucose on pure and adatoms modified Pt and Au electrodes. II: Alkaline medium.* Electrochim. Acta, 1992. **37**(11): p. 1909-1918.
4. Albery, W.J., et al., *Electrochemical sensors: theory and experiment.* J. Chem. Soc., Faraday Trans 1, 1986. **82**: p. 1033-1050.
5. Bartlett, P.N. and K.F.E. Pratt, *A study of the kinetics of the reaction between ferrocene monocarboxylic acid and glucose oxidase using the rotating disc electrode.* J. Electroanal. Chem., 1995. **397**: p. 53-60.
6. Albery, W.J., et al., *Amperometric enzyme electrodes Part 5. The homogeneous mediated mechanism.* J. Electroanal. Chem., 1992. **323**: p. 77-102.
7. Christie, I.M., et al., *Simplified measurement of serum alkaline phosphatase utilizing electrochemical detection of 4-aminophenol.* Anal. Chim. Acta, 1992. **257**: p. 21-28.
8. Thompson, R.Q., et al., *Zeptomole detection limit for alkaline phosphatase using 4-aminophenylphosphate, amperometric detection, and an optimal buffer system.* Anal. Chim. Acta, 1993. **271**: p. 223-229.

Chapter 8: The sensor

1 The Sensor

1.1 Introduction

This chapter describes the study of the detection capabilities of the sensor described in chapter 3. In chapter 3 we described the configuration of a new type of polymer transistor enzyme sensor. In chapter 4 we described the fabrication of the poly(aniline)-poly(vinylsulfonate) transistors where the polymer transistor is separated from the enzyme reaction. We will now use these transistors in our sensor, each transistor is only used once. By doing so we intend to prove the reliability of our sensor for the detection of 100 to 350 nM *p*-aminophenol and 0 to 4 nM alkaline phosphatase in a 100 µl sample volume corresponding to 0 to 3.5 10^{-11} moles of p-aminophenol and 0 to 4 10^{-13} moles of alkaline phosphatase.

First we will describe the design of the experiment. Then we will prove the relation between the loss of drain current through the polymer transistor and the concentration of *p*-aminophenol. This will be done using in-house built non-disposable electrodes as the disposable transistors are difficult to fabricate and very expensive because they are produced on a small production scale (of course this would not be true for an industrial production scale). The next step will be to produce a calibration curve for *p*-aminophenol using 5 transistors for each concentration. Similarly, we will produce a calibration curve for alkaline phosphatase.

The reason for testing alkaline phosphatase is due to the large number of monoclonal antibodies commercially available with alkaline phosphatase attached as a label. Therefore detecting alkaline phosphatase equates to detecting alkaline phosphatase attached to a monoclonal antibody. Because our sensor detects alkaline phosphatase, there is hope that it should be able to reveal diagnostic *in-vitro* immunoassays involving alkaline phosphatase as a label.

1.2 structure

The sensor combines the use of the poly(aniline)-poly(vinylsulfonate) film laid across two electrodes (chapter 3) through the use of a set of disposable polymer films characterised in chapter 4. The bioelectrochemical detection of this sensor involves the electrode oxidation of *p*-aminophenol at pH 9.5 studied in chapter 5. The mediator (*p*-aminophenol) is generated by the alkaline phosphatase catalysed *p*-aminophenyl phosphate hydrolysis. We showed in chapter 6 that *p*-aminophenyl phosphate did not interfere with *p*-aminophenol at 0 V vs SCE on carbon electrodes. As we explained in chapter 7, once *p*-aminophenol has reacted at the electrode, the reaction product (quinone imine) is recycled in *p*-aminophenol by the glucose / glucose oxidase system.

We recall the chain of reactions involved the sensing experiment in the following equations:

p-aminophenol phosphate + alkaline phosphatase > *p*-aminophenol + alkaline phosphatase.

(1)

p-aminophenol > quinone imine + $2e^- + 2H^+$

(2)

glucose oxidase(FAD^+) + glucose > glucose oxidase($FADH,H^+$) + gluconolactone

(3)

quinone imine + glucose oxidase($FADH,H^+$) > *p*-aminophenol + glucose oxidase(FAD^+)

(4)

The electrons afforded by *p*-aminophenol oxidation are conveyed to the conducting polymer by the wire connectingthe electrodes in cell A and B leading to the following reaction in cell A.

emeraldine + $2e^-$ > leucoemeraldine

(5)

The experimental set up of the sensor is described in Figure 1. We now explain how it is operated.

A 30 mV potential difference applied between the gates of the polymer transistor (drain potential) generates a drain current depending on the conductivity of the polymer (chapter 3). This current is recorded against time by a chart recorder connected to an ammeter. When the bioelectrochemical reaction takes place, the polymer is reduced from the conducting emeraldine state to the non-conducting, leucoemeraldine state as shown in chapter 3 and the drain current generated by the 30 mV drain potential decays. The rate of drain current decay against time was shown to be related to the kinetics of polymer reduction (Chapter 3). In this chapter we will prove that this is, in turn, related to the rate of *p*-aminophenol oxidation.

We showed in chapter 3 that the current decay through the transistor is exponentially related to the reduction charge applied to the polymer. We also studied the electron transfer kinetics in the *p*-aminophenol oxidation process in chapter 5. The re-oxidation constant of glucose oxidase by the reduction of quinone imine into *p*-aminophenol has been calculated at pH 9.5 (k_M = 1.38 10^5 mol^{-1} dm^{-3} s^{-1}) in chapter 7. The kinetic constants of alkaline phosphatase for *p*-aminophenylphosphate, K_m and k_{cat}, have also been determined in chapter 7. Finally the rate of amplification provided by the combined glucose oxidase-alkaline phosphatase enzyme system has been discussed in chapter 7.

A specific property of this sensor is the absence of a reference electrode. This role is fulfilled by the polymer itself. This means that the oxidation potential of the electrode at which *p*-aminophenol reacts, is imposed by the polymer. As seen in chapter 3, the reduction of the polymer causes its potential to drop from 0.2 V to 0 V vs SCE during the experiment. The change of polymer potential implies a change in the collecting electrode potential. This means a change of electrode potential against time as the *p*-aminophenol oxidation takes place. Therefore, the change in electrode potential induced by the reduction of the polymer will affect the current responsible for this same reduction.

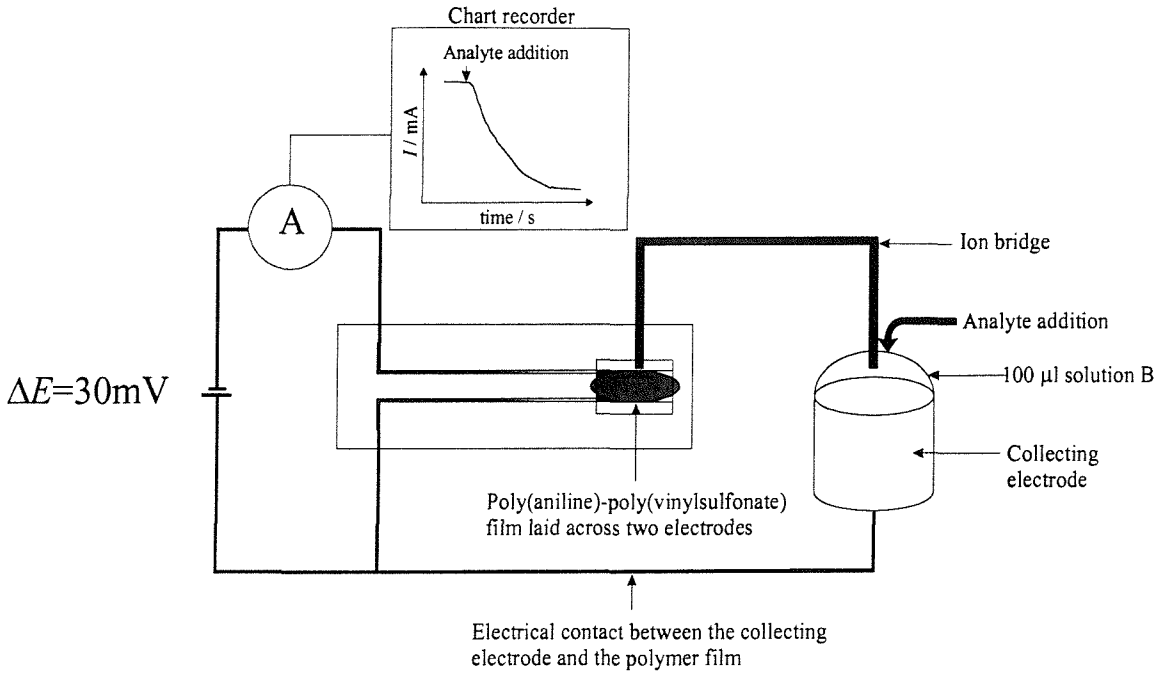

Figure 1: Sketch of the sensing device when ready to operate: the poly(aniline)-poly(vinylsulfonate) film is laid across two electrodes connected to an ammeter and a power supply maintaining a 30 mV potential difference between the two electrodes connected by the polymer. The polymer film bathes in a 2 M H_2SO_4 aqueous solution. The potential of the polymer is previously set at 0.2 V vs SCE in 2 M H_2SO_4 using a three electrode configuration (chapter 4). The polymer is in its conductive emeraldine state and a current flowing through it is detected by the ammeter and recorded on a chart recorder. The bioelectrochemistry takes place in 100 µl solution B (pH 9.5 Tris-HCl, 23 µM *p*-aminophenyl phosphate, 100 mM glucose, 38 µM glucose oxidase at 25°C) resting on a 1 cm^2 HOPG graphite electrode (basal plane). The collecting electrode is connected to one of the electrodes across which the polymer is laid. Therefore its potential is the same as the polymer connected to it. An ion bridge dipping both in acid on the polymer side and the sample on the collecting electrode side guarantees charge transfer. The detection experiment starts when alkaline phosphatase or *p*-aminophenol is added to the collecting electrode solution (solution B). The induced reaction results in a drop of current detected by the ammeter, which is recorded against time on the chart recorder.

At the start of the detection experiment, the stability of the polymer potential is shown by the steady current flowing through the transistor. It shows that no redox process is taking place at this stage. Glucose oxidase and glucose do not afford any current as shown in chapter 7. At this point the detection may be carried out by adding *p*-aminophenol to the solution. If *p*-aminophenyl phosphate is added, no current is recorded, and the detection is started when alkaline phosphatase is added to the solution.

The critical component of such calibration curves is the reproducibility of the transistor behaviour. We saw in chapter 3 that these can only be used once. The only information about the new transistor being used is the initial current flowing through it before the experiment is carried out.

Figure 2 displays the current transients for *p*-aminophenol detection. Time 0 stands for the addition of *p*-aminophenol to the solution. We see that all initial current values are not identical. Measurement 5 has a larger initial current by about 15%, and measurements 3 and 7 have a slightly lower initial current then the rest.

The set of data displayed in Figure 2 was obtained with in-house built transistors. This was done to investigate the detection properties of our sensing device without using our stock of disposable transistors.

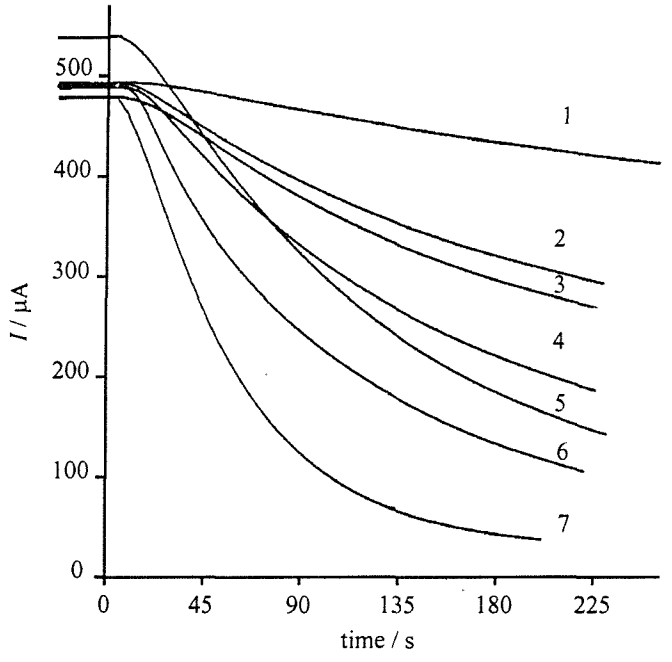

Figure 2: The drain current transients are plotted when various concentrations of *p*-aminophenol: **1** blank, **2** 100 nM, **3** 150 nM, **4** 200 nM **5** 300 nM, **6** 450 nM, **7** 900 nM. The polymerisation charge of the transistor was 0.78 mC and the drain voltage 30 mV. Here, the same transistor was used to obtain all seven measurements. Time 0 is the time of sample addition.

Figure 2 shows a different response from the sensor according to the concentration of *p*-aminophenol added to cell B. This set of data proves that our sensor is sensitive to different concentrations of mediator. Our sensor provides quantitative information on the concentration of mediator. The shape of the current transients in Figure 2 display a bend as the analyte is added, then a nearly linear slope is observed for a few seconds, and the slope decreases gradually. We observe that transient (1), which corresponds to a blank (100 mM glucose, 38 µM glucose oxidase) with no *p*-aminophenol present does not remain at the

same drain current intensity during the time of the experiment. Its slope, 0.5 μA / s, could be due to oxygen mediated reduction of the polymer transistor by glucose oxidase.

To correlate a current transient to the concentration of *p*-aminophenol added to cell B, we calculate the slope during the linear part of the transient. Results are shown in Figure 3.

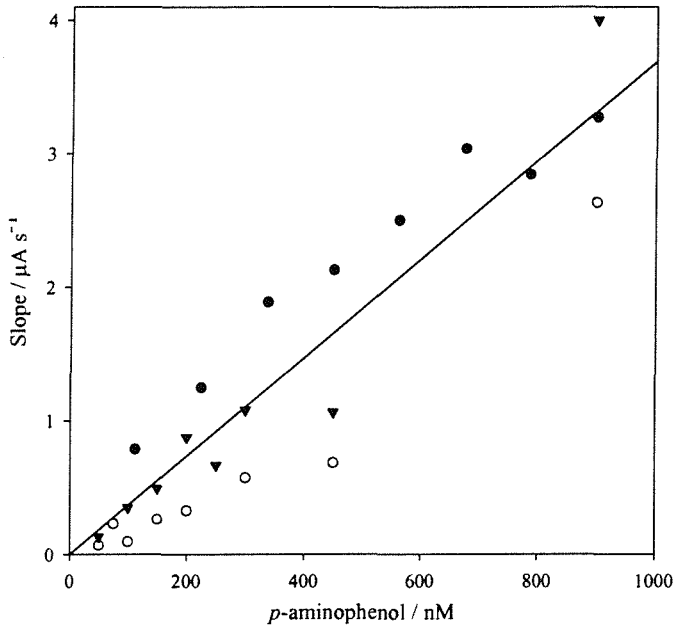

Figure 3: Scatter plot for several calibration experiments on several re-used home built transistors, each symbol represents the data collected from one individual transistor (polymerisation charge 0.78 mC) gold mylar gold (300 nm/25nm/300nm) 4 mm long supporting electrodes. Glucose 100 mM, glucose oxidase 38 μM at pH 9.5 Tris-HCl 0.1 M. A linear regression shows the limited accuracy of the device (+/- 300 nM).

Figure 3 shows calibration results obtained with re-used home built transistors, each symbol represents the data collected with each home made polymer transistor. These are made of gold coated mylar sheets where gold deposits on both sides of the mylar act as electrodes and the mylar acts as insulator between these electrodes. The structure is maintained by embedding it in epoxy resin. The polymer is formed on these electrodes by electro-polymerisation.

As we see from the scatter in Figure 3, good reproducibility of the results is difficult to achieve. To solve this problem, we had to use the polymer photolithography electrodes structure described in chapter 4.

2 Calibration of *p*-aminophenol

We tested the response of the disposable transistors described in chapter 4 to *p*-aminophenol concentrations ranging from 0 to 500 nM. The experiment was carried out as follows:

The polymer transistor is successively set at 0 V vs SCE (1 min), 0.35 V (1 min), and 0.2 V (1 min) in 2 M sulfuric acid. Meanwhile 100 µl pH 9.5 Tris-HCl buffer 0.1 M, 100 mM glucose, 38 µM glucose oxidase (solution B) are water jacketed at 37 °C in a multiwell plate. Dilutions of *p*-aminophenol are prepared in phosphate / citrate pH 5 buffer. When the transistor is set at 0.2 V vs SCE, solution B is deposited on a 1 cm^2 graphite electrode connected to the polymer transistor. The salt bridge makes contact between solution B and the sulfuric acid solution covering the polymer transistor. At this stage a 30 mV drain potential is applied to the transistor and the drain current intensity is recorded. *p*-aminophenol is added in a 1 µl fraction to solution B and the drain current intensity is recorded against time.

The results are displayed in Figure 4. These show no significant difference between the current slope value if no *p*-aminophenol is added and when 50 nM are added to cell B. On the contrary, we observe a regular increase in current slope value from 100 nM to 450 nM *p*-aminophenol concentration. In this experiment, each concentration is only tested once, and a new polymer transistor is used for each test.

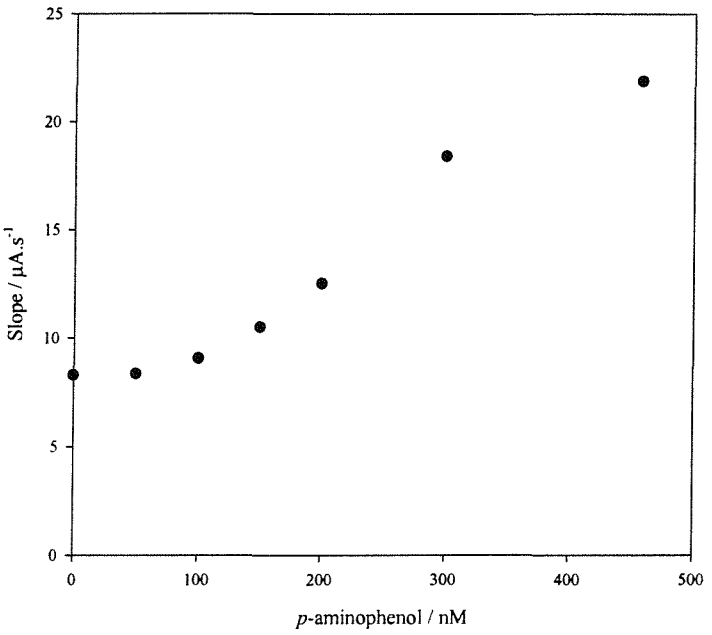

Figure 4: Calibration results from 0 to 500 nM *p*-aminophenol. With disposable commercial electrode bearing the polymer transistor. Glucose 100 mM, glucose oxidase 38 µM at pH 9.5 Tris-HCl 0.1 M.

In order to confirm the results showed in Figure 4 we repeated the experiment on *p*-aminophenol concentrations ranging from 100 nM to 350 nM. Each concentration was tested 5 times with 5 disposable transistors. The error bars are calculated from the variance of each result with the average value of these replicates.

The results in Figure 5 show that the slope is different from 0 when no *p*-aminophenol is present. Because the sample solution in which *p*-aminophenol is normally added is not degassed before the experiment, the reduction of the polymer transistor may be due to the oxidation of hydrogen peroxide formed from the reduction of dissolved oxygen by glucose oxidase. Although this is a possibility, we have no direct evidence to support this interpretation.

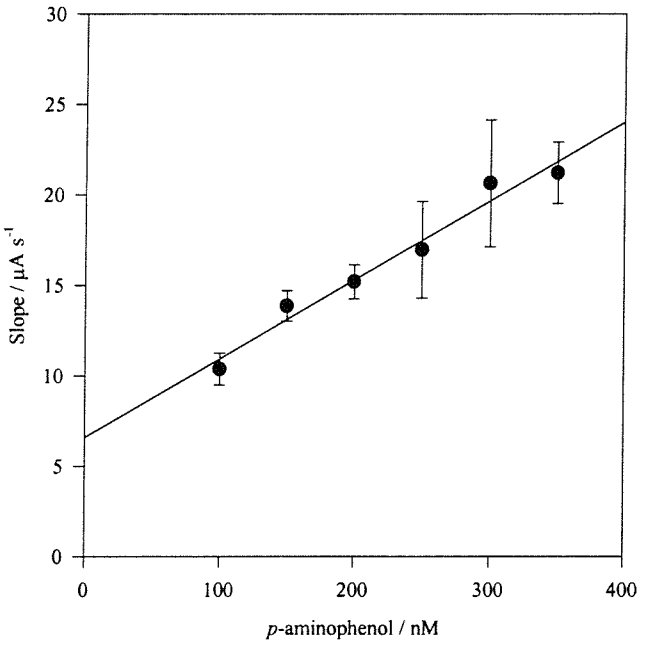

Figure 5: The measurements were carried out with the disposable transistors. Four values were taken for each concentration of *p*-aminophenol. The values for one concentration were measured on different days with fresh solutions. The Y scale indicates the slope of the initial linear drop of conductivity in µA / s. Glucose 100 mM, glucose oxidase 38 µM at pH 9.5 Tris-HCl 0.1 M.

Having showed that our sensor is able to display a linear response to *p*-aminophenol concentrations ranging from 100 nM to 350 nM, we are now interested in the detection capabilities of our sensor towards alkaline phosphatase. The *p*-aminophenol concentration range displayed here is purely indicative of our sensing device capabilities, we show which analyte concentration window may be detected within 60s.

3 Calibration of alkaline phosphatase

We are now interested in the response of our sensor to the addition of alkaline phosphatase. The experiment is carried out as follows.

The polymer transistor is successively set at 0 V vs SCE (1 min), 0.35 V (1 min), and 0.2 V (1 min) in 2 M sulfuric acid. Meanwhile 100 µl pH 9.5 Tris-HCl buffer 0.1 M, 100 mM glucose, 38 µM glucose oxidase, 20 µM *p*-aminophenyl phosphate (solution B) are water jacketed at 37 °C in a multiwell plate. Dilutions of alkaline phosphatase are prepared in Tris-HCl pH 9.5 buffer. When the transistor is set at 0.2 V vs SCE, solution B is deposited on a 1 cm^2 graphite electrode connected to the polymer transistor. The salt bridge makes contact between solution B and the sulfuric acid solution covering the polymer transistor. At this stage a 30 mV drain potential is applied to the transistor and the drain current intensity is recorded. Alkaline phosphatase is added in a 1 µl fraction to solution B and the drain current intensity is recorded against time.

To evaluate the sensitivity of our sensor, we tested alkaline phosphatase concentrations ranging from 0 nM to 10 nM in 100 µl (10^{-12} moles of analyte). Results are showed in Figure 6.

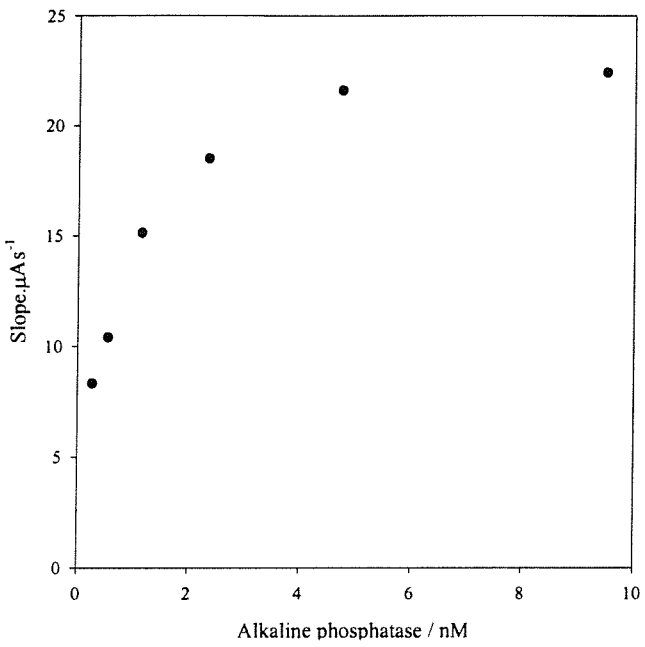

Figure 6: Calibration results from 0 to 9.7 nM alkaline phosphatase. With disposable commercial electrode bearing the polymer transistor. Glucose 100 mM, glucose oxidase 38 μM, *p*-aminophenyl phosphate 20 mM at pH 9.5 Tris-HCl 0.1 M.

Figure 6 shows a linear response of the sensor from 0 to 5 nM alkaline phosphatase, beyond this concentration, a plateau is observed. In this experiment each concentration is only tested once to determine the sensitivity range of our sensor. We tested the sensitivity of our device when no glucose oxidase is added to the solution. In these conditions, we found that the lowest alkaline phosphatase concentration that could be detected within 90s was 10 nM (not shown). Therefore we assume that the glucose/glucose oxidase system provides approximately a 10 fold amplification of the signal.

A calibration was carried out from 0 nM to 4 nM for each concentration, 5 replicates were obtained from 5 disposable transistors. To study the response of our sensor to the addition of alkaline phosphatase, the drain current is recorded against time. The data are shown in Figure 7.

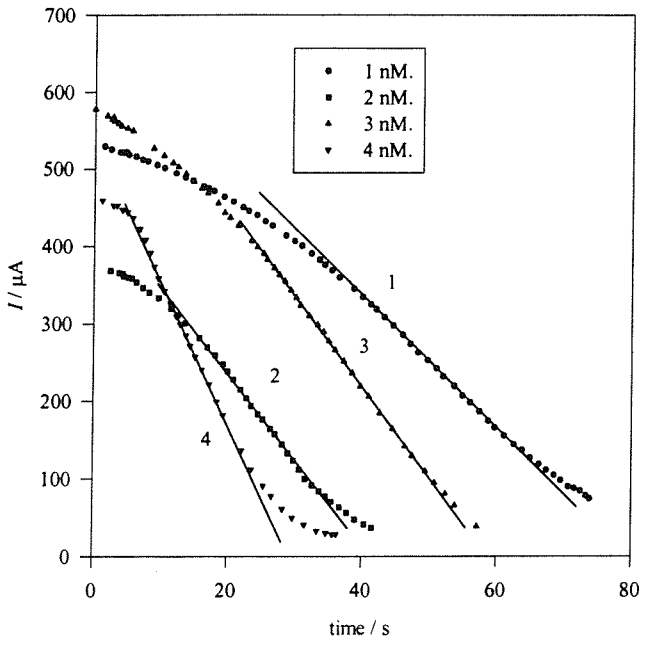

Figure 7: Drain current transients obtained with 4 transistors at 4 concentrations: (1) 1 nM, (2) 2 nM, (3) 3 nM, and (4) 4 nM alkaline phosphatase. The slopes are calculated from the straight lines.

Each replicate for each concentration of alkaline phosphatase display a similar slope as shown in Figure 8. However, as seen in chapter 3 most transistors display different drain current intensities at the start of each experiment. We observed that the intensity of the drain current at the start of each experiment had little influence on the variation of the slope for a given concentration of alkaline phasphatase.

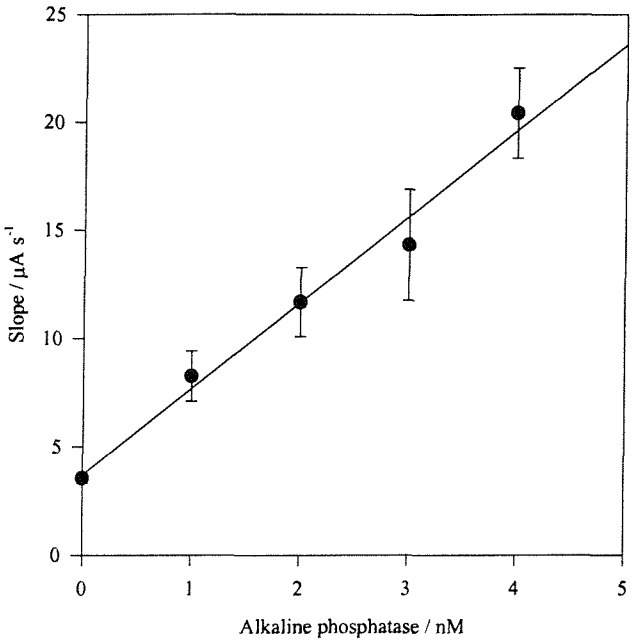

Figure 8: The measurements were carried out with the disposable transistors. Four values were taken for each concentration of alkaline phosphatase. The values for one concentration were measured on different days with fresh solutions. The Y scale indicates the slope of the initial linear drop of conductivity in µA / sec. Glucose 100 mM, glucose oxidase 38 µM, *p*-aminophenyl phosphate 20 mM at pH 9.5 Tris-HCl 0.1 M.

Figure 8 displays a linear relation between enzyme concentration and drain current slope value. However we see that the value of the slope with no alkaline phosphatase added is not 0. This could be explained by a slow non-enzyme catalysed hydrolysis of *p*-aminophenyl phosphate into *p*-aminophenol. Affording a small current before alkaline phosphatase is added. However, the intercept value at 0 nM for *p*-aminophenol calibration is similar (6 µA / s) to the intercept value observed in alkaline phosphatase calibration (4 µA / s), therefore this explanation seems wrong. It seems very likely that the current slopes at 0 nM are due to the same phenomenon in both the *p*-aminophenol and alkaline phosphatase calibration experiments.

4 Discussion

In this chapter, we proved the reliability of our sensor to detect 100 to 350 nM *p*-aminophenol and 0 to 4 nM alkaline phosphatase. These detection experiments were performed with the same set of polymer transistors described in chapter 4. All detection experiments were carried out in less then 60 s, which makes our sensor the most sensitive and fastest sensor to operate without a potentiostat. The accuracy of the sensor as well as its sensitivity window is encouraging in the prospect of fast highly sensitive portable devices. The range of concentration detected here may not be directly adapted to most analytes in human blood which range from pM to mM concentrations. But we proved in chapter 3 that when using a larger polymerisation charge to fabricate our polymer transistor, a larger reduction charge was required to perform the switch of the polymer film from conductive to insulating. This means that the electrodeposition charge of the polymer could be adapted to the range of analyte concentration to be tested. At the moment, with this range of sensitivity, our test could be used for 80 % of the analytes screened in routine blood tests.

It is worth stressing that any laboratory based immunoassay requires a trained technician working over up to 3 hours. The alternative possibility to carry out a portable immunoassay test in less than 60 s represents a major improvement in terms of time, as it could help the laboratory based analysis to be more targeted.

General conclusion

The sensor developed in this thesis, is not a viable commercial device as such. The reason for this is that the electrodeposition of poly(aniline)/poly(vinylsulfonate) is very delicate in terms of reproducibility, which is incompatible with cost effective industrial production. On the over hand this sensor has proved itself extremely sensitive and extremely fast as the results are obtained in less than 60 sec. This was achieved despite a large number of imperfections like the rapid decay of *p*-aminophenol in alkaline conditions, and the much lower than expected current amplification of *p*-aminophenol oxidation by glucose oxidase. However, the polymer electrodeposition can be greatly improved by experimenting different supporting electrode shapes. This is an issue that we were not able to explore. Secondly, the tendency of *p*-aminophenol to agglomerate and hence undermine the glucose oxidase current amplification process shows that this mode of current amplification would yield 1000 fold amplification rates if the agglomeration process was prevented.

These are reasons why this new type of sensor needs to be investigated further. The main advantage it provides is the absence of any reference electrode or counter electrode. To this date the electrode configuration on commercial electrochemical biosensors is the main cause for potential shift during the assay, leading to faulty readings. Despite the incredible progress of electronics, it is still difficult to build portable equipment able to detect small current intensities as the background noise is affecting the signal. The sensor developed in this thesis is unaffected by background noise because of its simplified electrode configuration.

Finally, in the area of biomedical assays, the use of blood to carry out electrochemistry in a three electrode configuration is a major problem in terms of potential distribution through the sample, the conductivity is very poor and the current intensities are greatly affected. Our sensor is less subject to these problems because the current is driven by the difference between the collecting electrode potential and the potential of the redox mediator in the diffusion layer. The salt bridge maintains the charge equilibrium between the two compartments of the sensor.

It is my conviction that if there was a true will to develop this sensor industrially it would be a success.